Building safety with nature

Salt marshes for flood risk reduction

Vuik, Vincent

DOI
10.4233/uuid:9339474c-3c48-437f-8aa5-4b908368c17e

Publication date
2019

Document Version
Final published version

Citation (APA)
Vuik, V. (2019). *Building safety with nature: Salt marshes for flood risk reduction*. [Dissertation (TU Delft), Delft University of Technology]. https://doi.org/10.4233/uuid:9339474c-3c48-437f-8aa5-4b908368c17e

BUILDING SAFETY WITH NATURE

SALT MARSHES FOR FLOOD RISK REDUCTION

Proefschrift

ter verkrijging van de graad van doctor
aan de Technische Universiteit Delft,
op gezag van de Rector Magnificus prof. dr. ir. T.H.J.J. van der Hagen,
voorzitter van het College voor Promoties,
in het openbaar te verdedigen op woensdag 27 maart 2019, 10.00 uur.

door

Vincent VUIK

civiel ingenieur, Technische Universiteit Delft, Nederland
geboren te Krimpen aan den IJssel, Nederland

Dit proefschrift is goedgekeurd door de

promotor: prof. dr. ir. S.N. Jonkman
copromotor: dr. ir. B.W. Borsje

Samenstelling promotiecommissie:

Rector Magnificus,	voorzitter
Prof. dr. ir. S.N. Jonkman,	Technische Universiteit Delft, promotor
Dr. ir. B.W. Borsje,	Universiteit Twente, copromotor

Onafhankelijke leden:

Prof. dr. R.J. Nicholls,	University of Southampton
Prof. dr. ir. A.J.H.M. Reniers,	Technische Universiteit Delft
Prof. dr. S. Temmerman,	Universiteit Antwerpen
Prof. dr. ir. P.H.A.J.M. Van Gelder,	Technische Universiteit Delft

Keywords: Flood risk, nature-based solutions, foreshore, salt marsh, vegetation

Printed by: GVO Drukkers & Vormgevers

Cover illustration: Jeroen Helmer / ARK Nature

ISBN 978-94-6332-470-0

An electronic version of this dissertation is available at
http://repository.tudelft.nl/.

The LORD on high is mightier
than the noise of many waters, yea,
than the mighty waves of the sea.

De HEERE in de hoogte is machtiger
dan het bruisen van machtige wateren,
de machtige golven van de zee.

Psalm 93

SUMMARY

Flood risk reduction in coastal areas is traditionally approached from a conventional engineering perspective, where dikes and dams are built to withstand the forces of tides, surges and waves. Recently, a nature-based approach to flood risk reduction is increasingly promoted, in which the benefits of coastal ecosystems for reducing the impact of extreme weather events are utilized. Ecosystems such as salt marshes, mangrove forests, coral reefs and sand dunes are preserved, enhanced or even created, in order to reduce flood risk in coastal areas. Nature-based flood defenses can work stand-alone, like sand dunes, but can also function in combination with engineered defenses, for example when vegetated foreshores reduce wave loads on dikes or dams.

The focus of this dissertation is on the case of hybrid flood defenses, where wave loads on a coastal dike or dam are reduced by a salt marsh, which functions as a vegetated foreshore in front of the engineered structure. There is limited knowledge on the functioning and stability of vegetated foreshores under severe storm conditions. Further, these natural systems are characterized by relatively high temporal and spatial variations. The lack of knowledge and high variability lead to a relatively high degree of uncertainty in flood risk reduction potential, compared to engineered structures. Uncertainty propagates into the failure probability of hybrid flood defenses. Therefore, the aim of this dissertation is to develop methods to assess how and how much nature-based flood defenses can reduce flood risks, taking into account uncertainties in their functioning and stability.

First, the effects of vegetated foreshores on wave heights, wave run-up and wave overtopping discharge were investigated, focusing on storm conditions. Wave energy dissipation was continuously measured for a period of approximately three years (2014-2017) on various salt marshes in the Western Scheldt estuary and in the Wadden Sea, both located in the Netherlands. The resulting dataset includes storms, with higher significant wave heights (maximum 0.85 m) and water depths (maximum 3.07 m) at the marsh edge than reported in any previous field study on wave attenuation by salt marshes. High wave attenuation rates over 50% per 300 m of marsh width were recorded during storms, notwithstanding reduced aboveground biomass in winter.

The process of wave energy dissipation was investigated, using the spectral wave model SWAN, which is able to distinguish different energy dissipation mechanisms such as depth-induced wave breaking, wave attenuation by standing vegetation, and bottom friction. Model results showed that wave energy dissipation was primarily caused by

wave attenuation by vegetation and (to a lesser extent) by wave breaking. Observed wave attenuation by *Spartina anglica* (common cord-grass) and *Scirpus maritimus* (sea club-rush) vegetation under storm conditions could best be described in the SWAN model by a calibrated bulk drag coefficient $\widetilde{C}_D \approx 0.4$.

The calibrated SWAN model was subsequently applied in combination with empirical EurOtop formulas, to predict how foreshores affect wave run-up and wave overtopping discharge at coastal dikes. This approach demonstrated that vegetated foreshores reduce wave loads on coastal dikes significantly. Pronounced reductions in wave run-up and wave overtopping were found, especially for situations with a large wave height to water depth ratio on the foreshore. Wave attenuation by vegetation has most added value at water depths for which waves are close to breaking, provided that the vegetation remains stable under the wave forcing.

The influence of salt marshes on wave run-up was confirmed by post-storm measurements of the position of flotsam lines (i.e., deposits of floating organic material) on the outer slopes of dikes along the Wadden Sea. Wave run-up height was found to be more than 2 m lower behind salt marshes during storms with a return period of ±5 years, compared to run-up at parts of the dike behind bare mudflats.

Secondly, the stability of vegetation under wave forcing was considered, in order to predict whether vegetation could still attenuate waves at storm conditions for which coastal dikes are usually built. A model has been developed to predict the threshold of stem breakage, by determining the wave load that a plant stem can withstand before it breaks or folds. This occurs when the wave-induced bending stress exceeds the stem's flexural strength.

Flexural strength was determined by means of three-point bending tests, which were carried out for two common salt marsh species: *Spartina anglica* (common cord-grass) and *Scirpus maritimus* (sea club-rush), at different stages in their seasonal cycle. The model expresses plant stability in terms of a critical orbital velocity, which is the velocity of particles due to wave motion. This critical orbital velocity depends on various plant characteristics that contribute to stability: flexural strength, flexibility, stem diameter and height, and the drag coefficient. A higher critical orbital velocity indicates greater stability of the stem.

The analytical formula was calibrated and validated, using information about stem breakage from the field sites in the Western Scheldt estuary (the Netherlands), and earlier laboratory tests. The short, thick and flexible stems of *Spartina* were found to be relatively stable compared to that of *Scirpus*. However, in design conditions, most coastal dikes are supposed to withstand high waves, which generate high near-bottom orbital velocities, thereby exceeding the critical orbital velocities of these two plant species.

Third, a method was set up to assess the failure probability of hybrid flood defenses, thereby incorporating relevant uncertainties in the characteristics and performance of the vegetated foreshore during extreme storms. Different models were integrated, which

describe wave propagation over a vegetated foreshore, stem breakage and dike failure. Two failure mechanisms were considered: failure due to (i) wave overtopping and (ii) wave impact on revetments.

Model results showed that vegetated foreshores cause a more pronounced reduction in failure probability for wave impact on revetments than for wave overtopping. For a case study in the Dutch Wadden Sea, the presence of a salt marsh allowed for a reduction of 0.5 m in dike crest level, compared to a dike behind tidal flats at mean sea level. Failure probabilities for asphalt and grass covers displayed a more pronounced reduction, by a factor 100 or more. The reason is that waves are able to damage revetments already at moderate water depths, for which the foreshore and vegetation have a relatively high influence.

The relevance of different uncertainties depends on the protection level and associated dike height and strength. For relatively low dikes (i.e., low protection levels, often found in developing countries, return periods below 100 years), vegetation remains stable in design conditions, and has significant added value in reducing wave loads. In the case of higher protection levels (like in the Netherlands, return periods larger than 1000 years), hence for more robust dikes, the effect of the vegetated foreshore reduces to the effect of its geometry only, because of expected stem breakage under these more extreme conditions.

Finally, the long-term effectiveness of nature-based flood defenses has been investigated, compared to conventional coastal engineering solutions. Previous studies have shown that marshes can generally keep pace with sea level rise, but this property of salt marshes has never been quantified in terms of future flood risk. No studies are currently available that compare hybrid solutions and traditional dike heightening in terms of long-term (i.e., ±100 years) effectiveness and life-cycle costs.

Cost-effectiveness of different measures for long-term (i.e., ±100 years) flood risk reduction depends on the ratio between long-term flood risk reduction and life-cycle costs. Benefits are expressed as differences in expected annual damage due to flooding. Several strategies were proposed, each with its own costs for construction and maintenance, and with different initial and future effects on flood risk. The most cost-effective strategy has the lowest total Net Present Value of flood risk and required investments. Expected damage reduction via vegetated foreshores was assessed via the probability of dike failure, which incorporates sea level rise, sediment accretion and wave energy dissipation over the foreshore.

Rising sea levels lead to higher nearshore waves during storms, and subsequently, to increasing probabilities of dike failure by wave overtopping. This study showed that marsh elevation change due to sediment accretion mitigates the increase in wave height, and elongates the lifetime of a dike-foreshore system. The performance of foreshores can be influenced by human interventions, such as foreshore construction via sediment nourishment, or by sheltering structures that enhance sediment accretion.

Cost-effectiveness depends on three main factors: (1) wave energy dissipation, which is lower for salt marshes with a natural elevation in the intertidal zone than for foreshores with artificial elements such as a high zone near the dike, or a detached breakwater; (2) investment costs for foreshore construction and maintenance, where continuous maintenance costs and delayed effects on flood risk make sheltering structures less attractive from a flood risk perspective; (3) economic value of the exposed area, where foreshores are relatively more attractive for protecting areas with low economic value against low costs.

Besides cost-effectiveness, also other factors may affect the site-specific choice for a certain type of flood risk reduction, such as legal boundaries, landscape development, environmental impacts and economic value of other ecosystems services.

Using the methods from this dissertation, hybrid flood defenses can now be assessed according to state-of-the-art safety standards based on failure probabilities. Knowledge from the fields of fluid mechanics, hydraulic engineering, ecology and morphology has been integrated into a modeling framework that couples dike failure calculations to descriptions of physical processes on the foreshore. This research is expected to facilitate more frequent application of vegetated foreshores and similar nature-based solutions, since their effectiveness and life cycle costs can now in a consistent manner be compared to more traditional engineering solutions.

SAMENVATTING

Bescherming van kustgebieden tegen overstromingen wordt van oudsher benaderd vanuit de traditionele waterbouwkunde, waarbij dijken en dammen worden aangelegd om de krachten van getij, stormvloeden en golven te weerstaan. Sinds kort krijgen echter ook natuurlijke oplossingen voor waterveiligheid steeds meer aandacht. Zulke oplossingen benutten de eigenschappen van ecosystemen langs de kust om de impact van extreme weersomstandigheden te beperken. Ecosystemen zoals schorren, mangrovebossen, koraalriffen en duinen worden beschermd, versterkt, of zelfs aangelegd om overstromingsrisico's te laten afnemen. Natuurlijke oplossingen kunnen zelfstandig het water keren, zoals duinen, maar kunnen ook functioneren in combinatie met harde waterkeringen, bijvoorbeeld in de vorm van begroeide voorlanden die de golfbelasting op de achterliggende dijk of dam beperken.

Dit proefschrift focust zich op hybride waterkeringen, waarbij golfbelastingen op een dijk of dam worden verlaagd door de aanwezigheid van een schor voor de dijk, wat daardoor functioneert als begroeid voorland. Er is slechts beperkte kennis beschikbaar over de werking en stabiliteit van begroeide voorlanden tijdens zware stormen. Verder vertonen dergelijke natuurlijke systemen relatief sterke variaties in ruimte en tijd. Beperkte kennis en grote variabiliteit veroorzaken een relatief grote onzekerheid over de mate waarin begroeide voorlanden bijdragen aan waterveiligheid, in vergelijking met harde keringen. De invloed van onzekerheid kan tot uitdrukking worden gebracht via de faalkans van de kering. Het doel van dit proefschrift is het ontwikkelen van methoden waarmee bepaald kan worden hoe en in hoeverre natuurlijke oplossingen overstromingsrisico's kunnen reduceren, rekening houdend met onzekerheden in hun werking en stabiliteit.

Allereerst is onderzoek gedaan naar de invloed van begroeide voorlanden op golfhoogtes, golfoploop en golfoverslagdebieten, met de focus op stormen. Er zijn gedurende een onafgebroken periode van ongeveer 3 jaar (2014-2017) golfmetingen uitgevoerd op schorren in de Westerschelde en kwelders in de Waddenzee, beide gelegen in Nederland. Deze metingen hebben geresulteerd in een dataset, waarin stormen aanwezig zijn met hogere significante golfhoogtes (maximaal 0.85 m) en waterdieptes (maximaal 3.07 m) bij de buitenrand van het schor dan in enig voorgaand veldonderzoek naar golfdemping door schorvegetatie. Er werd een sterke afname van golfhoogtes gemeten tijdens stormen, met meer dan 50% reductie over 300 m schorbreedte, ondanks afgenomen bovengrondse biomassa in de winter.

Het proces van golfenergiedissipatie is onderzocht met behulp van het spectrale golfmodel SWAN. Dit model is in staat om onderscheid te maken tussen verschillende dissipatiemechanismen, zoals golfbreking in ondiep water, golfdemping door staande vegetatie, en bodemwrijving. Modelresultaten toonden dat dissipatie voornamelijk veroorzaakt werd door golfdemping door vegetatie en (in mindere mate) door golfbreking. Waargenomen golfdemping tijdens stormen door *Spartina anglica* (Engels slijkgras) and *Scirpus maritimus* (zeebies) kon het best worden beschreven in SWAN met een gekalibreerde weerstandscoëfficiënt $\widetilde{C}_D$ van ongeveer 0.4.

Het gekalibreerde SWAN-model is vervolgens toegepast in combinatie met de empirische EurOtop formules, om te berekenen hoeveel invloed voorlanden hebben op golfoploop tegen en golfoverslagdebieten over zeedijken. Deze benadering liet zien dat begroeide voorlanden deze golfbelastingen op dijken significant kunnen laten afnemen. Er werden sterke reducties in golfoploop en golfoverslag gevonden, vooral voor situaties met een grote verhouding tussen golfhoogte en waterdiepte op het voorland. Golfdemping door vegetatie heeft de grootste toegevoegde waarde bij waterdieptes waarbij golven nog net niet breken, op voorwaarde dat de vegetatie stabiel blijft onder de golfwerking.

De invloed van schorren op golfoploop werd bevestigd door metingen aan veekrandhoogtes op de buitentaluds van de Waddenzeedijken na stormen. Veekranden zijn afzettingen van drijvend, hoofdzakelijk plantaardig materiaal, en laten zien hoe ver de golven tegen de dijk op zijn gelopen. Tijdens stormen met een terugkeertijd van circa 5 jaar waren de veekrandhoogtes achter de kwelders meer dan 2 meter lager dan bij delen van de dijk achter onbegroeide slikken.

Als tweede is onderzocht hoe stabiel vegetatie is onder golfwerking, om te kunnen voorspellen of vegetatie nog steeds golfdemping kan veroorzaken tijdens stormcondities waarvoor dijken gebruikelijk worden ontworpen. Daartoe is een model ontwikkeld wat een drempelwaarde voor de stabiliteit berekent, die uitgedrukt wordt als de golfbelasting die plantenstengels kunnen weerstaan voordat ze knakken of breken. Dit treedt op als de door golven veroorzaakte buigspanning de buigsterkte van de stengel overschrijdt.

De buigsterkte werd bepaald met behulp van drie-punts buigproeven, die zijn uitgevoerd voor twee algemene soorten schorvegetatie: *Spartina anglica* (Engels slijkgras) and *Scirpus maritimus* (zeebies), voor verschillende stadia binnen hun seizoenscyclus. Het model drukt stabiliteit van de stengel uit in termen van een kritieke orbitaalsnelheid, de door golven veroorzaakte snelheid van waterdeeltjes. Deze kritieke orbitaalsnelheid hangt af van verschillende eigenschappen van de plant: buigsterkte, flexibiliteit, stengeldiameter en -hoogte, en de weerstandscoëfficiënt. Een grotere kritieke orbitaalsnelheid duidt op een grotere stabiliteit van de stengel.

De analytische formule is gekalibreerd en gevalideerd met behulp van informatie over het afbreken van vegetatie op de onderzochte schorren in de Westerschelde (Nederland), en vanuit eerdere laboratoriumexperimenten. De korte, dikke en flexibele stengels van *Spartina* bleken stabieler te zijn dan de lange en stijve stengels van *Scirpus*.

De meeste dijken worden tijdens ontwerpcondities echter verondersteld hoge golven te kunnen keren, waardoor de orbitaalsnelheden bij de bodem de kritieke orbitaalsnelheden van deze twee plantensoorten veelal overschrijden.

Als derde is een methode ontwikkeld voor het bepalen van de faalkans van hybride keringen, rekening houdend met relevante onzekerheden in eigenschappen en gedrag van begroeide voorlanden tijdens extreme stormen. Daartoe zijn diverse modellen geïntegreerd voor het beschrijven van golfvoortplanting over begroeide voorlanden, afbreken van vegetatie en het bezwijken van de dijk. Twee faalmechanismen zijn in beschouwing genomen: bezwijken van de dijk door (i) golfoverslag en (ii) golfklappen op de bekleding van het buitentalud.

Modelresultaten lieten zien dat begroeide voorlanden meer effect hebben op de faalkans door golfklappen op de bekleding dan op de faalkans door golfoverslag. Voor een casestudie in de Nederlandse Waddenzee was bij aanwezigheid van een kwelder de benodigde kruinhoogte van de dijk 0.5 m lager, vergeleken met een situatie waarbij kale slikken op gemiddeld zeeniveau voor de dijk liggen. Faalkansen van gras- en asfaltbekledingen vertoonden een sterkere reductie, met een factor 100 of meer. De reden voor dat verschil is dat golven gewoonlijk schade veroorzaken aan bekledingen bij relatief lage waterstanden, waarbij het hooggelegen voorland en de kweldervegetatie een sterkere invloed hebben dan bij omstandigheden waarbij golfoverslag optreedt.

De relevantie van verschillende onzekerheden hangt af van het beschermingsniveau, en de daaraan gerelateerde dijkhoogte en -sterkte. Voor relatief lage dijken (dat wil zeggen, lage beschermingsniveaus, zoals vaak van toepassing in ontwikkelingslanden, met terugkeertijden van minder dan 100 jaar) blijft vegetatie stabiel tijdens ontwerpcondities, en heeft het aanzienlijke toegevoegde waarde voor het reduceren van golfbelastingen op de achterliggende kering. In het geval van hogere beschermingsniveaus (zoals in Nederland, met terugkeertijden van meer dan 1000 jaar), en daarmee voor robuustere dijken, reduceert de invloed van begroeide voorlanden tot enkel het effect van de kwelderbodem, vanwege het verwachte afbreken van vrijwel alle schorvegetatie onder de zwaardere maatgevende omstandigheden.

Tenslotte is ook onderzoek gedaan naar de lange-termijn effectiviteit van natuurlijke oplossingen voor waterveiligheid, in vergelijking met conventionele harde keringen. Eerdere studies hebben laten zien dat schorren veelal kunnen meegroeien met zeespiegelstijging door sedimentinvang, maar dit vermogen van schorren is nooit vertaald naar toekomstige invloed op overstromingsrisico's. Er zijn momenteel geen studies beschikbaar die een vergelijking maken tussen hybride keringen en traditionele dijkverhoging in termen van effectiviteit op lange termijn ($\pm$100 jaar) en kosteneffectiviteit over de levenscyclus.

Kosteneffectiviteit van verschillende maatregelen hangt af van de verhouding tussen de reductie van het overstromingsrisico en kosten over de levenscyclus. Baten worden uitgedrukt als verschillen in de op jaarbasis verwachte schade door overstromingen.

Er zijn verschillende strategieën onderzocht in dit proefschrift, elk met zijn karakteristieke kostenprofiel voor aanleg en onderhoud, en met zijn huidige en toekomstige effect op het overstromingsrisico. De meest kosteneffectieve strategie leidt tot de laagste totale netto contante waarde van het overstromingsrisico en de vereiste investeringskosten. Reductie van verwachte schade via begroeide voorlanden is bepaald op basis van de faalkans van de kering, waarin zeespiegelstijging, meegroeien van het voorland door sedimentatie en golfdemping over het voorland zijn verdisconteerd.

Een stijgende zeespiegel leidt tot hogere golven tijdens stormen, en vervolgens tot toenemende kansen op falen van de dijk door golfoverslag. Dit onderzoek heeft aangetoond dat het meegroeien van het schor door sedimentatie voorkomt dat de golfaanval op de dijk toeneemt, waardoor de levensduur van de hybride kering wordt verlengd. De prestaties van voorlanden kunnen worden beïnvloed door menselijke ingrepen, zoals het aanleggen van een voorland via een sedimentsuppletie, of via kwelderwerken die sedimentatie bevorderen.

Kosteneffectiviteit hangt af van drie belangrijke factoren: (1) de sterkte van de golfenergiedissipatie, die lager is voor schorren met een natuurlijke bodemhoogte in het intergetijdegebied dan voor voorlanden met kunstmatige elementen zoals een dam of een hoge zone direct voor de dijk; (2) investeringskosten voor aanleg en onderhoud, die hoog zijn voor kwelderwerken door voortdurend onderhoud, en niet opwegen tegen de vertraagde effecten op veiligheid; (3) economische waarde van het beschermde gebied, waarbij oplossingen met een voorland aantrekkelijker zijn in het geval van lage economische waarde.

Behalve kosteneffectiviteit kunnen ook andere factoren de locatiespecifieke keuze voor een bepaalde strategie beïnvloeden, zoals wet- en regelgeving, inpassing in het landschap, effecten op het grootschalige natuurlijke systeem, en waardering voor aanvullende ecosysteemdiensten die begroeide voorlanden te bieden hebben.

Door gebruik te maken van de methoden uit dit proefschrift kunnen hybride keringen nu worden beoordeeld volgens state-of-the-art veiligheidsnormen, gebaseerd op faalkansen. Kennis van de vakgebieden van vloeistofmechanica, waterbouwkunde, ecologie en morfologie is geïntegreerd in een raamwerk, waarin een koppeling is aangebracht tussen berekeningen van faalmechanismen van dijken en fysische processen op het voorland. Naar verwachting zal dit onderzoek bijdragen aan het vaker toepassen van begroeide voorlanden en vergelijkbare natuurlijke oplossingen voor waterveiligheid, omdat hun effectiviteit en kosten over de levenscyclus nu rechtstreeks kunnen worden vergeleken met traditionele waterbouwkundige constructies.

CONTENTS

1

INTRODUCTION

1.1. BACKGROUND

Throughout history, coastal areas have always attracted communities and settlements, because of possibilities for agriculture, fishery, industry, shipping and availability of well-sorted sand and gravel. The current population density in low-lying coastal zones is more than five times higher than the global mean, and there is an ongoing trend of coastal migration (Neumann et al., 2015). At the same time, low-lying coastal areas are particularly vulnerable to the impact of coastal hazards such as hurricanes, tsunamis, storm surges and wind waves. Furthermore, deltas are prone to hazards coming from multiple sides: from the sea, the river, and by intense rainfall.

Flood risk is generally defined as the product of the probability and consequences of flooding, and can be interpreted as the expected annual economic loss due to flooding. Consequences of coastal flooding are steadily increasing due to the ongoing economic and demographic development (Mendelsohn et al., 2012), and because of land subsidence (Syvitski et al., 2009). At the same time, the annual probability of flooding is expected to get higher due to climate-changed induced sea level rise (Nicholls and Cazenave, 2010), increasing storminess and rainfall intensification (Scaife et al., 2012). Interventions are evidently required to prevent a rapid increase of flood risks in coastal areas.

Traditionally, flood risk reduction in coastal areas is approached from a conventional engineering perspective, in which dikes and dams are built to withstand the forces of tides, surges and waves. Such structures should be regularly heightened and strengthened because of settlement, degradation of materials and sea level rise. Further, hard structures such as dikes and dams can induce negative effects on tidal flows, sediment fluxes, fish migration and ecosystem survival (Van Wesenbeeck et al., 2014). In this perspective, a nature-based approach to flood risk reduction is increasingly promoted, since

this strategy is supposed to be more sustainable, cost-effective and ecologically sound than conventional coastal engineering (Temmerman et al., 2013). At the same time, coastal ecosystems provide additional ecosystem services, such as providing habitats for fish and other wildlife, recreation, carbon sequestration, water purification and erosion control (Barbier et al., 2011).

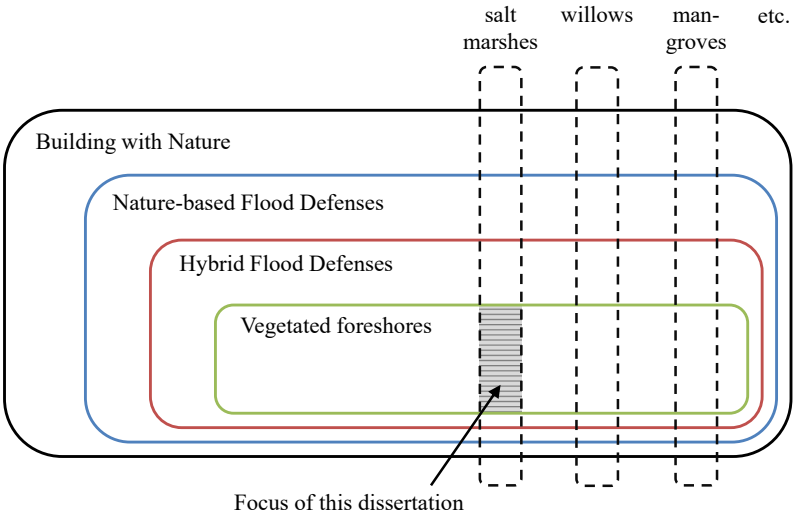

Figure 1.1: *Relations between key terms, used in this dissertation, in which the focus is on salt marshes, functioning as vegetated foreshores (shaded area).*

Nature-based flood defenses are based on the principles of Building with Nature (Fig. 1.1), in which society's infrastructural demands are met by starting from the functioning of the natural and societal systems in which this infrastructure is to be realized De Vriend et al. (2015). Nature-based flood defenses use natural dynamics and ecosystem services to reduce flood risk. Ecosystems such as salt marshes, mangrove forests, coral reefs and sand dunes are preserved, enhanced or even created, in order to protect the coastal zone from flooding. Nature-based flood defenses can work standalone, like sand dunes, but can also function in combination with engineered defenses. For example, in the form of vegetated foreshores that reduce the wave loads on dikes or dams (Borsje et al., 2011). A combination of an engineered hard structure and a vegetated foreshore is defined as a hybrid flood defense (Fig. 1.1). Various related terms are used in the literature, such as 'ecosystem-based coastal defenses' (Jones et al., 2012; Temmerman et al., 2013), 'ecological engineering' as an overarching term, and 'living shorelines' to indicate small-scale combinations of vegetation and hard structures (Davis et al., 2015).

Although many principles are generically applicable to nature-based flood defenses, the focus in this dissertation is on salt marshes, functioning as vegetated foreshores in

hybrid flood defenses (Fig. 1.1). Salt marshes are found at middle to high latitudes, while mangrove forests are abundant in tropical and subtropical environments where minimum sea surface temperatures are above 16 degrees Celsius (Fig. 1.2).

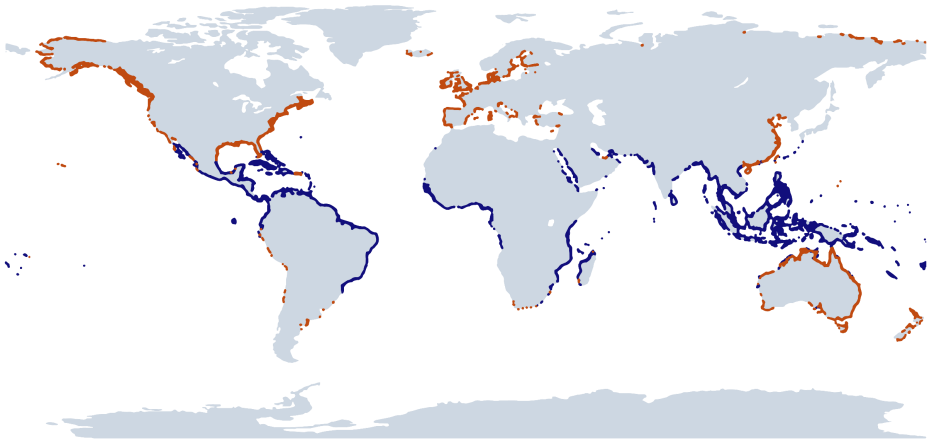

Figure 1.2: *Presence of coastal ecosystems at different latitudes. Sources: McOwen et al. (2017) (salt marshes, red), Giri et al. (2011) (mangroves, blue).*

Salt marshes are coastal ecosystems in the upper intertidal zone between land and water, regularly flooded by tides and surges[1]. They are covered with dense stands of salt-tolerant plants (so-called halophytes), such as herbs and grasses. These marshes are present worldwide, particularly in estuaries and barrier coasts in middle to high latitudes (Fig. 1.2), although threatened because of sediment starvation (Adam, 2002; Willemsen et al., 2016), land reclamation (Zhao et al., 2004), deforestation (Bradshaw et al., 2007) and eutrophication (Deegan et al., 2012). This has resulted in a global loss rate of 1-3% of total area per year (Duarte et al., 2013).

Salt marshes can exist in areas that roughly comply with two criteria. Firstly, mean hydrodynamic forcing by waves and currents should be limited, to enable sedimentation and vegetation establishment. Secondly, sediment concentrations should be high enough, to facilitate the raise of the salt marsh surface during high tides and storm surges (Davidson-Arnott et al., 2002). Vegetation plays a key role in the development of salt marshes. The presence of canopies accelerates sedimentation by reducing wave- and current-induced shear stresses on the bed material. Additionally, belowground root systems stabilize accumulated sediments and amplify the process of subsoil drainage, consolidation and compaction (Deegan et al., 2012). Salt marshes and the neighboring in-

[1] Part of this description is based on the author's original contribution to a book chapter: B.W. Borsje, S. de Vries, S.K.H. Janssen, A.P. Luijendijk, and V. Vuik (2017). Building with Nature as Coastal Protection Strategy in the Netherlands. In Living Shorelines: The Science and Management of Nature-Based Coastal Protection (1st ed., pp. 137–155). CRC Press.

tertidal flats form a coherent system with many mutual dependencies (Balke et al., 2016; Bouma et al., 2016).

Vegetation requires a certain time span for seedling establishment, during which disturbance is low or absent. Such periods, characterized by mild wave conditions and limited flow velocities, are often referred to as windows of opportunity (Balke et al., 2011). A distinction can be made between salt marshes that have developed in areas where windows of opportunity occur by nature, and salt marshes that can only persist due to artificial sheltering from waves and currents. An example of the latter can be found along the Dutch, German and Danish Wadden Sea coast, where an extensive system of earthen dams, brushwood dams (Fig. 1.3) and drainage channels has led to the presence of 3000 hectare of salt marsh habitat (Fig. 1.4). Starting from the 18th century, this technique was aimed at land reclamation, but nowadays, it is applied for nature conservation purposes (Bakker et al., 2002).

Figure 1.3: *Brushwood dams to create artificial shelter of salt marsh vegetation from waves and currents. The dike is visible in the background (Photo: V. Vuik).*

The benefits that ecosystems offer to humankind are known as ecosystem services. The most frequently quoted ecosystem services of salt marshes are wave attenuation, shoreline stabilization, nutrient removal, carbon sequestration, fisheries and recreation (Deegan et al., 2012; Temmerman et al., 2013). Salt marshes act as buffer zone against natural hazards such as floods, cyclones, tidal surges and storms, by reducing storm waves and storm surges (King and Lester, 1995; Wamsley et al., 2010; Gedan et al., 2011). Additionally, they protect shorelines from erosion by buffering wave action and trapping sediments (Shepard et al., 2011).

Figure 1.4: *Extensive salt marshes along the Dutch Wadden Sea coast, with the Wadden Sea and salt marshes on the right hand side, and the mainland on the left hand side of the dike (Photo: https://beeldbank.rws.nl, Rijkswaterstaat).*

1.2. FIELD EVIDENCE FOR WAVE LOAD REDUCTION

Before summarizing the knowledge gaps that are addressed in this study (Section 1.3), the current section first provides some clear evidence on the sheltering functioning of salt marshes during severe storms. Within the project, waves were measured on salt marshes before, during and after two storms (return period approximately 5 years). The field site is located at a wave-exposed marsh in the Dutch Wadden Sea, along the Emmapolder dike, 10 km west of the village Eemshaven in the Netherlands (Fig. 1.5). This marsh is 'man-made', as marsh development has been promoted by facilitating sedimentation, soil drainage and vegetation establishment since 1930s (Bakker et al., 2002). The site is characterized by a spatially homogeneous dike orientation and thereby homogeneous wind exposure, but a short-distance spatial gradient in front of the dike, from mature salt marsh to bare mudflat (Fig. 1.4).

Wave gauges (Ocean Sensor Systems, Inc., USA) were deployed at several locations on the salt marsh, to investigate spatial differences in wave characteristics. In January 2015, 8 wave gauges were deployed in total: 5 sensors in a transect over the salt marsh, perpendicular to the dike, and 3 additional sensors to measure spatial differences in wave loads on the dike (Fig. 1.6). In January 2017, a second severe storm occurred. The

Parts of this section were published in Zhu, Z., Vuik, V., ... and Bouma, T.J. (2019). Historic storms reveal overlooked value of saltmarshes for nature-based flood protection. (in review)

Figure 1.5: *Location of the field site in the Wadden Sea (blue marker) along the dike (red line). Bathymetry: echo soundings Rijkswaterstaat. Satellite image: Google Earth.*

set-up of the experiment was slightly altered by that time (Fig. 1.7), with 4 sensors in the same transect over the salt marsh, two sensors to measure wave propagation over the neighboring bare mudflat, and one sensor between both transects, close to the dike on the pioneer marsh.

Both storms produced higher incoming waves than ever reported in any previous field study on wave attenuation by marsh plants. High wave attenuation rates over 50% per 300 m of marsh width were recorded at a water depth of nearly 2 m above the highest part of the salt marsh (Figs. 1.6 and 1.7), even despite reduced standing vegetation biomass due to winter decay, and due to sheep grazing in 2017. In contrast, wave attenuation along the adjacent cross-shore transect of bare mudflat was only 18% over 300 m during the 2017 storm (Fig. 1.7).

As a result of wave dissipation by the marsh, wave run-up height, indicated by the flotsam position on the dike (Fig. 1.8), was found to be more than 2 m lower behind the salt marshes, compared to the dike behind the bare mudflats (Figs. 1.6 and 1.7). Lowered wave run-up reduces the risks of wave overtopping and dike breaching. Additionally, RTK-GPS measurements of bed level changes revealed that the presence of saltmarsh vegetation increased soil stability during the storm. No significant bed level changes were found on the salt marsh, against 2-3 centimeters erosion in a single storm on the bare mudflats (Fig. 1.7).

The same patterns were found at this dike after an even more severe storm of 8-9 November 2007, with a return period of the water level of approximately 20-30 years (Fig. 1.9). These findings suggest that, with a marsh foreshore of 300 m wide, the dike crest could be 2 m lower when supposed to defend against a storm with similar surge and waves as the 2007 and 2017 storms.

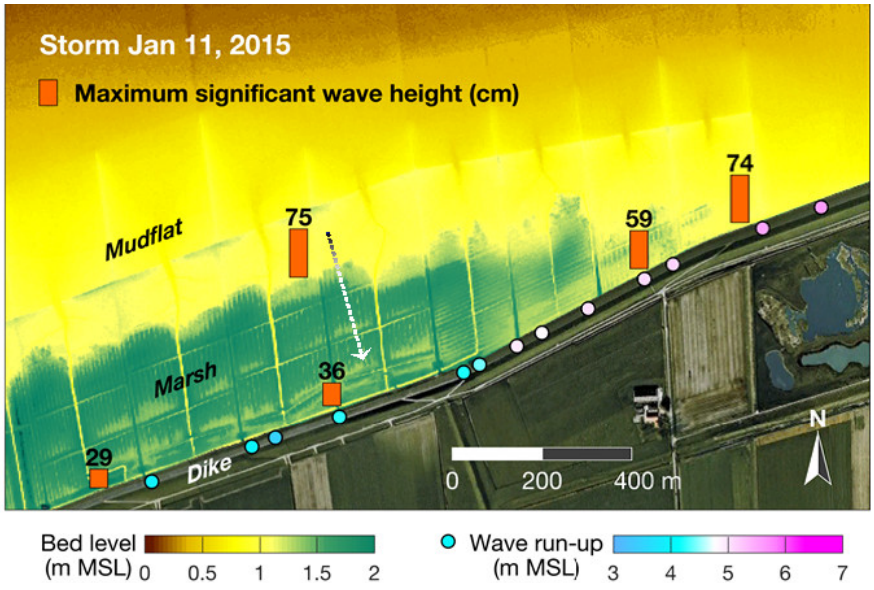

Figure 1.6: *Reduction of significant wave height and wave run-up level for the storm of 11 Jan. 2015, with a maximum still water level of 3.2 m MSL.*

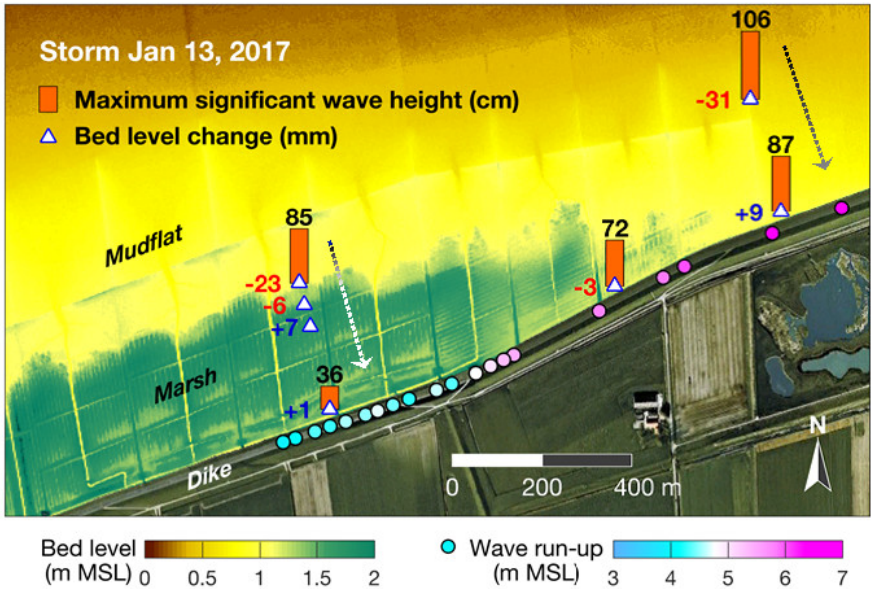

Figure 1.7: *Reduction of significant wave height and wave run-up level for the storm of 13 Jan. 2017, with a maximum still water level of 3.4 m MSL. Bed level changes caused by the storm are shown at the triangles.*

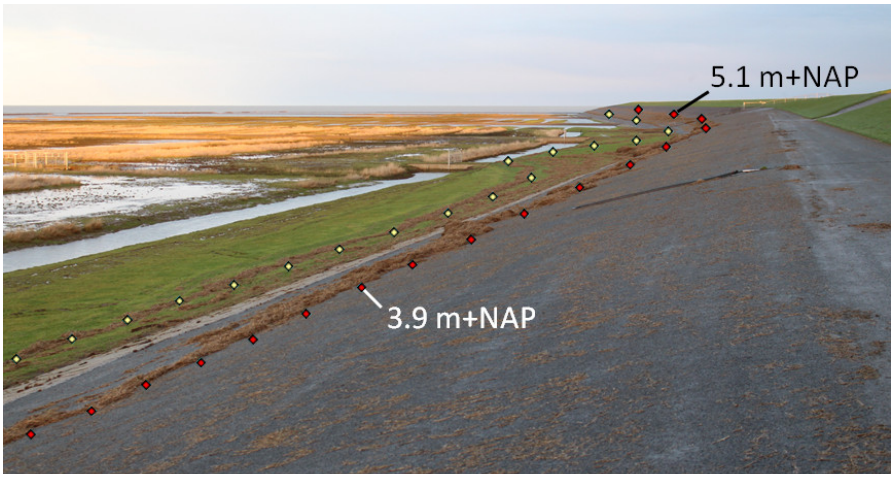

Figure 1.8: *An increase in flotsam level after the storm of January 2015, at the transition from salt marshes to bare mudflats (Photo: V. Vuik). NAP is the Dutch ordnance level, close to Mean Sea Level.*

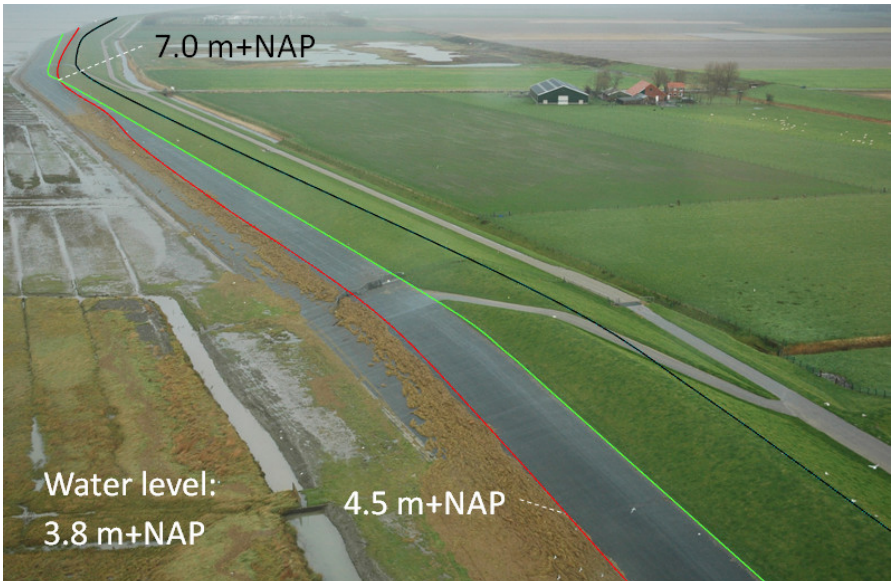

Figure 1.9: *Aerial photo after the storm of 8-9 November 2007 in the Wadden Sea, showing the flotsam line on the dike at the transition from salt marshes to bare mudflats (Photo: Waterboard Noorderzijlvest). The green line indicates the transition from asphalt to grass cover on the dike slope, at approximately 7 m+NAP. The red line highlights the maximum elevation of the flotsam line. NAP is the Dutch ordnance level, close to Mean Sea Level.*

1.3. KNOWLEDGE GAPS

The following knowledge gaps are addressed in this dissertation, related to flood protection via vegetated foreshores:

1. Although flood risk reduction by vegetated foreshores is often mentioned in the recent literature (Gedan et al., 2011; Temmerman et al., 2013), studies quantifying their functioning during storms are still scarce. Many studies describe wave attenuation by vegetation, but mostly for situations with a small water depth and low waves (Anderson et al., 2011). Therefore, there is a need for quantification of wave energy dissipation by vegetated foreshores during severe storms, and implications for wave loads on coastal dikes.

2. Furthermore, dikes are often built to withstand wave forces far beyond the range of measured conditions. Previous studies have speculated that marshes could lose their wave damping effect above a certain water depth (Möller et al., 1999). Calibration and validation of numerical models is needed, preferentially based on wave measurements during storm conditions. Furthermore, vegetation can disappear due to stem breakage or uprooting if wave-induced forces exceed a certain threshold (Liffen et al., 2013). Currently, no method is available that predicts the wave load that plant stems can withstand before they break or fold. This hampers implementation of vegetation into coastal protection schemes.

3. Another factor that complicates the application of nature-based flood defenses is the relatively high degree of uncertainty compared to engineered defenses, which is related to their inherently dynamic character. It is not well-known how to quantify, integrate and reduce the various uncertainties, and how to assess their overall effect on flood risk. Failure of dikes and levees can be caused by various failure mechanisms, from which erosion of the crest and inner slope due to overflow or wave overtopping is the most common mechanism (Danka and Zhang, 2015). For each failure mechanism, a probability of failure can be calculated, which is the probability that the hydraulic load (e.g., wave overtopping discharge) exceeds the dike strength (e.g., overtopping resistance of the grass cover). Probabilistic methods have frequently been applied for computing failure probabilities for traditional dikes (Vrijling, 2001). In contrast, no methods are currently available to assess the failure probability of hybrid flood defenses, thereby incorporating relevant uncertainties in the characteristics and performance of the vegetated foreshore during extreme storms. Consequently, it is difficult to compare flood risk reduction by hybrid flood defenses versus traditional engineering solutions.

4. Finally, nature-based flood defenses are often claimed to be more sustainable, cost-effective and ecologically sound, compared to conventional coastal engineering (Temmerman et al., 2013). Previous studies have shown that marshes can generally keep pace with sea level rise (Kirwan et al., 2016) because of sediment ac-

cretion (Temmerman et al., 2003; Mckee et al., 2007) and sub-surface expansion due to root growth (Nyman et al., 2006). However, this property of salt marshes has never been quantified in terms of future flood risk. No studies are currently available that compare hybrid solutions and traditional dike heightening in terms of long-term (i.e., ±100 years) effectiveness and life-cycle costs.

1.4. AIM OF THIS DISSERTATION

The aim of this dissertation is to develop new methods to assess how and how much nature-based flood defenses can reduce flood risks, taking into account uncertainties in their functioning and stability. The focus is on the case of hybrid flood defenses that combine hard structures, such as dikes and dams, with salt marshes functioning as vegetated foreshores.

Four research questions (RQ) are formulated, addressing the knowledge gaps described in Section 1.3:

RQ1. What is the influence of vegetated foreshores on wave run-up and wave overtopping?

RQ2. Until what threshold can plant stems withstand wave-induced forces before they fold or break?

RQ3. How to assess the failure probability of a dike, accompanied by a vegetated foreshore?

RQ4. What is the long-term effectiveness of salt marshes in reducing flood risk, in comparison to conventional dike strengthening?

1.5. APPROACH AND METHODS

The influence of vegetated foreshores on wave run-up and wave overtopping was investigated via a combination of field measurements, numerical modeling and empirical formulas. Field measurements were carried out at two salt marshes in the Western Scheldt estuary in the Netherlands, in order to obtain insights in wave energy dissipation on salt marshes for storm conditions with large waves and high water depths. These field measurements were used to calibrate and validate a SWAN wave model. The calibrated model was subsequently applied to predict wave attenuation over bare and vegetated foreshores under design conditions for dikes bordering the Western Scheldt. Wave conditions were translated into wave run-up height and wave overtopping discharge (Fig. 1.10) by application of the empirical EurOtop formulas (RQ1).

For determining a threshold for wave-induced stem breakage, a combination of field measurements and laboratory tests was deployed. Field measurements of vegetation characteristics and wave attenuation by vegetation were used to study seasonal variation

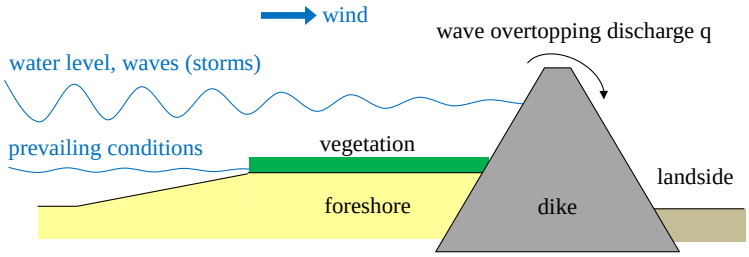

Figure 1.10: *Schematic representation of a dike-foreshore configuration (not to scale).*

in stem density (i.e., number of stems per square meter). In the laboratory, three-point-bending tests were applied to determine mechanical properties of the vegetation, such as modulus of elasticity and flexural strength. Based on plant characteristics, an analytical expression for a critical wave orbital velocity was derived. Plants stems are assumed to break if the wave orbital velocity exceeds this critical value. The analytical formula was calibrated and validated, using information about stem breakage from the field and earlier laboratory tests of Rupprecht et al. (2017) (RQ2).

A failure probability of a hybrid flood defense, consisting of a dike with vegetated foreshore, was calculated by coupling models for wave energy dissipation, stem breakage and dike failure. Probability distributions were defined for all relevant parameters, as well as correlations between parameters. Distributions and correlations were based on various data sources from the literature, combined with new measurements in the field and the laboratory. A probabilistic method was applied for running the integrated model, iteratively fed with input from all probability distributions. This resulted in a calculated probability of failure due to (1) wave overtopping and (2) wave impact on the outer slope, and insights regarding the relative importance of various uncertainties for the reliability of the system, specifically applied to a situation in the Wadden Sea, the Netherlands (RQ3).

Finally, long-term (i.e., 100 years) reliability of dike-foreshore configurations was investigated, considering sea level rise, sediment accretion, lateral marsh dynamics, probability of failure and life-cycle costs. Several human interventions were proposed, aiming to increase effectiveness of foreshores against low costs. Unit costs for construction and maintenance were collected, in order to compare traditional dike heightening with hybrid flood defenses (RQ4).

1

1.6. OUTLINE OF THE DISSERTATION

This dissertation is organized as follows:

- Chapter 2 describes wave attenuation by salt marsh vegetation, which is analyzed by wave measurements on salt marshes during severe storms and numerical modeling of wave propagation (RQ1).
- Chapter 3 deals with an upper limit on wave attenuation by vegetation, which is reached when wave loads exceed the flexural strength of the vegetation. A model is developed that predicts at what wave conditions vegetation will fold and break (RQ2).
- Chapter 4 demonstrates how a failure probability of a dike-foreshore system can be calculated, by incorporating uncertainties in hydraulic loads, dike strength and foreshore characteristics, integrating knowledge from the chapters 2 and 3 (RQ3).
- Chapter 5 compares traditional dike heightening with foreshore construction, considering long-term development under sea level rise, required maintenance and life-cycle costs (RQ4).
- Chapter 6 summarizes the main conclusions of this dissertation, and contains recommendations for future applications and research.

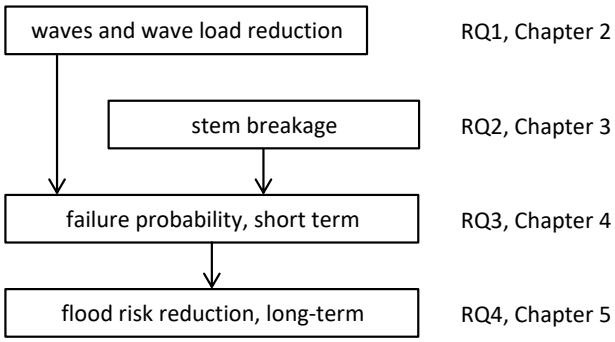

Figure 1.11: *Interaction between the main components, research questions (RQ) and chapters in this dissertation.*

1.7. EMBEDDING IN THE BE SAFE PROJECT

This research is part of the BE SAFE project, which stands for Bio-Engineering for Safety. This project focuses on flood risk reduction, using vegetated foreshores, by developing and integrating models and knowledge from the fields of hydraulic engineering, biogeomorphology and ecology. The BE SAFE project consists of four different subprojects at various research institutes in the Netherlands:

1. The Ecology subproject focuses on understanding thresholds driving long-term dynamics of salt marshes, and investigates trade-offs between benefits for coastal protection and other ecosystem services (NIOZ, Yerseke).

2. The Biogeomorphology subproject investigates long-term biogeomorphological dynamics for vegetated foreshores, focusing on interactions between vegetation and sediment dynamics (University of Twente, Enschede).

3. The Governance subproject analyzes how institutional arrangements affect the design, implementation and management of Building with Nature solutions (Delft University of Technology, Faculty of Technology, Policy and Management).

4. The Safety subproject considers vegetated foreshores from the perspective of the flood defense, by performing probabilistic analyses of dike-foreshore configurations (Delft University of Technology, Faculty of Civil Engineering). The result of this specific subproject is summarized in this dissertation.

Collaboration between the Safety subproject and the Ecology subproject has led to the field and laboratory data which was used in the Chapters 2, 3 and 4. Chapter 5 integrates knowledge from the Ecology and Biogeomorphology subprojects. Results from Chapter 5 can be used for research on the implementation of vegetated foreshores in the Governance subproject.

2

WAVE LOAD REDUCTION BY VEGETATED FORESHORES

ABSTRACT

This chapter analyzes the effect of vegetation on wave damping under severe storm conditions, based on a combination of field measurements and numerical modeling. The field measurements of wave attenuation by vegetation were performed on two salt marshes with two representative but contrasting coastal wetland vegetation types: cordgrass (*Spartina anglica*) and grassweed (*Scirpus maritimus*). The former is found in salty environments, whereas the latter is found in brackish environments. The measurements have added to the range with the highest water depths and wave heights presented in the literature so far. A numerical wave model (SWAN) has been calibrated and validated using the new field data. It appeared that the model was well capable of reproducing the observed decay in wave height over the salt marsh. The model has been applied to compute the reduction of the incident wave height on a dike for various realistic foreshore configurations and hydraulic loading conditions. Additionally, the efficiency of vegetated foreshores in reducing wave loads on the dike has been investigated, where wave loads were quantified using a computed wave run-up height and wave overtopping discharge. The outcomes show that vegetated foreshores reduce wave loads on coastal dikes significantly, also for the large inundation depths that occur during storms and with the vegetation being in winter state. The effect of the foreshore on the wave loads varies with wave height to water depth ratio on the foreshore. The presence of vegetation on the foreshore extends the range of water depths for which a foreshore can be

This chapter has been published as: Vuik, V., Jonkman, S. N., Borsje, B. W., & Suzuki, T. (2016). Nature-based flood protection: The efficiency of vegetated foreshores for reducing wave loads on coastal dikes. *Coastal Engineering*, **116**, 42–56.

applied for effective reduction of wave loads, and prevents intense wave breaking on the foreshore to occur. This research demonstrates that vegetated foreshores can be considered as a promising supplement to conventional engineering methods for dike reinforcement.

2.1. INTRODUCTION

Integration of ecosystems in coastal protection schemes is increasingly mentioned as a valuable supplement to conventional engineering methods (Jones et al., 2012; Temmerman et al., 2013; Van Wesenbeeck et al., 2014). Coastal ecosystems like sand dunes can fulfill the same function as man-made flood defenses, such as dikes and dams. Other ecosystem types, such as salt marshes (King and Lester, 1995; Möller et al., 1999; Möller and Spencer, 2002; Möller, 2006; Arkema et al., 2013), intertidal flats and mangrove forests (Mazda et al., 2006; Quartel et al., 2007; Horstman et al., 2014) can potentially be used as foreshore protection to reduce the impact of storm surges and wind waves on the flood defenses (Borsje et al., 2011; Gedan et al., 2011; Sutton-Grier et al., 2015). This study focuses on the latter ecosystem types: vegetated foreshores in front of coastal dikes (Fig. 2.1), since this system has only received limited attention in the literature, despite of the potential of these ecosystems to directly affect the flood risk in the area behind the flood defense.

A vegetated foreshore consists of a sediment body, covered with vegetation, in front of a dike. Surface waves, propagating from deep water towards a coastal dike, can significantly lose energy when a vegetated foreshore is present, due to depth-induced wave breaking, bottom friction and wave attenuation by vegetation. Wave run-up on the outer slope of coastal dikes is governed by the incident wave height and wave period. When the wave run-up exceeds the crest height of the dike, wave overtopping over the dike occurs. This might ultimately lead to erosion of the inner slope and breaching of the dike. Both wave run-up and wave overtopping discharge directly depend on the incoming wave height, which means that the presence of a vegetated foreshore influences the likelihood of dike breaching due to wave overtopping.

The first process that leads to wave energy reduction on vegetated foreshores is depth-induced wave breaking (Battjes and Janssen, 1978; Duncan, 1983) on the shallow foreshore in front of the dike. The maximum possible wave height depends primarily on the water depth. The ratio between both is the dimensionless breaker parameter. Several studies explain how the breaker parameter can vary due to differences in offshore wave steepness (Battjes and Stive, 1985; Nairn, 1990), bottom slope (Nelson, 1994) or wave length to water depth ratio (Ruessink et al., 2003). For a (nearly) horizontal bottom, the height of individual waves in a naturally occurring random wave train is at maximum 55 percent of the water depth (Massel, 1996; Nelson, 1994). On steep slopes, higher values can be found.

Additionally, wave energy can be dissipated by bottom friction on shallow foreshores with a surface covered with for instance vegetation, shells or sand ripples. Padilla-

(a) Westkapelle, sandy foreshore, North Sea. Foreshore elevation 4.0 m+NAP, 1:40 slope. Dike height 12.6 m+NAP, 1:6 slope. Design conditions: h = 4.9 m+NAP, H_{m0} = 4.6 m, $T_{m-1,0}$ = 9 s.

(b) Hellegat, salt marsh, Western Scheldt. Marsh elevation 3.0 m+NAP, width 200 m, slope 1:40. Dike height 9.5 m+NAP, slope 1:4. Design conditions: h = 6.0 m+NAP, H_{m0} = 1.9 m, $T_{m-1,0}$ = 5 s.

(c) Groningen, salt marsh, Wadden Sea. Marsh elevation 2.0 m+NAP, width 800 m, slope 1:750. Dike height 9.1 m+NAP, slope 1:4. Design conditions: h = 5.3 m+NAP, H_{m0} = 1.8 m, $T_{m-1,0}$ = 5 s.

(d) Texel, salt marsh Schorren, Wadden Sea. Marsh elevation 1.8 m+NAP, width 400 m, slope 1:250. Dike height 6.9 m+NAP, slope 1:3. Design conditions: h = 4.4 m+NAP, H_{m0} = 1.4 m, $T_{m-1,0}$ = 5 s.

Figure 2.1: *Examples of foreshores in the Netherlands and their characteristics: sandy foreshore near Westkapelle sea defence, bordering the North Sea (upper left), natural salt marsh Hellegatpolder in the Western Scheldt (upper right), man-made salt marsh along the Wadden Sea dikes of Groningen province (lower left), salt marsh Schorren at the Wadden Sea side of the barrier island Texel, with marsh edge protection (lower right). Source: https://beeldbank.rws.nl, Rijkswaterstaat. The numbers in this figure will be explained and used in Section 2.2.*

Hernández and Monbaliu (2001) have compared the capability of different bottom friction formulations in reproducing wave measurements in shallow water conditions, and argue that formulations for dissipation by bottom friction, like the models by Madsen et al. (1988) or Weber (1989), which explicitly take physical parameters for bottom roughness into account, should be preferred in wave modeling in shallow water areas.

And third, surface waves propagating through vegetation fields lose energy when they perform work on vegetation stems, branches and leaves (Dalrymple et al., 1984). This results in a decrease in wave height. Understanding wave attenuation by vegeta-

tion is crucial for determining the efficiency of vegetated foreshores in reducing wave loads on coastal dikes. Therefore, as part of this research, an inventory has been made of available studies that give insight in wave attenuation by vegetation (Fig. 2.2)[1]. Most of these studies are based on field or laboratory experiments with water depths of below one meter and/or wave heights of typically 10 to 30 centimeters.

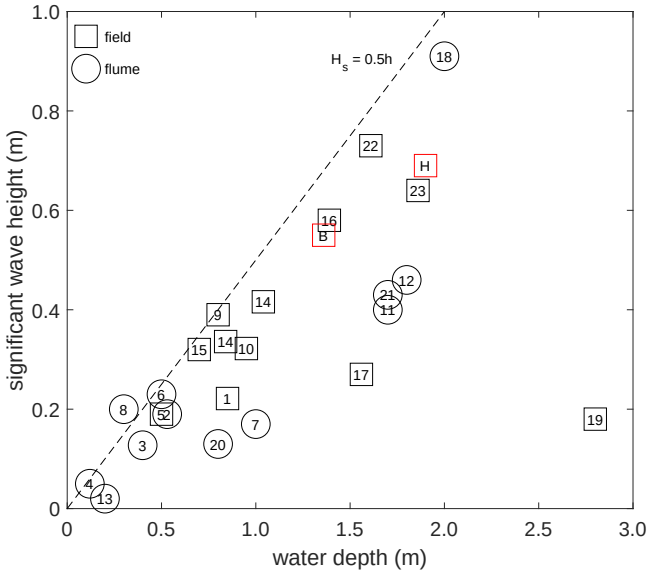

Figure 2.2: *Overview of maximum water depth and significant wave height, reported in previous studies with measurements of wave attenuation by vegetation. For regular waves, the plot position is determined by a computed equivalent significant wave height, using $H_s = 1.41H$. The dotted line roughly indicates depth-limitation due to breaking. Studies included: see Table 2.1. The letters H and B belong to the field measurements described in the current study at the salt marshes Hellegat and Bath, respectively (Section 2.2).*

Wave attenuation does not only depend on vegetation properties like vegetation height, stem diameter and spacing, but also on hydraulic characteristics such as the wave height, the water depth (Möller et al., 1999, 2014) and ambient currents (Hu et al., 2014). Therefore, wave attenuation rates measured in moderate conditions cannot be applied directly to severe storm conditions, and physical or semi-empirical modeling approaches are required for estimating the wave damping capacity of vegetated foreshores under these more extreme circumstances.

[1] This figure contains the original numbers, published in *Coastal Engineering* in 2016. After continuation of the measurement campaign, higher waves were observed, up to 0.85 m at a water depth of 2.16 m at Hellegat, and up to 0.69 m at a water depth of 1.73 m at Bath.

Table 2.1: *Studies included in Fig. 2.2, their characteristics, maximum water depth and maximum regular or significant wave height. Numbers indicated with an asterisk (*) are based on estimation.*

Nr.	Publication	Characteristics	max h	max H	max H_s
1	Allen et al. (2008)	Field, bulrush	0.85		0.22*
2	Anderson and Smith (2014)	Flume, synthetic plants	0.53		0.19
3	Augustin et al. (2009)	Flume, wooden pens & polyethylene	0.40	0.09	
4	Bouma et al. (2005)	Flume, *Spartina anglica* & *Zostera noltii*	0.12	0.05	
5	Cooper (2005)	Field, salt marsh species	0.50		0.19
6	Coops et al. (1996)	Artificial wave basin, *Phragmites* & *Scirpus*	0.50	0.23	
7	Dubi and Torum (1996)	Flume, synthetic plants	1.00		0.17
8	Fonseca and Cahalan (1992)	Flume, 4 plant species	0.30	0.20	
9	Jadhav and Chen (2013)	Field, *Spartina alterniflora*	0.80		0.39
10	Knutson et al. (1982)	Field, *Spartina alterniflora*	0.95		0.32*
11	Koftis et al. (2013)	Flume, polypropylene stripes	1.70		0.40
12	Manca et al. (2012)	Flume, polypropylene stripes	1.80		0.46
13	Mei et al. (2011)	Flume, perspex cylinders	0.20	0.02	
14	Möller and Spencer (2002)	Field, salt marsh species	1.04		0.42*
15	Möller (2006)	Field, salt marsh species	0.70		0.32
16	Möller et al. (1999)	Field, salt marsh species	1.39		0.58
17	Möller et al. (2011)	Field, *Phragmites australis*	1.56		0.27
18	Möller et al. (2014)	Flume, 3 salt marsh species	2.00		0.91
19	Paul and Amos (2011)	Field, *Zostera noltii*	3.50		0.18
20	Sánchez-González et al. (2011)	Flume, synthetic plants	0.80		0.13
21	Stratigaki et al. (2011)	Flume, polypropylene stripes	1.70	0.43	
22	Yang et al. (2012)	Field, *Scirpus* & *Spartina alterniflora*	1.61		0.73
23	Ysebaert et al. (2011)	Field, *Spartina alterniflora* & *S. mariqueter*	1.86		0.64
H	This study, Hellegat	Field, *Spartina anglica*	1.90		0.69
B	This study, Bath	Field, *Scirpus maritimus*	1.27		0.59

One modeling approach for describing the effect of vegetation on wave propagation is to apply an increased bottom friction coefficient (e.g. Möller et al. (1999)). The main drawback of this approach is the absence of information about vegetation height. Therefore, most modeling approaches make use of a cylinder approach (Dalrymple et al., 1984; Mendez and Losada, 2004), estimating the wave-induced drag force exerted on the vegetation stems, and optionally also on root systems or branches. This type of model relies on knowledge of the bulk drag coefficient $\widetilde{C}_D$, representing drag that is due to pressure differences and drag that is due to skin friction, but also processes that are not captured by the physical model, for example plant swaying (Dijkstra and Uittenbogaard, 2010; Méndez et al., 1999; Mullarney and Henderson, 2010; Riffe et al., 2011), attenuation of orbital motion by the vegetation canopy (Pujol et al., 2013) and interaction between individual wakes in dense vegetation fields (Suzuki and Arikawa, 2010).

Because of the complex physics underlying the bulk drag coefficient $\widetilde{C}_D$, a-priori determination of an appropriate value for a certain vegetation species and hydrodynamic conditions is precluded, and site-specific calibration of $\widetilde{C}_D$ is required. However, several authors have attempted to relate $\widetilde{C}_D$ to the Reynolds number Re (Kobayashi et al., 1993; Méndez et al., 1999; Pinsky et al., 2013) or to the Keulegan-Carpenter number K (Mendez

and Losada, 2004). Bradley and Houser (2009) and Anderson and Smith (2014) found no improvement when $\widetilde{C}_D$ was parameterized with K instead of Re. Coefficients in these relations are mostly obtained by calibration.

Formulations for vegetation bulk drag coefficients vary considerably in the literature (Table 2.2). Theoretically, drag coefficients of a smooth, rigid cylinder has a value of about 1.0-1.2 for sub-critical flow. However, it is difficult to estimate an appropriate bulk drag coefficient in wave conditions for different shapes, densities and flexibilities (Suzuki and Arikawa, 2010). Most studies that analyze bulk drag coefficients present a computed value that is based on observed wave attenuation. An exception is the study of Hu et al. (2014), where drag forces were directly measured. Because the bulk drag coefficient is usually a result of computations, it also reflects all processes that are not or incorrectly captured in the model involved.

Table 2.2: *Relations between Reynolds number Re and bulk drag coefficient $\widetilde{C}_D$ presented in the literature, based on a combination of a certain (synthetic or natural) vegetation type, vegetation height l_v, vegetation diameter b_v, water depth h and wave height H (regular waves) or H_s (irregular waves). The last column gives a comparison of the result for $Re = 1000$, which is a typical number for storm conditions at the measurement sites in the current study.*

Publication	Vegetation properties	Description of $\widetilde{C}_D$	Based on range	$\widetilde{C}_D$ for $Re = 1000$
Méndez et al. (1999)	Flexible plastic strips 52x0.03 mm (Asano et al., 1992), $l_v = 0.25$ m, $h \approx 0.50$ m, $H \leq 0.12$ m	$\widetilde{C}_D = (2200/Re)^{2.2} + 0.08$	200<Re<15500	$\widetilde{C}_D = 5.75$
Paul and Amos (2011)	*Zostera noltii*, sea grass, $l_v = 0.13$ m, $h = 1.5 - 3.5$ m, $H_s = 0.10 - 0.18$ m	$\widetilde{C}_D = (153/Re)^{1.45} + 0.06$	100<Re<1000	$\widetilde{C}_D = 0.13$
Jadhav and Chen (2012)	*Spartina alterniflora*, $l_v = 0.63$ m, $b_v = 8$ mm, $h \approx 0.4 - 0.6$ m, $H_s \leq 0.4$ m	$\widetilde{C}_D = 2,600/Re + 0.36$	600<Re<3200	$\widetilde{C}_D = 2.96$
Pinsky et al. (2013)	Statistical analysis of attenuation by several salt marsh vegetation species	$\log(\widetilde{C}_D) = \beta_0 + \beta_1 \log(c\,Re)$, $c = 3 \cdot 10^{-4}$, $\beta_0 = -1.72$, $\beta_1 = -1.67$	not specified	$\widetilde{C}_D = 0.14$
Anderson and Smith (2014)	Synthetic *Spartina*, $l_v = 0.42$ m, $b_v = 6.4$ mm, $h = 0.31 - 0.53$ m, $H_s = 0.05 - 0.19$ m	$\widetilde{C}_D = (744/Re)^{1.27} + 0.76$	500<Re<2300	$\widetilde{C}_D = 1.45$
Hu et al. (2014)	Stiff wooden rods, $l_v = 0.36$ m, $b_v = 10$ mm, $h = 0.25 - 0.50$ m, $H = 0.04 - 0.20$ m	$\widetilde{C}_D = (730/Re)^{1.37} + 1.04$	300<Re<4700	$\widetilde{C}_D = 1.69$
Möller et al. (2014)	Predominantly *Elymus athericus*, $l_v = 0.70$ m, $b_v = 1.3$ mm, $h = 2.0$ m, $H_s = 0.1 - 0.9$ m	$\widetilde{C}_D = (227/Re)^{1.62} + 0.16$	100<Re<1100	$\widetilde{C}_D = 0.25$

A calibrated relation between Re and $\widetilde{C}_D$ is generally used to estimate bulk drag coefficients under highly turbulent storm conditions, which are characterized by high Reynolds numbers. By using extrapolation to higher Reynolds numbers, possible physical thresholds are implicitly neglected, for example thresholds for swaying of vegetation

(Méndez et al., 1999; Bradley and Houser, 2009; Möller et al., 2014; Rupprecht et al., 2015) or vegetation collapse by uprooting or stem breakage (Seymour et al., 1989; Puijalon et al., 2011; Liffen et al., 2013; Möller et al., 2014). Additionally, seasonal variations in aboveground biomass and mechanical fragility can considerably influence wave damping capacity (Paul and Amos, 2011; Bouma et al., 2014).

As aforementioned, many authors describe the potential of vegetated foreshores for coastal protection. However, the capability of these ecosystems in serving as protection during extreme storm conditions with high waves and large water depths is not well understood. Most studies of wave attenuation by vegetation concern field or laboratory experiments with small water depths and low wave heights (Fig. 2.2). This means that most existing measurements are not directly suitable for drawing conclusions about the behavior of vegetation under conditions that are relevant to the design of coastal dikes: hydrodynamic conditions with severe waves and water depths of several meters. Empirical formulas and process-based descriptions of wave attenuation are mostly applied for bridging the gap between measured conditions and extreme conditions. These instruments are mainly based on measurements carried out during low-energy conditions (Anderson et al., 2011), which leads to uncertainties when applying them to storm conditions. This is reflected by the large variability in formulations that describe the drag coefficient as a function of wave properties and vegetation characteristics (Table 2.2).

Understanding the effect of vegetation on wave damping under storm conditions is for utmost importance to come up with design criteria for dikes with vegetated foreshores in front. The actual consequences of wave reduction by vegetated foreshores for hydraulic loads on dikes have never been quantified in the literature.

Therefore, the aim of this chapter is to provide understanding of the efficiency of vegetated foreshores for reducing wave run-up on and wave overtopping over coastal dikes. This insight is obtained utilizing a combination of field measurements and numerical modeling. New field measurements were required, because existing detailed field observations of storm wave attenuation by a characteristic north-west European vegetation canopy were absent. The new field data has been used to calibrate and validate a numerical model that simulates wave attenuation over vegetated foreshores. This model has been applied to some representative examples taken from the Netherlands, to show how and how much vegetated foreshores in front of coastal dikes can reduce wave loads on a dike under severe storm conditions.

This chapter is organized as follows. The field measurements are discussed in section 2.2. Section 2.3 describes the numerical modeling work on wave energy dissipation over vegetated foreshores. Section 2.4 shows the results of the application of the numerical model, to illustrate how much vegetated foreshores can affect the wave loads on dikes for some typical examples taken from the Netherlands. The chapter closes with a discussion and conclusions in the Sections 2.5 and 2.6.

2.2. FIELD MEASUREMENTS

A field measurement campaign was carried out, in which wave attenuation over vegetated foreshores was measured during severe storms in the Netherlands in the months November 2014 till January 2015. The measurements were performed on two salt marshes with two representative but contrasting coastal wetland vegetation types: cordgrass (*Spartina anglica*) and grassweed (*Scirpus maritimus*). The former is found in salty environments, whereas the latter is found in brackish environments. The obtained data set is used in this chapter for the calibration and validation of a numerical model that describes wave propagation over vegetated foreshores (Section 2.3).

2.2.1. WAVE MEASUREMENT CONFIGURATION

Field measurements were carried out at two exposed salt marshes in the Western Scheldt estuary in the Netherlands. Wave gauges were deployed between 23 November 2014 and 21 January 2015 at the salt marshes Hellegat and Bath (Fig. 2.3).

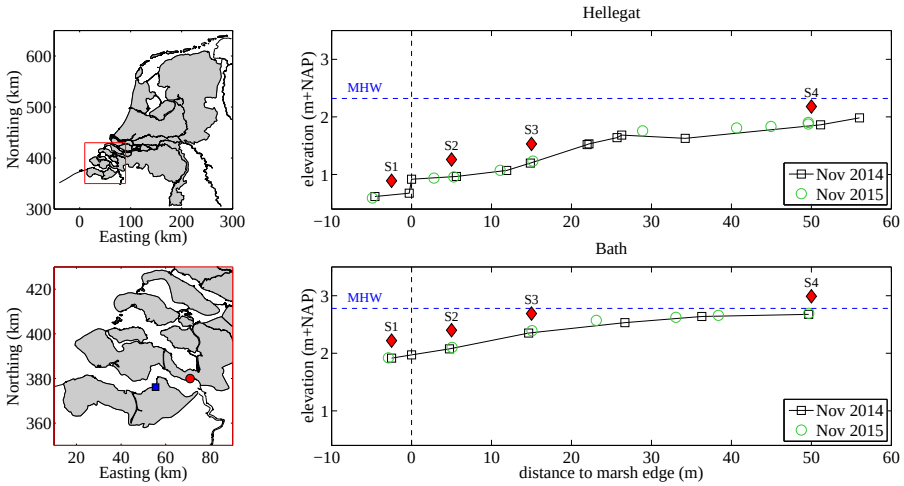

Figure 2.3: *Location of the salt marshes Hellegat (blue square) and Bath (red circle) in the Western Scheldt estuary (lower left) in the Netherlands (upper left), and the bathymetry at the measurement transects at Hellegat (upper right) and Bath (lower right) for November 2014 (black) and November 2015 (green). The position of the 4 wave gauges S1-S4 is indicated by red diamonds. The vertical dashed line is positioned at the marsh edge, the horizontal dashed line at Mean High Water.*

The marsh Hellegat is covered with the salt-tolerant species *Spartina anglica* (common cordgrass). Mixed vegetation is present on the higher marsh, but this is beyond the area where the wave gauges were deployed. At Bath, the discharge of the Scheldt river causes a brackish environment, which causes dominance of *Scirpus maritimus* (sea club-rush) at the measurement site. The tidal range in the Western Scheldt increases from approximately 4 m at the estuary mouth to 5 m at Bath. Under severe storm con-

ditions, both storm surge and wind waves can penetrate from the North Sea into the estuary. Significant inundation of the higher areas of the salt marsh only occurs when there is a combination of high tide and storm surge.

At both marshes, four wave gauges (Ocean Sensor Systems, Inc., USA) were deployed in the same configuration. One sensor was placed on the mudflat, directly in front of the marsh edge (S1). The three other sensors (S2, S3 and S4) were located in the vegetation, at distances of 5, 15 and 50 m from the marsh edge (Fig. 2.3, right). The elevation heights were determined using an RTK-GPS device with a precision in the order of 1 cm.

The wave gauges were programmed to record the pressure with a frequency of 5 Hz over a period of 7 minutes, every 15 minutes. This means that every burst contains 2100 samples. The measured pressure is the result of the local atmospheric pressure, the hydrostatic pressure and the dynamic wave pressure. In the post-processing, these three components were separated. The hydrostatic pressure provides information about the still water level, whilst the dynamic wave pressure depends on the surface waves. In the conversion of dynamic wave pressures to variations in the surface elevation due to waves, depth-attenuation of the pressure signal according to linear wave theory was taken into account. The pressure sensors were mounted approximately 0.10 m above the sediment surface.

2.2.2. VEGETATION MEASUREMENTS

Vegetation properties were determined by measuring the length, the diameter at the top, the diameter in the middle and the diameter at the base of individual stems. At Bath, the properties of all plants within a surface area of 0.5x0.5 m were investigated between sensors S1 and S2 and between sensors S2 and S3. This area was reduced to 0.25x0.25 m for the sampling between sensors S3 and S4 because of the high stem density. At Hellegat, an area of 0.25x0.25 m was used for all samples. The vegetation samples were collected on 19 November 2014, which means that vegetation was in its winter state (Fig. 2.4).

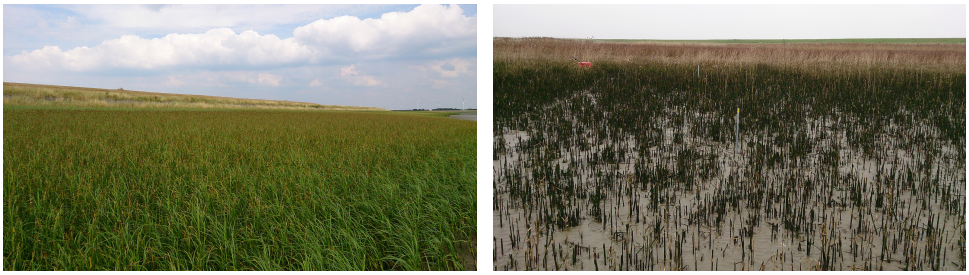

Figure 2.4: *Scirpus maritimus at Bath, Western Scheldt, the Netherlands in July 2014 (left) and November 2014 (right).*

The *Spartina anglica* at Hellegat had a mean height $h_{v,mean}$ ranging from 0.20 m at the marsh edge to 0.29 m further into the vegetation field (Table 2.3). A near-bottom

stem density $N_{v,0}$ of nearly 1000 stems/m^2 was present near the marsh edge, while a density of more than 1500 stems/m^2 was found between sensors S3 and S4. The near-bottom stem diameter $b_{v,0}$ was fairly constant at approximately 3 mm. The impact of wind and waves on the vegetation in its fragile winter state was more distinct at Bath. Near the marsh edge, the dense *Scirpus maritimus* that was present in summer has depreciated to broken stems with a mean height of approximately 0.15 m (Fig. 2.4). Between sensors S3 and S4, the disruption was less: the stem density, mean height and maximum height were all significantly larger than at the marsh edge. Remarkably, the mean stem diameter decreases from 8.7 mm at the marsh edge to 4.9 mm between sensors S3 and S4. The total biomass density M was estimated by multiplication of $h_{v,mean}$, $N_{v,0}$ and the near-bottom surface area $A_{v,0} = \pi b_{v,0}^2/4$.

Table 2.3: *Maximum plant height $h_{v,max}$, mean plant height $h_{v,mean}$, near-bottom stem density $N_{v,0}$, mean near-bottom stem diameter $b_{v,0}$ and total biomass density M for six sampling locations.*

Sample	$h_{v,max}$ (m)	$h_{v,mean}$ (m)	$N_{v,0}$ (stems/m^2)	$b_{v,0}$ (mm)	M (m^3/m^2)
Hellegat S1-S2	0.61	0.20	944	3.0	$1.3 \cdot 10^{-3}$
Hellegat S2-S3	0.78	0.29	1136	3.4	$3.0 \cdot 10^{-3}$
Hellegat S3-S4	0.84	0.27	1520	2.7	$2.3 \cdot 10^{-3}$
Bath S1-S2	0.48	0.17	144	8.7	$1.5 \cdot 10^{-3}$
Bath S2-S3	0.52	0.15	372	8.0	$2.8 \cdot 10^{-3}$
Bath S3-S4	1.23	0.35	1072	4.9	$7.1 \cdot 10^{-3}$

2.2.3. WAVE CHARACTERISTICS

Wave conditions and water depths were measured during 115 tides between 23 November 2014 and 21 January 2015 (Fig. 2.5). Inundation of the full transect only takes place during storms or spring tides. In the measurement period, this happened during 88 tidal cycles at Hellegat, and during 49 tidal cycles at Bath.

The wave height can be limited by depth, wind speed or wind direction. At Hellegat, both maximum water depths and maximum exposure to waves occurs at Western or North-Western winds. Therefore, at this site, the maximum wave height (Table 2.4) as well as the maximum water depth (Table 2.6) were recorded during the Western storm of 11 January 2015, although not at exactly the same time. The maximum significant wave height at Hellegat was equal to 0.69 m, with a corresponding water depth at the marsh edge of 1.90 m (Fig. 2.2). Wave conditions at Bath are at a maximum under South-Western wind conditions. This means that the wind direction that generates the maximum surge (NW) does not coincide with the wind direction that generates the largest waves (SW). The maximum significant wave height at Bath was equal to 0.55 m (Table 2.5), with a corresponding water depth at the marsh edge of 1.36 m (Fig. 2.2).

During storms, wave peak periods T_p were typically in the range of 2.5 to 4.0 s at Hellegat, and between 2.5 and 3.5 s at Bath. At these two sites in the Western Scheldt, the

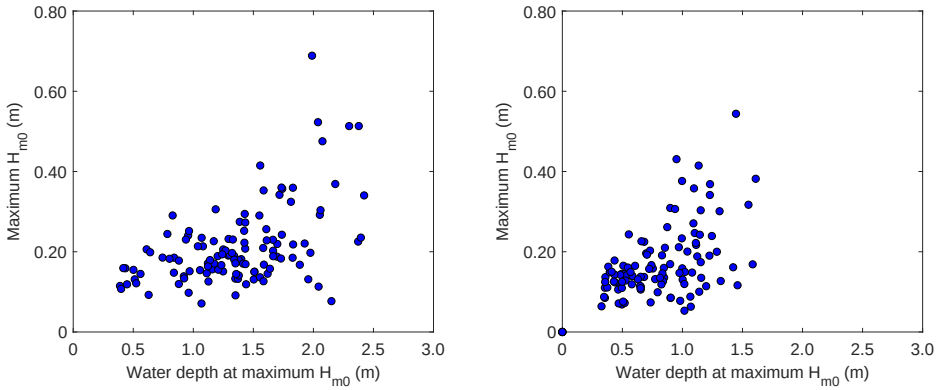

Figure 2.5: *Maximum significant wave height per tide and corresponding water depth at sensor S1, on the mud flat near the marsh edge of Hellegat (left) and Bath (right) for 115 tides between 23 November 2014 and 21 January 2015.*

fraction of wave energy in the infragravity wave band (0.005 Hz < f < 0.05 Hz) was less than 1 percent during severe storms.

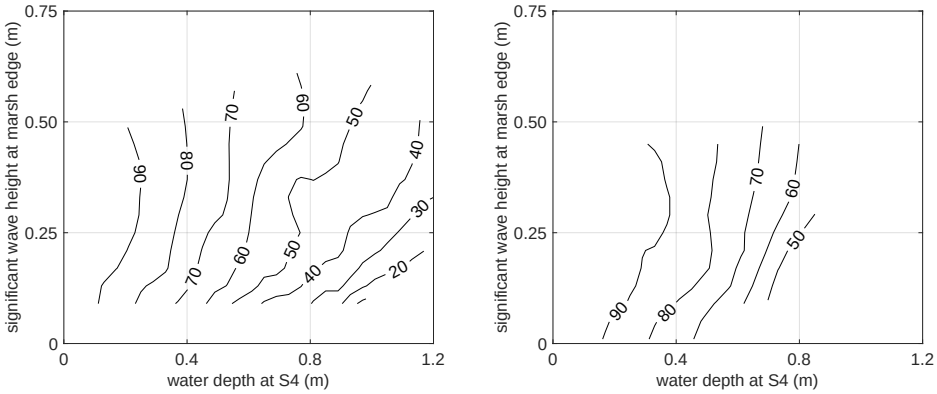

Figure 2.6: *Reduction in significant wave height Hm0 (%) over a distance of 50 m between sensor S1 and S4, depending on the lowest water depth over the transect, which is at sensor S4 (horizontal axis), and the incoming wave height at sensor S1 (vertical axis) for Hellegat (left) and Bath (right).*

Waves lose energy by depth-induced wave breaking, bottom friction and wave dissipation by vegetation. These processes all depend on the wave height to water depth ratio. The water depth on the salt marshes Hellegat and Bath decreases along the transects (Fig. 2.3). The reduction in significant wave height between the sensors S1 and S4 predominantly depends on incoming wave height and water depth (Fig. 2.6). For identical combination of wave height and water depth, the reduction in wave height was

larger at Bath than at Hellegat, despite of the larger difference in water depth between both ends of the transect at Hellegat. This difference is probably caused by the relatively high biomass density present at Bath (Table 2.3).

Table 2.4: *Five tides with the largest significant wave height (m) at station S1 with corresponding wave heights and water depths (m) at all stations S1-S4 for Hellegat.*

tide	time	H_{m0} S1	H_{m0} S2	H_{m0} S3	H_{m0} S4	h S1	h S2	h S3	h S4
96	11-01-2015 07:30	0.69	0.61	0.52	0.29	1.90	1.53	1.26	0.66
54	20-12-2014 14:00	0.53	0.46	0.39	0.21	1.95	1.58	1.31	0.70
58	22-12-2014 15:00	0.52	0.47	0.38	0.29	2.29	1.93	1.65	1.05
95	10-01-2015 17:45	0.51	0.46	0.40	0.29	2.19	1.82	1.56	0.94
94	10-01-2015 06:30	0.48	0.46	0.39	0.21	1.99	1.62	1.35	0.74

Table 2.5: *Five tides with the largest significant wave height (m) at station S1 with corresponding wave heights and water depths (m) at all stations S1-S4 for Bath.*

tide	time	H_{m0} S1	H_{m0} S2	H_{m0} S3	H_{m0} S4	h S1	h S2	h S3	h S4
94	10-01-2015 06:30	0.55	0.48	0.41	0.17	1.36	1.19	0.93	0.64
38	12-12-2014 06:30	0.44	0.36	0.23	0.00	0.88	0.73	0.43	0.00
100	13-01-2015 07:15	0.42	0.40	0.31	0.05	1.06	0.90	0.60	0.32
58	22-12-2014 15:30	0.38	0.34	0.29	0.15	1.43	1.26	0.98	0.69
92	09-01-2015 06:00	0.38	0.35	0.25	0.02	0.92	0.75	0.48	0.23

Table 2.6: *Five tides with the largest water depth (m) at station S1 with corresponding wave heights and water depths (m) at all stations S1-S4 for Hellegat.*

tide	time	H_{m0} S1	H_{m0} S2	H_{m0} S3	H_{m0} S4	h S1	h S2	h S3	h S4
96	11-01-2015 06:00	0.27	0.29	0.28	0.24	2.52	2.16	1.88	1.27
94	10-01-2015 05:15	0.31	0.31	0.31	0.24	2.41	2.05	1.78	1.17
95	10-01-2015 18:15	0.46	0.43	0.40	0.31	2.36	2.00	1.73	1.12
58	22-12-2014 14:30	0.38	0.38	0.33	0.23	2.34	1.98	1.71	1.10
59	23-12-2014 02:45	0.34	0.32	0.28	0.23	2.33	1.97	1.70	1.09

Table 2.7: *Five tides with the largest water depth (m) at station S1 with corresponding wave heights and water depths (m) at all stations S1-S4 for Bath.*

tide	time	H_{m0} S1	H_{m0} S2	H_{m0} S3	H_{m0} S4	h S1	h S2	h S3	h S4
96	11-01-2015 06:45	0.22	0.21	0.21	0.14	1.59	1.43	1.13	0.84
58	22-12-2014 15:15	0.35	0.36	0.32	0.17	1.57	1.40	1.10	0.81
94	10-01-2015 05:45	0.46	0.42	0.37	0.20	1.55	1.39	1.09	0.80
62	24-12-2014 16:45	0.17	0.15	0.13	0.07	1.48	1.32	1.03	0.73
64	25-12-2014 17:30	0.11	0.10	0.12	0.07	1.46	1.30	1.01	0.71

2.3. NUMERICAL MODELING OF WAVE PROPAGATION

To be able to distinguish between the processes of wave breaking, bottom friction and wave attenuation by vegetation, a numerical modeling investigation has been carried out. This section describes the modeling approach, calibration, validation and application of the model.

2.3.1. MODELING APPROACH

The measurements of wave propagation over vegetated foreshores have been reproduced with the spectral wave model SWAN (Simulating WAves Nearshore, (Booij et al., 1999; Ris et al., 1999)). The SWAN model includes the depth-induced wave breaking model of Battjes and Janssen (1978), different formulations for bottom friction, including Madsen et al. (1988), and the method for accounting wave damping by vegetation developed by Mendez and Losada (2004). Suzuki et al. (2012b) validated the performance of the vegetation module of SWAN. Additionally, they enabled schematization of vertical differences in vegetation characteristics in the model by specifying multiple layers. SWAN is capable of reproducing energy dissipation in shallow water, as long as the amount of long wave energy is limited. Total energy dissipation (i.e. wave heights) can be simulated relatively accurately with SWAN, compared to the simulation of the spectral shape (i.e. wave periods) (Van Gent and Doorn, 2001).

Three data sets were used for model calibration and validation: the data from Hellegat and Bath, described in this chapter, and wave data from a salt marsh covered with *Spartina alterniflora* (Smooth Cordgrass) at East Chongming island, China, reported in Yang et al. (2012). For the calibration and validation of the SWAN model, the bathymetry of the field sites (Fig. 2.3) was included in an 1D model schematization, with a resolution of 0.5 m. The significant wave height H_{m0} and mean wave period T_{m01} measured at the first sensor were used to define the incoming Jonswap wave spectrum. The measured significant wave heights at the other sensors were compared with the corresponding model outcomes during calibration and validation.

An area of 0.25x0.25 m = 0.0625 m^2 was sampled, in which 95 stems were found (Fig. 2.7), left). Four layers have been defined in the SWAN model, with a height of 0.20 m (Hellegat and Bath) or 0.25 m (East Chongming) each. For each stem, the diameter was measured at the base, in the middle, and at the top. Stem diameter and height of the diameter measurement were compared (Fig. 2.7), right). The stem diameter in the four layers of the SWAN model is equal to the mean stem diameter within each layer. The layering was based on the vegetation samples Bath S3-S4 and Hellegat S3-S4. For East Chongming, only one vegetation sample was available. The inter-sample variation in vegetation characteristics was expressed in the model by a spatial varying multiplication factor for the stem density, which was based on the variations in plant surface area $N_v \cdot b_v \cdot h_v$ with respect to sample S3-S4.

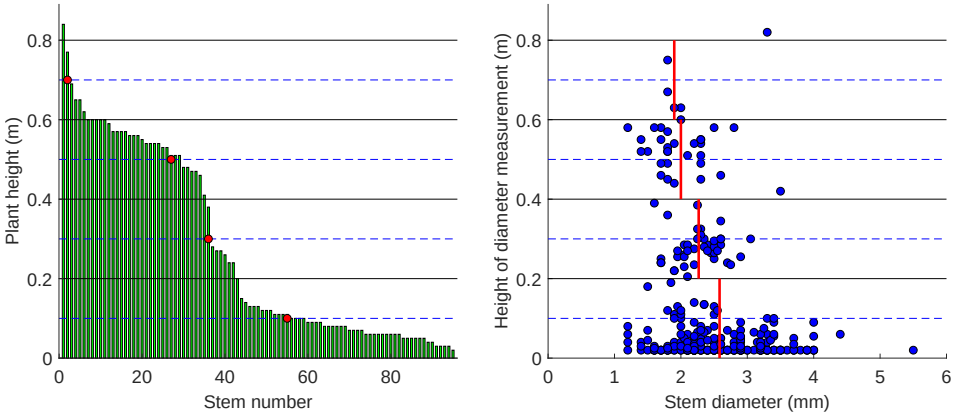

Figure 2.7: *Example of the method to determine vegetation characteristics, for Hellegat S3-S4 (Table 2.3). The stem density in the center of these layers is equal to 55, 36, 27 and 2 stems per sampled area, or 880, 573, 432 and 30 stems/m^2.*

2.3.2. MODEL CALIBRATION AND VALIDATION

As it is expected that wave dissipation by vegetation will prove to be the main dissipation mechanism on vegetated foreshores, the bulk drag coefficient $\widetilde{C}_D$ of the Mendez and Losada model in SWAN has been chosen as the main calibration parameter. The wave steepness based formula of Battjes and Stive (1985) has been used to determine suitable breaker parameters γ for the Battjes and Janssen (1978) model in SWAN. For bottom friction, the model of Madsen et al. (1988) has been selected, with a constant Nikuradse roughness length scale k_N = 0.02 m, which is a typical value for a bottom with ripples (Babanin et al., 2005).

For Hellegat and Bath, four tides between 9 Jan 2015, 15:00 and 11 Jan 2015, 9:30 have been selected for the model calibration, and six tides between 20 Dec 2014, 11:30 and 23 Dec 2014, 6:00 for the subsequent model validation. Most tides in the tables with five highest wave heights (Table 2.4 and 2.5) and inundation depths (Table 2.6 and 2.7) are included in these two selected periods.

For each burst, a best correspondence between measurement data and outcomes of the SWAN model was obtained, by calibrating the bulk drag coefficient $\widetilde{C}_D$ via the difference in wave height at S4. Wave attenuation in most bursts was best reproduced with a value of $\widetilde{C}_D$ between 0.2 and 0.9 (Fig. 2.8), given the method applied to schematize the vegetation with four layers. A decrease in $\widetilde{C}_D$ with increasing Re as described in the literature (Table 2.2) can be recognized. However, there is a considerable spread of drag coefficients around the mean trend, related to many factors that are of influence in the field, such as variations in water depth, wave height and wave period, wave obliqueness, and tidal currents.

Based on the calibration results and the range in Reynolds numbers that apply to the tides in the validation, one characteristic bulk drag coefficient $\widetilde{C}_D$ has been selected for

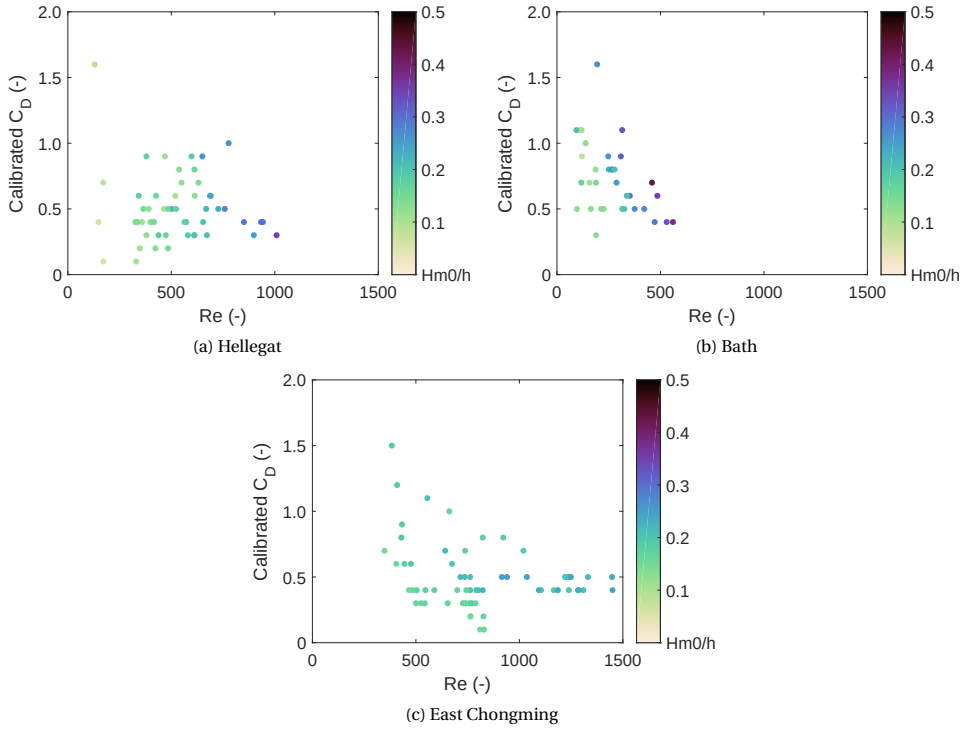

(a) Hellegat

(b) Bath

(c) East Chongming

Figure 2.8: *Results of the calibration of $\widetilde{C}_D$ in the SWAN model for the field sites Hellegat (top left), Bath (top right) and East Chongming (bottom). Reynolds numbers are plotted against calibrated $\widetilde{C}_D$ for each burst. The markers are colored by wave height to water depth ratio at sensor S1.*

each site: 0.5 for Hellegat ($Re \approx 700$), 0.6 for Bath ($Re \approx 400$) and 0.4 for East Chongming ($Re \approx 1200$). These values have been applied to tides outside the calibration period, to guarantee a statistically independent test of the SWAN model. Differences in optimal bulk drag coefficient between the sites are expected to be mainly related to plant stiffness and wave conditions. The validation computations demonstrate that the calibrated SWAN model is able to reproduce the wave height reduction over 50 m of vegetated foreshore with a deviation below 0.05 m (Fig. 2.9).

At Hellegat, the highest waves in the validation data are present in the tides 54 and 58. At Bath, no inundation of sensor S4 occurred during tide 56. The highest waves and water depths were present during tide 58. At East Chongming, waves and water depths were far higher during tide 10 than during tide 9. For all sites, the SWAN model gives an accurate reproduction of the tides with high waves and water depths, while for tides with lower waves, the wave attenuation is underestimated. Since for each site one constant value of $\widetilde{C}_D$ was used for all tides, the observed differences can be explained by the theoretical decline in $\widetilde{C}_D$ with Re.

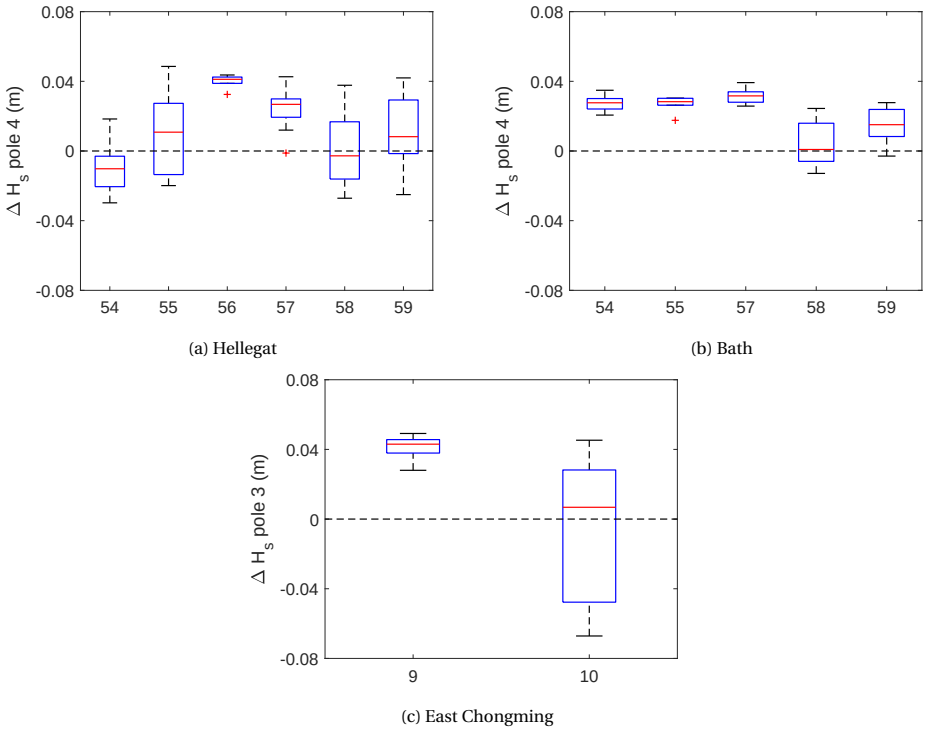

(a) Hellegat

(b) Bath

(c) East Chongming

Figure 2.9: *Results of the validation of the SWAN model for the field sites Hellegat (top left), Bath (top right) and East Chongming (bottom). For the tides included in the validation, the differences between modeled and measured significant wave height at sensor S4 are presented. The mean difference (model minus data) is shown in red, the 50 percent interval in blue, and the maximum differences in black.*

2.3.3. ANALYSIS OF WAVE ENERGY DISSIPATION MECHANISMS

Inclusion of vegetation in the model is essential to reproduce the decay in wave height properly. Wave attenuation by vegetation leads to a gradual decrease in wave height, and prevents intense wave breaking to occur (Fig. 2.10, right panel). In absence of vegetation in the model, waves can retain their energy further inland, and strong wave breaking occurs on the bar in the bottom profile of Hellegat (Fig. 2.10, left panel). Bottom friction is of minor importance for length scales in this order of magnitude. The same processes are present during other tides and at the other sites: Bath and East Chongming.

If wave energy dissipation by vegetation is excluded in the model, wave heights at sensor S4 are consequently overestimated. The relative importance of vegetation depends on the ratio between wave height and water depth (Fig. 2.11). For very small wave height to water depth ratios at the marsh edge (<0.15), depth-induced wave breaking is negligible and also wave energy dissipation by vegetation is relatively small. For moderate wave height to water depth ratios (0.15-0.30), depth-induced wave breaking on the

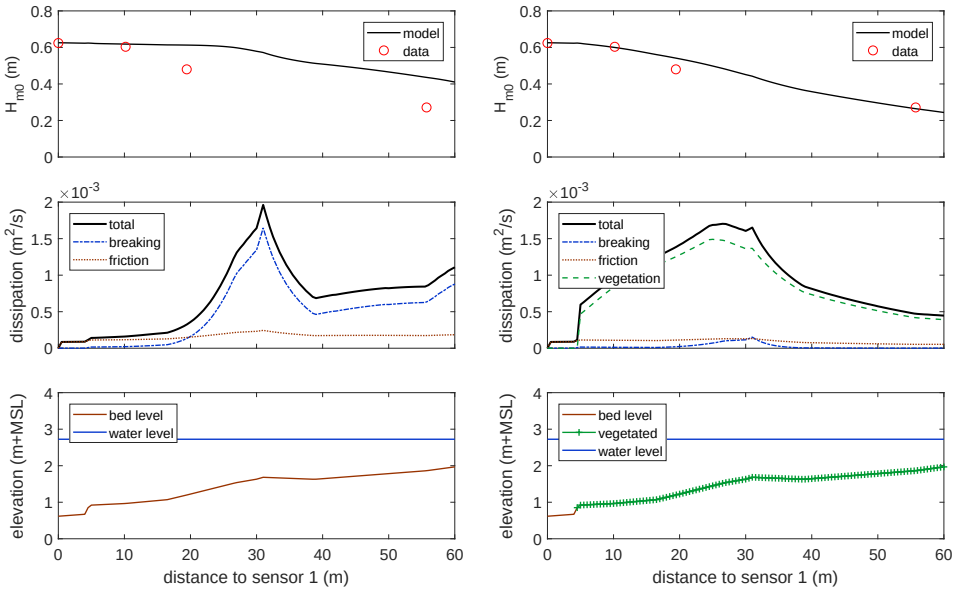

Figure 2.10: *Example of reproduction of measured wave heights at Hellegat for one individual burst, for $\widetilde{C}_D = 0$ (i.e., no vegetation effect, left panels) and $\widetilde{C}_D = 0.4$ (right panels). The upper panels present the observed versus modeled wave height. The middle panels show the magnitude of different dissipation mechanisms in the SWAN model. The lower panels show the bathymetry and indicate where vegetation is present.*

foreshore is still limited, but wave attenuation by vegetation can be substantial. The presence of vegetation leads to an additional reduction in significant wave height up to 50% of the total reduction. For larger wave height to water depth ratios at the marsh edge (>0.30), depth-induced wave breaking becomes significant, and the additional contribution of vegetation decreases. However, the model results show that the vegetation dissipates wave energy before intense breaking occurs, since the reduction of wave energy due to the presence of vegetation takes already place at smaller wave height to water depth ratios than the onset of wave breaking (Fig. 2.10). Consequently, the presence of vegetation leads to a more gradual dissipation of wave energy, and a distinct breaker zone is absent. The maximum contribution of vegetation is in the same order of magnitude as the value of 60%, presented in Möller et al. (2014). In their experiments, the contribution of depth-induced wave breaking was relatively low because of the horizontal bottom.

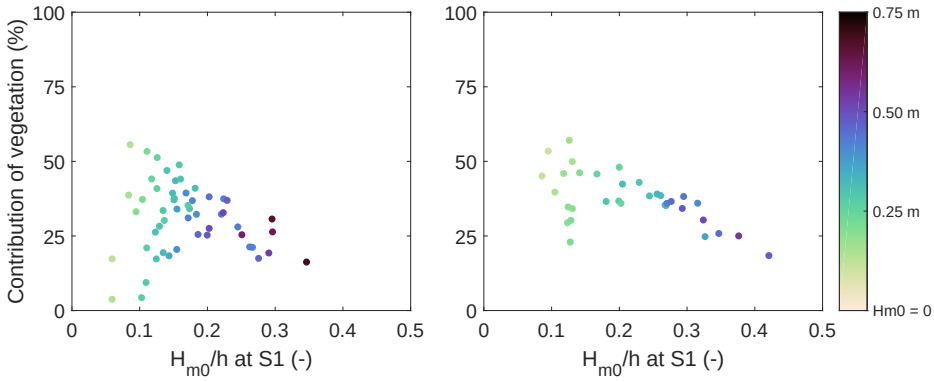

Figure 2.11: *Contribution of vegetation (%) to the total reduction in significant wave height between the sensors S1 and S4 at Hellegat (left) and Bath (right), when comparing observed reductions with reductions computed by a SWAN model in which vegetation is excluded. Numbers are given for different wave height to water depth ratios at sensor S1 (horizontal axes), and markers are colored by wave height at sensor S1.*

2.4. WAVE LOAD REDUCTION BY VEGETATED FORESHORES

The previous sections have demonstrated the wave damping capacity of vegetated foreshores. Since wave overtopping over the dike is strongly related to the incident wave height, wave energy dissipation by vegetated foreshores allows in principle for lower crest heights, and consequently, relatively slender dike bodies. This section shows some examples of the effect of vegetated foreshores on wave loads on coastal dikes for a range of foreshore configurations and hydraulic loading conditions.

2.4.1. APPROACH

The wave transformation over the vegetated foreshore is estimated by applying the validated SWAN model (Section 2.3). The formulas presented in EurOtop (2007) are used to calculate the characteristic two percent wave run-up height on the outer slope of the dike (formula 5.3) and the time-averaged wave overtopping discharge over the dike (formulas 5.8 and 5.11). Wave conditions at the toe of the dike should be supplied to these formulas. The validated SWAN model is used to compute wave height reduction over vegetated foreshores for various foreshore configurations and hydraulic loading conditions (Fig. 2.12), including the influence of the vegetated foreshore on the wave conditions as computed by SWAN. Because of the complex and context-dependent influence of vegetated foreshores on storm surge propagation (Wamsley et al., 2010; Zhang et al., 2012) and wave set-up (Battjes, 1974; Dean and Bender, 2006), we ignore these effects in the present study.

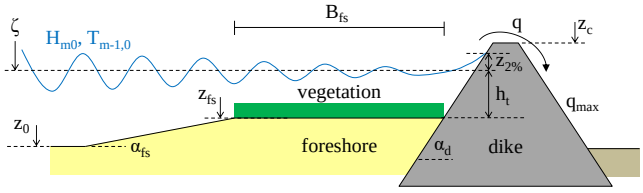

Figure 2.12: *Definition sketch of a schematized dike-foreshore system. Table 2.8 gives an overview of the variables involved.*

Table 2.8: *Definition of variables used to schematize the characteristics of the dike-foreshore system (Fig. 2.12) and the hydrodynamic loads on the system.*

Symbol	Parameter name	Units	Values
α_d	Slope angle dike	-	1:4
R_c	Relative freeboard	m	3.0
α_{fs}	Slope angle tidal flat	-	1:100
h_t	Water depth at dike toe	m	1.0-4.0
H_{m0}	Offshore significant wave height	m	1.5
$T_{m-1,0}$	Offshore spectral wave period	s	5.0
k_N	Roughness length scale	m	0.02
B_{fs}	Width of flat part of foreshore	m	0-800
N_v	Stem density	stems/m^2	0, 1200
b_v	Stem diameter	mm	3.0
h_v	Vegetation height	m	0.30
$\widetilde{C}_D$	Bulk drag coefficient vegetation	-	0.4
$z_{2\%}$	Two percent wave run-up height	m	-
q	Mean overtopping discharge	m^{3}s^{-1}m^{-1}	-

In the Netherlands, salt marshes are generally enclosed by a dike at the landward side, and an adjacent mudflat in front. The slope of these combined salt marsh-mudflat systems depends on the available space. For example in the Western Scheldt estuary, lateral dimensions of salt marshes similar to Hellegatpolder (Fig. 2.1, upper right) are limited by the presence of deep tidal channels, intensively used for navigation. At the salt marshes bordering the Wadden Sea in the north of the Netherlands, a smooth transition between the salt marshes and the extensive intertidal flats is often present. This is for example the case at the salt marshes near Groningen and Texel (Fig. 2.1, lower left and right). Sandy foreshores with relatively steep slopes (about 1:50) can be found in front of dikes directly bordering the North Sea, for example at the Westkapelle sea defense (Fig. 2.1, upper left). The hydrodynamic forcing at these foreshores is generally too intense to allow vegetation seeds and seedlings to settle.

Inundation depths depend on the salt marsh elevation and storm surge levels. The maximum elevation of the marshes is strongly related to the local tidal amplitude. Surge

levels depend on tidal amplitude and surge effects. Under design conditions in the Netherlands, inundation depths above salt marsh surface can typically reach values between 1.5 and 3.5 m near the dike toe. Depending on the location and orientation of the dike with respect to the prevailing wind direction during storms, incident wave heights vary roughly between 0.5 and 2.0 m. Salt marshes do generally not develop in areas that are exposed to even more energetic conditions. To achieve stable dike slope revetments, designers can opt for relatively steep slopes, typically around 1:3, combined with heavy armoring units. More gentle slopes, in the order of 1:6, allow for the use of lighter revetments. Depending on incident wave conditions, the relative freeboard is mostly in the range of 2.5 to 4.5 m.

Based on these different examples of salt marshes in the Netherlands, characteristic vegetated foreshore characteristics are defined (Table 8), with variation in water depth, foreshore width and vegetation coverage (no vegetation or vegetation resembling *Spartina anglica* in winter state). Based on the calibration results (Fig. 2.8), a bulk drag coefficient of $\widetilde{C}_D$ is considered as an initial estimate for salt marsh vegetation at large Reynolds numbers.

2.4.2. COMPUTATIONAL RESULTS

For the dike configuration and wave characteristics of Table 2.8, a two percent wave run-up height $z_{2\%}$ of approximately 3.2 m will occur without any disturbance of the waves on a foreshore. Because the relative freeboard in this case study is only 3.0 m, this would result in a mean overtopping discharge of 0.6 l/s/m. Fig. 2.13 shows the relative reduction of significant wave height (top panel), wave run-up height (middle panel) and reduction factor in wave overtopping discharge (bottom panel) due to the presence of bare foreshores (left panels) and vegetated foreshores (right panels), depending on foreshore width (horizontal axis) and depth on the foreshore (vertical axis).

If the depth on the foreshore is limited to just 1.0 m, the wave run-up is reduced by 60-100%, and the wave overtopping discharge diminishes to negligible amounts. For larger water depths, the influence of vegetation becomes more distinct. In the Netherlands, typical design water levels are in the order of 5 m above mean sea level, which is 3 m above the salt marsh surface. Where wave run-up under these conditions is only reduced by approximately 20% (0.6 m) for a 400 m wide, bare foreshore, the same foreshore covered by vegetation resembling *Spartina anglica* in winter state reduces the wave run-up by 55% (1.8 m). Wave overtopping discharges still have significant values for bare foreshores in case of large water depths, whereas the presence of vegetation fully prevents wave overtopping.

Some trends can be discerned. For foreshores with a small width, depth-induced wave breaking dominates the total wave energy dissipation. Bottom friction and wave attenuation by vegetation gain relative importance with increasing width. The dependence of wave load reduction with depth is non-linear, which is caused by the onset of wave breaking at a certain depth. For larger depths, the relative importance of vegetation

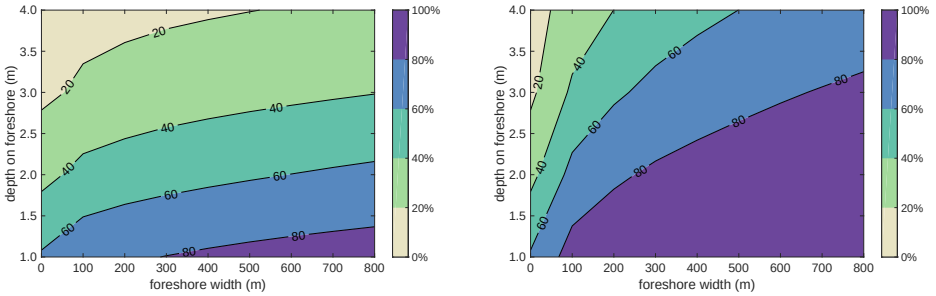

(a) Reduction in significant wave height (%)

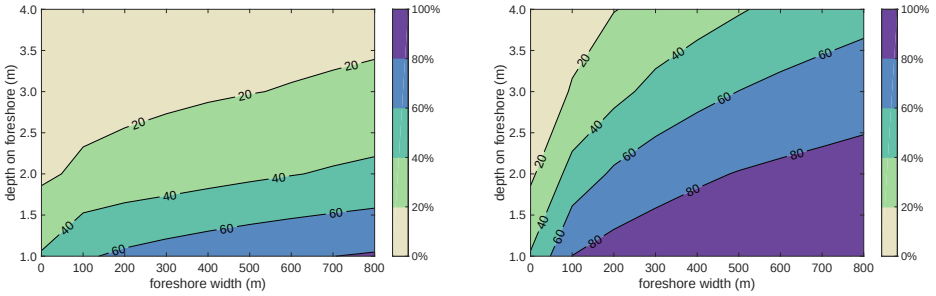

(b) Reduction in 2-percent wave run-up height (%)

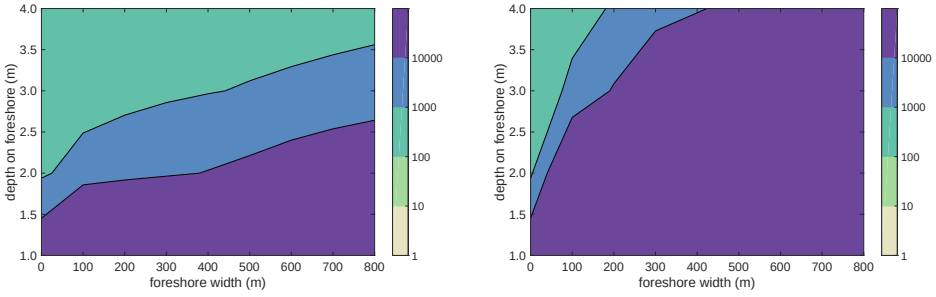

(c) Reduction in wave overtopping discharge (ratio)

Figure 2.13: *Relative reduction in significant wave height (top), 2 percent wave run-up height (middle) and reduction factor in wave overtopping discharge (bottom), in case of bare foreshores (left panels) and vegetated foreshores (right panels), for the values in Table 2.8.*

increases, since wave energy dissipation by vegetation already acts at lower wave height to water depth ratios than depth-induced wave breaking (Fig. 2.10). The relationship with foreshore width is non-linear as well, because of the dependence of wave energy dissipation on wave height.

The required crest height of a coastal dike is strongly related to the wave run-up height under design conditions. Because of the non-linear relation between wave run-up and wave height, the effect of foreshores on the wave run-up height is lower than their effect on the incident wave height. This difference is essential when interpreting

wave attenuation by vegetation and foreshores. Mostly, dikes are designed in such a way that the wave overtopping discharge is limited to a tolerable rate under design conditions. Because of the exponential relation between overtopping discharge and wave height (EurOtop, 2007), the presence of a vegetated foreshore might make the difference between a significant overtopping discharge and full absence of overtopping. The results of these explorative computations highlight the demand for integrating foreshore dimensions as well as vegetation characteristics in the design and assessment of coastal dikes.

2.5. DISCUSSION

This chapter has presented a combination of a literature review, field measurements and numerical modeling of wave attenuation by vegetation under storm conditions. The numerical model has been applied to assess the efficiency of vegetated foreshores in reducing wave loads on coastal dikes under design conditions. In this section, the field measurements and numerical modeling work is discussed. Additionally, attention is paid to the applicability of the results and demands for further research.

2.5.1. FIELD MEASUREMENTS

The field measurements of wave attenuation by vegetation, as described in this chapter, have added to the highest range of wave heights and water depths, as currently available in the literature. These new measurements reduce the gap between measured conditions and design conditions for the flood defenses. The current study is based on measurements of wave attenuation over salt marshes, in combination with computed wave run-up and wave overtopping. Quantification of the effect of vegetated foreshores can be improved when measurements of wave attenuation by vegetation are accompanied by measurements of wave run-up heights and wave overtopping discharges.

2.5.2. MODEL USED

To compute wave loads on coastal dikes with vegetated foreshore in front, a combination of SWAN for the wave transformation over the vegetated foreshore and analytical formulas for wave run-up and wave overtopping has been applied. Both components of this approach limit the applicability of the results to a certain range. SWAN is not able to compute the generation and propagation of infragravity waves, since it is a spectral domain model. At the salt marshes that were included in the calibration study of this research, the fraction of wave energy captured in long waves was very limited (less than 1% during storms). Application of the results of this study is restricted to situations where the wave regime is characterized by local wind sea and swell waves, and the presence of infragravity waves should be of minor importance for the wave loads on the dike. This is the case in many estuaries and coastal seas, where salt marshes are found. If significant infragravity wave energy is to be expected, it is better to use another numerical model,

such as SWASH (Zijlema et al., 2011) or XBeach (Roelvink et al., 2009).

The SWAN model contains approximations for wave energy dissipation by bottom friction and due to vegetation. Both dissipation models are based on linear wave theory, under the assumption of orbital velocity profiles according to linear wave theory. However, bottom friction affects near-bottom orbital velocities, and the presence of vegetation reduces orbital velocities in the submerged canopy. Consequently, the dissipation rates by both mechanisms are interdependent in reality. Higher bottom friction leads to lower dissipation due to vegetation and vice versa. In the SWAN model, their contributions are computed separately and added to the total wave energy dissipation. This methodological error influences model results such as the computed dissipation rates by both mechanisms and the bulk drag coefficient that follows by calibration.

The modeled rate of wave attenuation by vegetation strongly depends on the imposed bulk drag coefficient. In the calibration of the numerical model, a considerable variation in the calibrated drag coefficient was found. Many authors attempt to describe the bulk drag coefficient as a function of the vegetation Reynolds number or the Keulegan Carpenter number. In both quantities, the stem diameter is used as characteristic length scale. Differences in stem diameter is one of the main reasons for the large variation between the expressions that are proposed in the literature (Table 2.2). It is questionable whether such calibrated relations can be applied to vegetation types with significantly other characteristics such as stem diameter and flexibility. Studies that help to explain the physics behind the observed variation in vegetation drag coefficients can be useful in this context.

2.5.3. MORPHOLOGICAL STABILITY

The wave load reduction by vegetated foreshores relies on the stability of both bathymetry and vegetation. The bottom surface of salt marshes consists of consolidated clay and root systems. For such bottoms, significant surface erosion during storms is not to be expected. This is in agreement with post-storm observation (Dijkema et al., 2011; Spencer et al., 2015), large-scale wave flume experiments (Möller et al., 2014) and process descriptions (Winterwerp et al., 2012). The present study shows an additional reason for the stable character of salt marsh sediments. The presence of vegetation prevents intense wave breaking to occur, since the wave energy is dissipated more gradually by the vegetation. As wave breaking can lead to high sediment pick-up rates and severe erosion, this means that vegetation enhances the stable character of the salt marsh surface.

2.5.4. RELIABILITY OF DIKE-FORESHORE SYSTEMS

Before nature-based flood defenses can be considered as full alternatives for conventional flood defenses, they need to be tested according to engineering standards for probability of failure (Van Wesenbeeck et al., 2014). The probability of failure of a flood defense is defined as the probability that the flood defense fails in fulfilling its function:

the protection of social and economic value against flooding. To be able to assess the actual reliability of dike-foreshore systems in terms of a probability of failure, quantification of knowledge uncertainties as well as inherent uncertainties is required, see e.g. Vrijling (2001). The uncertainty in the choice of a suitable vegetation drag coefficient is one of the main knowledge uncertainties involved. This type of uncertainty is distinct from inherent uncertainty, which is related to the natural randomness in samples (Van Gelder, 2000). Examples of the latter include spatial and seasonal variations in vegetation properties. This study is part of the research project BE SAFE. Further research in this project should lead to more insights in the uncertainties regarding wave attenuation by vegetated foreshores.

2.5.5. IMPLICATIONS FOR MANAGEMENT

This study shows that vegetated foreshores with a width of several tens of meters can reduce wave loads on coastal dikes during severe storm significantly. Therefore, dike managers may consider construction or maintenance of vegetated foreshores as a serious supplement to the possibilities for traditional dike reinforcement such as raising the dike crest or strengthening the inner or outer slope revetment. In many deltas, vegetated foreshores such as salt marshes and reed fields are already present along the dikes. In that case, it is probably worth considering to take their influence on wave loads into account in flood risk assessments. Once the foreshores are formally part of the flood defense, the challenge shifts from the design of an appropriate foreshore to the establishment of assessment protocols and institutional arrangements for monitoring and management. The usage of a foreshore as a dike reinforcement strategy might be particularly attractive when a shallow foreshore is already present, or when site-specific conditions impede traditional reinforcements methods.

2.6. CONCLUSIONS

Application of vegetated foreshores has been increasingly mentioned as an effective method to reduce wave heights that act on coastal dikes. However, the efficiency of vegetated foreshores in reducing wave energy under severe storm conditions with high waves and large water depths is not well understood. Most existing empirical studies only quantify wave attenuation for moderate wave conditions in combination with limited water depths. The wave measurements described in this study have added to the range of observations with the highest water depths (up to 2.5 m) and wave heights (up to 0.7 m) presented in the literature so far. The measurements were performed on two salt marshes with two representative but contrasting coastal wetland vegetation types: cordgrass (*Spartina anglica*) and grassweed (*Scirpus maritimus*). The former is found in salty environments, whereas the latter is found in brackish environments. The measurements shed light on wave attenuation by vegetation under severe storm conditions, and have successfully been used to calibrate and validate the numerical model SWAN that

describes wave propagation over vegetated foreshores. It appeared that the observed wave attenuation by vegetation under storm conditions could best be described by a bulk drag coefficient $\widetilde{C}_D \approx 0.4$.

Vegetated foreshores can reduce wave energy during severe storm conditions significantly. Even though energy dissipation by vegetation is most effective at small water depths and with high biomass, the wave energy reduction for larger inundation depths and the vegetation being in winter state is still considerable. Vegetation drag substantially contributes to the total wave energy dissipation. The presence of vegetation leads to an additional reduction rate of the significant wave height of 25-50% with respect to the dissipation by only wave breaking and bottom friction on the sloping transects. Under storm conditions with relatively small wave height to water depth ratios, depth-induced wave breaking on the foreshore is limited, but wave attenuation by vegetation can already be substantial. For larger wave height to water depth ratios, the presence of vegetation prevents intense wave breaking to occur, since the wave energy is dissipated more gradually. The absence of intense wave breaking might contribute to the stable character of the salt marsh sediments.

The calibrated and validated SWAN model has been applied to compute wave height reduction over vegetated foreshores for various foreshore configurations and hydraulic loading conditions. The computed wave conditions at the toe of the dike have been used to determine the efficiency of vegetated foreshores in reducing the wave run-up height on the outer slope of the dike and the wave overtopping discharge over the dike. Both bare foreshores and vegetated foreshores can lead to a major decrease in wave run-up height and wave overtopping discharge when the water depth on the foreshore can be reduced to one or two times the significant wave height. However, when vegetation is present under these conditions, the main dissipation mechanism shifts from intense wave breaking to more gradual dissipation of wave energy due to the vegetation. For larger depths, the relative importance of vegetation increases, since wave energy dissipation by vegetation already acts at lower wave height to water depth ratios than depth-induced wave breaking. This means that vegetation extends the range of water depths for which a foreshore can be applied for effective reduction of wave loads. Bottom friction as well as wave attenuation by vegetation gain relative importance with increasing foreshore width. Since foreshores have a significant effect on wave run-up and overtopping, it is desirable to include the foreshore characteristics in the design and assessment of coastal dikes.

The reduction in wave loads that follows from observations in the field and computations with a calibrated numerical model shows that vegetated foreshores can be considered as a valuable supplement to conventional engineering methods for dike reinforcement.

3

STEM BREAKAGE OF SALT MARSH VEGETATION UNDER WAVE FORCING

ABSTRACT

One of the services provided by coastal ecosystems is wave attenuation by vegetation, and subsequent reduction of wave loads on flood defense structures. Therefore, stability of vegetation under wave forcing is an important factor to consider. This chapter presents a model which determines the wave load that plant stems can withstand before they break or fold. This occurs when wave-induced bending stresses exceed the flexural strength of stems. Flexural strength was determined by means of three-point-bending tests, which were carried out for two common salt marsh species: *Spartina anglica* (common cord-grass) and *Scirpus maritimus* (sea club-rush), at different stages in the seasonal cycle. Plant stability is expressed in terms of a critical orbital velocity, which combines factors that contribute to stability: high flexural strength, large stem diameter, low vegetation height, high flexibility and a low drag coefficient. In order to include stem breakage in the computation of wave attenuation by vegetation, the stem breakage model was implemented in a wave energy balance. A model parameter was calibrated so that the predicted stem breakage corresponded with the wave-induced loss of biomass that occurred in the field. The stability of *Spartina* is significantly higher than that of *Scirpus*, because of its higher strength, shorter stems, and greater flexibility. The model is validated by applying wave flume tests of *Elymus athericus* (sea couch), which produced reasonable results with regards to the threshold of folding and overall stem breakage percentage, despite the high flexibility of this species. Application of the stem break-

This chapter has been published as: Vuik, V., Suh Heo, H. Y., Zhu, Z., Borsje, B. W., & Jonkman, S. N. (2018). Stem breakage of salt marsh vegetation under wave forcing: A field and model study. *Estuarine, Coastal and Shelf Science*, **200**, 41–58.

age model will lead to a more realistic assessment of the role of vegetation for coastal protection.

3.1. INTRODUCTION

Coastal ecosystems, such as salt marshes, mangrove forests and reed swamps, provide a wide range of ecosystem services, including wave attenuation, shoreline stabilization and sediment trapping (Barbier et al., 2011; Duarte et al., 2013). Many studies quantify wave attenuation by vegetation, based on field and laboratory measurements (see Chapter 2 for an overview) or numerical models (Suzuki et al., 2012b; Tang et al., 2015). Its magnitude depends on hydrodynamic parameters, such as wave height (Anderson and Smith, 2014), wave period (Jadhav et al., 2013) and water depth (Paquier et al., 2017), and on vegetation characteristics, such as stem height, diameter and density (Marsooli and Wu, 2014) and flexibility (Luhar and Nepf, 2016; Paul et al., 2016).

The wave attenuation capacity of vegetation varies throughout the year, because of seasonal variations in above-ground biomass (Drake, 1976). One of the factors that drive the variation in biomass, is wave-induced stem breakage of the vegetation. This breakage process varies in time due to seasonal differences in storm frequency and intensity, and a seasonal cycle in the mechanical strength of the stems (Liffen et al., 2013).

Depending on the geographical location, extreme conditions may occur in different seasons. For instance, the Gulf coast of the USA is mainly affected by hurricanes from August to October, whereas coasts around the North Sea in Europe are primarily affected by storm surges between November and February. Vegetation also has its seasonal cycle: above-ground structures of mangroves and tropical seagrasses are present all year-round, while salt marsh plants in temperate climates lose much of their above-ground biomass during the winter (Gallagher, 1983; Koch et al., 2009; Bouma et al., 2014). The coinciding seasonal variations in storm intensity and vegetation characteristics determine to what extent vegetation may contribute to wave load reduction on flood defenses.

Puijalon et al. (2011) describe two strategies of plants to deal with drag forces due to wind or water movement: an avoidance strategy, where plants minimize the encountered forces, or a tolerance strategy, where plants maximize their resistance to breakage. Flexible plant species show an avoidance strategy, minimizing the risk of folding and breakage through reconfiguration. Stiff plants are more efficient in attenuating waves, as they maximize their resistance to stress (Paul et al., 2016), but may break at a certain threshold, which leads to a decline in wave attenuation capacity. A stem will fold or break when the wave-induced bending stress exceeds the stem's strength (Heuner et al., 2015; Silinski et al., 2015). Folding is an irreversible deformation, which leads to a lower effective plant height for wave attenuation. Folded stems may eventually break, and the biomass on the salt marsh decreases. The broken vegetation is frequently found in the form of accumulated debris on dike slopes after storms (Grüne, 2005). Remainders of broken vegetation will only contribute to wave energy reduction by enhancing the

roughness of the bottom compared to non-vegetated surfaces.

Vegetation causes wave attenuation due to the force exerted by the plants on the moving water. Following Newton's third law, the water simultaneously exerts a force equal in magnitude and opposite in direction on the plants. The flexibility of the plants determines how plant motion and wave motion interact, and determines the magnitude of the drag forces (Bouma et al., 2005; Dijkstra and Uittenbogaard, 2010; Mullarney and Henderson, 2010). Luhar and Nepf (2016) propose two dimensionless numbers to describe the motion of flexible vegetation under wave forcing: (1) the Cauchy number C_a, which represents the ratio of the hydrodynamic forcing to the restoring force due to stiffness, and (2) the ratio of the stem height to the wave orbital excursion, L. Plants will stand upright, and act as stiff cylinders, for $C_a < 1$. For $C_a > 1$, the vegetation will start to bend and move in the oscillatory flow. The ratio L determines the characteristics of the plant motion, with swaying motion for $L > 1$, and flattening of the vegetation for $L < 1$. Flattening of the vegetation leads to low flow resistance for a part of the wave cycle.

Several studies show that a significant loss of above-ground biomass can occur during storms (Seymour et al., 1989; Howes et al., 2010). Stem breakage was also observed in large-scale flume experiments on wave attenuation by vegetation (Möller et al., 2014). Recently, Rupprecht et al. (2017) determined the loss of biomass during these experiments, and related it to the measured wave orbital velocities in the canopy. They studied the impact of wave heights in the range of 0.1-0.9 m on two different salt marsh grasses: low-growing and highly flexible *Puccinellia maritima* and more rigid and tall *Elymus athericus*. *Puccinellia* survived even the highest wave forcing without substantial physical damage. This indicates that this species shows an avoidance strategy (Bouma et al., 2010).

Implementation of vegetation into coastal protection schemes is often hampered by a lack of knowledge on how vegetation behaves under extreme storm conditions (Anderson et al., 2011; Vuik et al., 2016). The quantification of wave-induced stem breakage by Rupprecht et al. (2017) is a major step forward in the assessment of the resilience of salt marsh vegetation to storm surge conditions. However, the quantification is purely empirical, and application to other plant species or hydrodynamic conditions is difficult. Further, large-scale flume experiments as in Möller et al. (2014) are expensive and labor-intensive. As a result, we aim to develop a method that predicts the relation between orbital velocity and biomass loss, as a function of plant characteristics such as plant morphology (stem height and diameter) and stem strength. We only consider biomass loss due to stem breakage. Uprooting may be another relevant mechanism, but we did not observe this phenomenon in the field. However, it may be relevant for different species, soil conditions or wave conditions (Liffen et al., 2013).

This chapter presents a model that predicts the wave load that plant stems can withstand before they break or fold. The model compares bending stresses, induced by the

orbital motion under waves, with the flexural strength of stems. Plant stability is expressed in terms of a critical orbital velocity, which combines plant morphology (stem height and diameter) and stem strength. The flexural strength is determined based on three-point bending tests, which were conducted in the laboratory for two common salt marsh species: common cord-grass (*Spartina anglica*) and sea club-rush (*Scirpus maritimus*). Stems were collected from salt marshes at different stages in the seasonal cycle of the plants, to capture the temporal variation in strength. The model is calibrated by relating the loss of biomass that took place on two salt marshes in the Netherlands to the wave conditions that were measured at these marshes over 19 months. Finally, the model is validated by applying flume tests of *Elymus athericus* (sea couch) presented in Rupprecht et al. (2017).

3.2. METHODS AND MATERIALS

3.2.1. FIELD SITES AND PLANT SPECIES

Two salt marshes in the Western Scheldt of the Netherlands were selected as field sites for the wave and vegetation measurements (Fig. 3.1). The first location is Hellegat, where *Spartina anglica* (common cord-grass) is the dominant plant species, and the second is Bath where *Scirpus maritimus* (sea club-rush) is prevalent. The bathymetry of both sites was measured using RTK-DGPS (Leica Viva GS12), see Fig. 3.1.

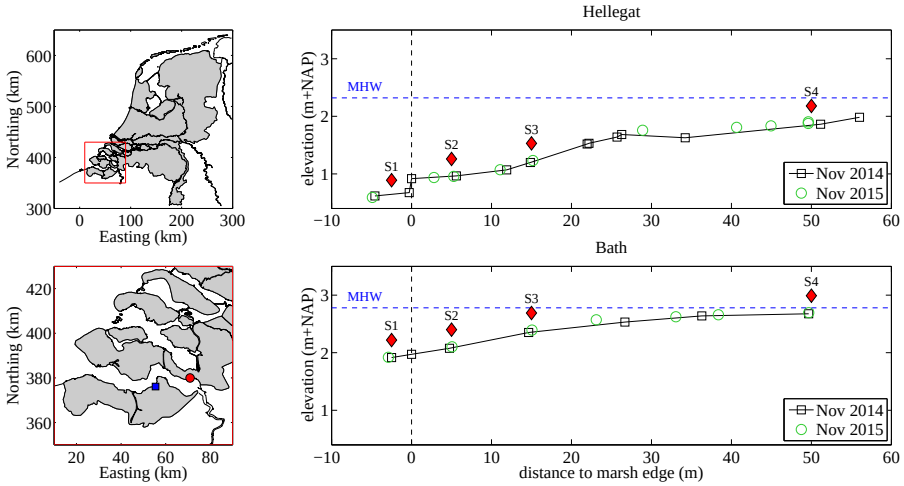

Figure 3.1: *Location of the salt marshes Hellegat (blue square) and Bath (red circle) in the Western Scheldt estuary (lower left) in the Netherlands (upper left), and the bathymetry at the measurement transects at Hellegat (upper right) and Bath (lower right) for November 2014 (black) and November 2015 (green). The position of the 4 wave gauges S1-S4 is indicated by red diamonds. The vertical dashed line is positioned at the marsh edge, the horizontal dashed line at Mean High Water.*

Hellegat is located at the southern shore of the Western Scheldt, and is exposed to

waves from directions between west and north. The marsh edge has an elevation of approximately NAP+1.0 m, where NAP is the Dutch reference level, close to mean sea level. A small cliff of 25 cm height is present at the marsh edge. Landward of the cliff, the bottom is sloping over a distance of approximately 50 m to the higher parts of the marsh, at NAP+2.0 m. The tide in the Western Scheldt leads to a local high water level of NAP+1.6 m at neap tide and up to NAP+2.9 m at spring tide. The highest water levels in the Western Scheldt occur during north-westerly storms in the North Sea region. That implies that Hellegat is regularly exposed to high waves and water levels at the same time. Bath is situated more upstream in the Western Scheldt, along the dike at the northern shore of the estuary, close to the bend towards Antwerp. High water levels in the tidal cycle are higher here, between NAP+1.9 m (neap tide) and NAP+3.4 m (spring tide). This has led to a high salt marsh elevation, sloping from NAP+2.0 m at the marsh edge to NAP+2.7 m at a distance of 50 m from the edge. No cliff is present at the marsh edge here. This marsh is more sheltered compared to Hellegat during north-westerly storms, due to its orientation towards the south-west.

While the salt marsh at Bath is dominated by *Scirpus*, there are also some patches with *Spartina* present (Fig. 3.2). In September, both species are standing up straight to a large extent. The difference in stem density is clearly visible. Especially for *Scirpus*, the start of the decay of the plants in autumn is already visible. In the photo from January, almost all *Scirpus* has disappeared, and only broken stems are remaining. In contrast, in the *Spartina* zone, there is still a lot of biomass present, with a mix of standing and folded stems.

3.2.2. WAVE MEASUREMENTS

Wave attenuation was measured for *Spartina* at Hellegat, and for *Scirpus* at Bath. At both sites, 4 wave gauges (Ocean Sensor Systems, Inc., USA) were deployed over a total distance of 50 m, measured from the marsh edge. One wave gauge (indicated by S1) was placed at 2.5 m in front of the marsh edge. The other gauges were placed at 5 (S2), 15 (S3) and 50 m (S4) in the vegetation. The pressure sensors on the gauges were mounted 10 cm from the bottom. The pressure was recorded with a frequency of 5 Hz over a period of 7 min, every 15 min. Wave energy spectra were determined, using Fast Fourier Transformation, taking into account the attenuation of the pressure signal with depth. A more detailed description of the measurements and processing of the data can be found in Chapter 2, where data was used from the period between November 2014 and January 2015. The present study analyzes wave data for a considerably longer period of 19 months, from November 2014 to May 2016, for which all wave gauges were continuously operational. This enables the analysis of seasonal variations in wave attenuation.

In order to analyze the seasonal differences in wave attenuation by vegetation, the mean wave height reduction between gauges S1 and S4 is computed for each month. However, the wave height reduction does not only depend on vegetation characteristics, but also on the prevalent hydrodynamic conditions such as water depth, wave height

Spartina (left) and *Scirpus* (right), 16 September 2015

Spartina (left) and *Scirpus* (right), 19 January 2017

Figure 3.2: *Photos of Spartina and Scirpus next to each other, in late summer (top) and in winter (bottom). Photos taken by Zhenchang Zhu at Bath.*

and wave period (Tschirky et al., 2001). When simply considering the mean wave height reduction per month, the numbers are strongly influenced by the fact that storms with large water depths and wave heights occur far more frequently in winter than in summer. To eliminate such seasonal differences in storm intensity and frequency, variations in wave attenuation are analyzed for different sea states. Sea states consist of a combination of a wave height range (e.g. 0.1-0.2 m) and a water depth range (e.g. 1.50-1.75 m) at the marsh edge. For all measurements in this range in each month, the average wave height reduction over 50 m transect length $(H_{m0,0} - H_{m0,50})/H_{m0,0}$ is computed. Sea states are selected, based on the criteria of (1) sufficient occurrence in all months and (2) inundation of the full transect (Table 3.1), where the water depth at 50 m in the marsh is 1.28 m and 0.77 m lower than on the mudflat at Hellegat and Bath, respectively.

Table 3.1: *Selected sea states, for which the monthly average wave height reduction over 50 m salt marsh was determined at Hellegat (H) and Bath (B).*

h (m)	H_{m0} (m)		
at mudflat	0.0-0.1	0.1-0.2	0.2-0.3
1.00-1.25	B	B	
1.25-1.50	B	B	
1.50-1.75	H	H	H
1.75-2.00	H	H	H
2.00-2.25	H	H	H

3.2.3. QUANTIFYING VEGETATION STRENGTH

At the two salt marshes, Hellegat and Bath, approximately 20-30 stems of each species were sampled four times in the seasonal cycle: 3 Dec. 2014, 7 Apr. 2015, 11 Sep. 2015 and 4 Nov. 2015 (*Spartina*), and 5 Dec. 2014, 1 Apr. 2015, 4 Sep. 2015 and 4 Nov. 2015 (*Scirpus*). For every stem, the stem diameter at approximately 5 cm from the bottom and the entire stem length were measured and then taken to the lab for further testing. As one of the important steps to quantify stem strength, three-point bending tests of the stems were performed at the Royal Netherlands Institute for Sea Research (NIOZ).

Conventionally, the three-point bending test is used to find the stress-strain relationship of a material in structural mechanics (or ecology), which in particular, focuses on the initial deflection behavior with a small amount of applied force (Usherwood et al., 1997; Dijkstra and Uittenbogaard, 2010; Miler et al., 2012; Paul et al., 2014; Rupprecht et al., 2015). However, this research considers the extreme situation when the stress-strain relation of the material (stem) is no longer linear and reaches its maximum flexural stress (Fig. 3.4). The stem is considered to break or fold when it reaches this maximum bending stress which is defined as the individual stem's flexural strength. This strength is determined for the bottom 5-10 cm of the stems (5cm for *Spartina* and 10 cm for *Scirpus*), as this is the location where the stems of both species normally break (see Fig. 3.2 and the information in Section 3.2.7). The stem density was measured by counting the number of standing stems in 10 sample areas of 25*25 cm at both Hellegat and Bath: 5 sample areas high in the marsh, and 5 close to the marsh edge.

For the hollow stemmed *Spartina*, the outer and inner diameter of each stem were measured with an electronic caliper (precision ± 0.5 mm), and the three-point bending test device's span length was fixed to 40 mm, resulting in a stem-diameter-to-span-length ratio between 1:10 and 1:14. *Scirpus* is not hollow, and the length of the three sides of the triangular cross-section was measured with the electronic caliper. In order to minimize the effect of shear stress, a maximum stem-diameter-to-span-length ratio of 1:15 was chosen for *Scirpus*. The three-point bending test's span length was adjusted to 15 times the mean side length. The bending tests were performed with an Instron EMSYSL7049 flexure test machine (precision ± 0.5%) using a 10 kN load cell (Instron Corporation, Canton, MA, USA) (Fig. 3.3). The stem test section was placed centrally onto two

supporting pins, and a third loading pin was lowered from above at a rate of 10 mm/min. The vertical deflection of the stem and the corresponding force were recorded.

Figure 3.3: *The Instron three-point bending test device*

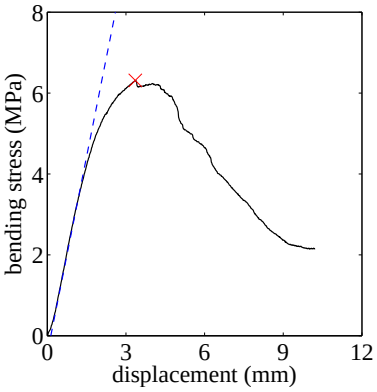

Figure 3.4: *Example of a stress-strain relation (solid black line) from results of a three-point bending test. Young's modulus (E) and flexural rigidity (EI) can be calculated from the slope of the initial linear part (blue dashed line). The plant breaks or folds when the line reaches its maximum bending stress, indicated with a red marker. This stress-strain relation is representative for many vegetation species including Spartina anglica and Scirpus maritimus.*

The flexural strength of the stem, expressed in terms of bending stress, is calculated by standard formulas in structural mechanics. The maximum tolerable bending stress

σ_{max} (Nm^{-2}) is calculated as

$$\sigma_{max} = M_{max} y / I, \tag{3.1}$$

where M_{max} is the maximum moment (Nm); y is the cross-sectional distance from the center of the cross-section to the convex surface (m), and I is the area moment of inertia (m^4). The maximum moment, $M_{max} = (1/4) F_{max} L_{span}$, is a function of the maximum force F_{max} (N) and the testing device's span length L_{span} (m). The two species studied in this research, *Spartina* and *Scirpus*, have different cross-sectional stem geometries. As a result, the cross-sectional distance and area moment of inertia are quantified differently (Fig. 3.5). Here, the stem diameter is indicated as b_v, and for vegetation with a hollow stem (*Spartina*), the inner diameter is represented as $b_{v,in}$.

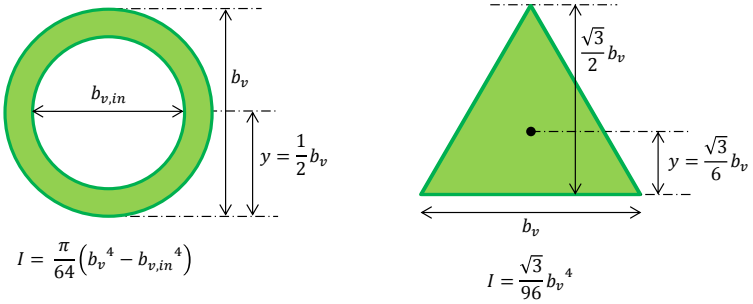

Figure 3.5: *The stem cross-section of Spartina anglica and Scirpus maritimus. Spartina anglica has a hollow circular stem (left panel), whereas Scirpus maritimus has a solid triangular stem, which is assumed to be equilateral (right panel). Formulas for calculating y (cross-sectional distance from center to convex surface) and I (area moment of inertia) are based on the stem geometry.*

Formulas for M_{max}, y and I (Fig. 3.5) are substituted in Eq. (3.1). The resulting flexural strength of the hollow, circular stems of *Spartina* is then expressed as

$$\sigma_{max,cir} = \frac{8 F_{max} L_{span} b_v}{\pi \left({b_v}^4 - {b_{v,in}}^4\right)}, \tag{3.2}$$

and for the triangular stems of *Scirpus* as

$$\sigma_{max,tri} = \frac{4 F_{max} L_{span}}{{b_v}^3}. \tag{3.3}$$

Mean values and standard deviations for the different parameters are determined for the sample locations close to the marsh edge and higher in the marsh separately. After that, the average mean value and average standard deviation are computed, and presented here. This means that the presented standard deviations reflect the average in-sample variation, rather than the inter-sample variation in vegetation properties.

3.2.4. QUANTIFYING WAVE-INDUCED BENDING STRESS

The amount of wave load acting on the stem is also quantified in terms of bending stress, in order to be comparable to the flexural strength. In Fig. 3.6 (left), vegetation is first schematized as a standing, cantilevering beam attached to a fixed bottom with a uniform horizontal load acting on the entire length of the stem.

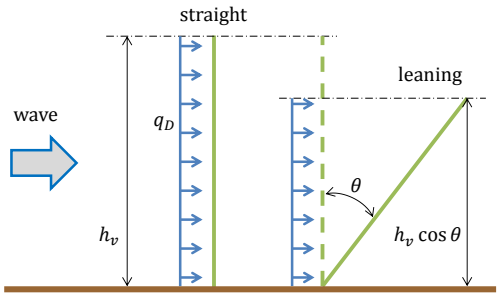

Figure 3.6: *The stem standing up straight (left) represents the preliminary consideration where the entire height of the stem (h_v) experiences the uniform horizontal wave loading. The leaning stem (right) represents the more realistic case, with a leaning angle θ which experiences a smaller horizontal wave load along the height of $h_v \cos\theta$.*

In such case, the critical bending stress at the bottom of the stem can be expressed as

$$\sigma_{wave} = \frac{q_D(\alpha h)^2 y}{2I}, \tag{3.4}$$

from standard structural mechanics (Gere and Goodno, 2013). Here, q_D is the drag force per unit plant height (N/m) and $\alpha = \min(h_v/h, 1)$ is the stem height h_v relative to the water depth h, maximized to 1 for emergent conditions. The drag force q_D is assumed to be uniform along the plant height which is in line with shallow water wave conditions.

In the wave-induced stress equation (σ_{wave}), stem height h_v and diameter b_v are known from field measurements, and the area moment of inertia I can be calculated based on the stem geometry and diameter (Fig. 3.5). The uniform wave load q_D is calculated by modifying the Morison-type equation F_x, previously used by Dalrymple et al. (1984) and Kobayashi et al. (1993). When dividing the Morison-type equation F_x by the stem density N_v (stems/m^2), this yields the uniform wave load q_D, which is expressed in terms of force per unit area per unit height (Nm^{-2}m^{-1}) as

$$q_D = \frac{F_x}{N_v} = \frac{1}{2}\rho C_D b_v u|u|, \tag{3.5}$$

where C_D is the drag coefficient (-), ρ the density of water (kg/m^3), and u is the horizontal orbital velocity of waves (m/s). The uniform horizontal wave load q_D yields the force per unit length of stem. Under shallow water conditions, the orbital velocity is expressed in terms of wave height H (m), water depth h (m) and gravitational acceleration g (m/s^2)

as $u = 0.5H\sqrt{g/h}$. Substituting the expressions for q_D and u into Eq. (3.4), the wave-induced bending stress at the bottom of the stem can be described with vegetation and wave parameters for circular and triangular stems.

There is no information available to identify which individual wave from the random wave field leads to stem breakage. However, it makes sense that it should represent the forces exerted by the highest fraction of the waves. Therefore, we assume that the mean of the highest one-tenth of waves breaks the stems ($H = H_{1/10}$). This measure is related to the significant wave height H_{m0} (=mean of the highest one-third of waves) via $H_{1/10} = 1.27H_{m0}$, assuming a Rayleigh distribution. The possible bias caused by this assumption will influence the results of the model calibration.

A correction factor is needed for the wave-induced load to take into account uncertainties involved in the selection of $H_{1/10}$, and in physical processes that are not explicitly included in the equations, such as fatigue and reduction of orbital velocities in the canopy. The equations for wave load are multiplied with an adjustable correction factor A_c, to account for such processes. The correction factors are calibrated for both species based on the amount of breakage in response to wave action in the field. Stem leaning and bending will be implemented as a separate factor, which will be discussed next.

Prior to calibrating the correction factor, the known but neglected process of stem leaning is assessed. So far, for the quantification of stem strength and wave-induced stress, the stem was assumed to be a relatively stiff beam standing up straight (90° from the sea bed). However, in reality the stems are quite flexible. This flexibility not only serves to reduce the amount of wave forcing but also prevents the weakest point along the stem (susceptible to breaking) from being directly exposed to strong wave forces.

The stem leaning angle varies widely depending on the combined direction and strength of the wave. However, in this research one representative leaning angle is chosen for each species based on field observations and its respective flexural rigidity (EI). From observations of Silinski et al. (2015), adult *Scirpus* has a maximum observed leaning angle of $\theta = 15°$ for short-period (2 s) waves and $\theta = 40°$ for long-period (10 s) waves. Wave peak periods at Bath are in the order of 3-4 s during storms, which is in between the two extremes of Silinski et al. Therefore, a leaning angle of 30° will be used in this research for *Scirpus*. Bouma et al. (2005) gives a maximum leaning angle of $\theta = 51°$ for *Spartina*, which is a larger angle than that of *Scirpus*. This is in line with the smaller flexural rigidity (EI) of *Spartina* (1000-4000 Nmm^2 in Rupprecht et al. (2015), 2100 ± 1000 Nmm^2 in the current study, Table 3.3), compared to *Scirpus* (40,000-50,000 Nmm^2 in Silinski et al. (2015), 52,000 ± 35,000 Nmm^2 in the current study, Table 3.4) With the maximum leaning angle (θ) for each species, the wave load is corrected by multiplying it with $\cos^2\theta$, as the submerged vegetation height ($h_v = \alpha h$) is squared as can be seen in Eq. (3.4).

The resulting wave-induced stress in shallow water wave conditions for the hollow, circular stems of *Spartina* is then expressed as

$$\sigma_{wave,cir} = 2A_c\rho g C_D \left(\frac{b_v^2(\alpha h)^2\cos^2\theta}{\pi\left(b_v^4 - b_{v,in}^4\right)}\right)\left(\frac{H_{1/10}^2}{h}\right), \tag{3.6}$$

and in the solid triangular stems of *Scirpus* as

$$\sigma_{wave,tri} = A_c\rho g C_D \left(\frac{(\alpha h)^2\cos^2\theta}{b_v^2}\right)\left(\frac{H_{1/10}^2}{h}\right). \tag{3.7}$$

3.2.5. DEFINITION OF VEGETATION STABILITY

Stem folding or breaking is identified as the point when the wave-induced bending stress exceeds the stem's flexural strength. The stability of vegetation under wave forcing can be investigated by comparing flexural strength σ_{max} (Eq. (3.2) or Eq. (3.3)) with the corresponding wave-induced stress σ_{wave} (Eq. (3.6) or Eq. (3.7)) for *Spartina* and *Scirpus*, respectively.

By combining the Eqs. (3.4) and (3.5), and including the leaning factor $\cos^2\theta$ and correction factor A_c, the critical orbital velocity for the circular stems of *Spartina* can be expressed as

$$u_{crit,cir} = \sqrt{\frac{\sigma_{max}\pi\left(b_v^4 - b_{v,in}^4\right)}{8A_c\rho C_D b_v^2(\alpha h)^2 cos^2\theta}}, \tag{3.8}$$

and for the triangular stems of *Scirpus* as

$$u_{crit,tri} = \sqrt{\frac{\sigma_{max}b_v^2}{4A_c\rho C_D(\alpha h)^2 cos^2\theta}}. \tag{3.9}$$

A higher critical orbital velocity indicates that the stem is more stable at a given location. Factors that contribute to stability are larger flexural strength (σ_{max}), smaller drag coefficient (C_D), and smaller correction factor (A_c). Further, vegetation parameters such as a large diameter (b_v), a small height ($h_v = \alpha h$), and a large leaning angle (θ) contribute to the stability by reducing the amount of wave force acting on the stem. The critical orbital velocity can be compared with an actual amplitude of the horizontal orbital velocity in the canopy, which is described by linear wave theory, based on water depth h, wave height H and wave period T via

$$u(z) = \frac{\omega H}{2}\frac{\cosh(k(z+h))}{\sinh(kh)}, \tag{3.10}$$

where $\omega = 2\pi/T$ is the angular wave frequency (rad/s), z the distance from the water surface (positive upward), with $z = -h$ at the bottom (m), and k the wave number (rad/m). The comparison between critical and actual orbital velocity indicates if the stems will break under the local storm conditions. The set of equations to determine wave-induced and critical orbital velocities is referred to as the stem breakage model.

3.2.6. IMPLEMENTATION IN A WAVE ENERGY BALANCE

Stems do not all break at the same wave conditions, as waves will predominantly break the weaker stems, see e.g. Rupprecht et al. (2017). Therefore, stem breakage will affect the stem density N_v, which subsequently influences wave energy dissipation by vegetation (Mendez and Losada, 2004). Stem breakage is applied to the quantification of wave height transformation over vegetated foreshores by means of a one-dimensional wave energy balance:

$$\frac{dEc_g}{dx} = -(\epsilon_b + \epsilon_f + \epsilon_v), \tag{3.11}$$

where $E = (1/8)\rho g H_{rms}^2$ is the wave energy density (J/m^2), $H_{rms} = H_{m0}/\sqrt{2}$ the root mean square wave height (m), c_g the group velocity, with which the wave energy propagates (m/s), x the distance along the transect (m), measured from the marsh edge, and on the right hand side wave energy dissipation (Jm^{-2}s^{-1}) due to wave breaking (ϵ_b), bottom friction (ϵ_f) and vegetation (ϵ_v).

For energy dissipation by breaking (ϵ_b), the formula of Battjes and Janssen (1978) is used, with the relation between the breaker index γ and the wave steepness according to Battjes and Stive (1985). Energy dissipation by bottom friction (ϵ_f) is described by the formulation of Madsen et al. (1988), where a relatively high Nikuradse roughness length scale of $k_N = 0.05$ m is used to account for the rough understory.

Energy dissipation by vegetation (ϵ_v) is based on the formula of Mendez and Losada (2004). These model descriptions correspond with the selection of energy dissipation formulations in the spectral wave model SWAN (Booij et al., 1999). Along vegetated foreshores, wave energy is strongly related to the wave energy dissipation due to vegetation. This dissipation mechanism is dominant for the two salt marshes under consideration, even under storm conditions (see Chapter 2). The formula for wave energy dissipation by vegetation of Mendez and Losada (2004) reads

$$\epsilon_v = \frac{1}{2\sqrt{\pi}} \rho C_D b_v N_v \left(\frac{kg}{2\omega}\right)^3 \frac{\sinh^3 k\alpha h + 3\sinh k\alpha h}{3k\cosh^3 kh} H_{rms}^3. \tag{3.12}$$

Here, it can be seen that vegetation parameters (b_v, N_v, h_v) affect the amount of wave energy dissipation. Stem breakage in particular affects the stem density N_v and height $h_v = \alpha h$, which is thus implemented in the wave energy balance, Eq. (3.11). The energy balance is discretized, using a simple first order numerical scheme with a grid cell size $\Delta x = 1.0$ m. The stem breakage model is evaluated in each computational grid cell. If the orbital velocity, Eq. (3.10), exceeds the stem's critical orbital velocity, Eq. (3.8) or (3.9), the stem height in the grid cell is reduced from h_v to a height of broken stems $h_{v,br}$. Such a reduction in stem height will subsequently influence the amount of wave height reduction.

The stem height reduction can be applied to all N_v stems per m^2 in the grid cell, solely based on the mean values for the vegetation characteristics. However, using sin-

gle average values does not take into account the variation in strength, height and diameter of the stems, which leads to a fraction of broken stems (Rupprecht et al., 2017). Therefore, instead of using one deterministic value, a Monte Carlo simulation is performed in each grid cell by drawing 1000 random samples from the probability distributions of σ_{max}, h_v and b_v, taking into account the correlations between these 3 variables. The fraction of broken stems f_{br} is equal to the fraction of the 1000 samples in which $u > u_{crit}$. This approach leads to a mix of broken stems (stem density $f_{br}N_v$, stem height $h_{v,br}$) and standing stems (stem density $(1 - f_{br})N_v$, stem height h_v), see Fig. 3.7. The total wave energy dissipation by vegetation is equal to the sum of the contributions by standing and broken stems. This superposition of dissipation rates is based on the assumption that orbital velocities in the bottom layer with broken stems are only weakly affected by the presence of the standing stems. This assumption is supported by the work of Weitzman et al. (2015), who found that the biomass of a low, secondary species in a multi-specific canopy significantly increases the attenuation of current- and wave-driven velocities.

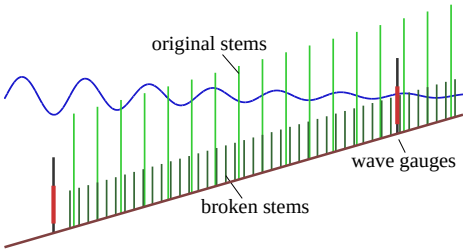

Figure 3.7: *Schematization of the breakage process. The original vegetation is shown in green, broken stems in darker green. The positions of the two wave gauges are indicated in red. A uniform fraction of broken stems is applied.*

A Gaussian distribution is applied for h_v and b_v, whereas a log-normal distribution is used for σ_{max} (Fig. 3.11). By choosing a log-normal distribution for σ_{max}, a positive number is guaranteed despite its large coefficient of variation (which is the ratio of standard deviation over mean value, σ/μ). In case of a small variation, the log-normal distribution resembles the Gaussian distribution. In addition, Pearson's correlation coefficients ρ between the 3 variables are incorporated to draw realistic combinations (Fig. 3.11). These correlation coefficients are determined for the sample locations close to the marsh edge and higher in the marsh separately. After that, the correlation coefficients are averaged over both sampling locations, and presented here. This means that the correlation coefficients reflect the average in-sample co-variation. The dependencies between the variables are included by drawing 1000 random numbers between 0 and 1 from a Gaussian copula with correlation coefficients based on the samples, collected from the salt marshes. Realizations for h_v, b_v and σ_{max} are calculated by sub-

stituting the 1000 random numbers into the inverse probability distributions of these 3 variables.

3.2.7. QUANTIFICATION OF STEM BREAKAGE IN THE FIELD

In order to investigate the validity of the stem breakage model, the results of the model are compared with observations of the stem breakage process in the field. However, the available vegetation measurements have an insufficient frequency, accuracy and spatial extent to reveal the response of the stem density to wave action. This makes a one-to-one comparison between wave conditions and stem density reduction impossible.

Alternatively, differences in stem density on the marsh are estimated from differences in wave attenuation. That means that the effect (wave attenuation) is observed, and the cause (stem density) is computed. Variations in wave attenuation are caused by variations in biomass on the salt marshes, since the bathymetry can be considered static at this time scale (see the limited difference in bed level in Fig. 3.1). As shown in Chapter 2, the presence of vegetation prevents wave breaking from occurring. Therefore, the observed differences in wave height reduction should be primarily attributed to differences in the vegetation on the marsh. The reconstructed variation of the stem density in time is used as data source in Section 3.2.8, to calibrate the correction factor A_c in the stem breakage model, Eqs. (3.8) and (3.9).

The approach to compute the fraction of broken stems in the field is shown in the left part of the flow chart in Fig. 3.8. The data underlying the analysis consists of the aforementioned wave data {1} and vegetation data {2}. The average wave height reduction over 50 m salt marsh is calculated for each month, for different combinations of water depth and wave height at the marsh edge {4}.

Before the wave energy balance can be applied, the drag coefficient C_D in Eq. (3.12) has to be defined {3}. The measured stem height, diameter and density for September 2015 are introduced in the model, for both sites and species. For the wave data, one period of non-stop wave measurements is used, from 16 July to 23 September 2015. A period of this length is required to include sufficient events with high waves in the time series. For each 15 minute time frame within this measurement period, the wave height reduction is modeled for a range of drag coefficients, from 0.0 to 5.0 with regular increments of 0.2. The drag coefficient in this range that leads to the best reproduction of the observed wave height reduction is selected, and related to the vegetation Reynolds number Re for the same 15 minute period.

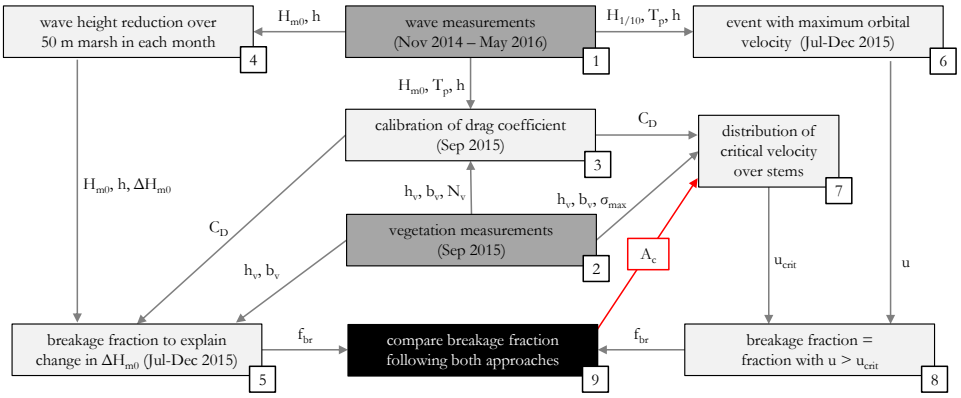

Figure 3.8: *Flow chart of the approach to calibrate the stem breakage model, which explains how data sources (dark gray) and modeling steps (light gray) interact. Numbers in the flow chart refer to numbers* {1} *to* {8} *mentioned in the text. The aim of the calibration (black box) is to choose the correction factor* A_c *in such way, that the breakage fraction modeled with the stem breakage model* {8} *equals the breakage fraction based on observations of the wave attenuation in the field* {5}.

The vegetation Reynolds number is defined as follows, see e.g. Méndez et al. (1999):

$$Re = \frac{ub_v}{\nu}, \tag{3.13}$$

where u is the orbital velocity at the marsh edge, halfway up the stem height ($z = -h + h_v/2$), computed with Eq. (3.10), and ν is the kinematic viscosity of water ($\approx 1.2 \cdot 10^{-6}$ m^2/s). Finally, a relation between Re and C_D is determined (assuming that the drag coefficient C_D is equal to the bulk drag coefficient $\widetilde{C}_D$ based on calibration of wave energy dissipation). Following Méndez et al. (1999); Paul and Amos (2011); Hu et al. (2014) and others, the following type of equation is used:

$$C_D = a + \left(\frac{b}{Re}\right)^c, \tag{3.14}$$

in which the parameters a, b and c are found by non-linear curve-fitting. This equation is fitted through the (Re,C_D) combinations for all 15 minute periods.

The wave energy balance, Eq. (3.11), is used to determine a time-varying fraction of broken stems f_{br}, which leads to the best reproduction of the wave height reduction over the Hellegat and Bath transects in each month {5}. The parameters stem height h_v, stem diameter b_v and the drag coefficient C_D according to Eq. (3.14) are based on the data set of September 2015, since this data is considered to be representative for the vegetation at the end of the summer. The data of September 2015 represents the properties of all stems, whereas the November 2015 or December 2014 samples only contain the subset of the stems that withstood the wave loads until November or December. The April 2015

data is not useful for this purpose, since the plants did not reach their full length yet. The bathymetry of November 2014 is included for both sites (Fig. 3.1). Vegetation does not change in height or diameter anymore from September onward. Therefore, the assumption is made that the vegetation in autumn consists of a mix of original long stems with September properties, and broken short stems, with a time-varying ratio between these two states.

The maximum wave height reduction occurs in summer, in June (*Scirpus*) or July (*Spartina*). It is assumed that all stems are standing upright at that time ($f_{br} = 0$), and the stem density N_v in these months is chosen in such way that the computed wave height reduction is equal to the measured reduction. For all other months, a fraction of this N_v stems is assumed to break, and a value $f_{br} > 0$ is computed for the 50 m salt marsh, to match the differences in wave height reduction throughout the year. These values of f_{br} are determined for each sea state of Table 3.1, and finally averaged over all sea states to obtain a robust value for each month.

A length of broken stems $h_{v,br}$ has to be specified to perform these computations. In December 2014, samples from *Scirpus* were collected near the marsh edge at Bath, where the vegetation was largely broken. 2/3 of the stems were lower than 20 cm, with a mean height of 10.4 cm. Therefore, $h_{v,br} = 0.10$ m is chosen for *Scirpus*. For *Spartina*, such samples were not available, but visual observations showed that this height is shorter than for *Scirpus* (see Fig 3.2). Therefore, a value of $h_{v,br} = 0.05$ m is selected. A sensitivity analysis has been carried out (not shown here), and the response of the correction factor A_c in the stem breakage model to a change of $h_{v,br}$ by a factor 2 was only 8%. So the exact choice of $h_{v,br}$ does not make a significant difference in case of *Spartina*.

3.2.8. MODEL CALIBRATION

The approach to calibrate the stem breakage model is shown on the right hand side of the flow chart in Fig. 3.8. The reconstructed fraction of broken stems (left hand side of the flow chart) is used as data source for the calibration. The period from June (*Scirpus*) or July (*Spartina*) to December 2015 is chosen for the calibration. June and July are the months with the maximum stem density, for which $f_{br} = 0$ is assumed. December 2015 was a relatively quiet month after a period with multiple storms in November, which had resulted in substantial (but not complete) stem breakage. Stems will break gradually during consecutive storm events. The standing stems at each point in time have a higher stability than required to withstand the most severe storm so far. Therefore, the total amount of broken stems in December 2015 is attributed to the event with the highest orbital velocity at 50 m in the marsh {6}. This event occurred on 28 November 2015 at Hellegat, with the following conditions at the marsh edge: $H_{m0} = 0.57$ m, $H_{1/10} = 0.72$ m, $T_p = 3.8$ s, $h = 3.0$ m, and the orbital velocity based on $H_{1/10}$ was $u = 0.52$ m/s. This orbital velocity is determined at halfway height of the stems. At Bath, the event with the highest orbital velocity occurred on 30 November 2015, with the following conditions at the marsh edge: $H_{m0} = 0.59$ m, $H_{1/10} = 0.75$ m, $T_p = 3.5$ s, $h = 1.6$ m, and $u = 0.79$ m/s.

In the right part of the flow chart, the stability-related vegetation characteristics, such as the flexural strength are introduced. The stems in the field vary in stability because of differences in length h_v, diameter b_v and flexural strength σ_{max}. This leads to a variation in the critical orbital velocity u_{crit} within the vegetation {7}, which is expressed in terms of a probability distribution. Correlation coefficients between stem height, diameter and strength are included to obtain a realistic distribution, as described before. The vegetation samples and three-point-bending tests from September 2015 are used for this purpose, for the same reasons as explained in Section 3.2.7. The fraction of broken stems is equal to the fraction of stems for which $u_{crit} < u$ {8}. The drag coefficient in the equations is based on the Reynolds number at the marsh edge, using Eq. (3.14).

The hydraulic conditions in the selected event are applied as boundary conditions in the wave energy balance, at the marsh edge of Hellegat and Bath. In each grid cell, a fraction of broken stems f_{br} is determined, by comparing the local wave orbital velocity with the distribution of the critical orbital velocity. The wave attenuation in this grid cell is based on the sum of the contributions by $(1 - f_{br})N_v$ standing stems and $f_{br}N_v$ broken stems. Finally, one average value of f_{br} is determined over all grid cells in the 50 m long transects of Fig. 3.1 with salt marsh vegetation. This value is compared with the estimated fraction of broken stems based on the wave attenuation in December {9}. The value of the correction factor A_c is set at the point when the fractions of broken stems according to both approaches are identical.

Since the correction factors A_c are known after the calibration, a critical orbital velocity can be determined for each sampled stem. The drag coefficient C_D in the expressions is determined iteratively via Eq (3.14) at $Re = u_{crit}b_v/\nu$. After that, a mean value and a standard deviation of u_{crit} are determined for each month with vegetation data.

3.2.9. MODEL VALIDATION

For model validation, the results of Rupprecht et al. (2017) for *Elymus athericus* (sea couch) are used. *Elymus* is a tall grass (70-80 cm), with thin stems (1-2 mm) and a high flexibility. The work of Rupprecht et al. (2017) was part of the Hydralab project, in which the interaction between salt marsh vegetation and waves was tested in a large-scale wave flume. Their paper gives a description of percentages of broken stems after several tests. For each tests, the statistics of the orbital velocity are available. Here, we validate the stem breakage model by comparing measured stem breakage fractions with the breakage fractions according to the stem breakage model. First, a mean and standard deviation of the critical orbital velocity are computed, based on the vegetation characteristics of the *Elymus*. After that, a breakage fraction is determined, which is the fraction of stems with a critical velocity lower than the mean value of the 10% highest orbital velocities ($u_{1/10}$, analogue to $H_{1/10}$), observed in the flume.

Since the flexible *Elymus* vegetation exhibits extreme leaning angles of more than 80 degrees, skin friction may significantly contribute to the forces on the plant. Form drag works over the reduced effective canopy height of roughly $h_{v,r} = 10$ cm, while a

shear stress works over the full length h_v of the leaning stems (60-70 cm). Therefore, we add a friction term to the equations for the critical orbital velocity. The force due to friction equals

$$F_F = \frac{1}{2} C_f \rho u^2 A, \tag{3.15}$$

where A is the cylindrical surface area over which the friction works, which is $\pi b_v (h_v - h_{v,r})$. We schematize the forces acting on the vegetation as in Fig. 3.9, with a reduced vegetation height, and the higher part of the stems leaning horizontally in the flow. This schematization is based on photos of leaning *Elymus* in Rupprecht et al. (2017). These photos are also used to estimate that $h_{v,r} = 9$ cm in the situation just before the stems start to fold and break.

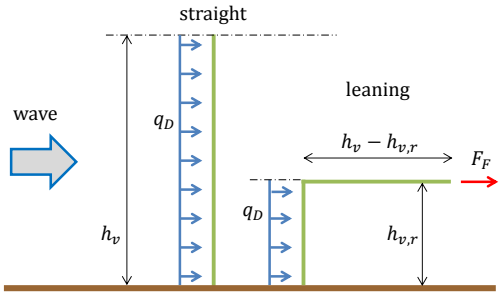

Figure 3.9: *Schematized representation of forces working on Elymus at extreme leaning angles, with a drag force acting on a reduced canopy height $h_{v,r}$, and a shear stress working over the horizontal part of the stem, which results in a friction force F_F that works as a point load at height $h_{v,r}$.*

This results in an adaptation to the expression for the critical velocity, Eq (3.8), which reads

$$u_{crit,cir} = \sqrt{\frac{\sigma_{max}\pi\left(b_v^4 - b_{v,in}^4\right)}{8A_c\rho b_v^2\left[C_D h_{v,r}^2 + 2\pi C_f (h_v - h_{v,r}) h_{v,r}\right]}}, \tag{3.16}$$

where h_v is the full length (m) of the plant stems, $h_{v,r}$ is the reduced height (m) of the canopy after leaning and bending, and C_f is the friction coefficient, which is set to 0.01, as in Luhar and Nepf (2011).

Application of the relation between Reynolds number and drag coefficient as proposed in Möller et al. (2014) leads to a drag coefficient C_D in the order of 0.2-0.3. This is a bulk drag coefficient, which is based on wave model calibration. Its value is strongly influenced by the rigid cylinder approximation of the highly flexible vegetation, in which the full stem length is used as effective vegetation height. Therefore, this bulk drag coefficient is not representative for the maximum force that works on the vegetation. In this

validation, C_D is set to 1.0, which is a characteristic value for drag forces on cylinders in wave motion (Hu et al., 2014).

From the considered plant species in this studies, the thinner and more flexible *Spartina* (EI≈2000 Nmm^2, see Table 3.3) comes closer to *Elymus* (EI≈300 Nmm^2, see Rupprecht et al. (2017)) than *Scirpus* (EI≈50,000 Nmm^2, see Table 3.4). Therefore, we apply the value of A_c that follows from the calibration for *Spartina*. Rupprecht et al. (2017) has presented the elasticity modulus E (2696 ± 1964 MPa) and flexural rigidity EI (299 ± 184 Nmm^2) of the stems, based on three-point-bending tests. However, the flexural strength σ_{max} (MPa) was not available. Therefore, we have analyzed the original data from these bending tests, and found that the flexural strength was 40 ± 28 MPa (sample size: 18 stems).

For each of the 18 sampled stems, the critical orbital velocity was computed using Eq. (3.16). This leads to a mean value and standard deviation of the critical orbital velocity. For each flume test, a mean and standard deviation of the measured orbital velocity is given in Rupprecht et al. (2017). Based on these normal distributions, a mean value is determined for the highest 10% of the orbital velocities ($u_{1/10}$). The computed fraction of broken stems f_{br} is equal to the fraction of stems for which the critical orbital velocity is lower than the actual orbital velocity $u_{1/10}$. These computed values are compared with the measurements of stem breakage.

3.3. RESULTS

3.3.1. SEASONAL VARIATIONS IN WAVE ATTENUATION

The wave height reduction over the salt marsh varies over the seasons. A selection is made of 4 storm events that have occurred in summer and winter respectively, for which water depth and wave conditions at the marsh edge were nearly identical (Table 3.2).

The ratio of wave height to water depth H_{m0}/h is chosen to illustrate the influence of vegetation on the wave height. For the storm of 25-07-2015 at Hellegat, H_{m0}/h decreases from 0.24 at gauge S1 (near the marsh edge) to 0.15 at gauge S4 (at 50 m in the marsh) due to the presence of dense *Spartina* vegetation (Chapter 2). In autumn (18-11-2015), this ratio is at S4 close to the value at S1, while in early spring (02-03-2016 and 26-04-2016), an increase over the salt marsh is visible, and the ratio of 0.31-0.33 approaches the limit for depth-induced wave breaking (e.g., Nelson (1994)). These results show a clear seasonal difference, as the greater decrease in this ratio in summer signifies stronger wave attenuation by vegetation. The same pattern is visible for *Scirpus* at Bath. In late spring, the wave height to water depth ratio at gauge S4 (19-05-2015, 0.07) is approximately half of this ratio in any other season (0.12-0.15).

Storm events such as in Table 3.2 do not occur in every month. Therefore, less energetic sea states were selected to analyze seasonal variations in wave attenuation for comparable wave height and water depth. Fig. 3.10 shows how the wave height reduction varies over the months at Hellegat (top panel) and Bath (lower panel).

Table 3.2: *Seasonal variations in the ratio of significant wave height H_{m0} over water depth h at gauge S4, 50 m in the salt marsh, for 4 events with nearly identical water level ζ, water depth h, significant wave height H_{m0} and wave peak period T_p at gauge S1 at Hellegat (top) and Bath (bottom).*

date		25-07-2015	18-11-2015	02-03-2016	26-04-2016
ζ (S1)	m+NAP	2.57	2.57	2.57	2.58
h (S1)	m	1.97	1.99	1.97	1.95
h (S4)	m	0.73	0.69	0.72	0.76
H_{m0} (S1)	m	0.47	0.48	0.46	0.47
H_{m0} (S4)	m	0.11	0.16	0.22	0.25
T_p (S1)	s	3.18	3.18	2.99	2.83
H_{m0}/h (S1)	-	0.24	0.24	0.23	0.24
H_{m0}/h (S4)	-	0.15	0.23	0.31	0.33

date		23-12-2014	19-05-2015	28-11-2015	26-04-2016
ζ (S1)	m+NAP	3.40	3.43	3.44	3.44
h (S1)	m	1.49	1.52	1.49	1.53
h (S4)	m	0.73	0.76	0.76	0.75
H_{m0} (S1)	m	0.27	0.28	0.30	0.27
H_{m0} (S4)	m	0.11	0.05	0.09	0.09
T_p (S1)	s	2.44	2.18	2.18	2.56
H_{m0}/h (S1)	-	0.18	0.18	0.20	0.18
H_{m0}/h (S4)	-	0.15	0.07	0.12	0.12

The highest wave attenuation by *Spartina* at Hellegat (Fig. 3.10, top panel) was observed in summer, roughly from May to September. In autumn and winter, the wave attenuation gradually decreased from September to a minimum in March. In spring, new shoots started growing, leading to a rapid increase in wave attenuation from March to May. The salt marsh at Bath with *Scirpus* (Fig. 3.10, lower panel) showed similar trends as that of Hellegat, but because of the smaller number of inundations, the results for Bath display larger variations compared to Hellegat. The minimum wave height reduction was found in winter, in the months January, February and March.

3.3.2. SEASONAL VARIATIONS IN VEGETATION CHARACTERISTICS

The vegetation characteristics demonstrate a seasonal dependence as can be seen in Tables 3.3 and 3.4. Only standing stems were sampled, regardless of the presence of broken or folded stems at some points in time.

In April, new shoots were measured, as can be seen from the relatively low stem height of 285 (*Spartina*) and 399 mm *Scirpus*. For both species, the diameter and height of the stems is larger in September than in April. In November, the flexural strength is much higher than in September, especially for *Spartina* (8.8 MPa in September, 17.0 MPa in November). This might be caused by breakage of stems with a lower flexural strength, but evidence is lacking to support this hypothesis. A statistically significant difference

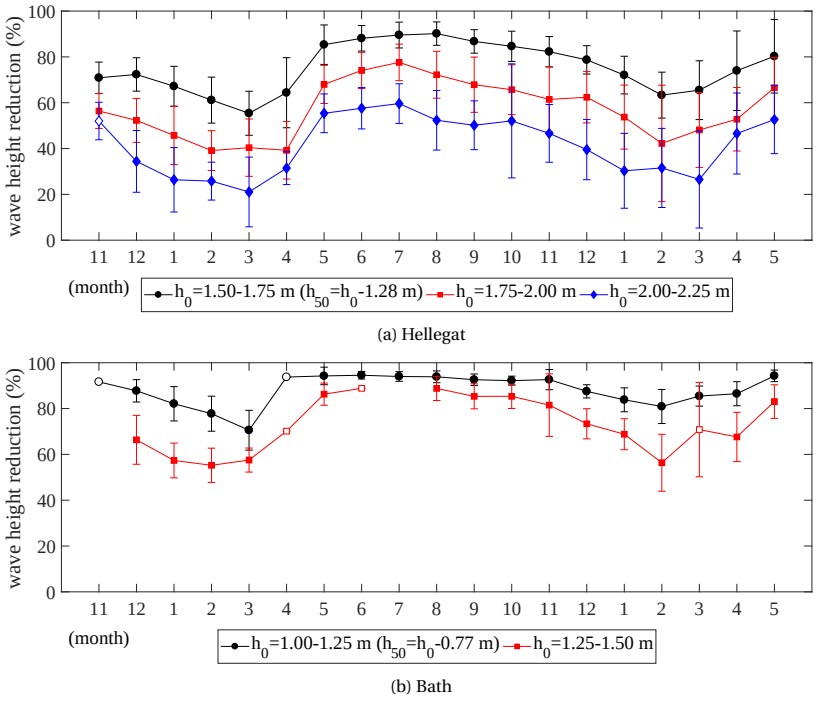

Figure 3.10: *Monthly average wave height reduction* $(H_{s,0} - H_{s,50})/H_{s,0}$ *(%) over 50 m salt marsh between wave gauges S1 and S4 at Hellegat (top panel) and Bath (lower panel) for the period Nov 2014 - May 2016, for an incoming significant wave height between 0.1 and 0.2 m, combined with a water depth at the marsh edge* h_0 *as shown in the legends. Open markers indicate that less than 5 occurrences were available in that month to compute the average reduction. Error bars give the mean value plus and minus one standard deviation.*

Table 3.3: *Characteristics of Spartina anglica (mean value ± standard deviation) per measurement period.*

Period		Dec 2014	Apr 2015	Sep 2015	Nov 2015	All
Samples		25	20	20	20	85
h_v	(mm)	327 ± 125	285 ± 63	544 ± 111	608 ± 50	441 ± 87
b_v	(mm)	3.1 ± 0.5	3.3 ± 0.5	4.1 ± 0.9	3.7 ± 0.5	3.5 ± 0.6
σ_{max}	(MPa)	13.9 ± 7.0	10.4 ± 5.1	8.8 ± 4.6	17.0 ± 5.8	12.5 ± 5.6
E	(MPa)	708 ± 560	318 ± 178	224 ± 151	503 ± 198	438 ± 272
EI	($Nmm^2 \times 10^3$)	2.0 ± 1.0	1.6 ± 0.5	2.5 ± 1.6	2.3 ± 1.1	2.1 ± 1.0
$\rho(h_v, b_v)$		0.29	0.43	0.70	0.25	0.42
$\rho(h_v, \sigma_{max})$		0.21	-0.11	-0.20	0.59	0.13
$\rho(b_v, \sigma_{max})$		-0.74	-0.09	-0.40	0.03	-0.30

Table 3.4: *Characteristics of Scirpus maritimus (mean value ± standard deviation) per measurement period.*

Period		Dec 2014	Apr 2015	Sep 2015	Nov 2015	All
Samples		20	20	19	19	78
h_v	(mm)	737 ± 169	399 ± 178	1015 ± 175	738 ± 208	722 ± 183
b_v	(mm)	6.8 ± 1.5	7.6 ± 1.9	8.0 ± 1.7	6.8 ± 1.4	7.3 ± 1.6
σ_{max}	(MPa)	6.8 ± 2.5	8.5 ± 4.1	9.5 ± 4.4	11.8 ± 6.2	9.2 ± 4.3
E	(MPa)	1130 ± 305	1625 ± 1120	917 ± 600	2052 ± 946	1431 ± 743
EI	($Nmm^2 \times 10^3$)	43 ± 29	58 ± 44	54 ± 35	51 ± 33	52 ± 35
$\rho(h_v, b_v)$		0.43	0.35	0.24	-0.02	0.25
$\rho(h_v, \sigma_{max})$		-0.40	0.04	0.16	-0.04	-0.06
$\rho(b_v, \sigma_{max})$		-0.06	-0.35	-0.64	-0.62	-0.42

is found (t-test, p=0.002) between the flexural strengths of both species, with a higher mean strength of *Spartina* (12.5 MPa) compared to *Scirpus* (9.2 MPa). A flexural strength of 12 ± 7 MPa was reported for *Spartina alterniflora* in Feagin et al. (2011), which is in the same range as the flexural strength of the *Spartina anglica* in the current study.

The correlation coefficients provide some additional information. They show that for both species, longer stems are generally thicker (positive ρ), and thicker stems tend to have a lower strength (negative ρ, see Fig. 3.11 for *Scirpus*). The latter observation is in line with Feagin et al. (2011), who found indications of an inversely proportional relationship between stem diameter and flexural strength of *Spartina alterniflora*.

In September 2015, a detailed stem density measurement was carried out. The mean stem density was 934 stems/m^2 for *Spartina* at Hellegat (842 and 1027 for the two individual locations), and 360 stems/m^2 for *Scirpus* at Bath (352 and 368 for the two individual locations).

3.3.3. SEASONAL VARIATIONS IN FRACTION OF BROKEN STEMS

Seasonal variations in the fraction of broken stems are computed based on the seasonal variations in wave attenuation (Fig. 3.10), using the one-dimensional wave energy balance, Eq. (3.11). Fig. 3.12 shows the relation between C_D and Re for both field sites. Fitting parameters of Eq. (3.14) are for Hellegat $a = 0.00$, $b = 943$, and $c = 0.48$, and for Bath $a = 1.59$, $b = 461$, and $c = 1.25$. The relatively high drag coefficient of *Scirpus maritimus* is related to the large frontal plant area with many leaves (Heuner et al., 2015). This relation between C_D and Re is used to reconstruct vegetation properties based on the measured wave attenuation.

The maximum wave height reduction occurs in summer, in July (*Spartina*) or June (*Scirpus*). With the drag coefficient, stem height and stem diameter as known variables, the wave energy balance is applied to determine the unknown maximum stem density: 1190 stems/m^2 (*Spartina*) and 850 stems/m^2 (*Scirpus*), assuming that $f_{br} = 0$ at that time. The lower wave height reduction in the other months is caused by breakage of a

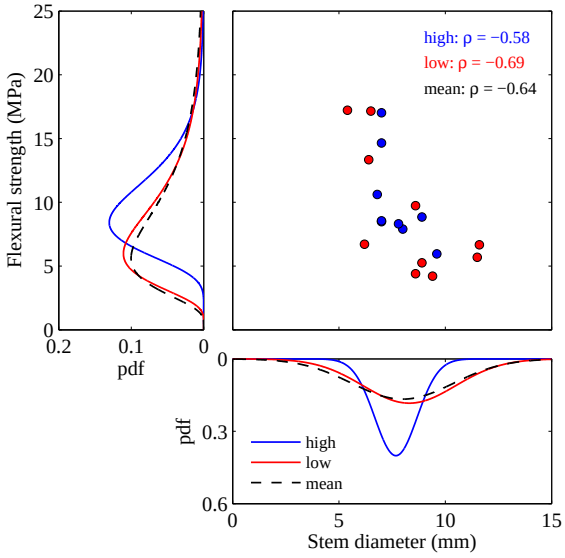

Figure 3.11: *Example of the stem diameter b_v and flexural strength σ_{max} for individual stems, their probability density functions, and the correlation coefficient between these variables, for Scirpus samples from September 2015 at Bath, with sample locations close to the marsh edge ('low') and higher in the marsh ('high').*

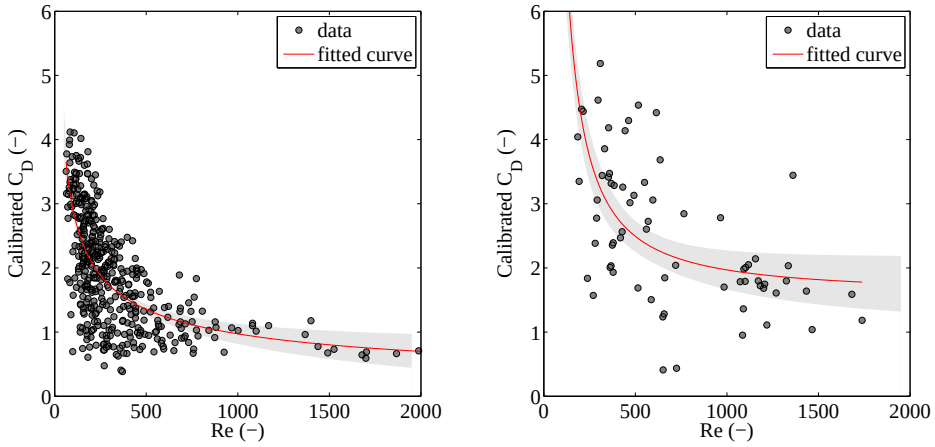

(a) Hellegat (b) Bath

Figure 3.12: *The relationship between calibrated bulk drag coefficients C_D and the corresponding Reynolds numbers Re for Hellegat (left) and Bath (right), and its 95% confidence interval (shaded area). Re is based on the hydrodynamics at the marsh edge. The curve is given by Eq. (3.14).*

part of the stems ($f_{br} > 0$, see Fig. 3.13). In September, the computed number of standing stems per m^2 was 950 stems/m^2 (*Spartina*) or 400 stems/m^2 (*Scirpus*). This is close to the measured values of 930 and 360 stems/m^2, respectively. The computed breakage fractions for December 2015 are equal to 0.52 (*Spartina*) and 0.85 (*Scirpus*). These values will be compared with the results of the stem breakage model, as indicated in the flow chart (Fig. 3.8).

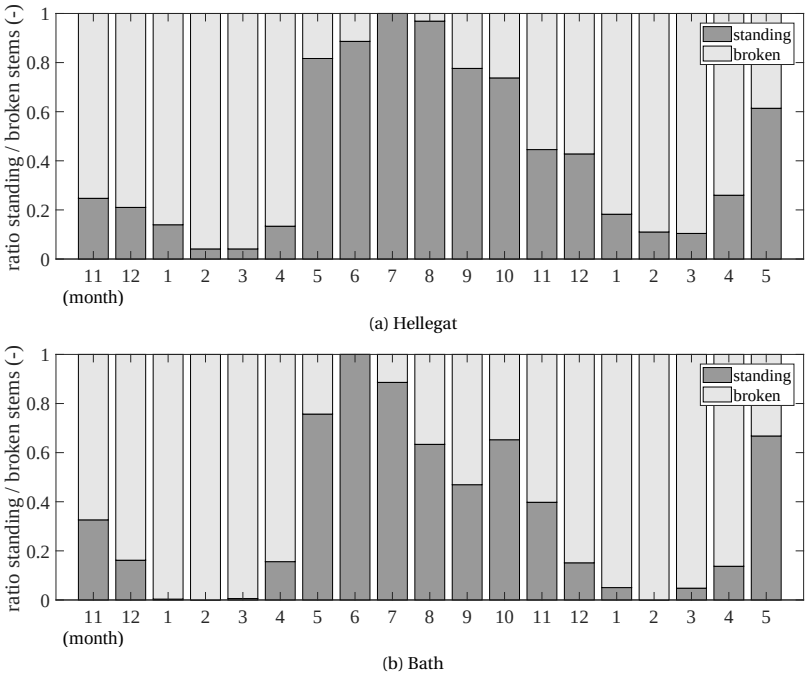

Figure 3.13: *The computed proportion of standing (1-f_{br}) and broken (f_{br}) stems for each month in the period November 2014 - May 2016, based on observations of wave attenuation.*

3.3.4. MODEL CALIBRATION

The performance of the stem breakage model is optimized by calibrating the correction factor A_c for wave-induced bending stress in the Equations (3.8) and (3.9). Following the right hand side of the flowchart in Fig. 3.8, a fraction of broken stems is computed with the stem breakage model, which is implemented in the wave energy balance. The distribution of the critical orbital velocity is based on the vegetation data of September 2015 in Tables 3.3 and 3.4, including the correlation coefficients.

The computed fraction of broken stems depends on A_c (Fig. 3.14). The stem density for A_c=0 (no breakage) represents the situation with a breakage fraction $f_{br} = 0$, which is assumed to be in July 2015 (*Spartina*) or June 2015 (*Scirpus*), see Fig. 3.13. The dashed lines in Fig. 3.14 indicate the fraction of broken stems in December 2015, and the cor-

rection factors that lead to these fractions. The stem density reduction from summer to December 2015 is best reproduced with A_c=1.7 for *Spartina* and A_c=1.3 for *Scirpus*.

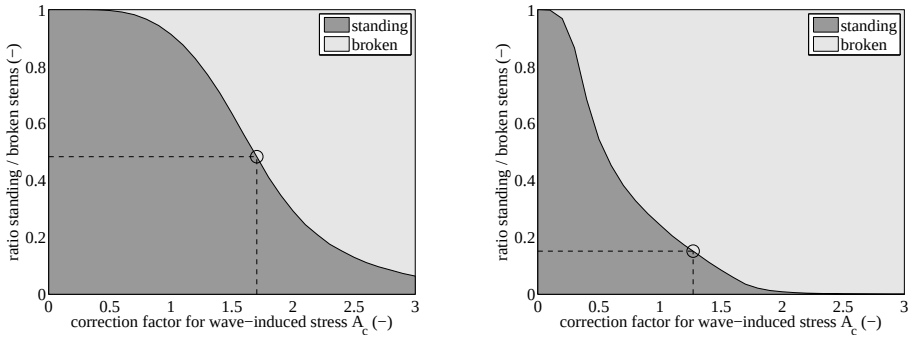

(a) Hellegat (b) Bath

Figure 3.14: *The fraction of broken stems f_{br} for Spartina anglica at Hellegat (left) and Scirpus maritimus at Bath (right), computed with the stem breakage model, as a function of the correction factor A_c.*

Stems break when the wave orbital velocity exceeds the critical orbital velocity u_{crit} of the vegetation, which is a measure for the stability of the stems. This velocity is determined for each sampled stem, including the calibrated correction factors A_c in the equations (Table 3.5).

Table 3.5: *Computed critical orbital velocity (m/s) for the sampled stems of Tables 3.3 and 3.4, mean value ± standard deviation.*

Species	Period	u_{crit}
Spartina anglica	2014 Dec	1.19 ± 0.60
	2015 Apr	1.14 ± 0.31
	2015 Sep	0.58 ± 0.13
	2015 Nov	0.52 ± 0.09
	All	0.86 ± 0.28
Scirpus maritimus	2014 Dec	0.51 ± 0.27
	2015 Apr	0.99 ± 0.38
	2015 Sep	0.30 ± 0.05
	2015 Nov	0.56 ± 0.19
	All	0.59 ± 0.22

In general, *Spartina* (u_{crit}=0.86 ± 0.28 m/s) is significantly (t-test, p=0.0003) more stable than *Scirpus* (u_{crit}=0.59 ± 0.22 m/s), which is also in agreement with visual observations, see Fig. 3.2. The stability of *Spartina* is relatively high in December 2014 and April 2015. This is related to the short stems, measured in these months (Table 3.3). In

November, the plants are most vulnerable to stem breakage, with a critical orbital velocity of 0.52 ± 0.09 m/s. Assuming a normal distribution, we see that the most stable 2.5% of the stems breaks at an orbital velocity of 0.70 m/s. The stability of newly growing *Scirpus* plants (April 2015) is quite high (u_{crit}=0.99 ± 0.38 m/s), because the plants have not reached their full length (399 mm in April, 1015 mm in September, Table 3.4), which is squared in Eq. (3.9). In other months, the tall plants are highly vulnerable to stem breakage, with breakage of the full-grown September vegetation already occurring for orbital velocities of 0.30 ± 0.05 m/s, with breakage of the 2.5% most stable stems at 0.40 m/s.

3.3.5. MODEL VALIDATION

The critical orbital velocity of *Elymus athericus* is 1.06 ± 0.34 m/s, according to Eq. (3.16). When neglecting friction, and using Eq. (3.8), this value increases to 1.28 ± 0.41 m/s. This means that incorporating skin friction decreases the critical orbital velocity by 17%.

Table 3.6: *Observed orbital velocities, computed mean value of the 10% highest orbital velocities ($u_{1/10}$), and observed and computed stem breakage fractions f_{br}.*

Test	u (m/s)	$u_{1/10}$ (m/s)	f_{br} (-) observed	computed
10	0.48 ± 0.07	0.61	>0	9%
14	0.83 ± 0.17	1.14	45%	59%
15	0.95 ± 0.10	1.13	80%	58%

Observed orbital velocities, and observed and computed stem breakage percentages are summarized in Table 3.6. Stems started to fold in test 10 from the Hydralab experiments, with medium orbital velocities (0.48 ± 0.07 m/s). The stem breakage model computes that 9% of the stems will fold or break in this test, which means that the threshold of stem folding is correctly predicted by the model. 45% of the stems were broken after test 14, with high orbital velocities (0.83 ± 0.17 m/s). The stem breakage model gives 59% stem breakage under these conditions, which is higher than the measured amount. The highest mean orbital velocity was generated in test 15 (0.95 ± 0.10 m/s). After this test, 80% of the stems were broken. The stem breakage model gives only 56% stem breakage. This is because the model uses $u_{1/10}$, which is smaller in test 15 compared to test 14, because of the relatively high standard deviation in test 14. Model results (58%) and measurements (80%) deviate here, which will be evaluated in the discussion section.

3.3.6. APPLICATION TO A SCHEMATIC SALT MARSH

This section gives an illustrative application of the calibrated stem breakage model for a schematic salt marsh with *Spartina anglica* (Fig 3.15). Vegetation characteristics of September 2015 are applied (Table 3.3). An arbitrary initial stem density of 1000 stems/m^2 is chosen. The bottom consists of a sloping part of 200 m from 2.0 to 3.0 m+MSL, followed by a flat part of 300 m at 3.0 m+MSL, further landward. Storm con-

ditions are applied with a water level at 5.0 m+MSL, with an incident significant wave height of 1.0 m and a peak period of 4.0 s. That means that the water depth is 3.0 m at the seaward boundary, and 2.0 m above the flat part of the salt marsh. There is no wind input active, so only dissipative mechanisms play a role.

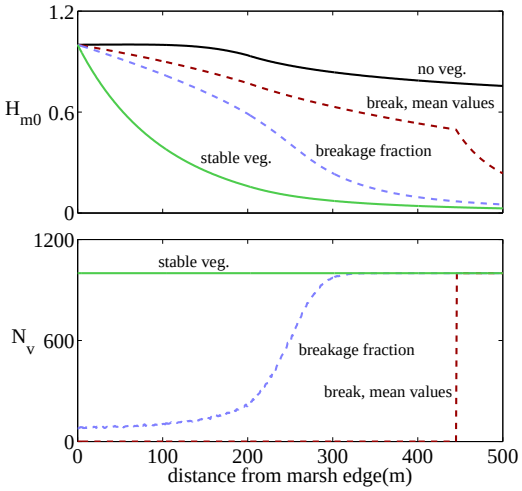

Figure 3.15: *Reduction in significant wave height H_{m0} (m) (upper panel) and stem density N_v (stems/m^2) (lower panel) for a Spartina marsh, which consists of a sloping part of 250 m and a flat part of 250 m. The curves show the computational result when applying no vegetation, stem breakage with mean values only, the approach with a fraction of broken stems, or stable vegetation.*

Without vegetation, the processes of depth-induced wave breaking and bottom friction lead to a wave height reduction of roughly 6% at 200 m and 25% at the landward end of the salt marsh. Addition of fully stable vegetation leads to a rapid decline in wave height, up to 97% at 500 m. The stem breakage model predicts breakage over 450 m, when solely based on mean values for the vegetation characteristics, for which all stems in each grid cell either stand or break. Further landward of this point, the original vegetation is undamaged (bimodal behavior). The 100% broken vegetation seaward of this point leads to some additional dissipation with respect to the case without vegetation.

Alternatively, when computing a fraction of broken stems in each computational grid cell, based on the variation in vegetation characteristics, the stem breakage gradually decreases from 92% at the marsh edge to nearly 0% at 300 m and further landward. The partially broken vegetation leads to wave energy reduction, and reduces the wave loads on the vegetation further landward. The two stem breakage approaches lead to different wave height reduction (difference in wave height up to 0.4 m), especially over the part of the marsh where the mean value approach leads to full breakage.

3.4. DISCUSSION

In this study, a model has been presented that determines the wave-induced forces that lead to vegetation stem breakage. Rupprecht et al. (2015) recommended studying both plant morphology (height and diameter) and mechanic characteristics when considering plant stability. The stem breakage model proposed in this chapter combines these two factors into an expression for a critical orbital velocity (Eqs. (3.8) and (3.9)). Three-point bending tests were utilized to investigate seasonal variability in flexural strength. Previous work only considered the strength of plants in its summer state, and recommended to measure the variability in mechanical properties due to differences in the stage of life cycle or vitality of plant stems (Rupprecht et al., 2015). The current study explicitly examines the seasonal variation in stem strength. We hypothesize that the presented strength variations are the result of a combination of internal biological processes and wave action that filters out the relatively weak plants.

Quantifying the thresholds of stem breakage is extremely challenging due to the complicated interaction between wave motion and vegetation motion, mechanical stresses due to dynamic wave loads in the swaying vegetation, and temporal and spatial variability in plant characteristics. The model proposed in this chapter simplifies this complicated process by combining linear wave theory and formulas from static mechanics. In spite of this simplification, the model captures the essence of the stem breakage process, as can be seen from the calibrated correction factors A_c (1.7 for *Spartina* and 1.3 for *Scirpus*), which are in the order of 1. Several assumptions and choices can lead to such a deviation from 1. We distinguish between (1) assumptions and simplifications where the model concept and its parameters are based on, and (2) assumptions and choices that were made in the procedure to calibrate the model.

The first category of assumptions is related to the model concept and the definition of its parameters.

- Orbital velocities in the model are based on linear wave theory (Mendez and Losada, 2004), while in-canopy velocities are known to decrease in dense canopies (Luhar et al., 2010). This means that stems may break for lower actual in-canopy velocities than the critical orbital velocities presented in this chapter.
- Another assumption is the choice of $H_{1/10}$, implying that the mean height of the highest 10% of the waves determines whether the vegetation breaks or not. No information is available to investigate which individual wave in the random wave field causes the vegetation to break. $H_{1/10}$ is one of the many options to describe the upper tail of the wave height distribution. Selection of a higher characteristic value from the wave height distribution would directly lead to a lower required A_c.
- Ship waves can also cause high wave loads at small water depths, which was specifically described for Bath by Schroevers et al. (2011). Such individual waves are not

included in the wave spectra and in $H_{1/10}$.

- Further, the leaning angle θ strongly influences the results. Stem bending was approximated by a constant leaning angle, which was based on a single experiment for each of the species. The selected value of 30 degrees for *Scirpus* was based on interpolation between measurements of leaning under low- and high-frequency wave forcing (Silinski et al., 2015). A sensitivity analysis (not presented) shows that the correction factor A_c reduces from 1.3 to 1.1 for an angle of 20 degrees, and increases to 1.6 for an angle of 40 degrees. A higher leaning angle reduces the flexural stress in the stems, and would require a higher value of A_c to obtain the same amount of stem breakage. Estimation of a leaning angle for different plant species requires mechanistic understanding of the relationship between wave properties, flexural rigidity EI and stem leaning.

- Finally, the correction factor A_c also accounts for processes that are not explicitly included in the stem breakage model, for instance the effects of dynamic loading (De Langre, 2012), fatigue due to repeated wave loads (Mach et al., 2007) and crowding, where neighboring plants provide physical support (Harley and Bertness, 1996). Further research is needed to determine whether these processes are influential.

The second category of assumptions that influence the model outcomes is related to the calibration procedure.

- Seasonal variations in wave attenuation were used to estimate the corresponding variations in the fraction of broken stems on the salt marshes, because in-situ vegetation measurements were not sufficient to assess the response to wave forcing. This is why the effect (wave attenuation) has been observed, and the cause (the number of standing and broken stems) has been computed. The computed fraction of broken stems was used as data source for the calibration of the model.

- Several choices and assumptions were made in reconstructing the seasonal variations in the fraction of broken stems, such as the length of broken stems and the selection of sea states (depth-wave height combinations). We have tested that application of a length of broken *Spartina* stems of 0.10 m instead of 0.05 m leads to a limited increase in A_c of 8%.

- Further, C_D was calibrated for vegetation data from September 2015 only, while seasonal differences, for instance in stem flexibility and amount of leaves, could lead to seasonal variations in C_D. The flexibility EI of both species in Sep. 2015 and Nov. 2015 is similar (Tables 3.3 and 3.4). A possible decrease in amount of leaves leads to a decrease in C_D in autumn, and a lower fraction of broken stems than shown in Fig 3.13. Such a decrease in computed stem breakage leads to a decrease of A_c (Fig. 3.14).

- Wave energy dissipation by standing and broken stems is summed up to obtain a total dissipation rate. This approach is based on the assumption that orbital velocities in the bottom layer with broken stems are only weakly affected by the presence of the standing stems. This is in line with the application of linear wave theory in Mendez and Losada (2004) and is supported by the findings of Weitzman et al. (2015) for a canopy composed of a tall upperstory and a short understory. For sparse standing vegetation or low-density canopies, this approach is valid. For high density vegetation, the wave orbital velocities in the broken vegetation may be lower than predicted by equations from linear wave theory. This effect could be taken into account via a reduced drag coefficient C_D for the broken fraction. On the other hand, the drag coefficient of short, broken stems may be higher, since they act as short, stiff cylinders (Hu et al., 2014). Detailed measurements on the complex interaction between the waves and the mix of broken and standing vegetation were not carried out. Therefore, for reasons of simplicity, the same drag coefficient was applied for both fractions.

Validation of the calibrated model ($A_c = 1.7$) was performed, using observations of stem breakage of *Elymus athericus* in a wave flume (Rupprecht et al., 2017). The very high flexibility of *Elymus* increases the complexity of the vegetation-wave interaction significantly. Nonetheless, the model was able to predict the initiation of stem breakage correctly. Rupprecht et al. (2017) gives two measurements of stem breakage: 45% after day 8 (test 14), and an additional 35% after day 10 (test 15, 80% in total). Where the first measurement was reproduced with reasonable accuracy (59%), the 80% of stem breakage after day 10 was not correctly reproduced (58%). Modeled fractions are based on the mean value of the 10% highest orbital velocities ($u_{1/10}$). This quantity does apparently not reflect the main differences between both tests.

A possible reason for the increase in breakage fraction is the long time span of 11 days over which wave tests were performed. The mechanical properties of the canopy after several days of testing may differ from the properties that were determined before the tests were performed. Another aspect is the extremely high non-linearity of the waves in the tests on day 11, with waves of 0.9 m at a water depth of 2.0 m and a substantial difference between forward and backward orbital velocity. Possibly, high turbulence levels have contributed to additional stem breakage. Further, a time lag up to 90° exists between wave orbital motion and vegetation motion (Rupprecht et al., 2017). This may lead to high bending moments in the stage before maximum leaning, which is not included in the model. We conclude that the stem breakage model did a reasonable job in reproducing the observed stem breakage, with the notion that the simplified description of waves and mechanics may lead to deviations, especially in situations with complex hydrodynamics and vegetation motion.

The number of measurements of stem breakage is still very limited. The reliability of the model predictions could be investigated further if additional measurements would be performed. Useful validation data could be obtained by frequent measure-

ments of the fraction of broken stems, by in-situ measurements, or by application of non-destructive methods such as time-lapse photography or satellite images (e.g., O'Donnell and Schalles (2016)). Preferably, several pre- and post-storm measurements should be carried out. These measurements should include vegetation characteristics (stem height, diameter and density) and flexural strength measurements by means of three-point bending tests. This should be combined with wave measurements during the storm. Alternatively, large-scale flume experiments as described in Rupprecht et al. (2017) can provide additional information for validation, if accompanied with measurements of the mechanical properties of the vegetation. In flume experiments, stem breakage can be more accurately linked to stem breakage, compared to field measurements.

Remarkable differences were visible between the two considered plant species, *Spartina anglica* and *Scirpus maritimus*. The relative change in A_c to reduce f_{br} from 90 to 10% is 50% larger for *Spartina*, compare the slopes of both panels of Fig. 3.14. That implies that *Scirpus* is more sensitive to the magnitude of wave-induced stresses than *Spartina*. The same conclusion follows from the computed critical orbital velocities (Table 3.5). *Scirpus* requires a location with a relatively mild wave climate, or when another species attenuates the waves to a certain extent, and provides a sheltered habitat further up the marsh (Heuner et al., 2015). The aforementioned pre- and post-storm measurements could help in determining the causes of the decline in biomass, including stem breakage by storm waves, stem breakage by fatigue (especially *Spartina* at Hellegat is frequently inundated and exposed to waves), and biological processes such as changing mechanical properties of the plants in autumn.

The partial stem breakage, observed in the wave flume tests of Rupprecht et al. (2017), indicates that individual *Elymus* stems vary in stability. This was also found in the current study for *Spartina* and *Scirpus*. From the 3 considered species, the flexible *Elymus* has the highest stability (u_{crit} =1.06 ± 0.34 m/s), whereas full-grown tall and stiff *Scirpus* is most vulnerable to stem breakage (u_{crit} =0.30 ± 0.05 m/s, September), with *Spartina* in between (u_{crit} =0.58 ± 0.13 m/s, September).

The critical orbital velocity as computed by the stem breakage model can be used for a first estimate of the (relative) stability of other plant species, provided that vegetation characteristics (height, diameter) and flexural strength are known. For such an estimate, preliminary values for A_c, C_D and θ can be used, with A_c between 1.0 and 2.0, in combination with a value for θ that reflects the flexibility of the considered plants. For the drag coefficient C_D, a value should be chosen that represents actual drag forces on the plants. Especially for highly flexible vegetation, this value may be substantially higher than a bulk drag coefficient that follows from calibration of a wave model. For a more quantitative description of the stem breakage of different plant species or locations, plant species-specific validation is recommended.

This chapter has shown how the stem breakage model can be implemented in a wave model such as a spectral wave model or a simple wave energy balance, to incorporate stem breakage in simulations of wave loads on dikes with a vegetated foreshore. The

wave load reduction on the flood defense due to vegetation decreases when stem breakage occurs, and declines in extreme cases to a situation where all vegetation is broken. Such extreme cases are equivalent to a wave flume test with completely mowed vegetation described in Möller et al. (2014), for which still some wave height reduction was measured. Including the variability in individual stem stability prevents bimodal model behavior, in which all stems either break or stand. Partial stem breakage leads to partial wave attenuation reduction. This results in a gradual decrease in wave-induced forces and, subsequently, in a gradual decrease in the fraction of broken stems, for increasing distance from the marsh edge. In this way, the role of vegetation can be more realistically included in flood risk assessments.

3.5. CONCLUSIONS

Wave measurements at two salt marshes revealed a strong seasonal variation in wave attenuation by salt marsh vegetation. Common cord-grass (*Spartina anglica*) and sea club-rush (*Scirpus maritimus*) were used as study species. From field observations and an analysis of the seasonal variation in wave attenuation, the above-ground biomass of these species was found to gradually diminish during the storm season (October to March in the Netherlands). At the end of winter, typically only a rough salt marsh bottom with remainders of folded and broken vegetation is present. From April onwards, new shoots start to grow, which eventually develop to dense vegetation with high wave damping capacity in summer.

Seasonal variations in biomass are caused by seasonal differences in storm intensity and mechanical properties of the stems. The stem height, stem diameter and flexural strength were measured for four measurement periods in the seasonal cycle, where the strength was determined by means of three-point bending tests. Both study species have their maximum flexural strength in the winter period. The stems of *Scirpus* have a lower flexural strength than that of *Spartina*.

A new model is presented in this chapter, which predicts the wave load that plant stems can withstand before they break or fold. The model compares plant stability, expressed in terms of a critical orbital velocity, Eqs. (3.8) and (3.9), with the amplitude of wave-induced orbital velocities in the canopy, Eq. (3.10). A higher critical velocity indicates greater stability of the stem. Factors that contribute to stability are a high flexural strength and large stem diameter. Further, vegetation characteristics such as a small stem height, low drag coefficient and high flexibility (i.e., a large leaning angle) contribute to the stability, by reducing the amount of wave force acting on the stem.

The model was calibrated, based on continuous measurements of water depth and wave conditions, over a period of 19 months. A correction factor in the stem breakage model (1.7 for *Spartina* and 1.3 for *Scirpus*) was required to reproduce the amount of stem breakage that occurred in the field. An independent validation of the model was carried out, by comparing model predictions of stem breakage of sea couch (*Elymus athericus*) with observations of Rupprecht et al. (2017) in a large-scale flume experiment

with wave heights up to 0.9 m. The stem breakage model correctly reproduced the starting point of folding. An observation of 45% stem breakage at high orbital velocities was reproduced with reasonable accuracy (57%). During the flume test with the highest orbital velocities, 80% stem breakage was observed, whereas the model predicted that 56% would break.

Spartina is relatively stable with a mean critical orbital velocity in the order of 0.5-1.2 m/s. The stability of *Scirpus* is lower, because of its smaller strength, lower flexibility and longer stems, with a mean critical orbital velocity of 0.3-1.0 m/s. These velocities are based on $H_{1/10}$, which is the mean height of the highest 10% of the waves. The stem breakage model was implemented in a wave energy balance to combine the calculations of wave attenuation and stem breakage. If the variation in individual stem properties is taken into account, a spatially varying fraction of broken stems can be calculated. In this way, bimodal model behavior is prevented, in which all stems either stand or break.

The stem breakage model can be used to predict the amount of remaining biomass on vegetated foreshores under design conditions for dikes. As a process-based model, it can be applied to different plant species and locations, provided that the characteristics (height and diameter) and flexural strength of the plants are determined. If possible, it is preferred to carry out a species-specific validation. Omitting stem breakage will lead to overestimation of wave height reduction, while application of the stem breakage model will lead to more realistic assessment of the role of vegetation for coastal protection.

4

ASSESSING SAFETY OF NATURE-BASED FLOOD DEFENSES

ABSTRACT

Vegetated foreshores adjacent to engineered structures (so-called hybrid flood defenses), are considered to have high potential in reducing flood risk, even in the face of sea level rise and increasing storminess. However, foreshores such as salt marshes and mangrove forests are generally characterized by relatively strong temporal and spatial variations in geometry and vegetation characteristics (e.g., stem height and density), which causes uncertainties with regards to their protective value under extreme storm conditions. Currently, no method is available to assess the failure probability of a hybrid flood defense, taking into account the aforementioned uncertainties. This chapter presents a method to determine the failure probability of a hybrid flood defense, integrating models and stochastic parameters that describe dike failure and wave propagation over a vegetated foreshore. Two dike failure mechanisms are considered: failure due to (i) wave overtopping and (ii) wave impact on revetments. Results show that vegetated foreshores cause a reduction in failure probability for both mechanisms. This effect is more pronounced for wave impact on revetments than for wave overtopping, since revetment failure occurs at relatively low water levels. The relevance of different uncertainties depends on the protection level and associated dike height and strength. For relatively low dikes (i.e., low protection levels), vegetation remains stable in design conditions, and plays an important role in reducing wave loads. In case of higher protection levels, hence for more robust dikes, vegetation is less important than foreshore

This chapter has been published as: Vuik, V., Van Vuren, S., Borsje, B.W., van Wesenbeeck, B.K., & Jonkman, S.N. (2018). Assessing safety of Nature-based Flood Defenses: dealing with extremes and uncertainties. *Coastal Engineering*, **139**, 47–64.

geometry, because of expected stem breakage of the vegetation under these more extreme conditions. The integrated analysis of uncertainties in hydraulic loads, dike geometry and foreshore characteristics in this chapter enables the comparison between nature-based flood defenses and traditionally engineered solutions, and allows coastal engineers to design hybrid flood defenses worldwide.

4.1. INTRODUCTION

Within the context of increasing flood risks in coastal areas (Chapter 1), efforts are being made to make greater use of nature-based approaches to flood risk reduction (Spalding et al., 2014; Bridges et al., 2015), including the use of vegetated foreshores in front of hard flood defenses. Such foreshores are present along many coastlines, but their role for coastal protection is rarely incorporated into flood protection strategies. Most examples of successful implementation concern small-scale pilot projects (Spalding et al., 2014). One of the causes is a lack of methods for testing hybrid solutions (Fig. 1.1) according to engineering standards for safety, often expressed by means of a failure probability (Van Wesenbeeck et al., 2014).

With state-of-the-art statistical and probabilistic techniques, it is possible to determine a failure probability and an optimal design of a traditional dike, considering the stochastic behavior of both load and strength (e.g. Vrijling (2001); Voortman (2003); Steenbergen et al. (2004)), with applications in for example the Netherlands (Jonkman et al., 2008), the UK (Buijs et al., 2004) and China (Zhang and Xu, 2011). Some studies have applied probabilistic methods to sandy shorelines, to describe coastal cliff recession (Hall et al., 2002) and dune erosion (Den Heijer et al., 2012; Vuik et al., 2017). Uncertainties are even more relevant for more complex flood defense systems like hybrid solutions, which combine ecological and engineering features. However, no methods are available to assess the failure probability of hybrid systems and to incorporate effects of relevant uncertainties, such as spatial and temporal variations in vegetation characteristics, wave attenuation by flexible vegetation, and stability of vegetation under extreme wave forcing. Consequently, it is difficult to assess effects of vegetated foreshores on safety.

The aim of this chapter is to assess the failure probability of nature-based flood defenses, more specifically, for a configuration with a dike accompanied by a vegetated foreshore. A probabilistic model framework is developed, in which uncertainties in hydraulic loads, characteristics and functioning of the vegetated foreshore, and strength of the dike are taken into account. The two most prevalent wave-driven failure mechanisms are considered: (i) erosion of the crest and inner slope of the dike due to wave overtopping, and (ii) erosion of the revetment or grass cover on the outer slope due to impact of breaking waves. Different foreshore configurations are defined, inspired by dikes and salt marshes bordering the Dutch Wadden Sea. This chapter shows how these foreshore configurations affect the failure probability of the flood defense, and to what extent different variables and processes influence this failure probability.

4.2. METHODS

4.2.1. SYSTEM DESCRIPTION

In hybrid solutions, ecosystems are utilized as vegetated foreshores along engineered structures. The combined dike-foreshore system is schematized, as shown in Fig. 4.1. Parameters will be introduced throughout the methods section, and are summarized in Appendix 4.A.

The combined characteristics of the dike, foreshore and vegetation determine the strength of the system. Hydrodynamic boundary conditions depend on the wind speed U_{10} (m/s) and are represented by a still water level ζ (m MSL), significant wave height H_{m0} (m) and a characteristics wave period, such as the peak period T_p (s) or the spectral mean wave period $T_{m-1,0}$ (s). The foreshore is characterized by a flat part of B_{fs} meter wide and an elevation z_{fs} (m MSL), which is naturally close to high water spring, because of sediment deposition by the tide (Allen, 2000; Borsje et al., 2017). Offshore from the marsh edge, the profile slopes under an angle α_{fs} to the bed level z_0 (m MSL) of the tidal flats. The marsh vegetation is described by a set of physical characteristics and model parameters, which together determine the wave attenuating capacity and stability against stem breakage. This will be discussed in Section 4.2.2.

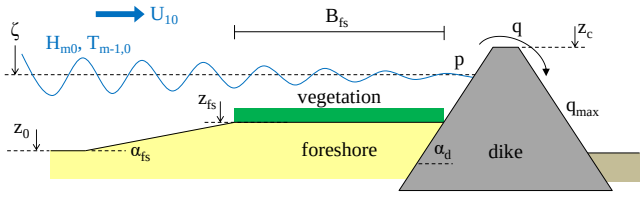

Figure 4.1: *Schematic representation of a dike-foreshore system (not to scale). System characteristics and computed quantities are shown in black, boundary conditions in blue, and model parameters in red. Parameters will be introduced throughout the methods section, and are summarized in Appendix 4.A.*

Two different failure mechanisms of the dike are considered. Firstly, failure due to wave overtopping over the dike with crest level z_c (m MSL) and slope angle α_d, which occurs when the wave overtopping discharge q (l/s per m width) exceeds a maximum tolerable value q_{max} that depends on the erosion resistance of the crest and inner slope of the dike (Section 4.2.3). Secondly, failure due to wave impacts p (N/m^2) on the outer slope, which leads to damage of the cover and subsequent erosion of the underlying dike core material if the storm duration exceeds a threshold value. For this second failure mechanism, covers with grass (Section 4.2.4) and asphalt (Section 4.2.5) are considered.

A model framework (Fig. 4.2) is applied to compute the failure probability of a dike, including the effect of a vegetated foreshore. Local water levels and wave characteristics are generated by wind and tide. Wind speed, water level and offshore wave conditions

are applied as boundary conditions. Without foreshore, a flat bottom at z_0 is considered. Presence of the vegetated foreshore affects the wave conditions, impact, run-up and, in extreme cases, overtopping over the dike. The framework consists of modules to account for foreshore effects (Section 4.2.2), wave overtopping (Section 4.2.3) or wave impact (Sections 4.2.4 and 4.2.5).

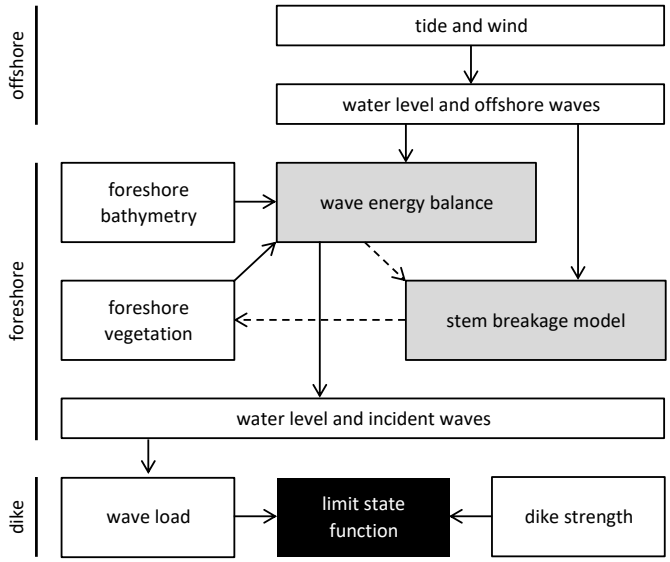

Figure 4.2: *Model framework to compute a probability of failure. A limit state function Z is defined, and given by the difference between strength and load. The definitions of dike strength and wave load differ per failure mechanism.*

A limit state function (LSF) describes dike failure in terms of the difference between strength (R) and load (S): $Z = R - S$. Both load and strength are considered as stochastic (i.e., uncertain) variables. Failure occurs when $Z < 0$. The corresponding probability that the dike fails is $P(Z < 0)$, shortly denoted as the probability of failure P_f. The framework is applied to compute this probability.

4.2.2. MODELING OF FORESHORE EFFECTS

The foreshore is included in the framework of Fig. 4.2 via a one-dimensional wave energy balance:

$$\frac{dEc_g}{dx} = S_{in} - S_{ds,w} - S_{ds,b} - S_{ds,f} - S_{ds,v}, \tag{4.1}$$

where $E = (1/8)\rho g H_{rms}^2$ is wave energy density (J/m^2), H_{rms} root mean square wave height (m), ρ density of water (kg/m^3), g gravitational acceleration (m/s^2), c_g group velocity (m/s), and x distance (m) along the foreshore. The right hand side of Eq. (4.1)

consists of different source terms ($\mathrm{J\,m^{-2}\,s^{-1}}$): energy input by wind (S_{in}), and energy dissipation due to whitecapping ($S_{ds,w}$), depth-induced wave breaking ($S_{ds,b}$), bottom friction ($S_{ds,f}$) and vegetation ($S_{ds,v}$).

The energy balance is discretized, using a simple first order numerical scheme with step size $\Delta x = 5$ m. The offshore wave period T_p is considered in the energy balance. In addition, the equation of Hofland et al. (2017) is used to account for a possible increase in spectral mean wave period $T_{m-1,0}$ over the shallow foreshore, based on the difference in depth between offshore mudflats (z_0) and foreshore (z_{fs}).

Dissipation due to wave breaking, bottom friction and vegetation will be dominant on vegetated foreshores. Vegetation is described by cylinders with stem height h_v (m), stem diameter b_v (m), stem density N_v (stems/m^2) and bulk drag coefficient $\widetilde{C}_D$ (-). The dissipation formula of Mendez and Losada (2004) is implemented to account for wave attenuation by this vegetation. For depth-induced wave breaking, the formula of Battjes and Janssen (1978) is used, in which the breaker parameter γ (-) follows from Battjes and Stive (1985). Bottom friction is represented by a roughness height k_N (m), following Madsen et al. (1988). The energy balance is primarily meant for computations over short distances, less than 1 or 2 km. For longer distances, a one-dimensional approach is mostly insufficient. However, to avoid an overestimation of the wave height reduction for relatively long foreshores, the processes wind input (due to Snyder et al. (1981)) and whitecapping (due to Komen et al. (1984)) are added. All these model descriptions correspond with the implementations in the spectral wave model SWAN (Booij et al., 1999).

If the wave-induced bending stresses exceed the plant's flexural strength, the stem will fold or break near the bottom (Rupprecht et al., 2017). The stem breakage model of Chapter 3 is implemented in the model framework of Fig. 4.2. This model compares the wave-induced bending stress with the flexural strength of the stems. Stem breakage occurs when the actual wave orbital velocity exceeds the stem's critical velocity, for stems with a circular cross-section expressed as

$$u_{crit} = \sqrt{\frac{\sigma_{max}\pi\left(b_v^4 - b_{v,in}^4\right)}{8A_c\rho b_v^2\left[C_D h_{v,r}^2 + 2\pi C_f (h_v - h_{v,r})h_{v,r}\right]}}, \tag{4.2}$$

in which A_c is an empirical correction factor for the wave-induced stress (-), $h_{v,r} = (1-f_r)h_v$ the reduced height (m) of the canopy after leaning and bending, $b_{v,in}$ the inner stem diameter in case of hollow stems (m), C_D the drag coefficient for forces on cylinders (-), and C_f the skin friction coefficient (-). This formula combines drag force over the reduced vegetation height and friction force over the part of the stem that leans horizontally in the flow (Luhar and Nepf, 2011). Stems are assumed to break if the amplitude of the in-canopy orbital velocity caused by the highest 10% of the waves ($H_{1/10} = 1.27H_{m0}$) exceeds the value of the critical velocity. Based on the variation of u_{crit} over the stems due to variations in stem height, strength and diameter, a fraction of broken stems is computed. The total wave attenuation consists of a contribution by standing stems (with

the original height h_v) and a contribution by broken stems (with a height of broken stems $h_{v,br}$). Details of this approach are described in Chapter 3.

4.2.3. FAILURE DUE TO WAVE OVERTOPPING

The limit state function Z (LSF) for wave overtopping is defined as the difference between tolerable and actual overtopping discharge:

$$Z_{ov} = q_{max} - q, \tag{4.3}$$

in which q is the wave overtopping discharge (l/s/m), according to EurOtop (2016), and q_{max} is the tolerable overtopping discharge, which depends on the erosion resistance of the dike crest and rear slope. The lower part of Fig. 4.2 is more specifically represented by the content of Fig. 4.3, in order to compute a probability of failure due to wave overtopping.

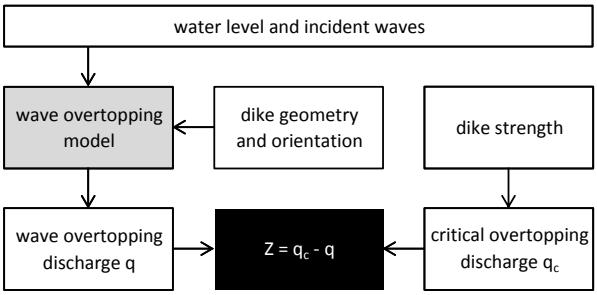

Figure 4.3: *Limit state function Z_{gr} for failure of a dike due to erosion of the crest and rear slope, caused by wave overtopping. The limit state is defined, as the difference between strength (tolerable overtopping discharge) and load (actual wave overtopping discharge).*

A shallow foreshore can affect the amount of overtopping by a change in wave height, wave period, and thereby wave steepness s_0 and Iribarren number $\zeta_{m-1,0} = \tan(\alpha_d)/\sqrt{s_0}$, in which α_d is the dike slope angle. Three situations are distinguished in EurOtop (2016), based on $\zeta_{m-1,0}$:

1. wind sea conditions and moderate to steep dike slopes ($\zeta_{m-1,0} < 2-3$), where waves will break on the dike slope;
2. a situation where a foreshore reduces wave steepness ($2-3 < \zeta_{m-1,0} < 5$), so that most waves will surge on the dike slope, without significant breaking;
3. a situation where heavy wave breaking on a very shallow foreshore leads to a flat wave energy spectrum without a clear peak, and where non-linear wave interactions transfer energy to infra-gravity wave frequencies ($\zeta_{m-1,0} > 7$).

The tolerable overtopping discharge q_{max} represents the erosion resistance of the grass cover on the crest and rear slope of the dike. Van der Meer et al. (2009) describe in-

situ overtopping tests on dikes with grass covers on clay, and the damage to the slope for different overtopping discharges. For actual dike failure, large-scale damage and erosion is relevant.

4.2.4. FAILURE DUE TO WAVE IMPACT ON GRASS COVERS

Where the cover of the crest and rear slope is affected by overtopping waves, the outer slope is primarily loaded by the impact of breaking waves. The limit state function Z_{gr} (LSF) for failure of grass covers due to wave impact is defined as the difference (hrs) between the time required to erode the top layer with grass roots t_{top} and the clay layer t_{sub}, and the effective duration $t_{load,eff}$ of wave loads at a certain location on the slope:

$$Z_{gr} = t_{top} + t_{sub} - t_{load,eff}. \tag{4.4}$$

The lower part of Fig. 4.2 is more specifically represented by the content of Fig. 4.4, in order to compute a probability of failure due to wave impact on grass covers.

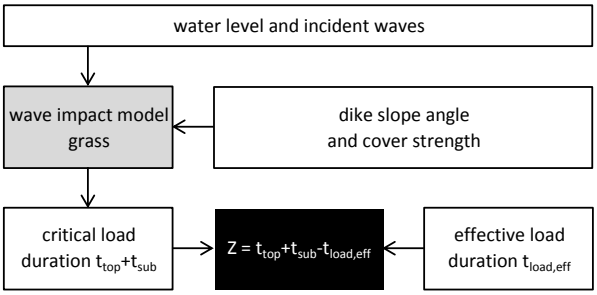

Figure 4.4: *Limit state function Z_{gr} for failure of a dike due to wave impact on a grass cover on the outer slope. The limit state is defined, as the difference between strength (time required to erode the grass and clay layer, $t_c = t_{top} + t_{sub}$) and load (effective duration of wave loads on a certain point on the dike, $t_{load,eff}$).*

Equations for the time required to erode the grass and clay layer ($t_{top}+t_{sub}$) are based on De Waal and Van Hoven (2015). The effective load duration $t_{load,eff}$ is the time span over which waves impact the dike slope at a certain location. This time span depends on (1) the time variation of the still water level and (2) the maximum distance to still water level for which waves are able to damage a grass cover. Appendix 4.B gives a more detailed description of the formulas for failure due to wave impact on grass covers.

4.2.5. FAILURE DUE TO WAVE IMPACT ON ASPHALT REVETMENTS

Failure of an asphalt revetment is a matter of fatigue. Breaking waves cause wave impacts on the dike, which leads to bending stresses in the asphalt layer. Theoretically, a crack can form when the bending stress due to an individual wave exceeds the flexural strength of the asphalt. In practice, it is more likely that asphalt will fail due to many repetitive

load cycles. The model described in De Looff et al. (2006) is used to compute failure of asphalt revetments, which is based on the principle that the asphalt layer will fail when the actual number of waves exceeds the critical number of waves (Fig. 4.5).

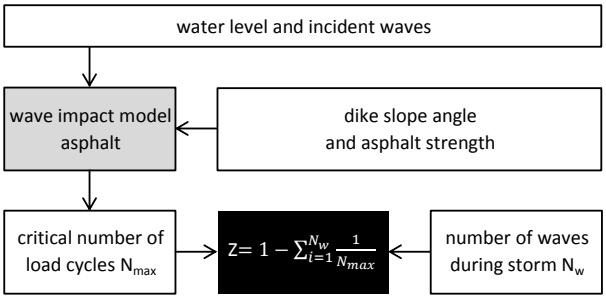

Figure 4.5: *Limit state function Z_{as} for failure of a dike due to wave impact on a asphalt revetment on the outer slope. For each wave, it is determined how many of such waves the asphalt can withstand (N_{max}). The limit state function becomes negative (i.e., failure occurs) if the sum of $1/N_{max,i}$ over all waves ($i = 1..N_w$) exceeds 1.*

The maximum number of tolerable load cycles N_{max} depends on the difference between the wave-induced bending stress σ (MPa) in the asphalt layer and the flexural strength σ_{br} (MPa), and reads

$$\log_{10} N_{max} = V_\beta \left(\log_{10}(\sigma_{br}) - \log_{10}(\sigma)\right)^{V_\alpha}, \tag{4.5}$$

in which V_α and V_β are dimensionless parameters that describe the fatigue curve, based on laboratory tests of asphalt.
Failure of the revetment occurs if the so-called Miner sum exceeds 1. A contribution to the Miner sum of $1/N_{max,i}$ is computed for all waves $i = 1..N_w$ within the load duration, where $N_{max,i}$ follows from Eq. (4.5).

$$Z_{as} = 1 - \sum_{i=1}^{N_w} 1/N_{max,i}. \tag{4.6}$$

This equation is included in logarithmic form in the model framework, to improve the convergence of the probabilistic computations:

$$Z_{as} = -\log_{10}\left(\sum_{i=1}^{N_w} 1/N_{max,i}\right). \tag{4.7}$$

The procedure to compute N_w bending stresses σ is included in Appendix 4.C.

4.2.6. PROBABILISTIC METHOD

The framework (Fig. 4.2) is used to compute the outcome of the LSF, Eqs. (4.3), (4.4) or (4.6), for any possible combination of input variables. Values of input variables are

selected from their probability density functions, see Appendix 4.A. The probabilistic method FORM (First Order Reliability Method, see Hasofer and Lind (1974)) is applied to compute a probability of failure P_f, using the open source implementation in OpenEarthTools (Van Koningsveld et al., 2010). In case of wave overtopping, this is the probability that the tolerable overtopping discharge is exceeded, i.e. $P_f = P(Z_{ov} < 0) = P(q > q_{max})$. FORM simplifies the mathematical problem by linearizing the LSF and transforming all probability distributions to equivalent normal distributions with mean value μ_i^N and standard deviation σ_i^N. The probability of failure P_f is expressed in terms of a reliability index β via the cumulative standard normal distribution Φ:

$$P_f = \Phi\left(-\beta\right), \tag{4.8}$$

FORM starts in a user-defined position in the probability density functions of all variables ($i = 1..n$), for example with a relatively high value for the boundary conditions, in combination with the mean value of all other parameters. This point is the first guess of the so-called design point X^*. The final design point should represent the most likely parameter values associated with failure. FORM uses an iterative method to update the design point until convergence of the design point and corresponding reliability index is reached.

Statistical dependence between different variables is taken into account via Gaussian correlation, characterized by Pearson's correlation coefficients. This choice is discussed in more detail in Section 4.3.2. Correlated input variables are transformed into independent standard normal variables via Rosenblatt transformation (Rosenblatt, 1952). See Jongejan et al. (2011) for an example of application of FORM in the context of flood risk.

In each iteration, FORM tests how strong the LSF responds to a perturbation of each individual variable X_i. The response is expressed in terms of the partial derivative $\partial Z / \partial X_i$. Based on these partial derivatives, importance factors α_i are calculated (where $\sum \alpha_i = 1$). For example, a large importance factor for the marsh width B_{fs} indicates a strong response of the limit state function to the standard deviation σ_i^N of this variable. The uncertainty in foreshore width has a strong influence on the failure probability in that case.

The design point and the partial derivatives are used to compute the reliability index of the system. The reliability index increases if the design point contains parameter values far from their mean values μ_i^N. A high reliability index (i.e., low P_f) is for example found if a dike only fails in case of extreme surge and waves, combined with a tolerable overtopping discharge far below the mean value. Based on the reliability index and the importance factors, the design point X^* is expressed as

$$X_i^* = \mu_i^N - \alpha_i \beta \sigma_i^N. \tag{4.9}$$

Based on the sign of α_i, load and strength variables can be distinguished. Negative importance factors correspond with load variables, such as the wind speed or the breaker

parameter. Higher values of these variables lead to higher wave loads on the dike, and a higher probability of failure. A positive importance factor indicates that a variable acts as a strength parameter, for which a higher value leads to a lower probability of failure. Examples are foreshore elevation and dike crest level. Their values in the design point are below the mean value μ_i^N.

The boundary conditions will usually dominate the probability of failure ($\alpha \approx -0.95$). The dike will obviously not fail without an extreme storm, whatever the foreshore characteristics or tolerable overtopping discharge will be. Therefore it is more interesting to investigate the relative influence of the other variables, disregarding the importance factors of the boundary conditions. For this means, a new quantity is defined: the relative contribution c_i of each system variable. System variables ($i = 1..n_{sys}$) are variables that describe the state and functioning of the dike-foreshore system, i.e., all variables in Appendix 4.A, except the boundary conditions. The relative contribution is given by

$$c_i = \frac{\alpha_i^2}{\sum_{n_{sys}} \alpha_i^2}. \tag{4.10}$$

4.2.7. CLASSIFICATION OF UNCERTAINTIES

Different types of uncertainty can be discerned. The nature of a source of uncertainty has implications for the possibilities of reducing this uncertainty. Van Gelder (2000) distinguishes between inherent (or natural) uncertainties, statistical uncertainties and model uncertainties. Statistical uncertainties and model uncertainties are often put together, and identified as knowledge uncertainties, related to incomplete knowledge about the process under investigation (Merz and Thieken, 2005).

Inherent (or natural) uncertainty is related to the inherent variability of nature, and can be subdivided into inherent uncertainty in time and space. Inherent uncertainty in time and space is caused by temporal and spatial variations in nature, which are inherently unpredictable. Examples are the maximum water level in the next 50 year, variations in properties of individual plants, asphalt aging, marsh edge erosion and seasonal variation in vegetation characteristics (Table 4.1). Inherent uncertainty cannot be reduced.

Table 4.1: *Examples of inherent uncertainties, statistical uncertainties and knowledge uncertainties in hybrid flood defenses, subdivided based on their location.*

Location	Inherent uncertainty	Statistical uncertainty	Knowledge uncertainty
Offshore	Future water levels	Wave height distribution	Distribution type wave height
Dike	Asphalt aging	Variations in dike height	Wave overtopping model
Foreshore	Marsh edge erosion	Spatial variations bathymetry	Wave breaking model
Vegetation	Seasonality	Variations in vegetation stability	Stem breakage model

Secondly, knowledge uncertainty is of interest, which can be subdivided into statis-

tical uncertainty and model uncertainty. Statistical uncertainty has to do with the finite length of measurement time series, which causes uncertainty in the choice of a certain probability distribution type and its parameters. Time series are usually too short to ensure reliable estimates of events with a low probability of exceedance, such as the wave height with an annual exceedance probability of 1/1000. Long-term measurement campaigns can help to reduce statistical uncertainty. Also a lack of information on spatial variations can lead to statistical uncertainty. Field measurements with high spatial extent and resolution can help in reducing this source of uncertainty.

Model uncertainty describes the imperfections of model concepts. Model concepts, concerning hybrid flood defenses, describe for example the processes of wave breaking, wave attenuation by vegetation, stem breakage due to wave action and wave overtopping over the dike (Table 4.1). These models can be imperfect because the physics are not fully understood, or model concepts are simplified to restrict computation time. Knowledge uncertainties can be reduced by developing more sophisticated models or probability distributions.

Uncertainties can, besides on basis of their nature, be subdivided based on their location (Walker et al., 2003). This is relevant in the context of vegetated foreshores, as there is a clear distinction between uncertainties related to the boundary conditions (wind, water level, wave conditions), the foreshore and the dike. Variables (see Appendix 4.A) are categorized, based on their nature (inherent, statistical, and model uncertainty) and location (boundary conditions, foreshore, vegetation, dike).

4.3. APPLICATION

4.3.1. SITE DESCRIPTION

The schematized system is based on a dike with foreshore in the Wadden Sea (Fig. 4.6). Many kilometers of the Wadden Sea dikes of Denmark, Germany and The Netherlands are bordered by salt marshes, see Fig. 1.4. An extensive system of brushwood dams and drainage ditches facilitates sediment trapping, soil consolidation and vegetation growth. The system was originally meant for land reclamation. Nowadays, it is maintained to preserve the natural and agricultural values of the salt marshes (Bakker et al., 2002; Reise et al., 2010; van Loon-Steensma, 2015). During storm surges, the wave loads on the dikes are reduced due to wave breaking, bottom friction, and wave attenuation by standing vegetation. The salt marshes are elevated around mean high water, due to sediment accretion, and are between a few hundred meters and two kilometers wide.

Plant species composition on these marshes progresses from a seaward zone of pioneer plants (forbs, grasses and low shrubs), such as *Salicornia europaea* (common glasswort), *Puccinellia maritima* (common saltmarsh-grass) and *Spartina anglica* (common cordgrass), to more mature, taller plant species landwards, such as *Elymus athericus* (couch grass), *Aster tripolium* (sea aster) and *Suaeda maritima* (seepweed).

The dikes are at some locations fully covered with grass, while revetments are present

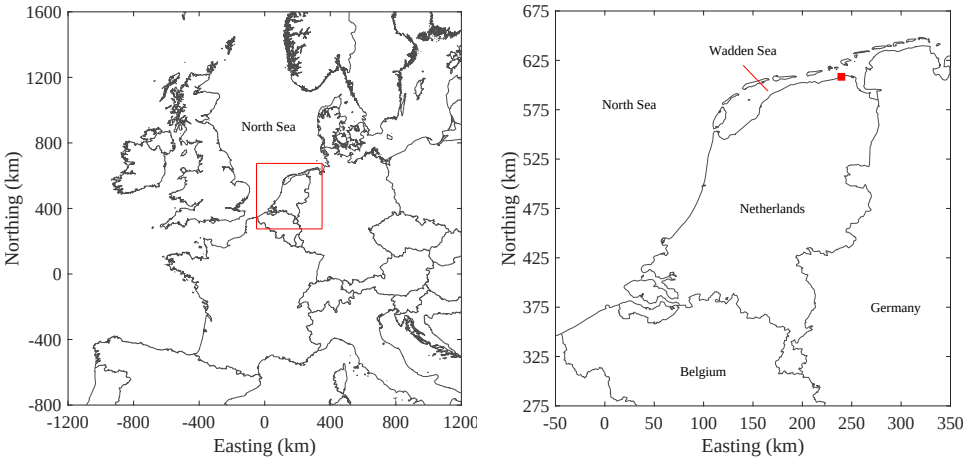

Figure 4.6: *Location of the Wadden Sea in Europe (left) and location of the salt marshes along a dike in the Netherlands (right panel, red square).*

at other places. These revetments are generally composed of different layers, with concrete elements in the tidal zone, an asphalt layer in the wave impact zone, and a grass cover in the wave run-up zone (Fig. 4.7). The crest and inner slope of the dike are normally covered with grass. The crest of the Dutch Wadden Sea dikes is situated at 8 to 9 m MSL. Outer slope angles vary between 1:3 and 1:8. A revetment is especially required at exposed locations and on steep slopes (1:3 or 1:4). Grass is only applied in the wave impact zone on gentle slopes (at least 1:6).

4.3.2. SPECIFICATION OF PARAMETERS AND PROBABILITY DISTRIBUTIONS

Appendix 4.A gives an overview of the variables, present in the model, including the nature and location of the uncertainty, the probability distribution type used in the simulations, and the parameters of this distribution. This section gives background information on the choice of input variables. Values are presented as mean value ± standard deviation.

DIKE GEOMETRY

The efficiency of vegetated foreshores in reducing failure probabilities is investigated for dike heights of 4, 6 and 8 m MSL, in combination with a 1:4 dike slope angle (Fig. 4.7). In this study, lower dike heights are considered as a proxy for areas with a lower level of protection than in the Netherlands. A standard deviation of 0.1 m in crest level and 5% in slope angle is considered, to account for spatial variations in dike geometry and measurement inaccuracies, corresponding with Jongejan et al. (2011). Effects of a berm, slope roughness and wave obliqueness are not considered here, for simplicity. The same 1:4 slope angle is considered to compute dike failure due to wave impact on asphalt

revetments in the wave impact zone, between 2 and 6 m MSL. For dikes with a grass cover, more gentle slopes are mostly applied on coastal dikes. Therefore, a slope angle of 1:8 is used for computations on grass covers.

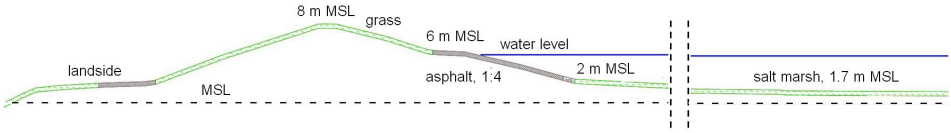

Figure 4.7: *Dike profile, based on the geometry of a dike along the Wadden Sea, with a crest level at 8 m MSL, an 1:4 sloping asphalt revetment in the wave impact zone between 2 and 6 m MSL, and a salt marsh foreshore at 1.7 m MSL.*

WAVE OVERTOPPING

The distribution of tolerable overtopping discharge is based on the mean value (63 l/s/m) and standard deviation (19 l/s/m) of the values presented in Van der Meer et al. (2009) for slopes, uniformly covered with grass on clay. Probability distributions for parameters in the formulas for the actual overtopping discharge are adopted from EurOtop (2016): a_1 (0.023 ± 0.003) and b_1 (2.70 ± 0.20) in the equation for breaking waves, a_2 (0.09 ± 0.0135) and b_2 (1.50 ± 0.15) for non-breaking waves, and a_3 (-0.79 ± 0.29) for very shallow foreshores (see Section 4.2.3).

GRASS COVERS

Grass covers can have different qualities: patchy grass on sand, open sods or homogeneous, closed sods. Only a strong grass cover on a mild slope is feasible at Wadden Sea dikes. Therefore, only a cover with closed sods on a 1:8 slope (indicated by G1) is considered here. For a description of grass quality (see Appendix 4.B), a log-normal distribution for C_a is used (1.82 ± 0.62 m). For C_b and C_c, deterministic values are applied (-0.035/hr and 0.25 m, respectively). These values are based on laboratory experiments, and adopted from Klerk and Jongejan (2016). The effect of the small slope angle of 1:8 is taken into account via the multiplication factor r_α in Eq. (4.B3) in Appendix 4.B. The sand fraction $f_{sand} = 0.35$, which does not influence the value of C_d in Eq. (4.B2). The total layer thickness d_{tot} (grass and clay) is 0.50 ± 0.10 m.

ASPHALT REVETMENTS

A new and correctly constructed asphalt revetment on a stable sandy subsoil can hardly be damaged by wave action. However, construction imperfections and asphalt aging may induce vulnerability to wave impact. Therefore, we consider the following two asphalt qualities (A1-A2): (A1) relatively low strength asphalt ($\sigma_{br} = 3.0 \pm 0.9$ MPa and $c_{sub} = 60 \pm 12$ N/m^3), and (A2) asphalt of poor quality, at the end of its lifetime ($\sigma_{br} = 1.5 \pm 0.45$ MPa and $c_{sub} = 30 \pm 6$ N/m^3). The asphalt thickness $d_a = 0.25 \pm 0.025$ m in both cases, and the stiffness modulus $S_a = 8000 \pm 2400$ N/m^2. All these parameters (see Appendix 4.C) are based on fatigue testing of asphalt taken from 5 dikes (Kanning

and Den Hengst, 2013). Log-normal distributions are chosen, since this distribution type fits the data well and cannot have negative values (Kanning and Den Hengst, 2013). The (deterministic) parameters that describe the fatigue curve, V_α and V_β, are 0.5 and 4.8, respectively.

FORESHORE CHARACTERISTICS

The foreshore bathymetry is schematized as a vegetated flat part and a 1:100 slope from the marsh edge to the adjacent tidal flats at 0 m MSL. The foreshore elevation is set to 1.7 m MSL (Fig. 4.7), close to mean high water spring (MHWS). Variations in bathymetry are not computed by means of a morphological model, but via a standard deviation on foreshore width and elevation. A standard deviation of 0.2 m is applied to the foreshore elevation, representing spatial and temporal variations in topographic data of the Dutch Wadden Sea. Storm impact on the bottom surface of salt marshes is very limited, according to post-storm observation (Spencer et al., 2015) as well as large-scale wave flume experiments (Spencer et al., 2016). However, lateral erosion may cause marsh edge retreat during storms (Francalanci et al., 2013). The magnitude of this lateral erosion is hard to predict. An arbitrary standard deviation of 50 m is taken into account to assess the sensitivity of the system's probability of failure to changes in foreshore width in the time scale of a single storm.

FORESHORE MODELS

Depth-induced wave breaking depends on the breaker parameter γ in the model, which is a function of the offshore wave steepness following Battjes and Stive (1985). A standard deviation of 0.05 is applied, estimated from Fig. 1 in Battjes and Stive (1985). Bottom friction is specified by means of a Nikuradse roughness length scale k_N. Typical Manning roughness values for bottom surfaces without vegetation range from 0.02 to 0.04 $m^{1/3}/s$. Conversion to k_N via Bretschneider et al. (1986) gives a k_N between 0 and 0.02 m for water depths between 0 and 3 m. This range is schematized by means of a uniform distribution with values between 0 and 0.02 m. The function to determine the increase in wave period $T_{m-1,0}$ is multiplied with a factor f_T with mean value equal to 1.0 and standard deviation of 0.09, to account for the uncertainty of the predictive formula proposed in Hofland et al. (2017). They prescribe this standard deviation for a wave height to water depth ratio of approximately 0.5, which is often found on salt marshes due to depth-limitation of the wave height.

VEGETATION PROPERTIES

The most abundant plant species at the study location is *Elymus athericus*, a tall, thin and densely growing flexible grass. Characteristics of this species are taken from flume tests of Möller et al. (2014) (mean values b_v = 1.30 mm, h_v = 700 mm, N_v = 1225 stems/m^2). Three-point-bending tests of the same vegetation were performed by Rupprecht et al. (2017) to assess mechanical properties, and reanalyzed by Vuik et al. (2018a) to determine the flexural strength (mean value σ_{max} = 40 MPa).

Two types of standard deviations are of interest. Firstly, inter-sample variation, which characterizes differences in mean values within the marsh. And secondly, in-sample variation, which characterizes variation of the individual stems within the sample. The inter-sample variation is used in the probabilistic calculations to select representative values for wave attenuation, whereas the in-sample variation is used to compute a fraction of broken stems in each grid cell. In-sample variation is based on the standard deviations mentioned in Möller et al. (2014), and expressed in terms of coefficients of variation (CV) with respect to the mean values ($CV = \sigma/\mu$), see Appendix 4.A. Inter-sample variation is based on variations between samples, taken from different locations on salt marshes along the coast of the province Friesland in the Netherlands, where extensive vegetation mapping and testing of mechanical properties was carried out in November 2016.

Apart from the vegetation characteristics, parameters have to be specified for the modeling of wave attenuation and stem breakage. For wave attenuation, a bulk drag coefficient $\widetilde{C}_D = 0.22 \pm 0.05$ is based on the parametrization proposed in Möller et al. (2014), given the stem diameter of 1.3 mm and an orbital velocity of 1.0 m/s. Although information on the variation of bulk drag coefficients is missing, $CV(\widetilde{C}_D) = 0.25$ is applied. For stem breakage, a theoretical value for the drag coefficient for cylinders in waves $C_D = 1.0$ is applied (Hu et al., 2014). The bulk drag coefficient $\widetilde{C}_D$ is lower than the drag coefficient C_D, since $\widetilde{C}_D$ includes the effects of swaying and leaning, which are not present in the description of wave attenuation by vegetation. For the skin friction coefficient C_f, a value of 0.01 is adopted from Luhar and Nepf (2011). Standard deviations of 0.25 for C_D ($CV = 0.25$) and 0.005 for C_f ($CV = 0.50$) are applied, to reflect the lack of knowledge on these parameters.

The reduction in stem height due to leaning $f_r = (h_v - h_{v,r})/h_v$ is based on observations in a wave flume by Rupprecht et al. (2017). For the tests just before the initiation of folding, a canopy height of 9 cm was observed, which leads to a reduction of $f_r = 0.87$. To determine a suitable standard deviation, a value of $h_{v,r} = 13$ cm is considered, which leads to a standard deviation in f_r of 0.04. The parameter $A_c = 1.7$ was found in the calibration of the stem breakage model for *Spartina anglica*, and applied in the validation for *Elymus athericus* in Chapter 3. A standard deviation of 0.5 is applied to account for the uncertainty in the model predictions of the complicated process of stem breakage. This standard deviation is based on the differences in A_c between the two plant species considered in Chapter 3. Finally, a height of broken stems $h_{v,br}$ is specified by means of a uniform distribution ranging from 2 to 8 mm. Stems are seen to fold and break near the bottom, both in the flume (Rupprecht et al., 2017) and in the field.

BOUNDARY CONDITIONS FOR WIND, WATER LEVEL AND WAVES

Boundary conditions are represented by the parameters wind speed U_{10}, still water level ζ, significant wave height H_{m0} and mean wave period $T_{m-1,0}$. The probability distributions of these parameters represent the situation at the marsh edge of the salt marshes in the Dutch Wadden Sea, along the coast of the province of Groningen (Fig. 4.6).

First, a joint probability distribution for wind speed and water level is determined, based on a time series with 30 years of measured still water levels, wind directions and wind speeds. A peak-over-threshold analysis is performed to select storms for which the 97.5% percentile value for wind speed and/or water level is exceeded, during at least 6 hours. Storms are selected with a wind direction at the peak water level within a sector of 45 degrees around North-West (292.5-337.5 nautical degrees). Only storms from this wind sector generate high surge in the Wadden Sea (Fig. 4.6). Adding storms outside this sector does only result in more scatter, without significant influence on the marginal distribution for the water level. Since the data exhibits greater dependence in the positive tail than in the negative, a Gumbel copula (with parameter $\alpha = 2.24$) is chosen to describe the correlation structure. See e.g. Salvadori et al. (2014, 2015) and Sebastian et al. (2017) for recent applications of copula's in the field of coastal engineering. Two Generalized Extreme Value (GEV) distributions are fitted through the data, to obtain marginal distributions for wind speed and water level. A Poisson distribution (with parameter $\lambda = 6.4$) describes the number of storms per year in the selected wind sector. This set of distributions defines statistics per storm event.

Statistics per storm event are converted into statistics per year, by simulating 10,000 years of data via Monte Carlo sampling. For each year, a number of storms N is sampled from the Poisson distribution, and N random realizations of wind speed and water level are drawn from the Gumbel copula. From these N realizations, the annual maximum still water level and corresponding wind speed are selected. This leads to a new data set, with 10,000 simulated annual maximum still water levels and corresponding wind speeds. Marginal GEV distributions are fitted through these new data, and the correlation between both variables is described by a Gaussian copula with $\rho = 0.43$, since no asymmetrical tail dependence is visible for the annual maximum values.

An existing database with the results of SWAN computations is deployed to determine wave conditions at the marsh edge. These SWAN computations were carried out to determine wave loads for the official assessment of the Dutch dikes surrounding the Wadden Sea (Groeneweg et al., 2010). 10,000 random data pairs with wind speed and water level are sampled from the Gaussian copula with $\rho = 0.43$. A wave height and wave period are coupled to these data pairs via 2D interpolation between the values in the database for the nearest wind direction (330 degrees). The extreme values of the sampled wave parameters could well be described by Weibull type marginal distributions, and Gaussian correlation between the variables. Parameters of all distributions and correlation coefficients are included in Tables 4.A5 and 4.A6 in Appendix 4.A. Some characteristic values from the marginal distributions are shown in Table 4.2.

Model uncertainty of the SWAN model was analyzed by Chbab and Groeneweg (2015), by comparing model results and measured wave conditions. Wave heights and wave periods are multiplied with a normally distributed model factor with a mean value (bias) and a standard deviation.

For wave impact on the outer slope, also load duration is of importance, Eq. (4.B4).

Table 4.2: *Characteristic values for boundary conditions.*

Boundary condition	Unit	Min	Max	
Spring tide	m MSL	-1.60	1.35	
Wind direction	naut. deg.	292.5	337.5	
Exceedance frequency	1/year	1/10	1/100	1/1000
Surge	m	1.88	2.56	3.12
Still water level	m MSL	3.23	3.91	4.47
Wind speed	m/s	21.2	25.5	28.9
Significant wave height	m	0.90	1.26	1.54
Mean wave period	s	4.08	4.92	5.49

Storms are selected from a time series, measured at a nearby measurement station at Eemshaven, deployed by Rijkswaterstaat. A mean value and standard deviation of the load duration have been determined for different values of the layer height Δz.

4.3.3. DEFINITION OF DEPENDENCIES

Variables are assumed to be independent, except for situations with physical or statistical arguments for correlation. In the latter situation, Gaussian correlation between input variables is applied (Section 4.2.6) for the following variables.

- dependence between wind, water level, wave height and wave period (see Section 4.3.2 and Table 4.A6 in Appendix 4.A)
- stem height h_v is positively correlated with stem diameter b_v in the *Elymus* samples ($\rho = 0.20$);
- thicker stems generally have a lower flexural strength σ_{max} ($\rho = -0.33$);
- the correlation between stem height and flexural strength is weak ($\rho = -0.07$);
- full dependence of the bulk drag coefficient and drag coefficient is applied, because of many reasons for dependence between these parameters, such as a large frontal area due to many leaves ($\rho = 1.00$);
- flexural strength σ_{br} and stiffness modulus S_a of the asphalt did not display significant correlation for the 5 tests ($\rho = 0.01$). However, if one divergent test is excluded, a considerably higher correlation is found ($\rho = 0.46$). An additional calculation (not shown) with the latter correlation coefficient incorporated displayed lower failure probabilities ($\Delta\beta = 0.15 - 0.90$, with biggest influence for high quality asphalt). Nonetheless, the relative effect of a vegetated foreshore is nearly the same in both calculations ($\Delta\beta = 1.05 - 1.45$ for $\rho = 0.01$ versus $\Delta\beta = 0.99 - 1.55$ for $\rho = 0.46$).

4.4. RESULTS

4.4.1. OVERVIEW OF SIMULATIONS

Failure probabilities are computed for various system configurations, based on the salt marshes in the Dutch Wadden Sea. System components (dike, foreshore bathymetry, vegetation, vegetation stability), and the corresponding models and variables, are stepwise added to the simulations to assess their effect on the probability of failure.

Table 4.3 explains which system components are included in the simulations. The reference case is a situation with only a dike, with a uniform foreshore at the level of the offshore tidal flats z_0. Next, a non-vegetated foreshore with the bathymetry of a salt marsh is considered. After that, vegetation is added, disregarding possible stem breakage. Finally, the model is completed by adding the stem breakage model and vegetation stability characteristics. A fraction of broken stems is computed in those simulations.

Table 4.3: *System components (rows), included in the 4 different simulations (columns), which are carried out in probabilistic (P) and deterministic (D) mode. System components are included via their mean value ('*') or its full probability distribution ('X').*

	dike only (foreshore at MSL)		foreshore, no vegetation		foreshore, stable vegetation		foreshore, breakable vegetation	
	D	P	D	P	D	P	D	P
dike characteristics	X	X	X	X	X	X	X	X
wave load model	X	X	X	X	X	X	X	X
wave model	*	X	*	X	*	X	*	X
foreshore bathymetry			*	X	*	X	*	X
vegetation properties					*	X	*	X
vegetation model					*	X	*	X
stability properties							*	X
stability model							*	X

For each system configuration, a probabilistic (P) and deterministic (D) simulation is performed (Table 4.3). In the deterministic simulations, a standard deviation of 0 is assigned to variables that describe the foreshore, vegetation, and associated models. In the probabilistic computations, uncertainties in these parameters are included.

4.4.2. PROBABILITY OF FAILURE DUE TO WAVE OVERTOPPING

An annual failure probability is computed for the different system configurations, considering erosion of the dike due to wave overtopping for three different crest levels (Fig. 4.8).

Without a foreshore (i.e., foreshore at MSL), an annual failure probability of 1/18 is computed for a crest level of 4 m MSL (i.e., dike failure would occur every 18 year, on average). This probability reduces to 1/2,200 for a 6 m MSL crest level, and to 1/1,500,000 for 8 m MSL. The ratio in dike volume (m^3/m) between these three dikes is approximately 1:2:4. Corresponding reliability indices β are 1.60, 3.32 and 4.83, respectively. Effects on the failure probability can best be expressed in terms of a change in reliability index ($\Delta\beta$), where a higher reliability index implies a lower failure probability, Eq. (4.8).

Addition of a foreshore without vegetation leads to $\Delta\beta = 0.21$ (4 m MSL) up to 0.32 (8 m MSL). A foreshore with stable vegetation has a considerably higher effect: $\Delta\beta = 0.60$ (4 m MSL) up to 0.70 (8 m MSL). However, if also stem breakage is taken into account, the probability of failure approaches the situation of a non-vegetated foreshore due to severe breakage of vegetation, especially for the dikes of 6 MSL and 8 m MSL (Table 4.4). Under such conditions, wave attenuation by vegetation reduces to the influence of short, broken stems only.

Fig. 4.8 also shows that the influence of uncertainties in foreshore bathymetry and wave model parameters is of minor importance, looking at the difference between a probabilistic (yellow bars) and deterministic description of the foreshore (gray bars underneath). Only for computations with stable vegetation, considerable differences are visible between the deterministic and probabilistic (green bars) simulations.

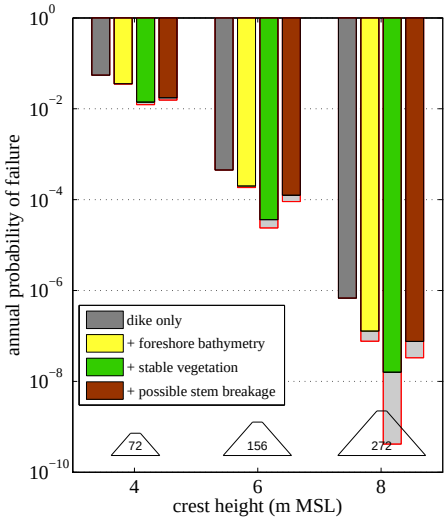

Figure 4.8: *Probability of failure for the four different system configurations of Table 4.3, for three different dike crest levels. Computations with a probabilistic (colored bars) and deterministic (gray bars with red lines) description of the foreshore are shown (see Table 4.3). Dike sections are shown (vertical scale exaggerated), with the dike volume above mean sea level (m^3/m) inside.*

Now we consider the design points of the simulations (Table 4.4). Presence of a salt marsh shifts the dominant hydrodynamic conditions. Failure of a dike with foreshore

Table 4.4: *Annual failure probabilities for different foreshore configurations and dike heights, with the hydrodynamic conditions in the corresponding design points.*

foreshore configuration	z_c (m MSL)	β (-)	P_f (-)	ζ (m MSL)	H_{m0} (m) in	H_{m0} (m) out	$T_{m-1,0}$ (s) in	$T_{m-1,0}$ (s) out	f_{br} (%)
dike only (foreshore at MSL)	4	1.60	$5.5\cdot10^{-2}$	3.38	1.00	1.08	4.1	4.1	x
foreshore, no vegetation		1.80	$3.6\cdot10^{-2}$	3.53	1.02	0.70	4.2	4.7	x
foreshore, stable vegetation		2.20	$1.4\cdot10^{-2}$	3.77	1.10	0.49	4.3	4.8	0%
foreshore, breakable vegetation		2.11	$1.7\cdot10^{-2}$	3.63	1.07	0.59	4.2	4.7	55%
dike only (foreshore at MSL)	6	3.32	$4.5\cdot10^{-4}$	4.50	1.62	1.64	5.5	5.5	x
foreshore, no vegetation		3.54	$2.0\cdot10^{-4}$	4.70	1.62	1.20	5.5	6.0	x
foreshore, stable vegetation		3.97	$3.6\cdot10^{-5}$	4.82	1.69	1.10	5.4	5.9	0%
foreshore, breakable vegetation		3.66	$1.3\cdot10^{-4}$	4.77	1.66	1.15	5.4	5.9	87%
dike only (foreshore at MSL)	8	4.83	$6.8\cdot10^{-7}$	5.39	2.17	2.07	6.7	6.7	x
foreshore, no vegetation		5.15	$1.3\cdot10^{-7}$	5.64	2.20	1.68	6.4	6.9	x
foreshore, stable vegetation		5.53	$1.6\cdot10^{-8}$	5.75	2.25	1.61	6.5	7.0	0%
foreshore, breakable vegetation		5.25	$7.6\cdot10^{-8}$	5.70	2.26	1.65	6.4	6.9	96%

occurs at higher water levels than without foreshore (i.e., at MSL). Waves are higher offshore, but lower at the dike. A distinct wave height reduction is visible for configurations with shallow foreshore, due to energy dissipation by breaking and vegetation, whereas energy gain can occur on low foreshores via wind input. An increase in mean wave period $T_{m-1,0}$ over the foreshore decreases its overall effect on wave overtopping. High waves lead to high fractions of broken stems for configurations with dike crest levels at 6 and 8 m MSL. The orbital velocities for these waves ($u_{1/10}$ = 1.6 m/s for z_c = 8 m MSL) are clearly higher than the critical velocity of most *Elymus* stems ($u_{crit} = 1.0 \pm 0.3$ m/s).

Alternatively, a required crest level can be determined for a fixed target probability, using logarithmic interpolation. For a target annual failure probability of e.g., 1/1000, a crest level of 5.67 m MSL is needed for a dike only (i.e., with foreshore at MSL). This value reduces to 5.38 m MSL (non-vegetated foreshore), 4.89 m MSL (foreshore with stable vegetation) or 5.16 m MSL (foreshore with breakable vegetation). The differences in required crest level at this target probability are 0.29, 0.78 and 0.51 m, respectively. Corresponding reductions in dike volume above MSL amount 10%, 25% and 16%, assuming a crest width of 2 m and inner and outer slope angles of 1:4. When neglecting uncertainties on the foreshore, and mean values for all foreshore characteristics and model parameters are used, the differences in required crest level at 1/1000 are only slightly larger: 0.29, 0.86 and 0.60 m, respectively. This confirms the earlier observation that uncertainties concerning the foreshore have less effect on the failure probability than uncertainties in boundary conditions, wave overtopping model, dike geometry and strength.

4.4.3. RELEVANCE OF UNCERTAINTIES FOR WAVE OVERTOPPING

Fig. 4.9 shows how the relative contribution of system components to the failure probability, Eq. (4.10), is distributed over the different system components listed in Table 4.3. 'dike characteristics' (i.e., uncertainty in geometry and strength), 'wave load model' (i.e., the wave overtopping formulas), 'foreshore bathymetry', 'wave model', 'vegetation properties', 'vegetation model', 'vegetation stability properties' and 'vegetation stability model'. For example, the relative contribution of the system component 'vegetation properties' is equal to the sum of the c_i of the variables stem density, stem height and stem diameter, see Appendix 4.A. The first three bars in the figure show the relative contribution of the different system components for a 'dike only' system with mean crest levels of 4, 6 and 8 m MSL. The other groups of three bars belong to the system configurations that include a non-vegetated foreshore, a foreshore with stable vegetation, and a foreshore with breakable vegetation, respectively.

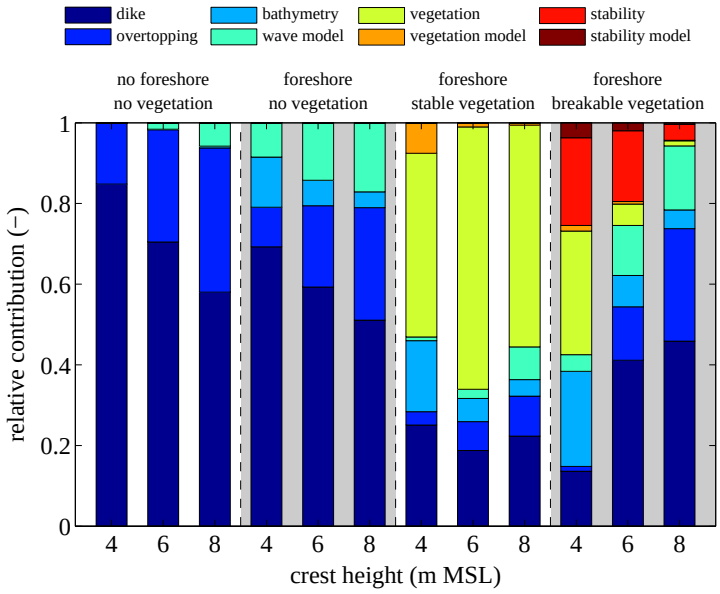

Figure 4.9: *The relative contribution of the different system components from Appendix 4.A to the probability of failure due to wave overtopping. System configuration are, from left to right: a dike without foreshore, a non-vegetated foreshore, a foreshore with stable vegetation, and a foreshore with breakable vegetation. The three bars per system configuration belong to the three different crest levels in the computations (4, 6 and 8 m MSL).*

The figure shows that uncertainties in dike geometry and dike strength dominate the probability of failure for a dike only (apart from the boundary conditions). Uncertainty in wave overtopping discharge (especially parameter b_1) gains relative importance with increasing dike height. This is partly due to an increase of its importance factor

(α = 0.05 for 4 m MSL and 0.16 for 8 m MSL), and partly due to a decrease of the importance factor for the uncertainty (σ = 0.10 m) in dike crest level (α = 0.11 for 4 m MSL and 0.08 for 8 m MSL). If a non-vegetated foreshore is added to the system, the components 'foreshore bathymetry' and 'wave model' come into play. Uncertainties in foreshore bathymetry (especially in the foreshore height z_{fs}) are mainly important for a low dike, whereas the influences of uncertainties in wave model parameters (especially the breaker parameter γ) increase with increasing dike height. In general, uncertainties in system characteristics are more important for low dikes and high failure probabilities. Model uncertainties show the opposite trend, with higher importance for high dikes with low failure probabilities.

The right half of the figure deals with vegetated foreshores. If the vegetation can be considered as fully stable, vegetation characteristics (especially the stem density N_v, due to its high spatial variation) and vegetation model (i.e., the bulk drag coefficient $\widetilde{C}_D$) dominate the uncertainty. However, most *Elymus* stems will break under these conditions. Therefore, addition of the stem breakage model changes the dominant uncertainties drastically. The influence of uncertainty in bulk drag coefficient (vegetation model) diminishes, as it does not only increase wave attenuation, but also stem breakage, due to the correlation between C_D and $\widetilde{C}_D$. Uncertainty in vegetation stability has the largest contribution for the system with a low dike (4 m MSL). Also vegetation characteristics are still important for this configuration. Stem density acts as a strength variable ($\alpha > 0$), whereas stem height acts as a load variable ($\alpha < 0$). This is because of the lower stability of longer stems, which dominates over the effect on wave attenuation. For the high dike (8 m MSL), uncertainty in the stem breakage process diminishes, as almost all stems will undoubtedly break. The distribution of relative contributions strongly resembles the situation of the non-vegetated foreshore.

4.4.4. SENSITIVITY ANALYSIS FOR WAVE OVERTOPPING

Different variations are applied with respect to the system characteristics of the base case, listed in Appendix 4.A, to test the response of the failure probability to different choices concerning important system characteristics. In the panels below, the effect of a vegetated foreshore (with breakable vegetation) is shown along different gradients, in the panels a-f:

(a) marsh width (base case: 300 m),
(b) tolerable overtopping discharge (base case: 63 l/s/m),
(c) flexural strength of vegetation (base case: 40 MPa),
(d) correlation between wind and water level (base case: ρ = 0.43),
(e) offshore wave height,
(f) sea level rise (base case: 0 m).

Effects can best be expressed in terms of the reliability index β, which is directly related to the failure probability via Eq. (4.8).

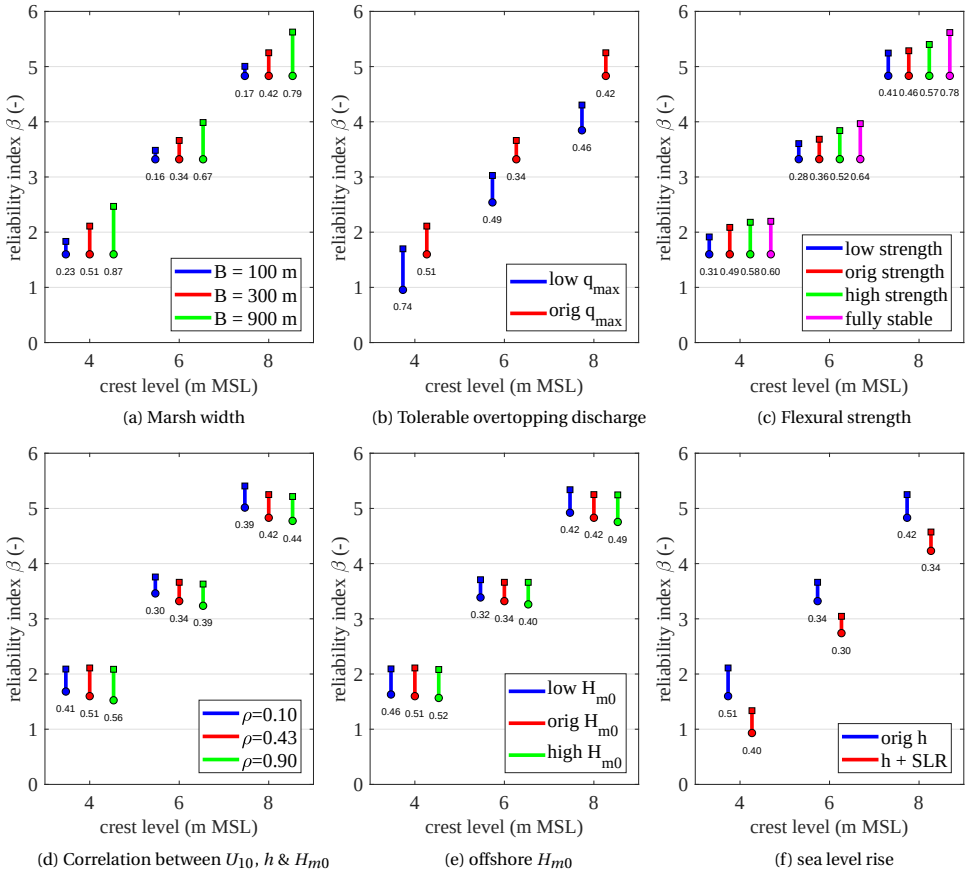

(a) Marsh width (b) Tolerable overtopping discharge (c) Flexural strength

(d) Correlation between U_{10}, h & H_{m0} (e) offshore H_{m0} (f) sea level rise

Figure 4.10: *Sensitivity of the reliability index β to different values of the marsh width (panel a), tolerable overtopping discharge (b), flexural strength of the vegetation (c), correlation coefficient between wind, water level and wave height (d), offshore wave height (e) and sea level rise (f). Circular markers at the lower end of the lines concern the dike only system; the square markers at the upper end of the lines concern the system with a vegetated foreshore. The numbers below the lines show the differences in β between both systems (i.e., the length of the lines).*

First, variations in foreshore width are applied (B_{fs} = 100 m, 300 m and 900 m), see Fig. 4.10, panel (a). Wider foreshores lead to lower failure probabilities, especially if the vegetation remains stable (low dike, 4 m MSL), since wave attenuation by vegetation is more dependent on marsh width than, for example, wave breaking. Logically, uncertainty in marsh width is more important for small marshes, for equal standard deviation of 50 m. However, even for the 100 m wide foreshore, the importance factor α for the uncertainty in marsh width (0.07-0.09, depending on crest level) is still smaller than for example the importance factor for the tolerable overtopping discharge (0.09-0.19).

The mean value of 63 l/s/m for the tolerable overtopping discharge q_{max} is valid for

healthy grass covers on clay. Dikes with a damaged grass cover, or a sandy subsoil, are characterized by a significantly lower erosion resistance. Panel (b) compares the failure probabilities for values of 63 (base case) and 6.3 l/s/m (factor 10 lower). Also the standard deviation is divided by 10. The effect of a vegetated foreshore compared to a dike only system is slightly larger ($\Delta\beta = 0.46 - 0.74$) for the lower tolerable overtopping discharge compared to the base case ($\Delta\beta = 0.34 - 0.51$). This means that vegetated foreshores are more effective for dikes with lower overtopping resistance.

Next, the effect of vegetation strength σ_{max} is investigated. Panel (c) contains failure probabilities for the base case (medium strength), strength values (both μ and σ) divided by 2 (low strength), multiplied by 2 (high strength), and fully stable vegetation. The vegetation in the high strength simulation behaves as fully stable for the low dike (only 8% breakage, against 48% in the base case). Differences between strength scenarios decrease for the medium dike and high dike, as the fractions of broken stems become 53% and 87%, respectively, versus 89% and 96% in the base case. A factor 2 in flexural strength is equivalent to a factor $\sqrt{2}$ in stem height or diameter, see Eq. (4.2), so shorter or thicker stems would display comparable behavior (disregarding correlation effects).

Panel (d) shows the system behavior when correlation between wind speed and water level is weaker ($\rho = 0.10$) or stronger ($\rho = 0.90$) compared to the base case ($\rho = 0.43$). The corresponding dependence of wave conditions on wind speed and water level is determined in the same way as for the base case, see Section 4.3.2. A lower correlation between wind and water level may occur if variations in river discharge or storage volume in a lake are more relevant. Lower correlation leads to higher reliability indices. However, also the effect of a vegetated foreshore (the length of the lines) becomes smaller. This is because the dominant loading conditions can shift to a situation with moderate waves combined with high water depths, for which the interaction between waves and the vegetated bottom surface is lower. Such a shift is more likely in case of low correlation.

Panels (e) and (f) show the effect of offshore wave height and sea level rise, which can both be induced by climate change. For the offshore wave height, the shape parameter of the Weibull distribution is 2.05 (base case), 2.26 (lower wave height) or 1.85 (higher wave height). Differences between offshore wave height reduce due to the presence of a foreshore, which makes a foreshore slightly more efficient in case of high offshore waves (panel e), which is in line with Van Wesenbeeck et al. (2017). For sea level rise, a scenario is added with an increase in still water level of 0.50 m with respect to the original water level statistics (panel f). Without morphological adjustment, sea level rise will also cause an increase in wave heights (Arns et al., 2017). Therefore, the incoming wave height is amplified as well, by applying a wave height to water depth ratio ($H_{m0}/(\zeta - z_0)$) identical to the situation without sea level rise. The computations show that the effect of a vegetated foreshore on β decreases in case of sea level rise.

4.4.5. PROBABILITY OF FAILURE DUE TO WAVE IMPACT ON REVETMENTS

Fig. 4.11 shows failure probabilities for a medium quality (A1, σ_{br} = 3 MPa, c_{sub} = 60 N/m^3) and low quality asphalt revetment (A2, σ_{br} = 1.5 MPa, c_{sub} = 30 N/m^3). For medium quality (A1), the presence of a salt marsh leads to an increase of the reliability index β by 1.04 (foreshore without vegetation), 1.21 (foreshore with breakable vegetation) or 1.40 (foreshore with stable vegetation). These differences in β are higher for low quality (A2): 1.13, 1.45 and 1.75, respectively. According to the model, 90 (A2) to 96% (A1) of the vegetation breaks. Effects of foreshores on reliability indices, and thus on failure probabilities, are considerably higher than for failure due to wave overtopping.

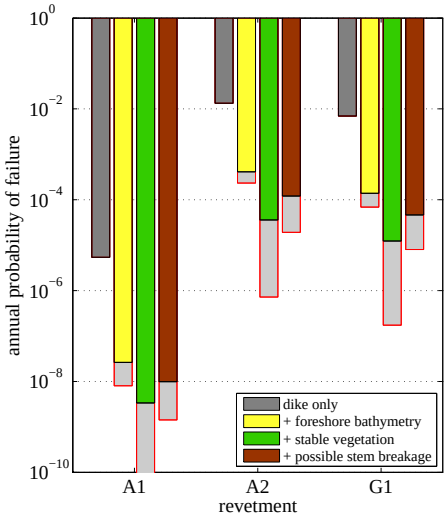

Figure 4.11: *Probability of failure due to wave impact on revetments for a revetment of medium strength (A1) and low strength asphalt on a 1:4 slope (A2), and closed grass sods on a 1:8 slope (G1). Computations with a probabilistic (colored bars) and deterministic (gray bars with red lines) description of the foreshore are shown (see Table 4.3).*

According to the implemented models for asphalt and grass, a high quality grass cover on a 1:8 slope has a strength comparable to low quality asphalt (A2) on a 1:4 slope. Presence of a salt marsh leads to an increase in β of 1.18 (foreshore without vegetation), 1.45 (foreshore with breakable vegetation) or 1.76 (foreshore with stable vegetation), which is similar to the results for an asphalt revetment.

4.4.6. RELEVANCE OF UNCERTAINTIES FOR WAVE IMPACT ON REVETMENTS

Generically speaking, the distribution of uncertainties for wave impact on revetments (Fig. 4.12) is similar to the case of failure due to wave overtopping (Fig. 4.9). The main difference is the contribution of uncertainty in dike strength. For wave overtopping, the overall uncertainty is dominated by the boundary conditions only, with a minor contribution ($\sum \alpha_i^2 \approx 0.02 - 0.05$) of dike characteristics and strength. For asphalt revetments,

uncertainty in asphalt properties is of significant importance ($\sum \alpha_i^2 \approx 0.30 - 0.55$), which implies that failure of asphalt revetments most likely occurs due to a moderate storm combined with a pessimistic scenario for the asphalt strength.

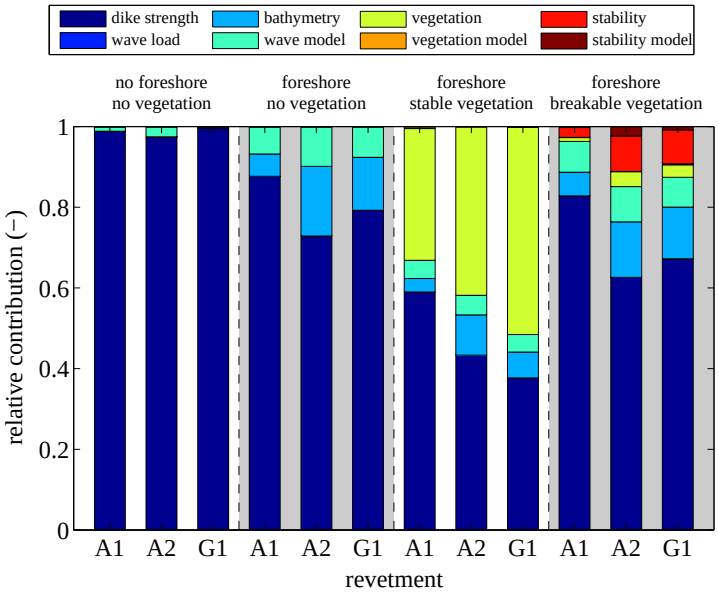

Figure 4.12: *The relative contribution of the different system components from Appendix 4.A to the probability of failure due to wave impact on revetments. System configuration are, from left to right: a dike with no foreshore, a non-vegetated foreshore, a foreshore with stable vegetation, and a foreshore with breakable vegetation. The three bars per system configuration belong to a revetment of medium strength (A1) and low strength asphalt on a 1:4 slope (A2), and closed grass sods on a 1:8 slope (G1).*

Since strong waves are required to break medium strength asphalt (A1), most vegetation will break, and the distribution of uncertainties of a foreshore with breakable vegetation strongly resembles the case of a foreshore without vegetation. For low strength asphalt (A2) and closed grass sods (G1), the uncertainty in vegetation stability is more relevant. However, considering the *Elymus* vegetation as fully stable is not realistic in both cases.

4.5. DISCUSSION

Uncertainties of nature-based flood defenses are not yet systematically evaluated. This study is a first assessment of uncertainties surrounding dikes with a grass or asphalt cover combined with a vegetated salt marsh foreshore. It shows how different foreshore configurations affect failure probabilities of hybrid flood defenses, and how uncertain-

ties in different system components contribute to this probability of failure.

4.5.1. DISCUSSION OF METHODS

The model framework consists of different connected modules, each with its own limitations. Formulas for dike failure due to wave overtopping or wave impact on asphalt and grass covers are simplified descriptions of complicated processes, as well as the description of wave attenuation by flexible vegetation that is prone to stem breakage. Marsh edge erosion is an example of a process that is simply taken into account via a standard deviation on the marsh width. There may be room for improvement in all these models. However, this is outside the scope of the current study, which focuses on integrating different models into one probabilistic calculation framework. The similarity in results for three independent models for dike failure mechanisms gives confidence in more general validity of the main conclusions in this chapter.

Results are based on a specific site with an exposed dike and salt marsh in the Dutch Wadden Sea, with vegetation characteristics of *Elymus athericus*. Choices regarding probability distributions are mostly based on field and flume observations, which results in a realistic case study. Some choices are generically valid, other choices will be more site-specific. The sensitivity analysis shows that trends and conclusions are more broadly applicable than the specific location only. Regardless, the probabilistic framework can be applied to any other location where a dike is loaded by waves, and bordered by a vegetated foreshore. Examples are wetlands surrounding the Mississippi delta (USA) and hybrid flood defenses with mangroves and levees in the Mekong delta (Vietnam).

The First Order Reliability Method (FORM) is a relatively simple probabilistic method, which is able to compute a failure probability in 20-40 iterations. Within each iteration, 2 computations are performed for each stochastic variable, since 2-sided derivatives are applied. Computation times are approximately 1 minute per failure probability on one CPU. Only computations with stem breakage take longer (ca. 10 minutes), since internal sampling from distributions is involved to determine a fraction of broken stems. Alternative probabilistic methods, such as Monte Carlo, Importance Sampling or Numerical Integration require considerably more computational time. We did not experience convergence problems of the iterative FORM computations, as long as continuous functions were used, and an initial design point was specified for which non-zero partial derivatives could be calculated.

4.5.2. DISCUSSION OF RESULTS

Presence of a salt marsh foreshore reduces the failure probability of the dike in behind, compared to a situation with a foreshore around mean sea level. This reduction is caused by depth-induced wave breaking, bottom friction and wave attenuation by vegetation. Stem breakage and an increase in mean wave period $T_{m-1,0}$ are factors that may reduce the efficiency of a vegetated foreshore. The reduction does not only apply to conditions with low water levels, since a system is considered here with positive correlation between

wind speed, water level and wave height, characterized by depth-limitation of the wave height. An increase in water level will be accompanied with an increase in wave height. The ratio between wave height and water depth determines the efficiency of a vegetated foreshore, not the water depth only (Chapter 2). The additional wave damping effect of vegetation on the salt marsh decreases with increasing water depth and wave height, as more stems will break.

The reduction in probability of failure due to wave impact on asphalt revetments or grass covers is more pronounced than for failure due to wave overtopping. The reason is that revetments can already be heavily impacted by waves at relatively low water levels. An increased water level is only needed to obtain a water depth for which high waves can reach the dike. With a foreshore at 0 m MSL, high waves can already damage the lower part of the revetment at a water level of approximately 4 m MSL. When a foreshore is present at 1.7 m MSL, such high waves can only reach the dike for higher water levels, with a much lower likelihood. This directly affects the probability of revetment failure. In contrast, severe wave overtopping and subsequent erosion requires high water levels, close to the dike crest level. The relative difference in water depth between situations with foreshores at 0 and 1.7 m MSL is smaller in that case.

This study shows that the total relative contribution of uncertainties concerning the vegetated foreshore is generally smaller than the contribution of uncertainties related to dike geometry and strength. This seems counter-intuitive, since especially vegetation characteristics are characterized by a high spatial and temporal variability. However, the probabilistic computations shed light on the relevance of such uncertainties for failure of hybrid flood defenses. Uncertainty in dike strength is still dominant in most cases. This finding allays concerns about a lack of certainty with respect to this kind of solutions (Bouma et al., 2014), on short time scales. This holds for both dike failure mechanisms that were considered in this study: erosion of the crest and rear slope due to wave overtopping and erosion of the outer slope revetment due to direct wave impact.

The relevance of different uncertainties depends on the protection level. In the application shown in this study, vegetation and the related uncertainties are only relevant for the low dike. Most vegetation will withstand the wave forcing, since relatively low waves already lead to overtopping of the dike. The amount of standing vegetation strongly depends on the stability characteristics. Also uncertainties in initial vegetation state (stem diameter, height and density) are important. These characteristics lose importance with increasing dike height and protection level. Eventually, for a very high dike, which should withstand high waves, it is very likely that almost all vegetation will break. It is not reasonable to take into account wave attenuation by vegetation, while disregarding the threshold of stem breakage. Wave forces that lead to failure of the dike are too strong for the vegetation, and the distribution of relevant uncertainties is very similar to the situation of a dike with a non-vegetated foreshore.

Flood defenses which provide a relatively low protection level are found in many countries in the world (Scussolini et al., 2016). These countries are confronted with other

relevant uncertainties than countries with a high protection level (Fig. 4.13). This finding can be used to make recommendations for future research. Inherent uncertainty and statistical uncertainty (Section 4.2.7) concerning the state of the foreshore and vegetation are especially important for low dikes with low strength. Monitoring and predicting the variability of the foreshore and vegetation is very important in such conditions, as well as restriction of the variability by management, for example by grazing, permeable dams or marsh edge protection. Research and measurements will decrease knowledge uncertainty, and will strongly affect failure probabilities.

In countries with high and strong dikes, uncertainty in vegetation characteristics and foreshore bathymetry is less important (Fig. 4.13). This leads to a paradox: in countries with a high protection level, there is often a lot of data available concerning the foreshore and vegetation, while the need for these detailed data is relatively low. Foreshore geometry is more relevant than the vegetation, because of expected stem breakage in design conditions. Given an initial foreshore state, the overall uncertainty is restricted to the severity of storm conditions (mostly beyond the measured range), and to the dike strength. Therefore, a simple description of foreshore characteristics and processes suffices for high and strong dikes. Further, research regarding the protective value of vegetated foreshores should focus on morphological development, including interactions with vegetation. While the direct role of vegetation under design conditions is limited, it does play an important indirect role in the medium to long term via

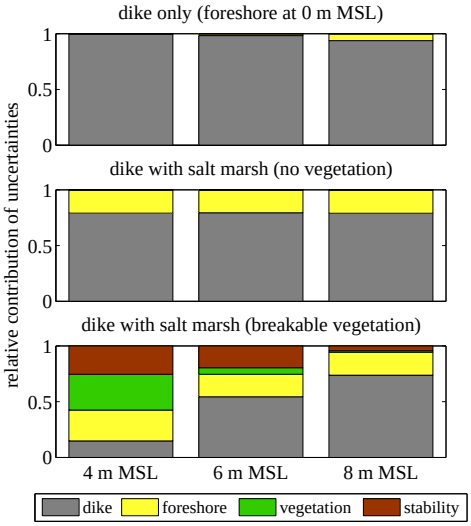

Figure 4.13: *The relative contribution of different uncertainties to the probability of failure due to wave overtopping. Uncertainties are subdivided into (1) dike (geometry, strength and overtopping model), (2) foreshore (geometry and wave model), (3) vegetation (characteristics and model parameters) and (4) vegetation stability (characteristics and model parameters). Contributions are shown for different foreshore configurations (three panels) and different crest levels (horizontal axes).*

bio-geomorphological interactions. Vegetation affects geomorphology via wave attenuation under moderate conditions (Möller et al., 2014), subsequent sediment trapping (Mudd et al., 2010), and stabilization of the salt marsh platform with its root systems (Francalanci et al., 2013; Lo et al., 2017).

Nature-based solutions for flood risk reduction are supposed to reduce the effect of climate change (Kirwan and Megonigal, 2013). This can partly be attributed to the aforementioned sediment trapping capacity, which makes that the foreshore can keep pace with sea level rise. This study confirms that accretion on the foreshore is required to retain its efficiency. Further, higher offshore waves lead to a greater effect of foreshores on the failure probability, which implies that the impact of increasing storminess (Jones et al., 2012) will be lower if a foreshore is present.

4.5.3. ADDED VALUE OF A PROBABILISTIC APPROACH

Application of a probabilistic approach gives insights in the absolute and relative importance of different uncertainties for flood risk reduction. Many parameters are needed to describe the characteristics and behavior of the hydrodynamics, dike, foreshore and vegetation. It is highly unlikely that unfavorable values for all those parameters occur simultaneously. Accumulation of conservative estimates would lead to an over-conservative design, which should be avoided. This can best be illustrated using a simple example with 2 parameters. We combine a water level with an annual probability of exceedance of 1% (once every 100 years, on average) with a conservatively chosen low bulk drag coefficient with a probability of non-exceedance of only 1%. This combination has a joint annual probability of occurrence of only 0.01% (assuming independence). Probably, the combination of a water level with an annual probability of exceedance of 0.01% (once every 10,000 years, on average) and the mean value of the bulk drag coefficient will lead to a worse situation. Both combinations have the same joint probability of occurrence. There is a need for a method that decides which variables should be chosen conservatively, and which variables may be chosen close to the expected value. The probabilistic method FORM, which was applied in this study, provides such guidance in the form of design points.

4.6. CONCLUSIONS

This study has investigated the probability of failure of a hybrid flood defense, which consists of a dike accompanied with a vegetated foreshore. An integrated modeling framework was developed, combining characteristics and model descriptions of the hydrodynamics, dike strength, foreshore bathymetry and vegetation. Probability distributions were based on field and flume observations. The probabilistic method FORM was applied to determine which uncertainties are most influential, and to compute the overall probability of failure of the dike-foreshore system. In this way, a hybrid flood defense can be assessed according to the same state-of-the-art standards as a standalone dike.

Two wave-driven failure mechanisms were considered: failure due to wave overtopping and failure due to wave impact on dike slope revetments. Vegetated foreshores cause a reduction in dike failure probability, which is caused by wave breaking, bottom friction and wave attenuation by vegetation. The effect of foreshores on wave impact on revetments is larger than their effect on wave overtopping, since waves are able to damage revetments already at moderate water depths, for which differences in foreshore configuration have a relatively high impact. Wave attenuation by vegetation has the highest effect on failure probabilities at low protection levels. This effect will become marginal if a high protection level is required. The flood defense should then be able to withstand high waves, which lead to stem breakage of most vegetation.

The effect of a vegetated foreshore on the probability of failure due to wave overtopping

- increases with foreshore width,
- decreases with overtopping resistance of the dike,
- increases with vegetation strength,
- increases with increasing dependence between wind, water level and wave height,
- increases with offshore wave height,
- and decreases with sea level rise, without change in foreshore elevation.

The model provides insights into the relative contribution of various uncertainties to the failure probabilities. The relevance of different uncertainties depends on system configuration and protection level. For low dikes, most vegetation will withstand the wave forces under design conditions, and uncertainties in vegetation characteristics and behavior strongly influence the probability of failure. For high dikes, the overall short-term uncertainty is restricted to the storm conditions and dike strength. The foreshore causes wave energy dissipation by depth-induced wave breaking on the salt marsh platform.

Hybrid flood defenses can now be assessed according to the state-of-the-art standards based on failure probabilities, in which both uncertainties in load and strength are considered. Different sources of uncertainties can be compared, involved in hydraulic loads, dike geometry and strength, and characteristics of the vegetated foreshore. This enables the assessment of nature-based solutions as an alternative to more traditional engineering solutions.

APPENDICES

4.A. OVERVIEW OF PROBABILITY DISTRIBUTIONS

This Appendix summarizes all parameters and probability distributions used in the calculations, with the following abbreviations. For nature of uncertainty: inherent (I), statistical (S) and/or model uncertainty (M); for location of uncertainty: boundary conditions (B), foreshore (F), vegetation (V), dike (D); for distribution type: normal (N), log-normal (L), uniform (U), Weibull (W), Generalized Extreme Value (G), deterministic (D).

Table 4.A1: *Parameters for dike strength (overtopping, asphalt, grass)*

Variable	Symbol	Units	Nature	Location	Distribution	Parameters
Dike crest level	z_c	m MSL	S	D	N	μ, 0.1
Dike slope angle	α_d	deg.	S	D	N	1/4, 1/80
Tolerable overtopping discharge	q_{max}	$\mathrm{ls}^{-1}\mathrm{m}^{-1}$	I,S	D	N	63, 19
Flexural strength asphalt, A1	σ_{br}	MPa	I,S	D	L	3.0, 0.90
Flexural strength asphalt, A2	σ_{br}	MPa	I,S	D	L	1.5, 0.45
Modulus of subsoil reaction, A1	c_{sub}	$\mathrm{N/m}^3$	S	D	L	60, 12
Modulus of subsoil reaction, A2	c_{sub}	$\mathrm{N/m}^3$	S	D	L	30, 6
Thickness asphalt layer	d_a	m	S	D	L	0.25, 0.025
Stiffness modulus asphalt	S_a	MPa	I,S	D	L	8000, 2400
Poisson's ratio of asphalt	v	-	I,S	D	D	0.35
Fatigue parameter asphalt	V_α	-	S	D	D	0.5
Fatigue parameter asphalt	V_β	-	S	D	D	4.8
Parameter grass strength	C_a	m	I,S	D	L	1.82, 0.62
Parameter grass strength	C_b	1/hr	I,S	D	D	-0.035
Parameter grass strength	C_c	m	I,S	D	D	0.25
Fraction of sand in clay	f_{sand}	-	S	D	D	0.35
Thickness clay layer with roots	d_{tot}	-	S	D	N	0.50, 0.10

Table 4.A2: *Parameters for wave load model (overtopping, grass)*

Variable	Symbol	Units	Nature	Location	Distribution	Parameters
Parameter wave overtopping	a_1	-	M	D	N	0.023, 0.003
Parameter wave overtopping	b_1	-	M	D	N	2.70, 0.20
Parameter wave overtopping	a_2	-	M	D	N	0.09, 0.0135
Parameter wave overtopping	b_2	-	M	D	N	1.50, 0.15
Parameter wave overtopping	a_3	-	M	D	N	-0.79, 0.29
Factor slope angle effect	r_α	-	M	D	N	1.51, 0.11

Table 4.A3: *Parameters for foreshore bathymetry and wave model*

Variable	Symbol	Units	Nature	Location	Distribution	Parameters
Foreshore width	B_{fs}	m	S	F	N	300, 50
Foreshore elevation	z_{fs}	m MSL	S	F	N	1.7, 0.2
Foreshore slope angle	α_{fs}	deg.	S	F	D	1/100
Offshore bed level	z_0	m MSL	S	F	D	0.0
Breaker parameter	γ	-	M	F	N	μ, 0.05
Roughness length scale	k_N	m	M	F	U	0, 0.02
Multiplier to increase $T_{m-1,0}$	f_T	-	M	F	N	1.00, 0.09

Table 4.A4: *Parameters for vegetation, vegetation stability, and model parameters*

Variable	Symbol	Units	Nature	Location	Distribution	Parameters
Stem height	h_v	mm	I,S	V	N	0.70, 0.05
Stem diameter	b_v	mm	I,S	V	N	1.30, 0.13
Stem density	N_v	stems/m^2	I,S	V	N	1225, 575
Stem flexural strength	σ_{max}	MPa	I,S	V	N	40, 12
Variation of h_v	CV(h_v)	-	I,S	V	N	0.02, 0.01
Variation of b_v	CV(b_v)	-	I,S	V	N	0.23, 0.05
Variation of σ_{max}	CV(σ_{max})	-	I,S	V	N	0.70, 0.12
Reduction factor for leaning	f_r	-	S	V	N	0.87, 0.04
Height of broken stems	$h_{v,br}$	mm	S	V	U	0.02, 0.08
Bulk drag coefficient	$\widetilde{C}_D$	-	M	V	N	0.22, 0.05
Drag coefficient	C_D	-	M	V	N	1.00, 0.25
Friction coefficient	C_f	-	M	V	L	0.010, 0.005
Correction factor stem breakage	A_c	-	M	V	N	1.7, 0.5

Table 4.A5: *Boundary conditions (wind, water level, waves)*

Variable	Symbol	Units	Nature	Location	Distribution	Parameters
Wind speed	U_{10}	m/s	I	B	G	2.70, 15.8, -0.11
Still water level	ζ	m MSL	I	B	G	0.38, 2.45, -0.08
Significant wave height	H_{m0}	m	I	B	W	0.60, 2.05
			M	B	N	0.99, 0.19
Mean wave period	$T_{m-1,0}$	s	I	B	W	3.26, 3.71
			M	B	N	0.96, 0.11
Wave impact zone below ζ	Δz	m	I	B	D	1.0
Load duration within Δz	t_{load}	hrs	I	B	N	4.97, 0.68

Table 4.A6: *Pearson correlation coefficients for Gaussian dependence between boundary conditions.*

Variable	U_{10}	ζ	H_{m0}	$T_{m-1,0}$
U_{10}	1.00	0.43	0.76	0.79
ζ	0.43	1.00	0.89	0.85
H_{m0}	0.76	0.89	1.00	0.99
$T_{m-1,0}$	0.79	0.85	0.99	1.00

4.B. FAILURE DUE TO WAVE IMPACT ON GRASS COVERS

This appendix summarizes the formulas describing dike failure due to wave impact on grass covers, and its implementation into a limit state function. Equations for the time required to erode the grass and clay layer are based on De Waal and Van Hoven (2015). Erosion of a grass cover starts at a certain threshold wave height c_c (m), and increases with H_{m0}, depending on the empirical parameters c_a (m) and c_b (1/hr). This relationship reads

$$t_{top} = f_{\alpha_d} 1/c_b \ln\left[\frac{\max((H_{m0} - c_c);0)}{c_a}\right]. \tag{4.B1}$$

The time required to erode the clay layer underneath the grass cover follows from

$$t_{sub} = f_{\alpha_d} \frac{\max((d_{tot} - 0.2);0)}{c_d (1/3)^{1.5} \max((H_{m0} - 0.5);0)}, \tag{4.B2}$$

in which d_{tot} is the layer thickness of the clay layer, including the top layer with grass roots, and c_d is a constant, depending on the sand fraction f_{sand} ($c_d = 1.1 + 8\max(f_{sand} - 0.7;0)$). Discontinuities in the functions may lead to instability of the probabilistic computations. Therefore, expressions of the form $\max(x - x_0);0)$ are replaced by a continuous hinge function ($\max((x - x0);0) = \delta \ln\left[1 + \exp((x - x0))/\delta\right]$), where the scale parameter δ is in the order of 0.01-0.1, depending on the magnitude of x. Kruse (2010) has studied the effect of other slope angles. Based on the differences in erosion duration for 1:3 slopes and 1:6 slopes, a linear correction factor for the slope angle is developed:

$$f_{\alpha_d} = \frac{(r_\alpha - 1)/3}{\tan \alpha_d} + 2 - r_\alpha, \tag{4.B3}$$

where the ratio r_α between 1:6 and 1:3 slopes is 1.51 on average, with a standard deviation of 0.11.

The load duration t_{load} is defined as the duration (hrs) of the period in which the water level is between the peak still water level ζ and a distance of Δz below the peak water level. Storm data were selected from time series with measured water levels, and a mean value and standard deviation of the load duration were determined for different values of Δz. The wave impact zone is assumed to range between still water level and 0.5 times the significant wave height below still water level. Outside this range, there is no wave impact (De Waal and Van Hoven, 2015). Application of a uniform distribution of

the water level over Δz leads to the following expression for the effective load duration (hrs):

$$t_{load,eff} = t_{load} \min\left(\frac{H_{m0}}{2\Delta z}; 1\right). \tag{4.B4}$$

Test simulations showed that the failure probability gradually decreases with increasing Δz, as long as $\Delta z > H_{m0}/2$. The dependence is only weak. Even extremely strong grass covers cannot withstand waves higher than 2.0 m. Therefore, a value of $\Delta z = 2.0/2 = 1.0$ m is selected. The location on the dike slope with the highest probability of exceedance of $Z < 0$ can not be determined beforehand, but follows from the probabilistic computations.

4.C. FAILURE DUE TO WAVE IMPACT ON ASPHALT REVETMENTS

This appendix summarizes the formulas describing dike failure due to wave impact on asphalt revetments. Equations are based on De Waal and Van Hoven (2015). The bending stress σ in Eq. (4.5) depends on the characteristics of the wave impact, the distance along the slope from the considered position on the asphalt layer to the location with the maximum wave impact, the asphalt characteristics, and the characteristics of the subsoil. According to De Looff et al. (2006), the asphalt layer is schematized as an elastic supported beam with small springs, loaded by a triangular-shaped wave impact. The asphalt layer (schematized as beam) is characterized by a thickness d_a (m), a flexural strength σ_{br} (MPa) and a stiffness modulus S_a (N/m^2). Elastic support is provided by the subsoil, which is usually sand. The elasticity of the subsoil is described by a modulus of subsoil reaction c_{sub} (N/m^3). These characteristics are combined into a parameter β, which reads

$$\beta = \sqrt[4]{\frac{3c_{sub}(1-\nu^2)}{S_a d_a^3}}, \tag{4.C1}$$

where ν (-) is the Poisson's ratio of asphalt.

The maximum wave impact can be calculated with a formula, originally proposed by Führböter and Sparboom (1988):

$$p_{max} = 4\tan(\alpha_d)\rho g q_p H_{m0}, \tag{4.C2}$$

where q_p is an impact factor (-) to account for the variability in wave impact of individual waves, given a significant wave height H_{m0}, ρ is the mass density of water (kg/m^3), and g is the gravitational acceleration (m/s^2). The impact factor q_p is described by a log-normal distribution with mean value 3.1 and standard deviation 0.72.

Besides of the impact factor, individual waves also vary in position of the maximum impact with respect to still water level, and in the width of the triangular-shaped wave

load. The position of the maximum wave impact equals $D_p = d_p H_{m0}$, in which the factor d_p follows a normal distribution with mean value -0.50 and standard deviation 0.25. This implies that the position of the maximum wave impact is on average half of the significant wave height below still water level.

Also the width of the wave load scales with the wave height, via $B_p = b_p H_{m0}$, where b_p is log-normally distributed, with mean value 0.65 and standard deviation 0.45. These distributions are continuous representations of the discrete probability distributions, given in De Looff et al. (2006).

Analogue to the model for grass covers, a layer height Δz is considered, with a corresponding load duration t_{load} (hrs). The number of waves N_w in Eq. (4.7) is equal to $3600 t_{load} / T_{mean}$, where T_{mean} is the mean wave period (s). A random water level between ζ and ζ-Δz is assigned to all N_w waves, and combined with a realization from the probability distributions of q_p, d_p and b_p. The same random realizations are used in all computations, to increase stability in the probabilistic computations. The most impacted point is situated at $z = \zeta - 0.5 H_{m0}$, according to the distribution of d_p. The layer height Δz should be large enough, to guarantee that waves at water levels outside the layer do not generate significant bending stresses at $z = \zeta - 0.5 H_{m0}$. However, for a very large layer height Δz, a long storm duration is found, although with only a small fraction of the waves causing high stresses at $z = \zeta - 0.5 H_{m0}$. Test simulations showed that results are nearly identical for approximately $\Delta z > 0.7$ m, so Δz is set to 1.0 m. All N_w waves cause a bending stress σ at this point, which depends on the distance along the slope x ($x \geq 0$) between this point to the position of the maximum wave impact (the center of the triangular-shaped load) via the equations given in De Looff et al. (2006), which depend on p_{max}, β, B_p, x and d_a.

5

LONG-TERM EFFECTIVENESS AND LIFE-CYCLE COSTS

ABSTRACT

Flood risks are increasing worldwide due to climate change and ongoing economic and demographic development in coastal areas. Salt marshes can function as vegetated foreshores that reduce wave loads on coastal structures such as dikes and dams, thereby mitigating current and future flood risk. This chapter aims to quantify long-term (100 years) flood risk reduction by salt marshes. Dike-foreshore configurations are assessed by coupled calculations of wave energy dissipation over the foreshore, sediment accretion under sea level rise, the probability of dike failure, and life-cycle costs. Rising sea levels lead to higher storm waves, and increasing probabilities of dike failure by wave overtopping. This study shows that marsh elevation change due to sediment accretion mitigates the increase in wave height, thereby elongating the lifetime of a dike-foreshore system. Further, different human interventions on foreshores are assessed in this chapter: realization of a vegetated foreshore via nourishment, addition of a detached earthen breakwater, addition of an unnaturally high zone, or foreshore build-up by application of brushwood dams that enhance sediment accretion. The performance of these strategies is compared to dike heightening for the physical boundary conditions at an exposed dike along the Dutch Wadden Sea. Cost-effectiveness depends on three main factors. First, wave energy dissipation, which is lower for salt marshes with a natural elevation in the intertidal zone, when compared to foreshores with a high zone or detached breakwater. Second, required costs for construction and maintenance. Continuous mainte-

This chapter has been published as: Vuik, V., Borsje, B.W., Willemsen, P.W.J.M., & Jonkman, S.N. (2019). Salt Marshes for Flood Risk Reduction: quantifying Long-Term Effectiveness and Life-Cycle Costs. *Ocean and Coastal Management*, **171**, 96–110.

nance costs and delayed effects on flood risk make sheltering structures less attractive from a flood risk perspective. Third, economic value of the protected area, where foreshores are particularly cost-effective for low economic value. Concluding, life-cycle cost analysis demonstrates that, within certain limits, foreshore construction can be more cost-effective than dike heightening.

5.1. INTRODUCTION

Increasing flood risks encourage implementation of coastal ecosystems in flood protection schemes (Chapter 1). In hybrid flood defenses (Fig. 1.1), nature-based elements such as salt marshes are utilized as vegetated foreshores, which reduce hydraulic loads on the flood defense structure behind (Chapter 2). Wave energy dissipation is caused by a combination of wave breaking, bottom friction, and attenuation by vegetation (Möller et al., 1999). The strength of these dissipation mechanisms depends on the wave height to water depth ratio (Chapter 2). In shallow coastal seas, waves are mostly depth-limited during severe storms, also during storms. Depth-limitation of waves makes foreshores highly effective. Salt marshes can retain their effectiveness under sea level rise (SLR) up to a certain rate, due to sedimentation (Kirwan and Megonigal, 2013) and sub-surface expansion by below-ground root growth (Nyman et al., 2006). Global measurements demonstrate that marshes are generally raising in elevation at rates similar to or exceeding historical SLR, and process-based models indicate that marshes are able to survive a wide range of future amplified SLR rates (Kirwan et al., 2016; Schuerch et al., 2018).

Costs are a crucial factor when selecting a certain measure for flood risk reduction. Since dikes with vegetated foreshores can adapt to SLR, proponents claim they are more sustainable and cost-effective than traditional engineering solutions, such as dikes and dams, in times of climate change (Temmerman et al., 2003; Sutton-Grier et al., 2015). According to Narayan et al. (2016), salt marshes and mangroves can be two to five times cheaper than submerged breakwaters for wave heights up to 0.5 m. Although this study made a great effort in collecting costs and benefits from many nature-based flood defenses, they only expressed benefits in terms of wave height reduction instead of in monetary value.

Further, most dikes and dams are supposed to withstand wave heights substantially higher than 0.5 m, for which a comparison of cost-effectiveness is still missing. Reguero et al. (2018) have taken this a step further in a case study for the Gulf Coast of the United States, by comparing investments and averted damage between traditional engineering approaches and nature-based solutions. However, they only expressed the effectiveness of nature-based solutions in the form of general hazard reduction percentages found in the literature, which they assumed to be generally applicable. Therefore, there is still a need for concrete comparison between hard structures and hybrid flood defenses in terms of long-term effectiveness for flood risk reduction, and associated life-cycle costs.

This chapter aims to quantify the long-term cost-effectiveness of salt marshes in reduc-

ing flood risk, in comparison to conventional dike heightening. Several possible human interventions on the foreshore are introduced, aiming to influence its biogeomorphological development and thereby the flood protection level and/or the expected lifetime of the hybrid flood defense. We express the performance of hybrid flood defenses in terms of reduction in probability of dike failure. Flood risk, which is the expected annual damage due to flooding, is generally defined as the product of probability and consequences of dike failure. Although foreshores affect multiple failure mechanisms, only dike failure due to wave overtopping is considered here, since (1) this is often one of the dominant mechanisms for coastal dikes (Danka and Zhang, 2015), (2) wave overtopping directly depends on dike crest level and SLR, and (3) it is affected by vegetated foreshores via wave height reduction (Chapter 2). The failure probability is calculated in a probabilistic assessment, in which the variabilities and uncertainties in storm, salt marsh, and dike characteristics are taken into account (Chapter 4). Cost-effectiveness of different measures is assessed in a life-cycle cost analysis by comparing initial and future investment costs with averted damage (Vrijling, 2001).

First, three issues relevant for implementing vegetated foreshores for long-term flood risk reduction are discussed: stability during storms, long-term morphological development, and strategies for influencing flood risk reduction (Section 5.2). This discussion is based on a combination of literature review and data analysis for evaluating morphological changes of salt marshes. Based on this discussion, the development in time of the failure probability of a dike with vegetated foreshore is computed, thereby taking into account SLR, vertical accretion in response to climate change, lateral foreshore dynamics, and the effect of several human interventions on foreshores (starting from Section 5.4.1). Subsequently, the performance of different strategies is assessed and compared to traditional dike heightening, based on costs and benefits (starting from Section 5.4.3). Finally, advantages and disadvantages of these strategies are discussed from a broader perspective, considering cost-effectiveness for flood risk reduction, required maintenance, environmental impact on the surrounding system, and provision of additional ecosystem services (Section 5.5).

5.2. FORESHORES IN FLOOD RISK MANAGEMENT

In this section, issues are discussed which are pertinent for implementing vegetated foreshores for long-term flood risk reduction: stability of salt marshes under storm conditions (Section 5.2.1), long-term vertical and lateral dynamics of salt marshes (Section 5.2.2), and strategies aiming to affect these dynamics and the associated effectiveness of the foreshore (Section 5.2.3).

5.2.1. STABILITY OF SALT MARSHES DURING STORMS

To consider the effect of a salt marsh foreshore for flood risk reduction, the dike manager has to be convinced that the foreshore will be effective during extreme storm surges or

hurricanes. Stability of salt marshes can be subdivided into morphological stability and vegetation stability. Morphological stability concerns the resistance against erosion and subsequent change in marsh elevation or marsh width. Vegetation stability is related to the strength of the vegetated top layer.

Concerning morphological stability, salt marshes are generally highly stable under wave forcing (Leonardi et al., 2016). For example, Gittman et al. (2014) reported absence of any change in marsh surface elevation due to a Category 1 hurricane with maximum wind speeds of 34 m/s, in contrast to significant damage and collapse of many bulkheads (vertical walls for shoreline protection) in the same area. Spencer et al. (2016) describe the impact of a sequence of simulated full-scale storm surge conditions in a wave flume, with only 6 mm average vertical lowering of the marsh surface. Storms can even cause net accretion on salt marshes (Turner et al., 2006).

However, other studies report extensive erosion of marshes during hurricanes (Morton and Barras, 2011), including large areas from which the marsh mat is torn away and immediately converted into open water (Cahoon, 2006). Marshes with such a substantial elevation loss commonly were either highly deteriorated and/or had a high organic matter content (Cahoon, 2006). According to Howes et al. (2010), differences in hurricane impact can be explained by soil composition and shear strength. Large-scale erosion only occurs in low-strength fresh and brackish marshes, with low day-to-day wave height and tidal amplitude. These marshes usually have a high organic content, and are sometimes affected by nutrients introduced via freshwater river diversions, which promotes poor rhizome and root growth (Kearney et al., 2011). Also sediment starvation can lead to increasing organic matter content, which results in structural weakness and edge failure (Peteet et al., 2018). Salt marshes rooted in mineral soils have much higher shear strengths, and are the most resilient wetlands to erosional storm impacts (Morton and Barras, 2011). Leonardi and Fagherazzi (2015) confirm that local variability in resistance of low-energy marshes might lead to unpredictable failure of large marsh portions with respect to average erosion rates. Marshes exposed to relatively high daily wave energy display constant and predictable average erosion rates, and low susceptibility to episodic severe storm events. In conclusion, marshes normally subject to significant wave energy are less susceptible to erosion during storms (Fig. 5.1), as long as windows of opportunity exist for plant seeds to germinate and seedlings to grow.

Second, stability of the vegetated top layer is important to maintain benefits from wave attenuation and bottom friction. Dense and tall vegetation is known to be highly effective in dissipating wave energy, both in emerged (e.g., Anderson and Smith (2014)) and submerged conditions (e.g., Vuik et al. (2016)). However, stem breakage may occur as wave height increase, thereby limiting the energy dissipating factors to bottom friction on a rough salt marsh surface with the remnants of vegetation (Liffen et al., 2013; Silinski et al., 2015). The maximum wave force that a plant stem can withstand depends on its mechanical properties, such as stem height and diameter, flexibility, and frontal area (see Chapter 3). For high waves (significant wave heights over 1 m), relatively tall

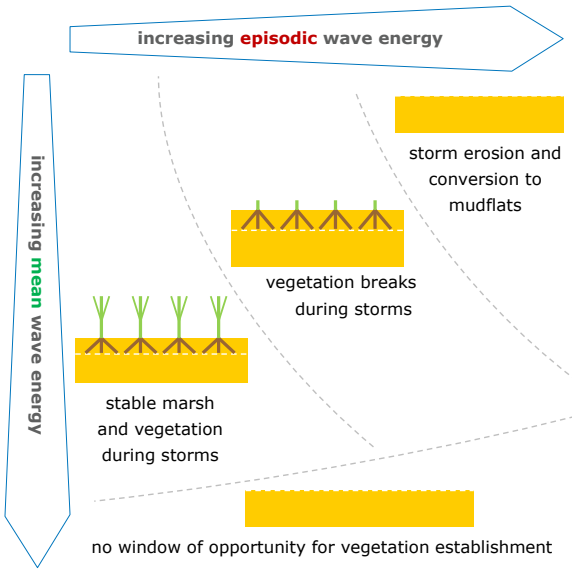

Figure 5.1: *Conceptual view on marsh stability during storms, with higher vulnerability for relatively low mean wave energy, both for vegetation stability (middle) and marsh surface erosion (upper right).*

plant species will lose the majority of their aboveground biomass; a large-scale flume experiment showed 80% stem breakage of *Elymus athericus* (Rupprecht et al., 2017), and 50% reduction in stem density of *Spartina alterniflora* was observed after a Category 1 hurricane (Gittman et al., 2014). Plants at locations exposed to higher mean wave energy develop shorter and thicker stems, which makes them less vulnerable to stem breakage (Silinski et al., 2018). This implies that, similar to morphological stability, locations with low mean wave energy are most sensitive to stem breakage during severe episodic storm events (Fig. 5.1).

5.2.2. TEMPORAL DEVELOPMENT OF SALT MARSHES

For taking into account the effect of a salt marsh foreshore in the design of a dike construction or reinforcement, a life-cycle analysis is required over the expected life time of the structure. This analysis takes into account SLR, as well as the response of marsh width and surface elevation to SLR.

Without adaptation, salt marshes will begin to disappear due to increased rates of SLR (Craft et al., 2009), as more frequent submersion will drown the vegetation and convert what was previously vegetated marsh to open water or bare mudflats (Kirwan and Megonigal, 2013). However, marshes can change in elevation due to biogeomorphological interactions such as sediment accretion (Temmerman et al., 2003) and sub-surface expansion due to root growth (Nyman et al., 2006). These processes result in marsh building at rates similar to or exceeding historical SLR (Kirwan et al., 2016). Marsh sur-

vival is expected to depend primarily on submergence time and suspended sediment concentrations (Kirwan et al., 2010; D'Alpaos et al., 2011), which explains the rapid loss of Jamaica Bay's salt marshes (Hartig et al., 2002). Recent simulations suggest that the resilience of wetlands is primarily driven by the accommodation space available for accumulation of fine sediments. Schuerch et al. (2018) state that coastal managers can strongly influence the survival of salt marshes under climate change, since accommodation space is mainly constrained by built infrastructure in the coastal zone. Tidal wetlands can be safeguarded by facilitating their landward migration under SLR, for example via inland displacement of hard coastal structures.

In addition to vertical variations, marshes can also display lateral dynamics due to seedling establishment and subsequent expansion, and lateral erosion of the marsh edge (Van der Wal et al., 2008). The marsh edge can shift several meters per year and shows cyclic alternations between erosion and expansion on decadal or longer timescales (Allen, 2000; Singh Chauhan, 2009). These variations in marsh width are driven by the interplay between sediment dynamics at the bare mudflat and within the salt marsh (Balke et al., 2016; Bouma et al., 2016).

Section 5.3.2 and Appendix 5.A of this chapter address the importance of vertical and lateral dynamics for failure probabilities.

5.2.3. STRATEGIES FOR INFLUENCING FLOOD RISK REDUCTION

Application of any kind of nature-based solution should fit in the surrounding physical system (De Vriend et al., 2015), and requires an analysis of technical feasibility, legal framework, integration in the landscape, and long-term influence on ecosystem services (Borsje et al., 2011). Generally speaking, vegetated foreshores can be realized or restored in front of a dike via human interventions, both for immediate flood risk reduction and in anticipation of future higher flood risk due to climate change. Here, we summarize several strategies considered in this chapter, including strategies that involve human interventions on the foreshore (Fig. 5.2).

1. The most common strategy in response to SLR is traditional dike heightening. However, dike heightening can be difficult, for example, in cases where buildings are close to the dike or when the subsoil is too soft to support a heavy dike.

2. The most straightforward engineering approach to realizing a vegetated foreshore is via sediment nourishment. After nourishing the original bottom, the core material is covered by a top layer of clayey silt, on which salt-tolerant salt marsh species can germinate, emulating a natural salt marsh. Costs depend on water depth, required elevation, construction method, and availability of local sediment. Use of dredged sediments from shipping channels and harbors can be considered here. High mean wave energy and nutrient-poor sediment diminish the chance of successful vegetation establishment on such a constructed foreshore (Penning et al., 2016). Therefore, salt marsh realization is only feasible in relatively sheltered

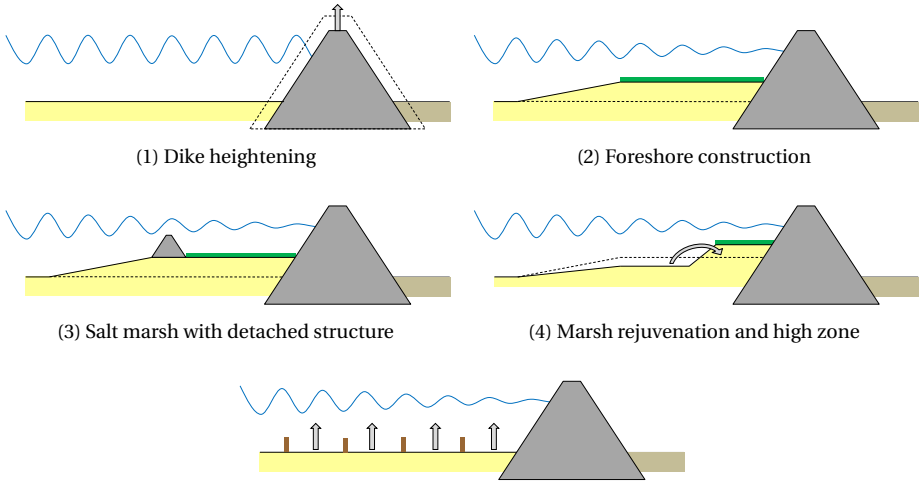

Figure 5.2: *Strategies for reducing flood risk, via dike heightening, or via human interventions on the foreshore.*

coastal systems. For sea dikes with severe waves, a sandy foreshore without vegetation may be more realistic than a vegetated foreshore (Oosterlo et al., 2018).

3. Salt marsh formation or restoration may also be enabled by detached structures, such as breakwaters or stone sills (Currin et al., 2008), which traps sediments from tidal flow to enable ongoing marsh accretion. Such hybrid combinations of natural and engineered shorelines are sometimes referred to as 'living shorelines' (Davis et al., 2015) or 'green infrastructure' (Silva et al., 2017). Presence of structures can lead to higher marsh elevations (Gittman et al., 2014), enhanced erosion resistance during storms, and higher stem densities (Smith et al., 2018), compared to natural marshes. During storms, both the detached structure and the salt marsh can help in reducing wave loads on the flood defense behind the living shoreline.

4. In many places, mature high salt marshes are present with generally lower species richness and nature value than lower, younger, and more dynamic pioneer marsh zones (Bakker et al., 2002). Here, safety and nature goals may be combined, by lowering and thereby rejuvenating the seaward part of the marshes. Dredged sediments can be used to construct a wave breaking high zone on the foreshore, directly in front of the dike. Since this zone is well above the level where natural accretion can be effective, newly accumulated sediments should be moved from the lower, natural part of the foreshore to the high zone, to preserve its wave damping functioning.

5. At exposed coasts, strong waves and currents may impede settling of fine sediments and establishment of salt marsh vegetation or mangroves (Winterwerp

et al., 2013). Construction of a system with brushwood dams (Fig. 1.3) creates shelter, facilitates sedimentation, and prevents lateral erosion. Combining these dams with drainage ditches improves consolidation and aeration of the settled sediment. This method (known as 'salt marsh works') has successfully been applied for centuries, and has led to artificial salt marshes along 450 km of the Dutch, German and Danish Wadden Sea coastline (Bakker et al., 2002; Hofstede, 2003), see Fig. 1.4.

5.3. METHODS

This section describes the methods for assessing long-term effects of vegetated foreshores on flood risk. Long-term development of foreshores is affected by marsh accretion induced by SLR (Section 5.3.2), lateral marsh dynamics (Appendix 5.A.1) and human interventions (5.3.4). Finally, the methods used to assess costs (5.3.5) and cost-effectiveness are described (5.3.6).

5.3.1. SYSTEM DESCRIPTION AND PROBABILISTIC MODELING APPROACH

Sea level rise, salt marsh dynamics, and human interventions affect the failure probability of a hybrid flood defense, which consists of a dike and a salt marsh foreshore (Fig. 1.10).

The probabilistic model of Chapter 4 is used for evaluating the failure probability of the hybrid flood defense for different points in time under SLR (see section 5.3.2). The main characteristics of this model are summarized here for clarity. A wave overtopping discharge q is computed using EurOtop (2016), including uncertainty in the associated model parameters. This wave overtopping discharge is compared with a tolerable wave overtopping discharge q_{max}, which depends on the erosion resistance of the dike crest and rear slope. Dike failure is described via the Limit State Function, represented by Eq. (4.3).

Comparison of failure probabilities for different foreshore configurations requires a relatively quick and simple calculation method. Therefore, wave propagation over the vegetated foreshore is computed by means of a one-dimensional wave energy balance:

$$\frac{dEc_g}{dx} = S_{in} - S_{ds,w} - S_{ds,b} - S_{ds,f}, \tag{5.1}$$

see Section 4.2.2 for a description of the elements in this equation. The energy balance is discretized, using a first order numerical scheme with step size $\Delta x = 10$ m. The offshore wave period T_p is considered in the energy balance, and the mean wave period $T_{m-1,0}$ in the overtopping calculations. A change in mean wave period $T_{m-1,0}$ on the foreshore is computed, using the equation of Hofland et al. (2017), with multiplication factor f_T with mean value of 1.00 and standard deviation of 0.09.

Most salt marsh vegetation will break under design conditions at exposed salt marshes (see Chapter 4). Therefore, the modeling approach with wave energy dissipation by cylindrical elements, combined with a calculated fraction of broken stems per grid cell (Fig. 4.2), is replaced by a much simpler representation by means of bottom friction according to Madsen et al. (1988). A Nikuradse roughness height $k_N = 0.05 \pm 0.02$ m is used, based on Manning values typically used for marshland in hurricane conditions (Wamsley et al., 2010). For bare tidal flats, $k_N = 0.001$ m is applied. The resulting simplified model framework is shown in Fig. 5.3.

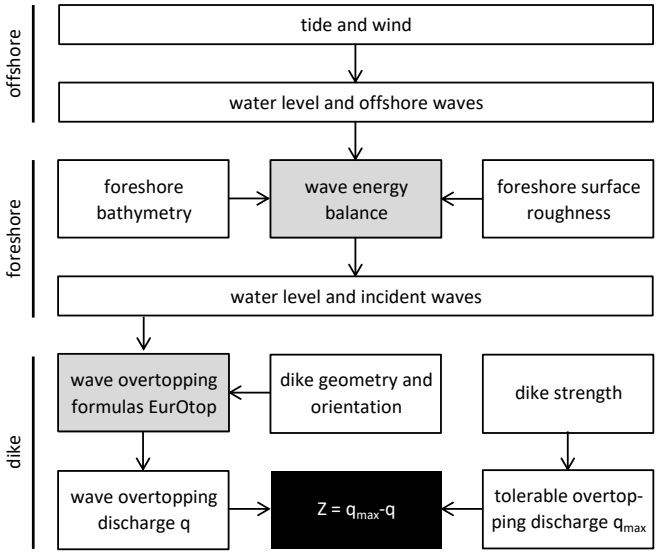

Figure 5.3: *Model framework to compute a probability of failure. The Limit State Function Z is defined as the difference between strength (tolerable overtopping discharge) and load (actual wave overtopping discharge).*

Boundary conditions for this model are a uniform wind speed and water level, and a wave height and period at the offshore boundary at the tidal flats, which are all specified via extreme value distributions with Gaussian correlation between parameters. For wave propagation over foreshores with submerged breakwaters, the formula of Van der Meer et al. (2005) for wave transmission over smooth, low-crested structures is added to the wave energy balance. The dike geometry, still water level, and wave conditions at the landward end of the foreshore are used for calculating a wave overtopping discharge.

The failure probability is computed using the probabilistic method FORM (Hasofer and Lind, 1974). This method iteratively draws numbers from all probability distributions and assesses the response of the Limit State Function via the model framework (Fig. 5.3). The end result is a probability of failure and the most likely combination of parameter values that leads to failure (the so-called design point). Table 5.1 shows how

the failure probability declines for increasing dike crest level. Further, the return period $T = 1/P_f$ is included, which can be interpreted as the average number of years between consecutive dike failures.

Table 5.1: *Annual failure probability P_f and return period T for dikes with different crest levels z_c and a foreshore at 0 m above mean sea level (MSL), including the boundary conditions in the design point: wind speed U_{10}, still water level ζ, offshore significant wave height H_{m0} and offshore mean wave period $T_{m-1,0}$.*

z_c (m MSL)	P_f (-)	T (year)	U_{10} (m/s)	ζ (m MSL)	H_{m0} (m)	$T_{m-1,0}$ (s)
4	$8.1{\cdot}10^{-2}$	12	22.2	3.29	1.03	4.27
5	$8.6{\cdot}10^{-3}$	120	25.2	3.92	1.34	4.80
6	$5.4{\cdot}10^{-4}$	1,900	27.9	4.55	1.62	5.22
7	$1.8{\cdot}10^{-5}$	56,000	30.3	5.14	1.89	5.58
8	$2.4{\cdot}10^{-7}$	$4.1{\cdot}10^{6}$	32.3	5.66	2.16	5.91
9	$1.1{\cdot}10^{-9}$	$9.5{\cdot}10^{8}$	33.8	6.08	2.40	6.19
10	$1.3{\cdot}10^{-12}$	$7.7{\cdot}10^{11}$	34.9	6.39	2.64	6.45

5

5.3.2. SEA LEVEL RISE AND MARSH ELEVATION CHANGE

Time-dependent scenarios for SLR are adopted from Table AII.7.7 of IPCC (2013). The mean values of the IPCC scenario with the highest sea level change in 2100 are used here: RCP8.5 with 0.74 m in 2100, compared to the reference period 1986-2005 ($t = 0$ in the central year 1996). Waves in the shallow Wadden Sea are depth-limited, implying that wave heights will increase as sea level rises (Arns et al., 2017). This effect is taken into account by keeping the wave height to water depth ratio and wave steepness equal to the situation without SLR.

For changes in marsh elevation, two basic situations are considered first: no temporal change at all ($dz_{fs}/dt = 0$), and a rate of change exactly equal to the rate of SLR ($dz_{fs}/dt = R(t)$), where $R(t)$ is the time-varying rate of SLR. In addition, a rate of change is estimated using the analytical approach by D'Alpaos et al. (2011). They describe how the accretion rate depends on the marsh elevation within the tidal range and suspended sediment concentration (SSC). The accretion rate decreases linearly from k at MSL to zero at Mean High Water H, according to the following differential equation proposed by D'Alpaos et al. (2011):

$$\frac{dz}{dt} = k\left(1 - \frac{z}{H}\right) - R(t), \tag{5.2}$$

in which z is the marsh elevation relative to a changing mean sea level, such that $dz/dt = dz_{fs}/dt - R(t)$, where z_{fs} is the foreshore elevation relative to MSL at $t = 0$. IPCC scenario RCP8.5 can be approximated by an accelerating sea level change $R(t) = R_0 + at$, with $R_0 = 2.14$ mm/year in 1996 and $a = 0.095$ mm/year^2.

For an arbitrary initial foreshore elevation $z_{fs,0}$, a time-varying elevation $z_{fs}(t)$ is found using the following solution of the differential equation, Eq. (5.2):

$$z_{fs}(t) = c_1 H + \left(z_{fs,0} - c_1 H\right) e^{-kt/H} - \frac{aH}{k} t, \tag{5.3}$$

in which the dimensionless constant c_1 reads

$$c_1 = 1 + \frac{aH}{k^2} - \frac{R_0}{k} \approx 1. \tag{5.4}$$

5.3.3. CASE STUDY CHARACTERISTICS

The development of the failure probability over time is investigated in this chapter for a case study located in the Dutch Wadden Sea. The Wadden Sea is a shallow coastal sea, separated from the North Sea by a series of barrier islands, stretching for over 500 km along the coasts of Denmark, Germany, and the Netherlands. It consists entirely of a sandy-muddy system of interconnected channels, tidal flats, and salt marshes. Barrier islands are separating the Wadden Sea from the North Sea.

The tidal flats and salt marshes form the largest coherent habitat of this type in Europe and are together an essential element of the Wadden Sea ecosystem, a biologically highly productive ecosystem of great natural, scientific, economic and social importance. Because of its unique size and ecological value, large parts of the Wadden Sea have been designated as UNESCO World Heritage Sites since 2009. Denmark, Germany, and the Netherlands have adopted the Trilateral Wadden Sea Plan (2010), which states that 'sustainable human use will continue and have to be continuously balanced in a harmonious relationship between the needs of society and ecological integrity' (CWSS, 2017). Future flood risk reduction strategies should be evaluated in that context.

Within the Wadden Sea, a case study location has been selected, situated along the dike that protects the province Groningen in the Netherlands (Fig. 4.6). Man-made salt marshes are present here along approximately 25 km of the dike between Eemshaven and Lauwersmeer. The same case study location is used in Vuik et al. (2018b), where a detailed description of all site parameters can be found (Section 4.3). Here, we only summarize the main characteristics of the dike and the existing salt marsh (stochastic parameters are presented as mean value ± standard deviation).

The dike has a crest level z_c at 8 m above MSL, and an outer slope angle $\tan(\alpha_d) = 1/4$. The tolerable overtopping discharge $q_{max} = 63 \pm 19\,\mathrm{l\,s^{-1}\,m^{-1}}$. For the actual dike height of 8 m MSL, no measure is needed, and the 'do nothing' strategy is economically most attractive. In this study, we would like to obtain a situation with a need for flood risk reduction via either traditional dike heightening or a nature-based solution with foreshores. Therefore, the dike height is lowered to 6 m MSL in all calculations, for which flood risk reduction should be considered.

The foreshore is simplified, with a flat vegetated part with a width B_{fs} of 300 ± 50 m, an elevation z_{fs} of 1.5 ± 0.2 m MSL (close to Mean High Water), and a 1:100 slope from

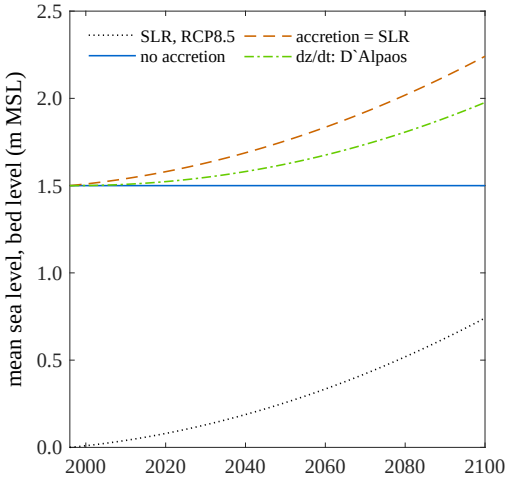

Figure 5.4: *Sea level rise (SLR) according to RCP8.5, and corresponding scenario's for marsh accretion: no accretion, accretion equal to SLR, and accretion according to Eq. (5.3).*

the marsh edge to the adjacent tidal flats at 0 m MSL (Fig. 1.10). The standard deviations reflect spatial variations, measurement inaccuracy, and possible erosion under design conditions. Vegetation is applied above 0.6 m MSL (including SLR), which is the actual marsh edge position in the Wadden Sea (Dijkema et al., 1990).

For Wadden Sea conditions, with a tidal amplitude H of approximately 1.5 m and a mean SSC of 70 mg/L (Borsje et al., 2008), a maximum vertical accretion rate of k = 54 mm/year is given in D'Alpaos et al. (2011). For these numbers, Eq. (5.2) results in 0.48 m gross accretion in 2100, which is less than 0.74 m SLR in the same year (Fig. 5.4). Table 5.2 summarizes characteristics of the boundary conditions for this location.

5.3.4. CHARACTERISTICS OF STRATEGIES

Different strategies for flood risk reduction are considered, as introduced in Section 5.2.3. This section describes how these strategies are technically accounted for in the failure probability calculations and cost estimates. All foreshores between the level above which vegetation establishes (0.6 m MSL) and Mean High Water (1.5 m MSL) are assumed to display an accretion rate according to Eq. (5.2), see Fig. 5.5.

1. First, we consider traditional dike heightening from 6 to 7 m MSL.

2. Next, we consider construction of a 300 m wide foreshore at 1.5 m MSL via nourishment, with standard deviations of 50 m and 0.2 m, respectively, to account for spatial variations. The bathymetry of this foreshore resembles that of a natural mature salt marsh. Vegetation is expected to establish, and accretion occurs in tandem with SLR (Fig. 5.5). High foreshores are most efficient from an engineering perspective, whereas low foreshores may be more suitable for establishment

Table 5.2: *Probability distributions, characteristic values and Pearson's correlation coefficients for boundary conditions.*

Parameter	Wind speed	Still water level	Significant wave height	Mean wave period
Symbol	U_{10}	ζ	H_{m0}	$T_{m-1,0}$
Units	m/s	m MSL	m	s
Distribution	GEV	GEV	Weibull	Weibull
Shape parameter	-0.14	-0.08	2.33	5.33
Scale parameter	2.70	0.38	0.70	3.62
Location parameter	17.5	2.45		
1/10 year value	22.7	3.23	1.00	4.23
1/100 year value	26.7	3.91	1.35	4.82
1/1000 year value	29.5	4.47	1.60	5.20
Correlations ρ:				
with ζ	0.80			
with H_{m0}	0.91	0.96		
with $T_{m-1,0}$	0.88	0.97	0.99	

of ecologically valuable salt-tolerant plant species. The foreshore elevation can be used for optimizing the performance of a design. For the computation, we only consider the value of 1.5 m MSL.

3. A possible design alternative is the addition of an earthen or rubble mound breakwater at the marsh edge of the same foreshore as (2.). A small detached earthen breakwater is considered, with a 3 m wide crest at 2.5 m MSL (i.e., 1.0 m above ground level of 1.5 m MSL) and 1:6 slopes. We neglect possible influence of the breakwater on accretion rates. The standard deviation for marsh width is set to zero in this simulation.

4. The constructed foreshore can also be designed with a geometry deviating from that of a natural salt marsh. In this chapter, we propose a foreshore with an identical volume to (2.), but consisting of a 100 m wide high zone at 3.20 m MSL directly in front of the dike (which is several wave lengths long, sufficient for wave breaking), bordered by a 200 m wide lower zone at 0.65 m MSL. This lower zone is higher than the level of 0.60 m MSL for which pioneer vegetation establishes (Section 5.3.3). The slope angle between both zones is 1:25, which is expected to be stable during storms. Every 20 years, newly accumulated sediments on the low zone are displaced to the high zone via earthmoving, in such way that the high zone keeps pace exactly with SLR (Fig. 5.5, two dashed lines). The initial elevation of the high zone is iteratively chosen, so that its initial effect (in 1996) is identical to that of 1 m dike heightening, due to intense wave breaking on the high zone.

5. Finally, we consider facilitation of accretion by means of brushwood dams, result-

ing in an initial constant accretion rate of 2 cm/year on the bare tidal flats, as typically found in salt marsh works in the Wadden Sea (Hofstede, 2003). When the bed level exceeds the threshold of 0.6 m MSL (MSL after SLR), vegetation starts to settle, and accretion follows Eq. (5.2).

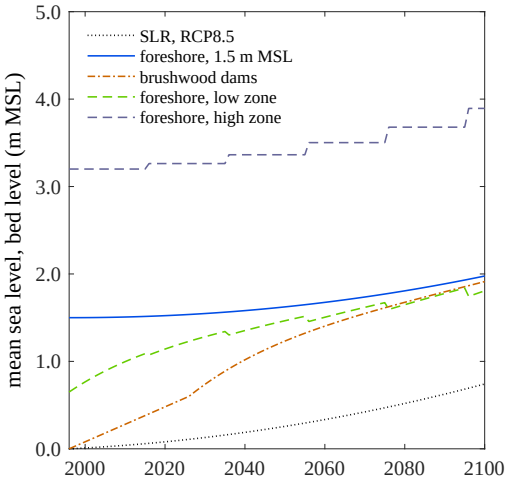

Figure 5.5: *Sea level rise (SLR) according to RCP8.5, and elevation in time for a nourished foreshore (1.50 m MSL at $t = 0$), brushwood dams, and a foreshore consisting of a low zone (0.65 m MSL at $t = 0$), and a high zone (3.20 m MSL at $t = 0$) which is regularly heightened.*

5.3.5. COSTS OF STRATEGIES

Construction and maintenance costs are estimated for the different strategies of Fig. 5.2, and included in Table 5.3. All unit prices are converted to 2018 price level, based on historic values of the consumer price index in the Netherlands, according to the Central Office for Statistics (CBS). Net Present Value (NPV) is calculated, using an interest rate of 3% per year over the period 1996-2100. Costs for maintenance of the dike itself are not taken into account, assuming that dike heightening or interventions on the foreshore do not affect the required maintenance for the dike.

1. Costs for 1 m heightening of 1 km dike are based on numbers for rural area in Jonkman et al. (2013).

2. Costs for foreshore construction (Fig. 5.2, configuration 2) are based on transforming tidal flats (0 m MSL) into 300 m wide marshland (1.5 m MSL) via dredging and nourishing, with a unit price of 2.4-7.0 €/m^3. The resulting costs of 1.3-3.7 M€ per km are equivalent to 3.6-10.4 €/m^2 marshland. Costs are relatively high, compared to the average costs of 0.9 €/m^2 (range 0.01-28 €/m^2) in Narayan et al. (2016) and 3.5 €/m^2 in Jonkman et al. (2013) (price level 2007 converted to 2018), due to

Table 5.3: *Cost comparison of the different strategies from Fig. 5.2. *The mentioned costs for the detached earthen breakwater and earthmoving to high zone are in addition to the costs for foreshore construction, which is also present in these strategies.*

	1	2	3	4	5
	Dike heightening, 1 m	Foreshore construction	Detached earthen breakwater*	Earthmoving to high zone*	Brushwood dams Wadden Sea
Unit price construction	4.5-12.4 M€	2.3-6.7 €	7.5-12.5 €	0.4 €	130 €
Unit price maintenance	x	x	x	3.0-10.0 €	22 €
Maintenance interval	x	x	x	20 years	1 year
Unit	km	m^3	m^3	m^3	m^1
Source	*1	*1	*2	*3	*4
Year of unit prices	2006	2013	1995	1995	2018
Unit price constr., 2018	5.4-14.9 M€	2.4-7.0 €	11.5-19.2 €	0.4 €	100 €
Unit price maint., 2018	x	x	x	4.6-15.4 €	22 €
Units/km, constr	1	525,000	20,500	525,000	2,200-5,000
Units/km, maint	x	x	x	6,000-21,000	2,200-5,000
Constr. costs/km (M€)	5.4-14.9	1.3-3.7	0.20-0.40	0.20	0.50
Maint. costs/km/interval	x	x	x	0.03-0.32	0.05-0.11
NPV 1996-2100 (M€)	5.4-14.9	1.3-3.7	0.20-0.40	0.25-0.37	1.9-3.6

Sources for unit costs:
*1 = Jonkman et al. (2013)
*2 = https://www.bodemrichtlijn.nl/Bibliotheek/bodemsaneringstechnieken/c-grondverzet/c6-herstellen-bodemprofiel/herstellen-bodemprofiel-kosten, visited 15-6-2018
*3 = https://www.bodemrichtlijn.nl/Bibliotheek/bodemsaneringstechnieken/c-grondverzet/c2-open-ontgraven/open-ontgraven-kosten-verwijderen-grond, visited 15-6-2018
*4 = Personal Communication Rijkswaterstaat, division Northern Netherlands

the substantial raising by 1.5 m. It is assumed that no significant maintenance is needed to preserve the foreshore.

3. Costs for a detached earthen low-crested breakwater (Fig. 5.2, configuration 3) are based on unit prices of clay for construction purposes, for a 1 m high dam on existing marshes, with slope angles of 1:6 and a crest width of 3 m. These costs are in addition to the costs for constructing the foreshore (configuration 2), which is also present in this alternative. It is assumed that maintenance costs for the earthen breakwater are negligible.

4. For constructing the foreshore with a high and low zone (Fig. 5.2, configuration 4), the volume is identical to that of a uniform foreshore at 1.5 m MSL. We assume that costs for dredging and nourishing are equal for both foreshore geometries, except for a surcharge of 2 €/m^2 for more accurate earthworks profiling on the high zone. This equates to 0.2 M€ per km dike, equivalent to an additional 0.4 € per m^3 foreshore volume. For periodic earthmoving on existing marsh, unit costs are

based on earthmoving of in-situ sediments, using land equipment in wet circumstances (4.6-15.4 €/m^3). All these costs are in addition to the costs of constructing the foreshore (configuration 2), which is also present in this alternative.

5. For salt marsh works with brushwood dams (Fig. 5.2, strategy 5), the contribution of maintenance to the overall costs will be substantial. Costs are based on two zones with sedimentation fields of 300 m wide (perpendicular to the dike) and 200 m long (parallel to the dike), based on the Dutch Wadden Sea (Fig. 5.6). The sedimentation fields at the seaside will lead to raising of the tidal flats, while salt marshes are supposed to emerge in the sedimentation fields at the landside. For constructing this system, a 5 km brushwood dam is needed per 1 km dike. For a stable, mature salt marsh system, only dams near the marsh edge have to be maintained. Currently, 111 kilometers of brushwood dams are maintained for approximately 50 km of coastline with salt marshes (Fig. 5.6, and personal communication with salt marsh manager at Rijkswaterstaat), which is 2.2 km of dam per 1 km of dike. Consequently, maintenance costs will become lower after several decades. Average maintenance costs in the Dutch Wadden Sea are equivalent to 22 €/m per year. In Indonesia, similar dams are applied for mangrove restoration. For comparison: a combination of bamboo poles and brushwoods is relatively expensive (170 €/m for construction, 80 €/m per year for maintenance, personal communication Witteveen + Bos, Indonesia, and Wilms et al. (2018)). Cheaper and more durable materials are currently being tested, such as horizontal bamboo beams between the poles (45 €/m for construction, 15 €/m per year for maintenance).

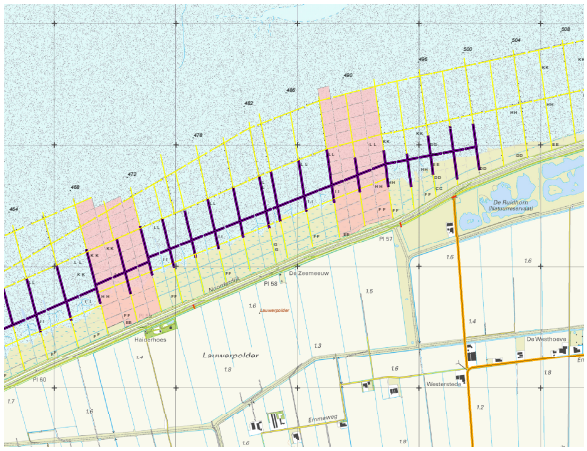

Figure 5.6: *Salt marsh works at the case study location in the Dutch Wadden Sea, with the dike (green line) salt marshes (green shading at the north of the dike), monitored sections (pink shading), maintained brushwood dams (purple lines) and abandoned brushwood dams (yellow lines). Source: Rijkswaterstaat Northern Netherlands. Distance between grid lines is 1 km.*

5.3.6. COST-EFFECTIVENESS OF STRATEGIES

In this study, we determine which strategy is most cost-effective, depending on the damage in case of dike breaching. We only consider benefits in terms of flood risk reduction, the primary objective of flood risk reduction projects, either traditional or nature-based. Although relevant for decision making, economic value of other ecosystem services is not quantified in this study. The most cost-effective strategy leads to the minimum sum of investment costs and expected damage. Investment costs I consist of initial construction costs and the NPV of maintenance costs. Expected damage is defined as the product of time-varying annual failure probability $P_f(t)$ and damage D in case of dike breaching: the expected value of the annual damage.

Total costs C_{tot} are defined as

$$C_{tot} = \sum_t \frac{I}{(1+r)^t} + \sum_t \frac{P_f(t)\,D}{(1+r)^t}, \tag{5.5}$$

in which r is the interest rate (3%) and t the time since $t = 0$ (1996). For this assessment, the mean values of all cost ranges in Table 5.3 are used. Total costs depend on the damage in the area that is being protected. The optimal strategy will thus also be influenced by this damage.

5.4. RESULTS

This section presents computed failure probabilities of dike-foreshore configurations, affected by SLR and vertical accretion (Section 5.4.1), lateral marsh edge dynamics (5.4.2) and human interventions on the foreshore (5.4.3). The influence on failure probabilities is evaluated in relation to the associated costs (5.4.4).

5.4.1. SEA LEVEL RISE AND ACCRETION RATES

The development of the annual failure probability P_f in time is investigated for a dike with existing foreshore, under different accretion rates (Fig. 5.4). The failure probability increases in time, since SLR leads to a decline in freeboard (i.e., crest level minus still water level) of the dike (Fig. 5.7, upper panel).

The base case is a 'dike only' system, with stationary, non-vegetated foreshore at 0 m MSL. SLR in the period 1996-2100 leads to an increase in failure probability by a factor of 18, from an initial value of $5 \cdot 10^{-4}$ to $1 \cdot 10^{-2}$ in 2100 (Fig. 5.7, middle panel), which is equivalent to a difference in dike height of more than 1 m (Table 5.1). The effect is larger than SLR only, because higher waves can reach the dike at a greater depth. The addition of a vegetated foreshore at 1.5 m MSL (strategy 2, Section 5.2.3) leads initially to a reduction in P_f by a factor of 2.8 (Fig. 5.7, lower panel), compared to the 'dike only' system. Without morphological adjustment to SLR, this effect decreases to a factor of 2.1 in 2100.

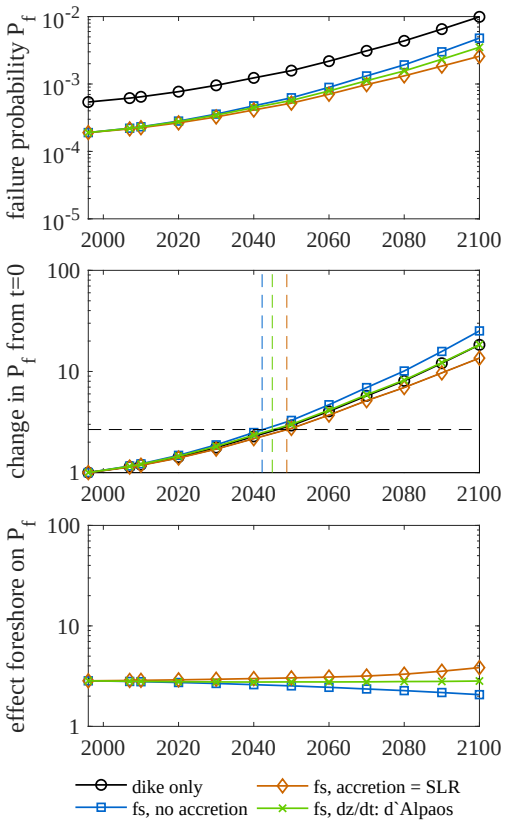

Figure 5.7: *Top panel: annual failure probability P_f in time for different accretion rates of the foreshore (abbreviation 'fs'). Middle panel: the change in P_f with respect to $t = 0$ due to the combination of SLR and accretion (multiplication factor). Bottom panel: reduction factor of P_f with respect to the 'dike only' system.*

Contrastingly, an increasing effect is found in case of accretion equal to SLR (from 2.8 in 1996 to 3.8 in 2100). More realistic accretion, according to Eq. (5.2), results in a more or less constant factor of 2.8 in P_f. After 50 years (a typical lifetime for structures like seawalls), the failure probability of the 'dike only' system has increased by a factor of 2.7 (Fig. 5.7, middle panel, black dashed lines). The same increase is reached 4 years earlier in the case of a foreshore without accretion, and 3 years later with accretion equal to SLR. Therefore, foreshore adjustment to SLR leads to a 7 year difference in lifetime (14%) for this system.

5.4.2. LATERAL MARSH DYNAMICS

At the case study site in the Wadden Sea, lateral marsh dynamics are small due to the presence of brushwood dams. Therefore, temporal variations in marsh width B_{fs} are investigated for unprotected salt marshes in the Western Scheldt, an estuary in the South-

West of the Netherlands. This analysis is included in Appendix 5.A. Fig. 5.8 shows, as an example, the result for the salt marsh with the largest variation in width.

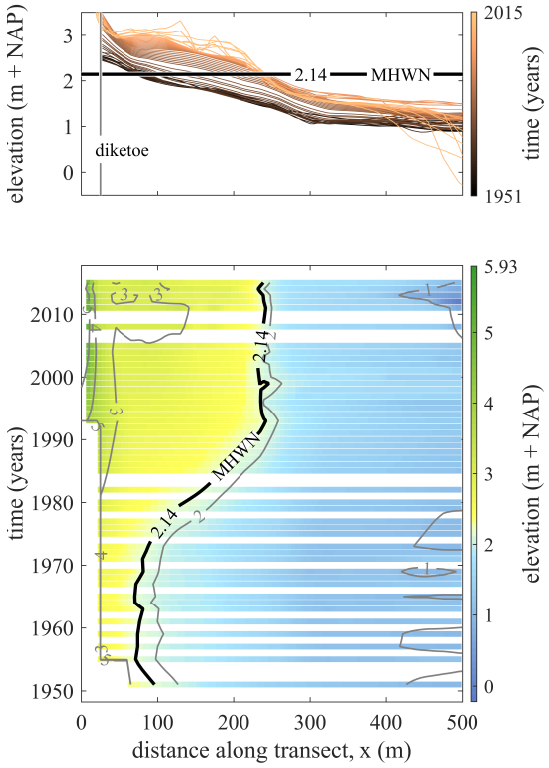

Figure 5.8: *Profiles of the salt marsh and mudflat at 'Zimmermanpolder' between 1951 and 2001 (top panel), including the vertical position of the marsh edge at MHWN (2.14 m+NAP) and the fixed dike toe position. Old profiles are indicated with darker colors, and recent profiles with light colors. Lateral marsh edge dynamics display marsh expansion (bottom panel). Colors indicate elevation. The higher landward side of the profiles is at $x = 0$, while the lower seaward side is at $x = 500$ m. Gray contour lines are added for clarity; the black line indicates the marsh edge at MHWN.*

Fig. 5.9 shows how such variations in foreshore width would affect the failure probability of the case study system, with a foreshore at 1.5 m MSL (Fig. 1.10). Most marshes in the Western Scheldt displayed a limited variation in the considered period of 65 year, see Appendix 5.A. The maximum difference in marsh width of 170 m (Table 5.A1) leads to a change by a factor of 1.34 with respect to the failure probability at a marsh width of 300 m (Fig. 5.9, 385 to 215 m). This is equivalent to a difference in dike crest level of 9 cm and a difference in foreshore elevation of 38 cm. As marsh width increases, variations in width have decreasing influence on failure probabilities. The influence of foreshore width does not change noticeably after SLR and subsequent accretion is considered according to Eq. (5.2) (lower panel).

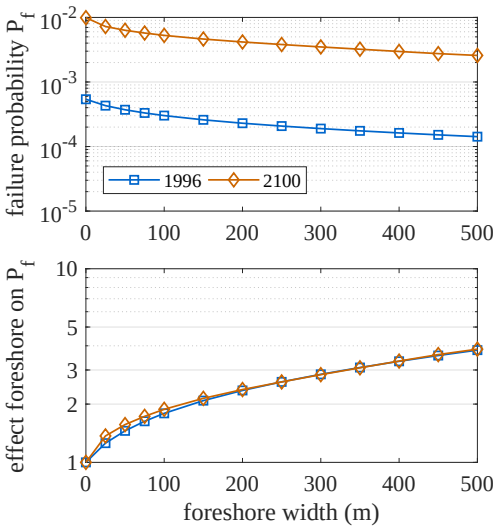

Figure 5.9: *Variation with foreshore width of (1) the failure probability in 1996 and (after sea level rise) in 2100 (top panel), and (2) the factor with which P_f decreases with respect to a 'dike only' system (bottom panel).*

5.4.3. PERFORMANCE OF STRATEGIES FOR FLOOD RISK REDUCTION

Different strategies for flood risk reduction are considered, as introduced in Section 5.2.3. These strategies are compared in terms of failure probabilities in the period 1996-2100. Effects are expressed in terms of a reduction factor on the failure probability of the 'dike only' system (Fig. 5.10, lower panel), with crest level at 6 m MSL and foreshore at 0 m MSL.

0. In case of the 'do nothing' strategy, the 'dike only' system with crest level at 6 m MSL displays an increase in failure probability by a factor of 18 in the period 1996-2100 (mentioned in Section 5.4.1 and visible in Fig. 5.10, middle panel).

1. Dike heightening from 6 to 7 m MSL initially has an effect of a factor of 31, decreasing to 14 in 2100 (Fig. 5.10, lower panel). This decrease is primarily caused by SLR, and secondly due to subsequent higher exposure to waves.

2. Construction of a 300 m wide foreshore at 1.5 m MSL leads to a reduction of the system's failure probability by a factor of 2.8, with respect to a dike only (Fig. 5.10, lower panel). This effect is rather constant in the period 1996-2100 due to sediment accretion.

3. Addition of an earthen or rubble mound breakwater at the marsh edge of the same foreshore initially has a relatively large effect: a reduction factor of 5.6, which is 2.0 times larger than the effect of a foreshore only (2.). However, going to 2100, the breakwater's additional effect declines due to increasing submergence. This

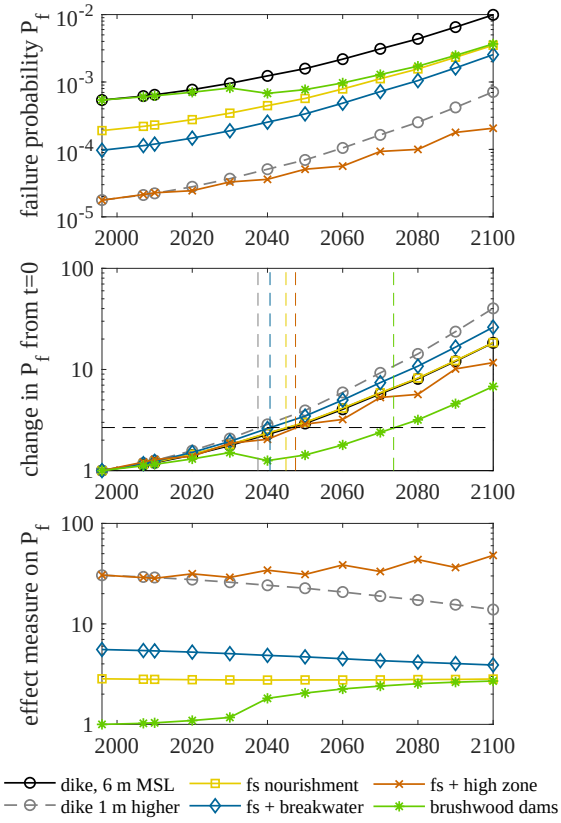

Figure 5.10: *Top panel: annual failure probability P_f in time for different strategies, including dike heightening and human interventions on the foreshore (abbreviation: fs). Middle panel: the change in P_f with respect to $t = 0$ (multiplication factor). Bottom panel: reduction factor of P_f with respect to the 'dike only' system.*

leads to a decrease in the added value of the breakwater in 2100: only a factor of 1.4 compared to the situation with a constructed foreshore (where a factor of 1.0 means no effect).

4. Further, we consider the foreshore that consists of a high zone directly in front of the dike and a low zone with pioneer vegetation. The initial effect of the foreshore is identical to that of 1 m dike heightening (a factor of 30 in 1996), since the foreshore elevation was iteratively chosen to obtain this failure probability. The repetitive earthmoving from the natural marsh to the high zone leads to a reduction factor of 47 in 2100, significantly higher than the factor of 14 of 1 m dike heightening at the same time (Fig. 5.10, lower panel).

5. Application of brushwood dams results in accretion and salt marsh establishment. This intervention has initially no effect on the system's failure probability. How-

ever, in 2100, its effect approaches that of a system with a constructed foreshore (factors of 2.7 and 2.8, respectively, see Fig. 5.10, lower panel), provided that the dams are continuously maintained and heightened. In 2034, vegetation establishes, and the effect of roughness is added to the wave calculations. In this way, the lifetime of the flood defense can be elongated by 28 years, if 50 years is considered as a reference situation (dashed vertical lines in middle panel of Fig. 5.10).

5.4.4. COST-EFFECTIVENESS

In comparing dike heightening and foreshore construction in terms of cost-effectiveness, we first consider 1 m dike heightening and the foreshore with high zone. The high zone initially has an identical effect on the system's failure probability as 1 m dike heightening. This enables straightforward cost-effectiveness comparison of two measures that induce an instantaneous decrease in flood risk. A 1 m dike heightening costs 5.4-14.9 M€, while construction of a 300 m wide foreshore with 100 m wide high zone costs 1.5-3.9 M€. This shows that a high foreshore is a cheaper strategy for coastal protection than dike heightening in this case study, provided that sufficient space and relatively shallow water is present in front of the dike.

Further, we investigate which strategy is most cost-effective, taking into account costs for construction, maintenance, and expected damage after dike failure. Fig. 5.11 shows for different strategies how the NPV of total costs (annual investments plus annual expected damage) depends on the damage after dike failure.

Without damage ($D = 0$), the 'do nothing' strategy obviously has the minimum total costs. For damage above 70 M€, construction of a foreshore with high zone is more cost-effective. Constructing a foreshore with natural elevation at 1.5 m MSL is more cost-effective than 1 m dike heightening for expected damages between roughly 100 M€ and 600 M€ (without breakwater) and between 90 M€ and 1100 M€ (with breakwater). For higher damage, dike heightening is more appropriate. Although sheltering structures such as brushwood or bamboo dams require low initial investments, costs for maintenance are considerable. Further, their effect on safety is only significant after some decades. This postponed effect on flood risk is penalized in the NPV calculation. Therefore, sheltering structures in the current form and associated costs are not attractive from a purely flood risk perspective.

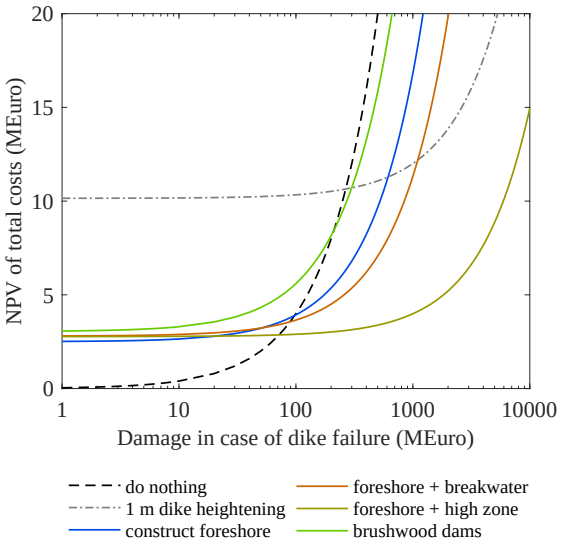

Figure 5.11: *Total costs (in million €, vertical axis) as a function of damage in case of dike failure (in million €, horizontal axis), for different strategies (different lines). The most cost-effective strategy for a given damage is that with the lowest total costs, which is the net present value of all investments and expected damage.*

5.5. DISCUSSION

5.5.1. MULTI-DISCIPLINARY EVALUATION

This chapter has assessed the efficiency of vegetated foreshores, primarily looking from the perspective of engineering, flood risk, and economics. However, these are not the only factors that determine the suitability of solutions in the local situation. For example, in the Wadden Sea, each strategy should be carefully assessed in terms of short-term and long-term effects on the large-scale physical system, including its ecology and associated ecosystem services, and should fit into legal boundaries. For the case of (man-made) salt marshes, an assessment is required of the viability of salt marshes within the physical boundary conditions of the large-scale system, including available space, tidal range, sediment concentration, flow intensity, and wave action. Further, the ecological value of the salt marsh itself should be investigated, as well as interactions between the salt marsh and neighboring aquatic ecosystem.

Traditionally, flood defenses are located within their predefined narrow borders, fully apart from the ecosystem in front. Dike reinforcement and ecological restoration are performed separately by different institutions. Dike heightening can easily be applied within the zone that is designated for flood protection. In contrast, when working with foreshores, measures should fit in the large-scale physical and ecological system, which requires a multi-disciplinary approach to flood protection. Although decision making can be more challenging and time-consuming, combined benefits for flood protection

and nature conservation can potentially be improved if such an integrated approach is adopted (Janssen et al., 2015).

Adaptive flood risk management comprises flexibility in measures and strategies, in order to allow for speeding up or slowing down. This way, flood risk managers avoid undesirable exposure to flood risk and exorbitant investments that may be done in response to uncertain future climate change and demographic developments (Klijn et al., 2015). Working with vegetated foreshores fits well into an approach based on adaptive flood risk management for two main reason: the ability of vegetated foreshores to raise with sea level by natural sediment accretion, and ease of incremental upscaling of a foreshore compared to repetitive dike reinforcement.

Important criteria for choosing a certain flood risk reducing strategy are (1) cost-effectiveness for flood risk reduction, (2) required maintenance, (3) initial impact on the local ecosystem during construction, and (4) long-term additional ecosystem services. Here, we qualitatively evaluate the strategies considered in this chapter, looking at those four aspects (Fig. 5.12).

	Dike heightening	Foreshore construction	Foreshore + breakwater	Foreshore + high zone	Brushwood dams
Cost-effective flood risk reduction	✔	✔	✔	✔✔	o
Required maintenance	o	o	o	✘	✘✘
Initial ecological impact	o	✘	✘	✘	o
Additional ecosystem services	o	✔✔	✔	✔	✔✔

Figure 5.12: *Qualitative assessment of arguments for choosing different strategies for flood risk reduction (checkmark = positive, cross = negative, zero = neutral).*

1. Dike heightening and construction of a foreshore with a high zone are considered most positive for **cost-effective flood risk reduction**. Both strategies have a large effect on flood risk, but dike heightening is more expensive. Construction of a foreshore that resembles a natural salt marsh (either with or without breakwater) has less effect on flood risk, since its elevation is limited to approximately mean high water, where natural accretion can take place. The effect of brushwood dams on flood risk is on the long run similar to that of foreshore construction. However, due to continuous maintenance costs and postponed benefits for safety, it is less attractive in terms of life-cycle costs than the other strategies considered here.

2. Concerning **required maintenance**: dike maintenance is needed in all strategies, and is neglected in this comparison. In addition, periodic earthmoving is applied

for the foreshore with high zone, in order to keep pace with sea level rise. Brushwood dams demand more or less continuous maintenance. Foreshores with gentle slopes are assumed to be morphologically stable here, although this is highly case-specific. At locations where marsh edge erosion is to be expected, periodic sediment nourishment is needed, which seriously increases life-cycle costs and ecological impact. Addition of brushwood dams or other sheltering structures may be considered here for erosion mitigation.

3. **Initial ecological impact** of dike heightening is neutral, since it does not significantly affect the estuary or coastal sea, either positively or negatively. Foreshore construction and earthmoving have adverse ecological impacts, due to for example disturbance of underwater habitats and increased turbidity due to dredging and nourishment. Impact can be reduced by using sediment with similar grain size as the native bed material (McLachlan, 1996), and by avoiding nourishments in spring, considering the reproduction cycle of many benthic species (Menn et al., 2003). Brushwood dams have negligible adverse environmental effects. These scores are only related to short-term impact.

4. Systems with a high nature-based character provide **additional ecosystem services**, such as providing habitats for fish and other wildlife, recreation, carbon sequestration, water purification, and erosion control (Barbier et al., 2011). Long-term effects on the surrounding ecosystem, either positive or adverse, should be investigated in a site-specific ecological impact assessment. Here, salt marsh realization via nourishment or brushwood dams are considered most positive on this aspect, since these strategies aim to realize a foreshore that resembles a natural salt marsh, with salt-tolerant vegetation, inundated during high tide. These strategies can be considered as 'Building with Nature', since natural materials and processes are exploited for safety. Artificial elements, such as a breakwater or high zone, decrease the nature-based character of the system. More research is required to quantify ecological performance of different foreshore configurations.

5.5.2. GENERAL APPLICABILITY

This study demonstrates that the cost-effectiveness of vegetated foreshores depends on three main factors:

1. The original failure probability of the system, and how much this probability can be affected by foreshores, both initially and after sea level rise;

2. The investments required to construct and maintain foreshores, in comparison to hard structures;

3. The economic value of the protected area, where nature-based solutions are relatively more attractive for low economic value.

These three factors should be quantified on a local scale, accompanied by assessments of (1) viability in the surrounding physical system and (2) ecological impact, in order to decide whether nature-based solutions can outcompete traditionally engineered structures.

This chapter's integrated analysis of wave load reduction, probability of failure, vertical salt marsh adaptation to sea level rise, and life-cycle costs can be applied to other estuaries and coastal seas worldwide. Examples of interesting future applications in low-lying coastal regions are mangrove coasts in the Mekong delta (Vietnam), or coastal wetlands along the coasts of Virginia and Louisiana (US). Previous studies in these areas have quantified effects on surge and waves (e.g., Bao (2011); Glass et al. (2018); Wamsley et al. (2010)). By applying an approach similar to that in the current study, quantitative insights can be obtained on the cost-effectiveness of such nature-based solutions for flood risk reduction.

5.5.3. FUTURE WORK

Starting from the current study, research concerning salt marshes for flood risk reduction can be brought a step further by collecting and describing more practical examples where vegetated foreshores have been implemented, including construction and maintenance costs. We encourage to extend existing studies on cost-effectiveness of nature-based solutions, such as Reguero et al. (2018), with site-specific calculations of flooding probabilities and the influence of nature-based solutions.

In most tables and handbooks, bottom roughness values are prescribed for various vegetation types, without taking into account the disruption of vegetation during storms and hurricanes. Also in this chapter, a standard empirical roughness value has been used. Predictions of wave attenuation over wetlands can be improved by calibrating bottom roughness in numerical models for flow and waves, specifically for salt marsh surfaces that have experienced extensive stem breakage.

The D'Alpaos equation for vertical marsh accretion, Eq. (5.2), is a rather simple analytical formula, which could easily be used to estimate the response of marshes to sea level rise, tidal amplitude, and sediment concentration. We did not validate its performance. The purpose of this study was to show the importance of a realistic vertical accretion rate for long-term effectiveness of foreshores in reducing flood risk. There was no need to select the best possible model. More sophisticated models such as SLAMM, used in e.g., Craft et al. (2009), could provide more precise estimates in future studies, provided that the simulations do include the feedback mechanisms that allow marshes to adapt to SLR by accelerating rates of elevation change (Kirwan et al., 2016).

This chapter puts central the flood risk reduction and associated cost-effectiveness of nature-based solutions, which are the main criteria for choosing a certain flood risk reduction strategy. Nature-based solutions however, typically require joint action of multiple different stakeholders, including nature organizations and local governments. First, because these measures provide more services than flood risk reduction only. And sec-

ond, because these solutions should often be realized in ecologically sensitive and protected areas. Therefore, successful implementation of nature-based solutions requires different governance and institutional arrangements compared to traditional flood risk management (Janssen et al., 2015; Borsje et al., 2017). More research on this aspect can help in getting nature-based solutions in the mainstream of coastal protection. In addition, the interplay between human interventions in salt marshes and biodiversity needs to be studied, to optimize the whole spectrum of ecosystem services provided by natural and man-made salt marshes.

The economic value of ecosystem services other than flood risk reduction have not been taken into account in the current study. This aspect should be added to the comparison between different strategies, in order to perform a fully integrated cost-benefit analysis. In this study, vegetated foreshores are considered as ecologically valuable components of the large-scale physical system. However, connectivity between the terrestrial high salt marsh and the lower aquatic parts of the system influences certain ecosystem services (Barbier et al., 2011). Therefore, for actual applications of vegetated foreshores, we underline the recommendations made in Bockstael et al. (2000), who stressed that the overall ecosystem services provided by the large-scale system should be investigated, instead of valuing specific and localized components of the small-scale ecosystem only.

5.6. CONCLUSIONS

This chapter presented an approach to assess the cost-effectiveness of salt marshes for flood risk reduction by coupled calculations of wave attenuation, sediment accretion under sea level rise, probability of dike failure, and life-cycle costs. Different interventions on the foreshore were compared with traditional dike heightening, considering the net present value of benefits (failure probability reduction) and costs (for construction and maintenance).

Sea level rise leads to increasing probabilities of dike failure by wave overtopping, caused by a combination of rising still water levels and decreasing wave height reduction over the foreshore. Marsh elevation change due to sediment accretion mitigates the increase in wave height, and elongates the lifetime of a dike-foreshore system.

Cost-effectiveness of nature-based solutions versus hard structures depends on various local conditions, most importantly: economic value of the protected area, current failure probability, reduction of this probability via foreshores, and costs for construction and maintenance.

Different strategies were assessed for a case study in the shallow Dutch Wadden Sea in the Netherlands. Salt marshes here are exposed to relatively high day-to-day waves and tidal currents, which leads to stable plant species, firmly rooted in mineral soils. Such marshes are highly resistant to surface erosion, even during extreme storms. The calculations give rise to the following conclusions from an engineering perspective:

- Salt marsh construction is cheaper than dike heightening. However, salt marshes are limited in effect on failure probabilities because of their dependence on sediment accretion in the intertidal zone. For the considered case study, salt marsh construction is only more cost-effective than dike heightening, if small to moderate economic damage occurs in case of dike breaching.
- Artificial high zones and breakwaters on the salt marsh improve the flood defense's reliability substantially, against relatively low costs. A foreshore with high zone is even more cost-effective than dike heightening if it is constructed well above mean high water. Without human interventions, breakwaters and high zones lose effect because of SLR and absence of natural sediment accretion. However, periodic earthmoving from the pioneer zone to the high zone is an effective alternative for obtaining persistent flood risk reduction.
- Sheltering structures such as brushwood or bamboo dams enhance sediment accretion and lead on the long term to similar foreshore effects as instant construction via nourishment. However, continuous maintenance costs and postponed benefits for safety discard brushwood dams as attractive strategy for flood risk reduction.

These conclusions are valid for the considered case study and design options. We emphasize that similar site-specific analyses are required, before results can be universally applied to other systems and locations.

APPENDIX

5.A. TEMPORAL VARIATIONS IN MARSH WIDTH

This appendix contains an analysis of temporal variations in marsh width, based on historical bathymetric survey data. At the case study site in the Wadden Sea, lateral marsh dynamics are small due to the system of brushwood dams. Therefore, we investigate temporal variations in marsh width B_{fs} for unprotected salt marshes in the Western Scheldt, an estuary in the South-West of the Netherlands. For these marshes, a lot of data is available, in contrast to the Wadden Sea, where only a limited number of bathymetric surveys have an extent that covers the salt marshes. The selection of study sites in the Western Scheldt is identical to that of Van der Wal et al. (2008).

5.A.1. METHODS

Lateral dynamics of salt marshes in the Netherlands are captured in an extensive bathymetrical dataset (so-called 'Vaklodingen') of the Dutch nearshore areas. These bathymetric data are collected since 1925-1935 by the Ministry of Infrastructure and the Environment (former Ministry of Transport, Public Works and Water Management), interpolated over a 20 x 20 m grid (De Kruif, 2001; Wiegman et al., 2005).

Temporal dynamics of the salt marsh and tidal flats are obtained by linear interpolation of the Vaklodingen data to a transect perpendicular to the marsh edge. For determining the marsh width, the (most recent) position of the dike toe is used as the landward boundary. Since salt marsh area was not collected for the full period, the marsh edge position is determined by using a tidal benchmark. Different tidal benchmarks have been used in the literature for defining marsh edge positions (Balke et al., 2016), e.g. 20-40 cm below Mean High Water (MHW) in the Dutch Wadden sea (Bakker et al., 2002), or Mean High Water Neap (MHWN) in the Western Scheldt Van der Wal et al. (2008). In this analysis, MHWN is used.

Finally, the marsh width is defined as the distance from the dike toe (landward reference) to the marsh edge (seaward reference). Missing data at the intertidal area were interpolated in time. To prevent extrapolation above MHWN, measurements obtained in years before the first measurement reached up to MHWN, were removed.

5.A.2. RESULTS

The width of the analyzed marshes varied over the assessed period of 65 years (Table 5.A1). The largest variation was observed at Zimmermanpolder, with a marsh width increasing from 50 m in 1951 to 220 m in 2015 (Fig. 5.8). The marsh width of most marshes remained constant or increased in time, except of Paulina, where net erosion was found. In general, the marsh width of the salt marshes located at the northern shore of the estuary were smaller than the marshes at the southern shore, although the standard deviation in marsh width at the northern shore was on average larger. These find-

ings are in line with Callaghan et al. (2010) and Van der Wal et al. (2008). For Hellegat, no results were obtained, since the profiles did not exceed MHWN.

Table 5.A1: *Characteristics of the marsh width (mean, minimum, maximum, largest difference and standard deviation) of multiple marshes along the Northern (N) and Southern (S) shore of the Western Scheldt estuary in the Netherlands. The table includes the assumed vertical position of the marsh edge (m+NAP, where NAP is the Dutch ordinance level, close to MSL), the assessed period and available years of data (vaklodingen).*

Salt marsh	Mean (m)	Minimum (m)	Maximum (m)	Diff. (m)	St. dev. (m)	MHWN (m+ NAP)	Period assessed (years)	Available years
Zuidgors (N)	255	230	280	50	13	1.85	1955-2015	37
Baarland (N)	109	95	135	40	12	1.83	1958-2015	36
Biezelingsche Ham (N)	62	50	80	30	7	1.80	1957-2015	46
Zimmermanpolder (N)	148	50	220	170	71	2.14	1951-2015	47
Paulina (S)	246	215	320	105	31	1.73	1955-2015	37
Thomaespolder (S)	90	70	150	80	16	1.71	1955-2015	37
Hoofdplaat (S)	139	130	155	25	8	1.59	1999-2015	13
Hellegat (S)	-	-	-	-	-	1.81	-	-
Average (N)	144	106	179	73	26	1.91	-	42
Average (S)	158	138	208	70	18	1.71	-	29
Average (overall)	150	120	191	71	23	1.81	-	36

6

CONCLUSIONS AND RECOMMENDATIONS

6.1. CONCLUSIONS

The aim of this dissertation was to develop new methods to assess how and how much nature-based flood defenses can reduce flood risks, taking into account uncertainties in their functioning and stability. The focus was on hybrid flood defenses that combine engineered structures such as dikes and dams with vegetated foreshores, particularly concentrating on salt marshes.

Here, the four Research Questions (RQ) formulated in Section 1.3 are answered.

RQ1. What is the influence of vegetated foreshores on wave run-up and wave overtopping?

Field measurements of wave energy dissipation on salt marshes have resulted in a dataset that contains storm conditions with higher significant wave height (maximum 0.85 m) and water depth (maximum 3.07 m) at the marsh edge than reported in any previous field study on wave attenuation by salt marshes. High wave attenuation rates over 50% per 300 m of marsh width were recorded during storms, notwithstanding reduced aboveground biomass in winter. Numerical modeling with the SWAN wave model showed that wave energy dissipation was primarily caused by wave breaking and wave attenuation by vegetation. Observed wave attenuation by *Spartina anglica* (common cord-grass) and *Scirpus maritimus* (sea club-rush) vegetation under storm conditions could best be described in SWAN by a calibrated bulk drag coefficient $\widetilde{C}_D \approx 0.4$.

Coupling of the calibrated SWAN model to the empirical EurOtop formulas demonstrated that vegetated foreshores reduce wave loads on coastal dikes significantly. Pronounced reductions in wave run-up and wave overtopping were found, including for the

large water depths that occur during storms and with reduced aboveground biomass in the winter. Wave load reduction is highest for large wave height to water depth ratios on the foreshore. Wave attenuation by vegetation has most added value at water depths for which waves are close to breaking, provided that the vegetation remains stable under the wave forcing.

The influence of salt marshes on wave run-up was confirmed by post-storm measurements of the position of flotsam lines (i.e., deposits of floating organic material) on the outer slopes of dikes along the Wadden Sea. Wave run-up height was found to be more than 2 m lower behind salt marshes during storms with a return period of ±5 years, compared to the run-up at parts of the dike behind bare mudflats. (Chapter 2).

RQ2. Until what threshold can plant stems withstand wave-induced forces before they fold or break?

Winter storms caused significant stem breakage of salt marsh vegetation at the field sites, and a subsequent reduction in stem density. In order to predict how much vegetation will withstand the wave forcing during extreme storms, a model has been developed which determines the wave load that a plant stem can withstand before it breaks or folds. This occurs when the wave-induced bending stress exceeds the stem's flexural strength.

Flexural strength was determined by means of three-point bending tests, which were carried out for two common salt marsh species: *Spartina anglica* (common cord-grass) and *Scirpus maritimus* (sea club-rush), at different stages in their seasonal cycle. The model expresses plant stability in terms of a critical orbital velocity, which is the velocity of particles due to wave motion. This critical orbital velocity depends on various plant characteristics that contribute to stability: flexural strength, flexibility, stem diameter and height, and the drag coefficient. A higher critical orbital velocity indicates greater stability of the stem.

The analytical formula was calibrated and validated, using information about stem breakage from the field sites in the Western Scheldt estuary (the Netherlands), and earlier laboratory tests of Rupprecht et al. (2017). The short, thick and flexible stems of *Spartina* were found to be relatively stable (mean critical orbital velocity 0.5-1.2 m/s) compared to that of *Scirpus* (0.3-1.0 m/s), where the velocities are based on the mean height of the highest 10% of the waves ($H_{1/10}$). However, in design conditions, most coastal dikes are supposed to withstand high waves, which generate high near-bottom orbital velocities (>1.0 m/s), thereby exceeding the critical orbital velocities of these two plant species and resulting in large-scale stem breakage. (Chapter 3).

RQ3. How to assess the failure probability of a dike, accompanied by a vegetated foreshore?

A failure probability of a hybrid flood defense can be determined by integrating models that describe wave propagation over a vegetated foreshore, stem breakage and dike failure. Two failure mechanisms were considered: failure due to (i) wave overtopping and (ii) wave impact on revetments.

Model results showed that vegetated foreshores cause a more pronounced reduction in failure probability for wave impact on revetments than for wave overtopping. For a case study in the Dutch Wadden Sea, presence of a salt marsh allowed for a reduction of 0.5 m in dike crest level, compared to a dike behind tidal flats at mean sea level. Failure probabilities for asphalt and grass covers displayed a more pronounced reduction in failure probability, by a factor 100 or more. The reason is that waves are able to damage revetments under moderate water depths, for which the foreshore and vegetation have a relatively high influence on wave height.

The relevance of different uncertainties depends on the protection level and associated dike height and strength. For relatively low dikes (i.e., low protection levels, often found in developing countries), vegetation remains stable in design conditions, and plays an important role in reducing wave loads. In case of higher protection levels, hence for more robust dikes, the effect of the vegetated foreshore reduces to the effect of its geometry only, because of expected stem breakage under these more extreme conditions. (Chapter 4).

RQ4. What is the long-term effectiveness of salt marshes in reducing flood risk, in comparison to conventional dike heightening?

The cost-effectiveness of different measures for long-term (i.e., ±100 years) flood risk reduction depends on the ratio between long-term flood risk reduction and life-cycle costs. Rising sea levels lead to higher nearshore waves during storms, and subsequently, to increasing probabilities of dike failure by wave overtopping.

Marsh elevation change due to sediment accretion mitigates the increase in wave height, and extends the lifetime of a dike-foreshore system. The performance of foreshores can be influenced by human interventions, such as foreshore construction via sediment nourishment, or by sheltering structures that enhance sediment accretion.

Cost-effectiveness depends on three main factors: (1) wave energy dissipation, which is lower for salt marshes with a natural elevation in the intertidal zone than for foreshores with artificial elements such as a high zone near the dike, or a detached breakwater; (2) investment costs for foreshore construction and maintenance, where continuous maintenance costs and delayed effects on flood risk make sheltering structures less attractive from a flood risk perspective; (3) economic value of the protected area, where foreshores are relatively more attractive for protecting areas with low economic value.

Besides cost-effectiveness, also other factors may affect the site-specific choice for a certain type of flood risk reduction, such as legal boundaries, landscape development, environmental impacts and economic value of other ecosystems services. (Chapter 5).

6.2. LIMITATIONS

This research has provided new insights into flood risk reduction by vegetated foreshores, by quantifying effects on waves, wave loads, probability of failure and cost-effectiveness. Knowledge and data from different disciplines were integrated in this study. However, the following aspects related to physical processes deserve further investigation:

- This thesis has shown the essence of including possible stem breakage of salt marsh vegetation during extreme storms. After stem breakage, a rough bottom surface remains, with remainders of folded and broken stems. There is currently no information about representative roughness values for such disturbed salt marsh surfaces. Measurements in the field or in a wave flume are recommended to fill this knowledge gap.

- On shallow foreshores, infragravity waves can be generated by non-linear wave interactions that displace wave energy from high to low frequencies. These infragravity waves are only weakly dissipated on the foreshore, and might significantly affect wave run-up and wave overtopping (Suzuki et al., 2012a). In this dissertation, the overall effect of foreshores on the mean wave period was taken into account by means of a simple empirical formula (Hofland et al., 2017). It is currently not well-known how to quantify wave overtopping for a combination of short wind waves and long infragravity waves. The often-used EurOtop formulas (EurOtop, 2016), based on the spectral mean wave period $T_{m-1,0}$, are not meant for such clearly bimodal wave spectra (Oosterlo et al., 2018). More research is needed to assess to what extent and under what conditions infragravity waves can develop on vegetated foreshores, and negatively affect the performance of dike-foreshore configurations.

- Foreshores may require regular maintenance, for example via sediment nourishment, vegetation mowing or grazing. Especially man-made foreshores can be prone to erosion, if constructed at unfavorable locations. Maintenance significantly affects life-cycle costs, and thereby the cost-effectiveness of vegetated or sandy foreshores. Vegetation can contribute to soil stability via wave and flow attenuation, reduction of wave breaking induced turbulence (Chapter 2), changed soil composition (Feagin et al., 2009) and soil stabilization via root systems (Gedan et al., 2011). The aspect of maintenance only received minor attention in this research, and should be thoroughly investigated when considering site-specific application of foreshores for coastal protection.

6.3. APPLICATIONS

In this study, the developed methods were applied to a case study in the Wadden Sea, a shallow coastal sea in the Netherlands. Variations were applied by means of a sensitivity analysis, in order to show the broader applicability of results. However, the developed models and knowledge can more widely be applied to other locations. Additional case studies, pilots and full-scale applications will increase confidence in reduction of flood risks by vegetated foreshores.

- Three aspects can be used while exploring opportunities for application of vegetated foreshores. Firstly, a flood defense structure can only be impacted and overtopped by waves, if a water level occurs, significantly higher than the elevation of the foreshore; secondly, the foreshore elevation is related to the tidal amplitude; and thirdly, wave energy dissipation depends on the wave height to water depth ratio on the foreshore. Considering these three aspects, we argue that foreshores are most effective at locations with (1) a large tidal amplitude, (2) high waves, and (3) a relatively small wind set-up. When disregarding the effect of tide, foreshores (either sandy or vegetated) are also supposed to be highly effective along lake shores. A broad exploration, based on this search window, can help in demonstrating at which locations foreshores are most valuable.

- This dissertation has mainly focused on salt marshes. However, the same methods and considerations are applicable to mangrove forests in tropical regions. Mangroves are expected to experience less stem breakage than salt marsh vegetation, which can rather easily be investigated by applying the formulas from this dissertation (Chapter 3), with measured or estimated stem height, diameter, flexibility and flexural strength as input. The effect of mangroves on flood risk can subsequently be assessed by coupling models for wave energy dissipation by mangrove roots, trunks and branches, and wave loads on settlements or levees behind the mangroves.

- The research has shown that vegetated foreshores are particularly effective in situations with relatively low protection levels (Chapter 4), which calls for case studies, pilots and applications in countries with lower protection levels than in the Netherlands, such as mangrove coasts in the Mekong delta (Vietnam), or coastal wetlands along the coasts of Virginia and Louisiana (USA).

- The developed models can be applied to assign intervention values to e.g., marsh width, marsh elevation or vegetation density. If a maximum tolerable failure probability is defined for a dike-foreshore system, the probabilistic model of Chapter 4 can be used to assess at which foreshore characteristics an intervention is required. The calculation results can be used as input for setting up a monitoring and maintenance strategy.

6.4. RELATED WORK

Finally, several aspects were not considered in the scope of this dissertation, but are expected to be relevant:

- This dissertation has focused on quantifying effects of foreshores on the failure probability for two wave-induced dike failure mechanisms: erosion of the inner slope due to wave overtopping, and failure of the outer slope revetment due to wave impact. However, vegetated foreshores may affect geotechnical failure mechanisms as well, which can occur for water levels significantly below the crest level of the dike (Schweckendiek, 2014). The chance of dike failure due to piping is lower when a solid impermeable clay layer on the foreshore increases the seepage length (Vorogushyn et al., 2009). Further, the mass of the foreshore can reduce the chance of macro-instability due to sliding of the outer slope. The effects of (vegetated) foreshores on other failure mechanisms could be investigated in future studies.

- This dissertation has approached the effect of vegetated foreshores on flood risk via the probability of dike failure. However, vegetated foreshores with a stable top layer can also affect consequences of dike failure, by vertically confining breach dimensions (Rijkswaterstaat and KNMI, 1961) and thereby limiting the volume of water that enters the flooded area (Zhu et al., 2018). This aspect adds to the value of salt marshes for flood risk reduction, and deserves more attention in the future.

- Flotsam lines were used as field evidence for the effect of salt marshes on wave run-up during severe storms (Section 1.2). These lines may provide a useful and cheap source of information about spatial variations in wave run-up, including the influence of vegetated foreshores. However, knowledge is lacking to accurately relate flotsam levels to often-used measures for wave run-up, such as the two-percent wave run-up. Simultaneous measurements of waves, time-varying wave run-up and post-storm flotsam levels may help in increasing the value of flotsam lines for assessing wave run-up on coastal structures.

- Vegetated foreshores should often be realized in valuable nature areas. Implementation can only be successful if the foreshore fits into the large-scale physical and ecological system. This requires multi-disciplinary research to ecological impact, ecosystem services, legal aspects and agreements about investments and maintenance between different organizations. This dissertation has considered flood risk reduction by salt marshes from the perspective of hydraulic engineering. Ongoing collaboration between experts (from the fields of ecology, morphology and governance) and stakeholders is required for realizing vegetated foreshores at suitable locations.

BIBLIOGRAPHY

Adam, P. (2002). "Saltmarshes in a time of change." *Environmental Conservation*, 29(1), 39–61.

Allen, J. H., Nuechterlein, G. L., and Buitron, D. (2008). "Bulrush mediation effects on wave action: implications for over-water nesting birds." *Waterbirds*, 31(3), 411–416.

Allen, J. R. L. (2000). "Morphodynamics of Holocene salt marshes: a review sketch from the Atlantic and Southern North Sea coasts of Europe." *Quaternary Science Reviews*, 19(12), 1155–1231.

Anderson, M. E. and Smith, J. M. (2014). "Wave attenuation by flexible, idealized salt marsh vegetation." *Coastal Engineering*, 83, 82–92.

Anderson, M. E., Smith, J. M., and McKay, S. K. (2011). "Wave dissipation by vegetation." *Report No. CHETN-I-82*, US Army Engineer Research and Development Center (sep).

Arkema, K. K., Guannel, G., Verutes, G., Wood, S. A., Guerry, A., Ruckelshaus, M., Kareiva, P., Lacayo, M., and Silver, J. M. (2013). "Coastal habitats shield people and property from sea-level rise and storms." *Nature Climate Change*, 3(10), 913–918.

Arns, A., Dangendorf, S., Jensen, J., Talke, S., Bender, J., and Pattiaratchi, C. (2017). "Sea-level rise induced amplification of coastal protection design heights." *Scientific Reports*, 7, 40171.

Asano, T., Deguchi, H., and Kobayashi, N. (1992). "Interaction between water waves and vegetation." *Proc. 23rd Intern.Coastal Engrg. Conf., ASCE*, 3(23), 2710–2723.

Augustin, L. N., Irish, J. L., and Lynett, P. (2009). "Laboratory and numerical studies of wave damping by emergent and near-emergent wetland vegetation." *Coastal Engineering*, 56(3), 332–340.

Babanin, A. V., Young, I., and Mirfenderesk, H. (2005). "Field and laboratory measurements of wave-bottom interaction." *Coasts and Ports 2005*, Australia, Institution of Engineers, 293.

Bakker, J. P., Esselink, P., Dijkema, K. S., Van Duin, W. E., and De Jong, D. J. (2002). "Restoration of salt marshes in the Netherlands." *Hydrobiologia*, 478, 29–51.

Balke, T., Bouma, T. J., Horstman, E. M., Webb, E. L., Erftemeijer, P. L. A., and Herman, P. M. J. (2011). "Windows of opportunity: thresholds to mangrove seedling establishment on tidal flats." *Marine Ecology Progress Series*, 440, 1–9.

Balke, T., Stock, M., Jensen, K., Bouma, T. J., and Kleyer, M. (2016). "A global analysis of the seaward salt marsh extent: The importance of tidal range." *Water Resources Research*, 52(5), 3775–3786.

Bao, T. Q. (2011). "Effect of mangrove forest structures on wave attenuation in coastal Vietnam." *Oceanologia*, 53(3), 807–818.

Barbier, E. B., Hacker, S. D., Kennedy, C., Koch, E. W., Stier, A. C., and Silliman, B. R. (2011). "The value of estuarine and coastal ecosystem services." *Ecological Monographs*, 81(2), 169–193.

Battjes, J. A. (1974). "Computation of set-up, longshore currents, run-up and overtopping due to wind-generated waves." Phd thesis, Delft University of Technology, Delft University of Technology.

Battjes, J. A. and Janssen, J. P. F. M. (1978). "Energy loss and set-up due to breaking of random waves." *Proceedings of 16th International Conference on Coastal Engineering, Am. Soc. of Civ. Eng., New York*, 32(1), 569–587.

Battjes, J. A. and Stive, M. J. F. (1985). "Calibration and verification of a dissipation model for random breaking waves." *Journal of Geophysical Research*, 90(C5), 649–660.

Bockstael, N. E., Freeman, A. M., Kopp, R. J., Portney, P. R., and Smith, V. K. (2000). "On measuring economic values for nature." *Environmental Science and Technology*, 34(8), 1384–1389.

Booij, N., Ris, R. C. R., and Holthuijsen, L. H. L. (1999). "A third-generation wave model for coastal regions. I- Model description and validation." *Journal of Geophysical Research*, 104(C4), 7649.

Borsje, B. W., de Vries, M. B., Hulscher, S. J. M. H., and De Boer, G. J. (2008). "Modeling large-scale cohesive sediment transport affected by small-scale biological activity." *Estuarine, Coastal and Shelf Science*, 78(3), 468–480.

Borsje, B. W., van Wesenbeeck, B. K., Dekker, F., Paalvast, P., Bouma, T. J., van Katwijk, M. M., and de Vries, M. B. (2011). "How ecological engineering can serve in coastal protection." *Ecological Engineering*, 37(2), 113–122.

Borsje, B. W., Vries, S. D., Janssen, S. K. H., Luijendijk, A. P., and Vuik, V. (2017). "Building with Nature as Coastal Protection Strategy in the Netherlands." *Living Shorelines: The Science and Management of Nature-Based Coastal Protection*, CRC Press, 1 edition, 137–155.

Bouma, T. J., de Vries, M. B., and Herman, P. M. J. (2010). "Comparing ecosystem engineering efficiency of two plant species with contrasting growth strategies.." *Ecology*, 91(9), 2696–2704.

Bouma, T. J., De Vries, M. B., Low, E., Peralta, G., Tánczos, I. C., van de Koppel, J., and Herman, P. M. J. (2005). "Trade-Offs Related To Ecosystem Engineering: a Case Study on Stiffness of Emerging Macrophytes." *Ecology*, 86(8), 2187–2199.

Bouma, T. J., van Belzen, J., Balke, T., van Dalen, J., Klaassen, P., Hartog, A. M., Callaghan, D. P., Hu, Z., Stive, M. J. F., Temmerman, S., and Herman, P. M. J. (2016). "Short-term mudflat dynamics drive long-term cyclic salt marsh dynamics." *Limnology and Oceanography*, 61(6), 2261–2275.

Bouma, T. J., van Belzen, J., Balke, T., Zhu, Z., Airoldi, L., Blight, A. J., Davies, A. J., Galvan, C., Hawkins, S. J., Hoggart, S. P. G., Lara, J. L., Losada, I. J., Maza, M., Ondiviela, B., Skov, M. W., Strain, E. M., Thompson, R. C., Yang, S., Zanuttigh, B., Zhang, L., and Herman, P. M. J. (2014). "Identifying knowledge gaps hampering application of intertidal habitats in coastal protection: Opportunities & steps to take." *Coastal Engineering*, 87, 147–157.

Bradley, K. and Houser, C. (2009). "Relative velocity of seagrass blades: Implications for wave attenuation in low-energy environments." *Journal of Geophysical Research: Earth Surface*, 114(1), 1–13.

Bradshaw, C. J. A., Sodhi, N. S., Peh, K. S. H., and Brook, B. W. (2007). "Global evidence that deforestation amplifies flood risk and severity in the developing world." *Global Change Biology*, 13(11), 2379–2395.

Bretschneider, C. L., Krock, H. J., Nakazaki, E., and Casciano, F. M. (1986). "Roughness of typical Hawaiian terrain for tsunami run-up calculations: A users manual." *Report No. 1*, University of Hawaii, Honolulu.

Bridges, T. S., Wagner, P. W., Burks-copes, K. A., Bates, M. E., Collier, Z. A., Fischenich, C. J., Gailani, J. Z., Leuck, L. D., Piercy, C. D., Rosati, J. D., Russo, E. J., Shafer, D. J., Suedel, B. C., Vuxton, E. A., and Wamsley, T. V. (2015). "Use of Natural and Nature-Based Features (NNBF) for Coastal Resilience." *Report No. ERDC SR-15-1*, US Army Corps of Engineers - Engineer Research and Development Center.

Buijs, F. A., Van Gelder, H. A. J. M., and Hall, J. W. (2004). "Application of reliability-based flood defence design in the UK." *Heron*, 49(1), 33–50.

Cahoon, D. (2006). "A Review of Major Storm Impacts on Coastal Wetland Elevations." *Estuaries and coasts*, 29(6A), 889–898.

Callaghan, D. P., Bouma, T. J., Klaassen, P., van der Wal, D., Stive, M. J. F., and Herman, P. M. J. (2010). "Hydrodynamic forcing on salt-marsh development: Distinguishing the relative importance of waves and tidal flows." *Estuarine, Coastal and Shelf Science*, 89(1), 73–88.

Chbab, H. and Groeneweg, J. (2015). "Modelonzekerheid belastingen [Model Uncertainty Hydraulic Loads]." *Report No. 1209433-008*, Deltares, Delft, The Netherlands.

Cooper, N. J. N. (2005). "Wave dissipation across intertidal surfaces in the Wash Tidal Inlet , Eastern England." *Journal of Coastal Research*, 21(1), 28–40.

Coops, H., Geilen, N., Verheij, H. J., Boeters, R., and van der Velde, G. (1996). "Interactions between waves, bank erosion and emergent vegetation: an experimental study in a wave tank." *Aquatic Botany*, 53(3-4), 187–198.

Craft, C., Clough, J., Ehman, J., Jove, S., Park, R., Pennings, S., Guo, H., and Machmuller, M. (2009). "Forecasting the effects of accelerated sea-level rise on tidal marsh ecosystem services." *Frontiers in Ecology and the Environment*, 7(2), 73–78.

Currin, C. A., Delano, P. C., and Valdes-Weaver, L. M. (2008). "Utilization of a citizen mon-

itoring protocol to assess the structure and function of natural and stabilized fringing salt marshes in North Carolina." *Wetlands Ecology and Management*, 16(2), 97–118.

CWSS (2017). "Introduction." *Wadden Sea Quality Status Report 2017*, R. Strempel, A. Bostelmann, J. Busch, and S. Klöpper, eds., Common Wadden Sea Secretariat, Wilhelmshaven, Germany, 2017 edition.

D'Alpaos, A., Mudd, S. M., and Carniello, L. (2011). "Dynamic response of marshes to perturbations in suspended sediment concentrations and rates of relative sea level rise." *Journal of Geophysical Research: Earth Surface*, 116(4), 1–13.

Dalrymple, R. A., Kirby, J. T., and Hwang, P. A. (1984). "Wave diffraction due to areas of energy dissipation." *Journal of Waterway, Port, Coastal and Ocean Engineering*, 110(1), 67–79.

Danka, J. and Zhang, L. M. (2015). "Dike Failure Mechanisms and Breaching Parameters." *Journal of Geotechnical and Geoenvironmental Engineering*, 141(9), 04015039.

Davidson-Arnott, R. G., Van Proosdij, D., Ollerhead, J., and Schostak, L. (2002). "Hydrodynamics and sedimentation in salt marshes: Examples from a macrotidal marsh, Bay of Fundy." *Geomorphology*, 48(1-3), 209–231.

Davis, J. L., Currin, C. A., O'Brien, C., Raffenburg, C., and Davis, A. (2015). "Living shorelines: Coastal resilience with a blue carbon benefit." *PLoS ONE*, 10(11), 1–18.

De Kruif, A. C. (2001). "Bodemdieptegegevens van Nederlandse kustsysteem: Beschikbare digitale data en een overzicht van aanvullende analoge data [Bathymetric data of the Dutch Coastal system: available digital data and an overview of additional analog data]." *Report No. 2001.041*, Rijkswaterstaat RIKZ, <uuid:1163bef6-00b8-4dd1-8d20-f17dcf8abb54%0A%0A>.

De Langre, E. (2012). "Methodological advances in predicting flow-induced dynamics of plants using mechanical-engineering theory." *Journal of Experimental Biology*, 215, 914–921.

De Looff, A. K., 't Hart, R., Montauban, K., and Van de Ven, M. F. (2006). "Golfklap, a model to determine the impact of waves on dike structures with an asphalt concrete layer." *Coastal Engineering Proceedings*, Vol. 30, San Diego, 1–10.

De Vriend, H. J., Van Koningsveld, M., Aarninkhof, S. G. J., De Vries, M. B., and Baptist, M. J. (2015). "Sustainable hydraulic engineering through building with nature." *Journal of Hydro-environment Research*, 9(2), 159–171.

De Waal, J. P. and Van Hoven, A. (2015). "Failure Mechanism Module Grass Wave Impact Zone; Requirements and Functional Design." *Report No. 1220043-002*, Deltares, Delft, The Netherlands.

Dean, R. G. and Bender, C. J. (2006). "Static wave setup with emphasis on damping effects by vegetation and bottom friction." *Coastal Engineering*, 53(2-3), 149–156.

Deegan, L. A., Johnson, D. S., Warren, R. S., Peterson, B. J., Fleeger, J. W., Fagherazzi, S.,

and Wollheim, W. M. (2012). "Coastal eutrophication as a driver of salt marsh loss." *Nature*, 490(7420), 388–392.

Den Heijer, C. K., Baart, F., and van Koningsveld, M. (2012). "Assessment of dune failure along the Dutch coast using a fully probabilistic approach." *Geomorphology*, 143-144, 95–103.

Dijkema, K. S., Bossinade, J. H., Bouwsema, P., and de Glopper, R. J. (1990). "Salt Marshes in the Netherlands Wadden Sea: Rising High-Tide Levels and Accretion Enhancement." *Expected Effects of Climatic Change on Marine Coastal Ecosystems*, J. J. Benkema, ed., Kluwer, Dordrecht, The Netherlands, 173–188.

Dijkema, K. S., Van Duin, W. E., Dijkman, E. M., Nicolai, E., Jongerius, H., Keegstra, H., Van Egmond, L., Venema, H. J., and Jongsma, J. J. (2011). "Fifty years monitoring and maintenance of salt marshes in Friesland and Groningen: 1960-2009. [Vijftig jaar monitoring en beheer van de Friese en Groninger kwelderwerken: 1960-2009.]." *Report No. 229*, Wageningen UR, Wageningen.

Dijkstra, J. T. and Uittenbogaard, R. E. (2010). "Modeling the interaction between flow and highly flexible aquatic vegetation." *Water Resources Research*, 46(12), 1–14.

Drake, B. G. (1976). "Seasonal changes in reflectance and standing crop biomass in three salt marsh communities.." *Plant physiology*, 58(5), 696–9.

Duarte, C. M., Losada, I. J., Hendriks, I. E., Mazarrasa, I., and Marbà, N. (2013). "The role of coastal plant communities for climate change mitigation and adaptation." *Nature Climate Change*, 3(11), 961–968.

Dubi, A. and Torum, A. (1996). "Wave energy dissipation in kelp vegetation." *Coastal Engineering Proceedings*, 2626–2639.

Duncan, J. H. (1983). "The breaking and non-breaking wave resistance of a two-dimensional hydrofoil." *Journal of Fluid Mechanics*, 126, 507–520.

EurOtop (2007). *Wave overtopping of sea defences and related structures: assessment manual*. EurOtop.

EurOtop (2016). *Manual on wave overtopping of sea defences and related structures An overtopping manual largely based on European research, but for worldwide application*. Van der Meer, J.W.; Allsop, N.W.H.; Bruce, T.; De Rouck, J.; Kortenhaus, A.; Pullen, T.; Schüttrumpf, H.; Troch, P.; Zanuttigh, B.

Feagin, R. A., Irish, J. L., Möller, I., Williams, A. M., Colón-Rivera, R. J., and Mousavi, M. E. (2011). "Short communication: Engineering properties of wetland plants with application to wave attenuation." *Coastal Engineering*, 58(3), 251–255.

Feagin, R. A., Lozada-Bernard, S. M., Ravens, T. M., Moller, I., Yeager, K. M., and Baird, A. H. (2009). "Does vegetation prevent wave erosion of salt marsh edges?." *Proceedings of the National Academy of Sciences*, 106(25), 10109–10113.

Fonseca, M. S. and Cahalan, J. A. (1992). "A preliminary evaluation of wave attenuation by four species of seagrass." *Estuarine, Coastal and Shelf Science*, 35(6), 565–576.

Francalanci, S., Bendoni, M., Rinaldi, M., and Solari, L. (2013). "Ecomorphodynamic evolution of salt marshes: Experimental observations of bank retreat processes." *Geomorphology*, 195, 53–65.

Führböter, A. and Sparboom, U. (1988). "Shock pressure interactions on prototype sea dykes caused by breaking waves." *Proc. SOWAS '88 (Modelling Soil-Water-Structure interactions), ISBN 90.6191.8154*.

Gallagher, J. L. (1983). "Seasonal patterns in recoverable underground reserves in Spartina alterniflora Loisel (Delaware, Georgia)." *American Journal of Botany*, 70(2), 212–215.

Gedan, K. B., Kirwan, M. L., Wolanski, E., Barbier, E. B., and Silliman, B. R. (2011). "The present and future role of coastal wetland vegetation in protecting shorelines: answering recent challenges to the paradigm." *Climatic Change*, 106(1), 7–29.

Gere, J. M. and Goodno, B. J. (2013). *Mechanics of Materials*. Cengage Learning, Stamford, USA, 8th edition.

Giri, C., Ochieng, E., Tieszen, L. L., Zhu, Z., Singh, A., Loveland, T., Masek, J., and Duke, N. (2011). "Status and distribution of mangrove forests of the world using earth observation satellite data." *Global Ecology and Biogeography*, 20(1), 154–159.

Gittman, R. K., Popowich, A. M., Bruno, J. F., and Peterson, C. H. (2014). "Marshes with and without sills protect estuarine shorelines from erosion better than bulkheads during a Category 1 hurricane." *Ocean and Coastal Management*, 102(PA), 94–102.

Glass, E. M., Garzon, J. L., Lawler, S., Paquier, E., and Ferreira, C. M. (2018). "Potential of marshes to attenuate storm surge water level in the Chesapeake Bay." *Limnology and Oceanography*, 63(2), 951–967.

Groeneweg, J., Beckers, J., and Gautier, C. (2010). "A probabilistic model for the determination of hydraulic boundary conditions in a dynamic coastal system." *Coastal Engineering Proceedings*, Vol. 32, Shanghai, China, 1–13.

Grüne, J. (2005). "Evaluation of wave climate parameters from benchmarking flotsam levels." *Proceedings of the International Conference on Coastlines, Structures and Breakwaters, 2005*, Thomas Telford, 468.

Hall, J. W., Meadowcroft, I. C., Lee, E. M., and Van Gelder, P. H. A. J. M. (2002). "Stochastic simulation of episodic soft coastal cliff recession." *Coastal Engineering*, 46(3), 159–174.

Harley, C. D. G. and Bertness, M. D. (1996). "Structural interdependence: An ecological consequence of morphological responses to crowding in marsh plants." *Functional Ecology*, 10(5), 654–661.

Hartig, E., Gornitz, V., Kolker, A., Mushacke, F., and Fallon, D. (2002). "Anthropogenic and climate-change impacts on salt marshes of Jamaica Bay, New York City." *Wetlands*, 1(March), 71–89.

Hasofer, A. M. and Lind, N. C. (1974). "Exact and Invariant Second-Moment Code Format." *Journal of the Engineering Mechanics Division*, 100(1), 111–121.

Heuner, M., Silinski, A., Schoelynck, J., Bouma, T. J., Puijalon, S., Troch, P., Fuchs, E., Schröder, B., Schröder, U., Meire, P., and Temmerman, S. (2015). "Ecosystem engineering by plants on wave-exposed intertidal flats is governed by relationships between effect and response traits." *PLoS ONE*, 10(9), 1–18.

Hofland, B., Chen, X., Altomare, C., and Oosterlo, P. (2017). "Prediction formula for the spectral wave period Tm-1,0 on mildly sloping shallow foreshores." *Coastal Engineering*, 123, 21–28.

Hofstede, J. L. A. (2003). "Integrated management of artificially created salt marshes in the Wadden Sea of Schleswig-Holstein, Germany." *Wetlands Ecology and Management*, 11, 183–194.

Horstman, E. M., Dohmen-Janssen, C. M., Narra, P. M., van den Berg, N. J., Siemerink, M., and Hulscher, S. J. (2014). "Wave attenuation in mangroves: A quantitative approach to field observations." *Coastal Engineering*, 94, 47–62.

Howes, N. C., FitzGerald, D. M., Hughes, Z. J., Georgiou, I. Y., Kulp, M. A., Miner, M. D., Smith, J. M., and Barras, J. A. (2010). "Hurricane-induced failure of low salinity wetlands." *Proceedings of the National Academy of Sciences*, Vol. 107, 14014–14019.

Hu, Z., Suzuki, T., Zitman, T., Uittewaal, W., and Stive, M. (2014). "Laboratory study on wave dissipation by vegetation in combined current-wave flow." *Coastal Engineering*, 88, 131–142.

IPCC (2013). "Annex II: climate system scenario tables." *Climate Change 2013: The Physical Science Basis. Contribution of Working Group I to the Fifth Assessment Report of the Intergovernmental Panel on Climate Change [Stocker, T.F., D. Qin, G.-K. Plattner, M. Tignor, S.K. Allen, J. Boschung, A. Nauels, Y. Xia,*, M. Prather, G. Flato, P. Friedlingstein, C. Jones, J. F. Lamarque, H. Liao, and P. Rasch, eds., Cambridge, United Kingdom and New York, NY, USA, Cambridge University Press, 1395–1445.

Jadhav, R. S. and Chen, Q. (2012). "Field Investigation of Wave Dissipation Over Salt Marsh Vegetation During Tropical Cyclone." *Coastal Engineering Proceedings*, 1(33), 41.

Jadhav, R. S. and Chen, Q. (2013). "Probability distribution of wave heights attenuated by salt marsh vegetation during tropical cyclone." *Coastal Engineering*, 82, 47–55.

Jadhav, R. S., Chen, Q., and Smith, J. M. (2013). "Spectral distribution of wave energy dissipation by salt marsh vegetation." *Coastal Engineering*, 77, 99–107.

Janssen, S. K., van Tatenhove, J. P., Otter, H. S., and Mol, A. P. (2015). "Greening Flood Protection—An Interactive Knowledge Arrangement Perspective." *Journal of Environmental Policy and Planning*, 17(3), 309–331.

Jones, H. P., Hole, D. G., and Zavaleta, E. S. (2012). "Harnessing nature to help people adapt to climate change." *Nature Climate Change*, 2(7), 504–509.

Jongejan, R. B., Stefess, H., Roode, N., Ter Horst, W., and Maaskant, B. (2011). "The VNK2

project: a detailed, large-scale quantitative flood risk analysis for the Netherlands." *International Conference on Flood Management*, Vol. 5, 27–29.

Jonkman, S. N., Hillen, M. M., Nicholls, R. J., Kanning, W., and van Ledden, M. (2013). "Costs of adapting coastal defences to sea-level rise— New estimates and their implications." *Journal of Coastal Research*, 29(5), 1212–1226.

Jonkman, S. N., Kok, M., and Vrijling, J. K. (2008). "Flood risk assessment in the Netherlands: A case study for dike ring South Holland." *Risk Analysis*, 28(5), 1357–1373.

Kanning, W. and Den Hengst, S. (2013). "Probabilistic assessment of asphalt revetments in the WTI2017." *Report No. 1207805-007*, Deltares, Delft, The Netherlands.

Kearney, M. S., Riter, J. C. A., and Turner, R. E. (2011). "Freshwater river diversions for marsh restoration in Louisiana: Twenty-six years of changing vegetative cover and marsh area." *Geophysical Research Letters*, 38(16), 1–6.

King, S. E. and Lester, J. N. (1995). "The value of salt-marsh as a sea defense." *Marine Pollution Bulletin*, 30(3), 180–189.

Kirwan, M. L., Guntenspergen, G. R., D'Alpaos, A., Morris, J. T., Mudd, S. M., and Temmerman, S. (2010). "Limits on the adaptability of coastal marshes to rising sea level." *Geophysical Research Letters*, 37(23), 1–5.

Kirwan, M. L. and Megonigal, J. P. (2013). "Tidal wetland stability in the face of human impacts and sea-level rise." *Nature*, 504(7478), 53–60.

Kirwan, M. L., Temmerman, S., Skeehan, E. E., Guntenspergen, G. R., and Fagherazzi, S. (2016). "Overestimation of marsh vulnerability to sea level rise." *Nature Climate Change*, 6(3), 253–260.

Klerk, W. J. and Jongejan, R. B. (2016). "Semi-probabilistic assessment of wave impact and runup on grass revetments." *Report No. 1220080-005*, Deltares, Delft, The Netherlands.

Klijn, F., Kreibich, H., de Moel, H., and Penning-Rowsell, E. (2015). "Adaptive flood risk management planning based on a comprehensive flood risk conceptualisation." *Mitigation and Adaptation Strategies for Global Change*, 20(6), 845–864.

Knutson, P. L., Brochu, R. A., Seelig, W. N., and Inskeep, M. (1982). "Wave damping in Spartina alterniflora marshes." *Wetlands*, 2, 87–104.

Kobayashi, N., Raichle, A. W., and Asano, T. (1993). "Wave Attenuation by Vegetation." *Journal of Waterway, Port, Coastal, and Ocean Engineering*, 119(1), 30–48.

Koch, E. W., Barbier, E. B., Silliman, B. R., Reed, D. J., Perillo, G. M., Hacker, S. D., Granek, E. F., Primavera, J. H., Muthiga, N., Polasky, S., Halpern, B. S., Kennedy, C. J., Kappel, C. V., and Wolanski, E. (2009). "Non-linearity in ecosystem services: Temporal and spatial variability in coastal protection." *Frontiers in Ecology and the Environment*, 7(1), 29–37.

Koftis, T., Prinos, P., and Stratigaki, V. (2013). "Wave damping over artificial Posidonia

oceanica meadow: A large-scale experimental study." *Coastal Engineering*, 73(1), 71–83.

Komen, G. J., Hasselmann, K., and Hasselmann, K. (1984). "On the existence of a fully developed wind-sea spectrum." *Journal of physical oceanography*, 14(8), 1271–1285.

Kruse, G. A. M. (2010). "Studie voor richtlijnen klei op dijktaluds in het rivierengebied [Study for guidelines for clay on dike slopes in riverine areas]." *Report No. 1202512-000*, Deltares, Delft, The Netherlands.

Leonardi, N. and Fagherazzi, S. (2015). "Effect of local variability in erosional resistance on large-scale morphodynamic response of salt marshes to wind waves and extreme events." *Geophysical Research Letters*, 42(14), 5872–5879.

Leonardi, N., Ganju, N. K., and Fagherazzi, S. (2016). "A linear relationship between wave power and erosion determines salt-marsh resilience to violent storms and hurricanes." *Proceedings of the National Academy of Sciences*, 113(1), 64–68.

Liffen, T., Gurnell, M. A., O'Hare, M. T., Pollen-Bankhead, N., Simon, A., Gurnell, A. M., O'Hare, M. T., Pollen-Bankhead, N., and Simon, A. (2013). "Associations between the morphology and biomechanical properties of Sparganium erectum: Implications for survival and ecosystem engineering." *Aquatic Botany*, 105, 18–24.

Lo, V. B., Bouma, T. J., van Belzen, J., Van Colen, C., and Airoldi, L. (2017). "Interactive effects of vegetation and sediment properties on erosion of salt marshes in the Northern Adriatic Sea." *Marine Environmental Research*, 131, 32–42.

Luhar, M., Coutu, S., Infantes, E., Fox, S., and Nepf, H. M. (2010). "Wave-induced velocities inside a model seagrass bed." *Journal of Geophysical Research: Oceans*, 115(12), 1–15.

Luhar, M. and Nepf, H. M. (2011). "Flow-induced reconfiguration of buoyant and flexible aquatic vegetation." *Limnology and Oceanography*, 56(6), 2003–2017.

Luhar, M. and Nepf, H. M. (2016). "Wave-induced dynamics of flexible blades." *Journal of Fluids and Structures*, 61, 20–41.

Mach, K. J., Hale, B. B., Denny, M. W., and Nelson, D. V. (2007). "Death by small forces: a fracture and fatigue analysis of wave-swept macroalgae.." *The Journal of experimental biology*, 210(Pt 13), 2231–2243.

Madsen, O. S., Poon, Y.-K., and Graber, H. C. (1988). "Spectral Wave Attenuation by Bottom Friction: Theory." *Coastal Engineering Proceedings*, 21, 492–504.

Manca, E., Cáceres, I., Alsina, J. M., Stratigaki, V., Townend, I., and Amos, C. L. (2012). "Wave energy and wave-induced flow reduction by full-scale model Posidonia oceanica seagrass." *Continental Shelf Research*, 50-51, 100–116.

Marsooli, R. and Wu, W. (2014). "Numerical investigation of wave attenuation by vegetation using a 3D RANS model." *Advances in Water Resources*, 74(October), 245–257.

Massel, S. R. (1996). "On the largest wave height in water of constant depth." *Ocean Engineering*, 23(7), 553–573.

Mazda, Y., Magi, M., Ikeda, Y., Kurokawa, T., and Asano, T. (2006). "Wave reduction in a mangrove forest dominated by Sonneratia sp.." *Wetlands Ecology and Management*, 14(4), 365–378.

Mckee, K. L., Cahoon, D. R., and Feller, I. C. (2007). "Caribbean mangroves adjust to rising sea level through biotic controls on change in soil elevation." *Global Ecology and Biogeography*, 16(5), 545–556.

McLachlan, A. (1996). "Physical factors in benthic ecology: Effects of changing sand particle size on beach fauna." *Marine Ecology Progress Series*, 131(1), 205–217.

McOwen, C., Weatherdon, L., Bochove, J.-W., Sullivan, E., Blyth, S., Zockler, C., Stanwell-Smith, D., Kingston, N., Martin, C., Spalding, M., and Fletcher, S. (2017). "A global map of saltmarshes." *Biodiversity Data Journal*, 5, e11764.

Mei, C. C., Chan, I.-C., Liu, P. L.-F., Huang, Z., and Zhang, W. (2011). "Long waves through emergent coastal vegetation." *Journal of Fluid Mechanics*, 687, 461–491.

Mendelsohn, R., Emanuel, K., Chonabayashi, S., and Bakkensen, L. (2012). "The impact of climate change on global tropical cyclone damage." *Nature Climate Change*, 2(3), 205–209.

Mendez, F. J. and Losada, I. J. (2004). "An empirical model to estimate the propagation of random breaking and nonbreaking waves over vegetation fields." *Coastal Engineering*, 51(2), 103–118.

Méndez, F. J., Losada, I. J., and Losada, M. A. (1999). "Hydrodynamics induced by wind waves in a vegetation field." *Journal of Geophysical Research: Oceans*, 104(C8), 18383–18396.

Menn, I., Junghans, C., and Reise, K. (2003). "Buried alive: Effects of beach nourishment on the infauna of an erosive shore in the North Sea." *Senckenbergiana Maritima*, 32(1), 125–145.

Merz, B. and Thieken, A. H. (2005). "Separating natural and epistemic uncertainty in flood frequency analysis." *Journal of Hydrology*, 309(1-4), 114–132.

Miler, O., Albayrak, I., Nikora, V., and O'Hare, M. (2012). "Biomechanical properties of aquatic plants and their effects on plant-flow interactions in streams and rivers." *Aquatic Sciences*, 74(1), 31–44.

Möller, I. (2006). "Quantifying saltmarsh vegetation and its effect on wave height dissipation: Results from a UK East coast saltmarsh." *Estuarine, Coastal and Shelf Science*, 69(3-4), 337–351.

Möller, I., Kudella, M., Rupprecht, F., Spencer, T., Paul, M., Van Wesenbeeck, B. K., Wolters, G., Jensen, K., Bouma, T. J., Miranda-Lange, M., and Schimmels, S. (2014). "Wave attenuation over coastal salt marshes under storm surge conditions." *Nature Geoscience*, 7(10), 727–731.

Möller, I., Mantilla-Contreras, J., Spencer, T., and Hayes, A. (2011). "Micro-tidal coastal

reed beds: Hydro-morphological insights and observations on wave transformation from the southern Baltic Sea." *Estuarine, Coastal and Shelf Science*, 92(3), 424–436.

Möller, I. and Spencer, T. (2002). "Wave dissipation over macro-tidal saltmarshes: Effects of marsh edge typology and vegetation change." *Journal of Coastal Research*, 36(36), 506–521.

Möller, I., Spencer, T., French, J. R., Leggett, D. J., and Dixon, M. (1999). "Wave transformation over salt marshes: A field and numerical modelling study from North Norfolk, England." *Estuarine, Coastal and Shelf Science*, 49(3), 411–426.

Morton, R. A. and Barras, J. A. (2011). "Hurricane Impacts on Coastal Wetlands: A Half-Century Record of Storm-Generated Features from Southern Louisiana." *Journal of Coastal Research*, 275(6), 27–43.

Mudd, S. M., D'Alpaos, A., and Morris, J. T. (2010). "How does vegetation affect sedimentation on tidal marshes? Investigating particle capture and hydrodynamic controls on biologically mediated sedimentation." *Journal of Geophysical Research: Earth Surface*, 115(3), 1–14.

Mullarney, J. C. and Henderson, S. M. (2010). "Wave-forced motion of submerged single-stem vegetation." *Journal of Geophysical Research*, 115(C12), C12061.

Nairn, R. B. (1990). "Prediction of cross-shore sediment transport and beach profiles evolution." Ph.D. thesis, Imperial College London, London.

Narayan, S., Beck, M. W., Reguero, B. G., Losada, I. J., Van Wesenbeeck, B., Pontee, N., Sanchirico, J. N., Ingram, J. C., Lange, G. M., and Burks-Copes, K. A. (2016). "The effectiveness, costs and coastal protection benefits of natural and nature-based defences." *PLoS ONE*, 11(5), 1–17.

Nelson, R. C. (1994). "Depth limited design wave heights in very flat regions." *Coastal Engineering*, 23(1), 43–59.

Neumann, B., Vafeidis, A. T., Zimmermann, J., and Nicholls, R. J. (2015). "Future coastal population growth and exposure to sea-level rise and coastal flooding - A global assessment." *PLoS ONE*, 10(3).

Nicholls, R. and Cazenave, A. (2010). "Sea-Level Rise and Its Impact on Coastal Zones." *Science*, 328(5985), 1517–1520.

Nyman, J. A., Walters, R. J., Delaune, R. D., and Patrick, W. H. (2006). "Marsh vertical accretion via vegetative growth." *Estuarine, Coastal and Shelf Science*, 69(3-4), 370–380.

O'Donnell, J. P. and Schalles, J. F. (2016). "Examination of abiotic drivers and their influence on Spartina alterniflora biomass over a twenty-eight year period using Landsat 5 TM satellite imagery of the Central Georgia Coast." *Remote Sensing*, 8(6).

Oosterlo, P., McCall, R., Vuik, V., Hofland, B., van der Meer, J., and Jonkman, S. (2018). "Probabilistic Assessment of Overtopping of Sea Dikes with Foreshores including In-

fragravity Waves and Morphological Changes: Westkapelle Case Study." *Journal of Marine Science and Engineering*, 6(2), 48.

Padilla-Hernández, R. and Monbaliu, J. (2001). "Energy balance of wind waves as a function of the bottom friction formulation." *Coastal Engineering*, 43(2), 131–148.

Paquier, A. E., Haddad, J., Lawler, S., and Ferreira, C. M. (2017). "Quantification of the Attenuation of Storm Surge Components by a Coastal Wetland of the US Mid Atlantic." *Estuaries and Coasts*, 40(4), 930–946.

Paul, M. and Amos, C. L. (2011). "Spatial and seasonal variation in wave attenuation over Zostera noltii." *Journal of Geophysical Research: Oceans*, 116(C08019), 1–16.

Paul, M., Henry, P. Y. T., and Thomas, R. E. (2014). "Geometrical and mechanical properties of four species of northern European brown macroalgae." *Coastal Engineering*, 84, 73–80.

Paul, M., Rupprecht, F., Möller, I., Bouma, T. J., Spencer, T., Kudella, M., Wolters, G., van Wesenbeeck, B. K., Jensen, K., Miranda-Lange, M., and Schimmels, S. (2016). "Plant stiffness and biomass as drivers for drag forces under extreme wave loading: A flume study on mimics." *Coastal Engineering*, 117, 70–78.

Penning, E., Steetzel, H., Santen, R. V., Lange, M. D., Ouwerkerk, S., Vuik, V., and Fiselier, J. (2016). "Establishing vegetated foreshores to increase dike safety along lake shores." *E3S Web of Conferences*, Vol. 12008, 1–6.

Peteet, D. M., Nichols, J., Kenna, T., Chang, C., Browne, J., Reza, M., Kovari, S., Liberman, L., and Stern-Protz, S. (2018). "Sediment starvation destroys New York City marshes' resistance to sea level rise." *Proceedings of the National Academy of Sciences*, 115(41), 201715392.

Pinsky, M. L., Guannel, G., and Arkema, K. K. (2013). "Quantifying wave attenuation to inform coastal habitat conservation." *Ecosphere*, 4(August).

Puijalon, S., Bouma, T. J., Douady, C. J., van Groenendael, J., Anten, N. P. R., Martel, E., and Bornette, G. (2011). "Plant resistance to mechanical stress: Evidence of an avoidance-tolerance trade-off." *New Phytologist*, 191(4), 1141–1149.

Pujol, D., Serra, T., Colomer, J., and Casamitjana, X. (2013). "Flow structure in canopy models dominated by progressive waves." *Journal of Hydrology*, 486, 281–292.

Quartel, S., Kroon, A., Augustinus, P., Van Santen, P., and Tri, N. H. (2007). "Wave attenuation in coastal mangroves in the Red River Delta, Vietnam." *Journal of Asian Earth Sciences*, 29(4), 576–584.

Reguero, B. G., Beck, M. W., Bresch, D. N., Calil, J., and Meliane, I. (2018). "Comparing the cost effectiveness of nature- based and coastal adaptation : A case study from the Gulf Coast of the United States." *PLoS ONE*, 1–24.

Reise, K., Baptist, M., Bubridge, P., Dankers, N., Fischer, L., Flemming, B., Oost, A. P., and Smit, C. (2010). "The Wadden Sea Quality Status Report- Synthesis Report." *Report No. 29*, Common Wadden Sea Secretariat, Wilhelmshaven, Germany.

Riffe, K. C., Henderson, S. M., and Mullarney, J. C. (2011). "Wave dissipation by flexible vegetation." *Geophysical Research Letters*, 38(18).

Rijkswaterstaat and KNMI (1961). "Verslag over de stormvloed van 1953 [Report on the 1953 Flood]." *Report no.*, The Hague.

Ris, R. C., Holthuijsen, L. H., and Booij, N. (1999). "A third-generation wave model for coastal regions: 2. Verification." *Journal of Geophysical Research*, 104(C4), 7667.

Roelvink, D., Reniers, A., van Dongeren, A., van Thiel de Vries, J., McCall, R., and Lescinski, J. (2009). "Modelling storm impacts on beaches, dunes and barrier islands." *Coastal Engineering*.

Rosenblatt, M. (1952). "Remarks on a Multivariate Transformation." *The Annals of Mathematical Statistics*, 23(3), 470–472.

Ruessink, B. G., Walstra, D. J. R., and Southgate, H. N. (2003). "Calibration and verification of a parametric wave model on barred beaches." *Coastal Engineering*, 48(3), 139–149.

Rupprecht, F., Möller, I., Evans, B., Spencer, T., and Jensen, K. (2015). "Biophysical properties of salt marsh canopies - Quantifying plant stem flexibility and above ground biomass." *Coastal Engineering*, 100, 48–57.

Rupprecht, F., Möller, I., Paul, M., Kudella, M., Spencer, T., van Wesenbeeck, B. K., Wolters, G., Jensen, K., Bouma, T. J., Miranda-Lange, M., and Schimmels, S. (2017). "Vegetation-wave interactions in salt marshes under storm surge conditions." *Ecological Engineering*, 100, 301–315.

Salvadori, G., Durante, F., Tomasicchio, G. R., and D'Alessandro, F. (2015). "Practical guidelines for the multivariate assessment of the structural risk in coastal and off-shore engineering." *Coastal Engineering*, 95, 77–83.

Salvadori, G., Tomasicchio, G. R., and D'Alessandro, F. (2014). "Practical guidelines for multivariate analysis and design in coastal and off-shore engineering." *Coastal Engineering*, 88, 1–14.

Sánchez-González, J. F., Sánchez-Rojas, V., and Memos, C. D. (2011). "Wave attenuation due to Posidonia oceanica meadows." *Journal of Hydraulic Research*, 49(4), 503–514.

Scaife, A. A., Spangehl, T., Fereday, D. R., Cubasch, U., Langematz, U., Akiyoshi, H., Bekki, S., Braesicke, P., Butchart, N., Chipperfield, M. P., Gettelman, A., Hardiman, S. C., Michou, M., Rozanov, E., and Shepherd, T. G. (2012). "Climate change projections and stratosphere-troposphere interaction." *Climate Dynamics*, 38(9-10), 2089–2097.

Schroevers, M., Huisman, B. J. A., Van Der Wal, M., and Terwindt, J. (2011). "Measuring ship induced waves and currents on a tidal flat in the Western Scheldt Estuary." *2011 IEEE/OES/CWTM 10th Working Conference on Current, Waves and Turbulence Measurement, CWTM 2011*, 123–129.

Schuerch, M., Spencer, T., Temmerman, S., Kirwan, M. L., Wolff, C., Lincke, D., McOwen, C. J., Pickering, M. D., Reef, R., Vafeidis, A. T., Hinkel, J., Nicholls, R. J., and Brown,

S. (2018). "Future response of global coastal wetlands to sea-level rise." *Nature*, 561(7722), 231–234.

Schweckendiek, T. (2014). "On Reducing Piping Uncertainties: A Bayesian Decision Approach." Phd thesis, Delft University of Technology, Delft.

Scussolini, P., Aerts, J. C. J. H., Jongman, B., Bouwer, L. M., Winsemius, H. C., De Moel, H., and Ward, P. J. (2016). "FLOPROS: an evolving global database of flood protection standards." *Natural Hazards and Earth System Sciences*, 16(5), 1049–1061.

Sebastian, A., Dupuits, E. J., and Morales-Nápoles, O. (2017). "Applying a Bayesian network based on Gaussian copulas to model the hydraulic boundary conditions for hurricane flood risk analysis in a coastal watershed." *Coastal Engineering*, 125, 42–50.

Seymour, R. J., Tegner, M. J., and Seymour M.J. Tegner, P.K. Dayton, & P.E. Parnell., R. J. (1989). "Storm wave induced mortality of Giant Kelp, Macrocystis pyrifera, in southern California.." *Estuarine, Coastal and Shelf Science*, 28(3), 277–292.

Shepard, C. C., Crain, C. M., and Beck, M. W. (2011). "The protective role of coastal marshes: a systematic review and meta-analysis.." *PloS one*, 6(11), e27374.

Silinski, A., Heuner, M., Schoelynck, J., Puijalon, S., Schröder, U., Fuchs, E., Troch, P., Bouma, T. J., Meire, P., and Temmerman, S. (2015). "Effects of wind waves versus ship waves on tidal marsh plants: A flume study on different life stages of scirpus maritimus." *PLoS ONE*, 10(3), 1–16.

Silinski, A., Schoutens, K., Puijalon, S., Schoelynck, J., Luyckx, D., Troch, P., Meire, P., and Temmerman, S. (2018). "Coping with waves: Plasticity in tidal marsh plants as self-adapting coastal ecosystem engineers." *Limnology and Oceanography*, 63(2), 799–815.

Silva, R., Lithgow, D., Esteves, L. S., Martínez, M. L., Moreno-Casasola, P., Martell, R., Pereira, P., Mendoza, E., Campos-Cascaredo, A., Winckler Grez, P., Osorio, A. F., Osorio-Cano, J. D., and Rivillas, G. D. (2017). "Coastal risk mitigation by green infrastructure in Latin America." *Proceedings of the Institution of Civil Engineers - Maritime Engineering*.

Singh Chauhan, P. P. (2009). "Autocyclic erosion in tidal marshes." *Geomorphology*, 110(3-4), 45–57.

Smith, C. S., Puckett, B., Gittman, R. K., and Peterson, C. H. (2018). "Living shorelines enhanced the resilience of saltmarshes to Hurricane Matthew (2016)." *Ecological Applications*, 28(4), 871–877.

Snyder, R. L., Dobson, F. W., Elliott, J. A., and Long, R. B. (1981). "Array measurements of atmospheric pressure fluctuations above surface gravity waves." *Journal of Fluid mechanics*, 102, 1–59.

Spalding, M. D., Mcivor, A. L., Beck, M. W., Koch, E. W., Möller, I., Reed, D. J., Rubinoff, P., Spencer, T., Tolhurst, T. J., Wamsley, T. V., van Wesenbeeck, B. K., Wolanski, E., and Woodroffe, C. D. (2014). "Coastal ecosystems: A critical element of risk reduction." *Conservation Letters*, 7(3), 293–301.

Spencer, T., Brooks, S. M., Evans, B. R., Tempest, J. A., and Möller, I. (2015). "Southern North Sea storm surge event of 5 December 2013: Water levels , waves and coastal impacts." *Earth-Science Reviews*, 146, 120–145.

Spencer, T., Möller, I., Rupprecht, F., Bouma, T. J., van Wesenbeeck, B. K., Kudella, M., Paul, M., Jensen, K., Wolters, G., Miranda-Lange, M., and Schimmels, S. (2016). "Salt marsh surface survives true-to-scale simulated storm surges." *Earth Surface Processes and Landforms*, 41(4), 543–552.

Steenbergen, H. M. G. M., Lassing, B. L., Vrouwenvelder, A. C. W. M., and Waarts, P. H. (2004). "Reliability analysis of flood defence systems." *Heron*, 49(1), 51–73.

Stratigaki, V., Manca, E., Prinos, P., Losada, I. J., Lara, J. L., Sclavo, M., Amos, C. L., Cáceres, I., and Sánchez-Arcilla, A. (2011). "Large-scale experiments on wave propagation over Posidonia oceanica." *Journal of Hydraulic Research*, 49(SUPPL.1), 31–43.

Sutton-Grier, A. E., Wowk, K., and Bamford, H. (2015). "Future of our coasts: The potential for natural and hybrid infrastructure to enhance the resilience of our coastal communities, economies and ecosystems." *Environmental Science and Policy*, 51, 137–148.

Suzuki, T. and Arikawa, T. (2010). "Numerical analysis of bulk drag coefficient in dense vegetation by immersed boundary method." *Coastal Engineering Proceedings*.

Suzuki, T., Verwaest, T., and Veale, W. (2012a). "A numerical study on the effect of beach nourishment on wave overtopping in shallow foreshores." *Coastal Engineering Proceedings*, 1–13.

Suzuki, T., Zijlema, M., Burger, B., Meijer, M. C., and Narayan, S. (2012b). "Wave dissipation by vegetation with layer schematization in SWAN." *Coastal Engineering*, 59(1), 64–71.

Syvitski, J. P. M., Kettner, A. J., Overeem, I., Hutton, E. W. H., Hannon, M. T., Brakenridge, G. R., Day, J., Vörösmarty, C., Saito, Y., Giosan, L., and Nicholls, R. J. (2009). "Sinking deltas due to human activities." *Nature Geoscience*, 2(10), 681–686.

Tang, J., Shen, S., and Wang, H. (2015). "Numerical model for coastal wave propagation through mild slope zone in the presence of rigid vegetation." *Coastal Engineering*, 97(March), 53–59.

Temmerman, S., Govers, G., Wartel, S., and Meire, P. (2003). "Spatial and temporal factors controlling short-term sedimentation in a salt and freshwater tidal marsh, scheldt estuary, Belgium, SW Netherlands." *Earth Surface Processes and Landforms*, 28(7), 739–755.

Temmerman, S., Meire, P., Bouma, T. J., Herman, P. M. J., Ysebaert, T., and De Vriend, H. J. (2013). "Ecosystem-based coastal defence in the face of global change." *Nature*, 504(7478), 79–83.

Tschirky, P., Hall, K., and Turcke, D. (2001). "Wave attenuation by emergent wetland vegetation." *Coastal Engineering*, 865–877.

Turner, R. E., Baustian, J. J., Swenson, E. M., and Spicer, J. S. (2006). "Wetland sedimentation from huricanes Katrina and Rita." *Science*, 314(May), 449–452.

Usherwood, J. R., Ennos, A. R., and Ball, D. J. (1997). "Mechanical and anatomical adaptations in terrestrial and aquatic buttercups to their respective environments." *Journal of Experimental Botany*, 48(312), 1469–1475.

Van der Meer, J. W., Briganti, R., Zanuttigh, B., and Wang, B. (2005). "Wave transmission and reflection at low-crested structures: Design formulae, oblique wave attack and spectral change." *Coastal Engineering*, 52(10-11), 915–929.

Van der Meer, J. W., Schrijver, R., Hardeman, B., Hoven, A. V., Verheij, H., and Steendam, G. J. (2009). "Guidance on erosion resistance of inner slopes of dikes from three years of testing with the Wave Overtopping Simulator." *Proc. ICE 2009*, Vol. 162, 1–14.

Van der Wal, D., Wielemaker-Van den Dool, A., and Herman, P. M. J. (2008). "Spatial patterns, rates and mechanisms of saltmarsh cycles (Westerschelde, The Netherlands)." *Estuarine, Coastal and Shelf Science*, 76(2), 357–368.

Van Gelder, P. (2000). "Statistical methods for the risk-based design of civil structures." *Phd thesis*, Delft University of Technology, Delft, The Netherlands.

Van Gent, M. and Doorn, N. (2001). "Numerical model simulations of wave propagation and wave run-up on dikes with shallow foreshores." *Proceedings of Coastal Dynamics*, Lund, Sweden, ASCE, 1–10.

Van Koningsveld, M., De Boer, G. J., Baart, F., Damsma, T., Den Heijer, C., Van Geer, P., and De Sonnevile, B. (2010). "OpenEarth: Inter-company management of: Data, Models, Tools and Knowledge." *WODCON XIX: Dredging Makes the World a Better Place*, 14 pp.

van Loon-Steensma, J. M. (2015). "Salt marshes to adapt the flood defences along the Dutch Wadden Sea coast." *Mitigation and Adaptation Strategies for Global Change*, 20(6), 929–948.

Van Wesenbeeck, B. K., De Boer, W., Narayan, S., Van der Star, W. R. L., and De Vries, M. B. (2017). "Coastal and riverine ecosystems as adaptive flood defenses under a changing climate." *Mitigation and Adaptation Strategies for Global Change*, 22(7), 1087–1094.

Van Wesenbeeck, B. K., Mulder, J. P. M., Marchand, M., Reed, D. J., de Vries, M. B., De Vriend, H. J., and Herman, P. M. J. (2014). "Damming deltas: A practice of the past? Towards nature-based flood defenses." *Estuarine, Coastal and Shelf Science*, 140, 1–6.

Voortman, H. G. (2003). "Risk-Based Design of Large-Scale Flood Defence Systems." Phd thesis, Delft University of Technology, Delft, The Netherlands.

Vorogushyn, S., Merz, B., and Apel, H. (2009). "Development of dike fragility curves for piping and micro-instability breach mechanisms." *Natural Hazards and Earth System Science*, 9(4), 1383–1401.

Vrijling, J. K. (2001). "Probabilistic design of water defense systems in The Netherlands." *Reliability Engineering & System Safety*, 74(3), 337–344.

Vuik, V., Jonkman, S. N., Borsje, B. W., and Suzuki, T. (2016). "Nature-based flood protection: The efficiency of vegetated foreshores for reducing wave loads on coastal dikes." *Coastal Engineering*, 116, 42–56.

Vuik, V., Suh Heo, H. Y., Zhu, Z., Borsje, B. W., and Jonkman, S. N. (2018a). "Stem breakage of salt marsh vegetation under wave forcing: A field and model study." *Estuarine, Coastal and Shelf Science*, 200, 41–58.

Vuik, V., van Balen, W., and van Vuren, S. (2017). "Fully probabilistic assessment of safety against flooding along the Dutch coast." *Journal of Flood Risk Management*, 10(3), 349–360.

Vuik, V., Van Vuren, S., Borsje, B. W., van Wesenbeeck, B. K., and Jonkman, S. N. (2018b). "Assessing safety of Nature-based Flood Defenses: dealing with extremes and uncertainties." *Coastal Engineering*, 139, 47–64.

Walker, W., Harremoës, P., Rotmans, J., Van der Sluijs, J., Van Asselt, M., Janssen, P., and Krayer von Krauss, M. (2003). "Defining uncertainty: a conceptual basis for uncertainty management in model-based decision support." *Integrated Assessment*, 4(1), 5–17.

Wamsley, T. V., Cialone, M. a., Smith, J. M., Atkinson, J. H., and Rosati, J. D. (2010). "The potential of wetlands in reducing storm surge." *Ocean Engineering*, 37(1), 59–68.

Weber, S. L. (1989). *Surface gravity waves and turbulent bottom friction*.

Weitzman, J. S., Zeller, R. B., Thomas, F. I. M., and Koseff, J. R. (2015). "The attenuation of current- and wave-driven flow within submerged multispecific vegetative canopies." *Limnology and Oceanography*, 60(6), 1855–1874.

Wiegman, N., Perluka, R., Oude Elberink, S., and Vogelzang, J. (2005). "Vaklodingen: de inwintechnieken en hun combinaties. Vergelijking tussen verschillende inwintechnieken en de combinaties ervan [Vaklodingen: measurement techniques and their combinations]." *Report No. AGI-2005-GSMH-012*, Adviesdienst Geo-Informatica en ICT (AGI), Delft, <http://www.vliz.be/imisdocs/publications/112037.pdf>.

Willemsen, P. W., Horstman, E. M., Borsje, B. W., Friess, D. A., and Dohmen-Janssen, C. M. (2016). "Sensitivity of the sediment trapping capacity of an estuarine mangrove forest." *Geomorphology*, 273, 189–201.

Wilms, T., Van Wesenbeeck, B. K., and Tonneijck, F. (2018). "Permeable structures; Building with Nature to restore eroding tropical muddy coasts." *Report no.*, Ecoshape, Dordrecht.

Winterwerp, J. C., Erftemeijer, P. L., Suryadiputra, N., Van Eijk, P., and Zhang, L. (2013). "Defining eco-morphodynamic requirements for rehabilitating eroding mangrove-mud coasts." *Wetlands*, 33(3), 515–526.

Winterwerp, J. C., van Kesteren, W. G. M., van Prooijen, B., and Jacobs, W. (2012). "A conceptual framework for shear flow–induced erosion of soft cohesive sediment beds." *Journal of Geophysical Research*, 117(C10), C10020.

Yang, S. L., Shi, B. W., Bouma, T. J., Ysebaert, T., and Luo, X. X. (2012). "Wave Attenuation at a Salt Marsh Margin: A Case Study of an Exposed Coast on the Yangtze Estuary." *Estuaries and Coasts*, 35(1), 169–182.

Ysebaert, T., Yang, S.-L. L., Zhang, L., He, Q., Bouma, T. J., and Herman, P. M. J. (2011). "Wave Attenuation by Two Contrasting Ecosystem Engineering Salt Marsh Macrophytes in the Intertidal Pioneer Zone." *Wetlands*, 31(6), 1043–1054.

Zhang, K., Liu, H., Li, Y., Xu, H., Shen, J., Rhome, J., and Smith, T. J. (2012). "The role of mangroves in attenuating storm surges." *Estuarine, Coastal and Shelf Science*, 102-103, 11–23.

Zhang, L. and Xu, Y. (2011). "Assessment of Levee Breaching Risks to the Pearl River Delta." *Geotechnical Safety and Risk. ISGSR 2011.*, N. Vogt, B. Schuppener, D. Straub, and G. Bräu, eds., Karlsruhe, BAW, 613–621.

Zhao, B., Kreuter, U., Li, B., Ma, Z., Chen, J., and Nakagoshi, N. (2004). "An ecosystem service value assessment of land-use change on Chongming Island, China." *Land Use Policy*, 21(2), 139–148.

Zhu, Z., Vuik, V., Visser, P. J., Soens, T., van Wesenbeeck, B. K., van de Koppel, J., Jonkman, S. N., Temmerman, S., and Bouma, T. J. (2018). "Historic support for nature-based mitigation of coastal flooding under future sea level rise." *(in review)*.

Zijlema, M., Stelling, G., and Smit, P. (2011). "SWASH: An operational public domain code for simulating wave fields and rapidly varied flows in coastal waters." *Coastal Engineering*, 58(10), 992–1012.

LIST OF SYMBOLS

Symbol	Name	Units
α	Stem height to water depth ratio (Chapter 2)	-
α	Importance factor (Chapter 4)	-
α_d	Slope angle dike	-
α_{fs}	Slope angle tidal flat	-
β	Reliability index	-
ϵ_b	Energy dissipation due to wave breaking	$Jm^{-2}s^{-1}$
ϵ_f	Energy dissipation due to bottom friction	$Jm^{-2}s^{-1}$
ϵ_v	Energy dissipation due to vegetation	$Jm^{-2}s^{-1}$
γ	Breaker parameter	-
ν	Kinematic viscosity of water (Chapter 3)	m^2/s
ν	Poisson's ratio of asphalt (Chapter 4)	-
ω	Angular wave frequency	rad/s
ρ	Mass density of water	kg/m^3
σ_{br}	Flexural strength asphalt	MPa
σ_{max}	Flexural strength	MPa
σ_{wave}	Wave-induced bending stress	MPa
θ	Leaning angle	deg.
ζ	Still water level	m MSL
a, b, c	Fitting parameters in relation C_D and Re	-
A_c	Correction factor wave-induced stress	-
B_{fs}	Width of flat part of foreshore	m
b_v	Stem diameter	m
$b_{v,in}$	Inner stem diameter	m
C_a, C_b, C_c	Parameters grass strength	m, 1/hr, m
C_D	Drag coefficient	-
$\widetilde{C}_D$	Bulk drag coefficient	-
C_f	Friction coefficient	-
c_g	Group velocity	m/s
c_{sub}	Modulus of subsoil reaction	N/m^3
D	Damage after flooding	€
d_a	Thickness asphalt layer	m
d_{tot}	Thickness clay layer with roots	m
E	Young's modulus (Chapter 3)	N/m^2
E	Wave energy density	J/m^2
f_{br}	Fraction of broken stems	-
F_{max}	Maximum force	N
f_{sand}	Fraction of sand in clay	-
g	Gravitational acceleration	m/s^2
h	Water depth	m
H	Wave height	m
$H_{1/10}$	Mean of highest 1/10th of waves	m

Symbol	Name	Units
H_{m0}	Significant wave height	m
H_{rms}	Root mean square wave height	m
h	Water depth	m
h_t	Water depth at dike toe	m
h_v	(Total) vegetation height	m
$h_{v,r}$	Reduced vegetation height after leaning	m
$h_{v,br}$	Stem height broken stems	m
I	Area moment of inertia (Chapter 3)	m^4
I	Investment costs (Chapter 5)	€
k	Wave number	rad/m
k_N	Nikuradse roughness length scale	m
L_{span}	Span length	m
M_{max}	Maximum moment	Nm
N_v	Stem density	stems/m^2
P_f	(Annual) failure probability	-
q	Wave overtopping discharge	$ls^{-1}m^{-1}$
q_D	Wave-induced distributed load	N/m
q_{max}	Tolerable overtopping discharge	$ls^{-1}m^{-1}$
r	Interest rate	-
R_c	Relative freeboard	m
Re	Vegetation Reynolds number	-
S_a	Stiffness modulus asphalt	MPa
T	Wave period	s
t_{load}	Load duration	hr
$T_{m-1,0}$	Spectral mean peak period	s
T_p	Wave peak period	s
u	Amplitude of horizontal orbital velocity	m/s
U_{10}	Wind speed at 10 m	m/s
u_{crit}	Critical orbital velocity for breakage	m/s
V_α, V_β	Fatigue parameters asphalt	-
x	Distance along transect	m
y	Distance center to convex surface	m
z	Distance from water surface	m
z_0	Offshore bed level	m MSL
$z_{2\%}$	2% wave run-up height	m
z_{fs}	Foreshore elevation	m MSL

NAWOORD

Met veel plezier kijk ik terug op bijna vijf jaar promotieonderzoek, waarin ik me heb mogen verdiepen in de mogelijkheden die de natuur ons biedt voor bescherming tegen de dreiging van het water. Naast het onderzoek heb ik bij HKV de gelegenheid gehad om de onderzoeksresultaten toe te passen in verschillende projecten, wat mij dwong om tot praktisch toepasbare en concrete resultaten te komen. Na afloop van mijn promotiecontract heb ik tussen de bedrijven door dit proefschrift kunnen voltooien. Die periode was intensief, maar de afronding levert veel voldoening op. Graag wil ik dit nawoord gebruiken om iedereen te bedanken die op wat voor wijze dan ook heeft bijgedragen aan de totstandkoming van dit proefschrift.

Allereerst wil ik mijn promotor Bas Jonkman bedanken. In december 2012 benaderde je mij vanwege mijn interesse voor promotieonderzoek. Je beschrijving van een interessante kernvraag zou, nu ik het zo teruglees, zo in de samenvatting van dit proefschrift kunnen: “Hoeveel helpen natuurlijke oplossingen zoals wetlands of zand in termen van waterveiligheid, en tegen welke kosten? Hoe gedragen deze natuurlijke oplossingen zich op lange termijn, en welke eisen stelt dit aan onderhoud en beheer?”. Je was dus niet alleen de projectleider, maar ook de geestelijk vader van BE SAFE. Bas, bedankt voor je visie, gedrevenheid en sturing in de afgelopen jaren. Ondanks je volle agenda was je telkens in staat om binnen korte tijd een reactie te geven op mijn schrijfwerk, en heb je ervoor gezorgd dat ik de belangrijkste uitdagingen voor het project in beeld hield.

Ik wil hier ook mijn waardering uitspreken richting Bas Borsje. Vanaf het schrijven van het onderzoeksvoorstel hebben we gezamenlijk opgetrokken, en je hebt in de loop van de jaren steeds meer de rol van dagelijks begeleider op je genomen. Door je altijd constructieve houding en je feedback op de artikelen heb je elk hoofdstuk van dit proefschrift naar een hoger niveau helpen tillen. Daarbij was het altijd prettig om met je van gedachten te wisselen, bijvoorbeeld over de uiteenlopende reacties en reviewcommentaren op onze publicaties. Ik ben erg blij dat je bijdrage uiteindelijk ook gewaardeerd mag worden door je formele aanstelling als mijn copromotor.

Veel mensen hebben bijgedragen aan het BE SAFE project. De inspirerende inbreng van Tjeerd Bouma, Mindert de Vries, Leon Hermans en anderen heeft meegeholpen voor het financieren van dit prachtige multidisciplinaire project. Gedurende het project zelf heb ik mogen samenwerken met Isabella Kratzer, Zhenchang Zhu, Pim Willemsen en Stephanie Janssen. Ik zie veel onderzoeksprojecten waarbij de onderzoekers vrijwel onafhankelijk hun weg gaan. Zo niet bij ons. Met Zhenchang, en eerder met Isabella, heb ik prettig samengewerkt bij het veldwerk op de kwelders en andere voorlanden. Vooral de metingen rond stormen waren een belevenis. In dat verband wil ik ook Henk Schol

en Henry Rijploeg van Waterschap Noorderzijlvest noemen vanwege het mede mogelijk maken van onze veldmetingen langs de Waddenzeedijken. Zhenchang en Pim, ik ben blij dat we tot gezamenlijke publicaties zijn gekomen. De week in Providence was onvergetelijk! Stephanie, de energie die je in het project hebt gestoken was erg waardevol, bijvoorbeeld rond gebruikersbijeenkomsten en de gezamenlijke casestudie in Friesland.

Verschillende studenten hebben in de afgelopen jaren hun steentje bijgedragen aan dit onderzoek. Patrick Oosterlo, Yi Mou, Timor Post, Gerald Songy, Merijn Janssen, Hannah Suh, Karel van Osselen, Maartje Godfroy, Zsofia Habetler, Martine Stam en Jan-Willem van Lente: ik heb jullie met veel plezier begeleid. Jullie inzet en nuttige werk rond vegetatie en voorlanden heeft op allerlei manieren bijgedragen aan dit proefschrift. Hetzelfde geldt voor het werk van fulbright student Madeline Keefer, in het toepassen van dit onderzoek in de Verenigde Staten.

Ik wil mijn kamergenoten bedanken voor de prettige tijd op de TU, en wel in het bijzonder Duong Bach, Guy Dupuits en Kasper Lendering, met wie ik de meeste tijd heb doorgebracht. Anne Ton, we hebben al een prettige samenwerking opgestart rond de zandige versterking van de Houtribdijk. Bedankt voor je begrip voor mijn soms wat verdeelde focus op het nieuwe project en het afronden van dit proefschrift. Ik zie uit naar de jaren die komen gaan. Verder dank aan alle mensen van de vakgroep: promovendi, docenten en het ondersteunend personeel.

Veel waardering gaat uit naar mijn werkgever, de directie van HKV. Jullie hebben mij gestimuleerd om aan dit avontuur te beginnen, en hiervoor alle mogelijke randvoorwaarden in orde gemaakt. Bedankt dat jullie mij de ruimte hebben gegund om min of meer naar eigen inzicht de twee banen met elkaar te combineren. Ik ben ervan overtuigd dat jullie opstelling ervoor zorgt dat het bijzondere karakter van HKV ook richting de toekomst behouden blijft. Ook alle andere collega's van HKV wil ik bedanken voor de interesse, bijdragen aan het onderzoek, en natuurlijk de fijne collegiale sfeer.

Verder wil ik mijn familie bedanken, in het bijzonder mijn ouders voor jullie onvoorwaardelijke steun en hulp tijdens alle jaren van schoolgaan, studeren, werken en promoveren, en voor jullie oprechte interesse in mijn onderzoek. Charlene, een speciaal plekje in dit dankwoord voor jou. De voortdurende druk om voortgang te boeken en uiteindelijk het proefschrift te schrijven heeft heel wat tijd opgeslokt die ik ook met jou had kunnen doorbrengen. Ik hoop dat er straks meer plek vrijkomt in mijn hoofd voor belangrijkere dingen in het leven dan een promotieonderzoek. Ik wil je bedanken omdat je er altijd voor me bent! Myrthe en Noëlle, ik ben blij dat jullie er elke dag weer voor hebben gezorgd dat ik mijn werk los kon laten zodra ik thuis kwam. Zo hebben ook jullie mij fantastisch geholpen.

Bovenal dank ik God dat Hij mij het verstand, de mogelijkheden en de gezondheid heeft gegeven om dit werk te doen en te volbrengen. Dat ik al deze jaren zonder problemen aan het onderzoek heb mogen werken, zie ik als een bijzondere gave, terugdenkend aan de tijd waarin er grote zorgen waren over mijn gezondheid. *'Wat heb ik, wat ik niet heb ontvangen?' 'Wie roemt, die roeme in de Heere.'*

ACKNOWLEDGMENTS

This research was part of the research programme BE SAFE, which was financed by the Netherlands Organisation for Scientific Research (NWO) (850.13.010). Additional financial support was provided by Deltares, Boskalis, Van Oord, Rijkswaterstaat, World Wildlife Fund and HZ University of Applied Science.

We thank Benwei Shi for his willingness for providing wave data from East Chongming, China (Chapter 2), Franziska Rupprecht for providing the three-point-bending test data from the Hydralab experiments (Chapter 3), Robert 't Hart and André van Hoven (Deltares) for sharing their knowledge on asphalt revetments and grass covers (Chapter 4), and Hessel Jongerius (Rijkswaterstaat) and Tom Wilms (Witteveen+Bos) for providing construction and maintenance costs for brushwood and bamboo dams (Chapter 5).

We also gratefully acknowledge the comments of all anonymous reviewers, who helped us to improve and clarify the different chapters of this dissertation.

CURRICULUM VITÆ

VINCENT VUIK

1987/05/31	Born in Krimpen aan den IJssel, The Netherlands.
1999–2005	VWO, Wartburg College, locatie Revius, Rotterdam
2005–2010	MSc. Civil Engineering *(cum laude)*, Delft University of Technology, Delft
2010-present	Consultant Rivers, Estuaries and Coasts HKV Consultants, Lelystad and Delft
2014-2018	PhD researcher, Section of Hydraulic Structures and Flood Risk, Faculty of Civil Engineering and Geosciences, Delft University of Technology, Delft
2018-present	Postdoctoral researcher, Section of Coastal Engineering, Faculty of Civil Engineering and Geosciences, Delft University of Technology, Delft

List of Publications

Peer-reviewed journal papers

1. **Vuik, V.**, Borsje, B. W., Willemsen, P. W. J. M., and Jonkman, S. N. (2019). Salt Marshes for Flood Risk Reduction: quantifying Long-Term Effectiveness and Life-Cycle Costs. *Ocean and Coastal Management*, **171**, 96-110. (Chapter 5)
2. Zhu, Z., **Vuik, V.**, Visser, P. J., Soens, T., Van Wesenbeeck, B. K., Van de Koppel, J., Jonkman, S. N., Temmerman, S., and Bouma, T. J. (2019). Historic storms reveal overlooked value of saltmarshes for nature-based flood protection (under review).
3. **Vuik, V.**, Van Vuren, S., Borsje, B. W., van Wesenbeeck, B. K., and Jonkman, S. N. (2018). Assessing safety of Nature-based Flood Defenses: dealing with extremes and uncertainties. *Coastal Engineering*, **139**, 47–64. (Chapter 4)
4. **Vuik, V.**, Suh Heo, H. Y., Zhu, Z., Borsje, B. W., and Jonkman, S. N. (2018). Stem breakage of salt marsh vegetation under wave forcing: A field and model study. *Estuarine, Coastal and Shelf Science*, **200**, 41–58. (Chapter 3)
5. Oosterlo, P., McCall, R. T., **Vuik, V.**, Hofland, B., van der Meer, J. W., and Jonkman, S. N. (2018). Probabilistic assessment of overtopping of sea dikes with foreshores including infragravity waves and morphological changes: Westkapelle case study. *Journal of Marine Science and Engineering*, **6** (2), 48.
6. **Vuik, V.**, van Balen, W., and Van Vuren, S. (2017). Fully probabilistic assessment of safety against flooding along the Dutch coast. *Journal of Flood Risk Management*, **10**, 349–360.
7. **Vuik, V.**, Jonkman, S. N., Borsje, B. W., and Suzuki, T. (2016). Nature-based flood protection: The efficiency of vegetated foreshores for reducing wave loads on coastal dikes. *Coastal Engineering*, **116**, 42–56. (Chapter 2)
8. Giardino, A., Santinelli, G., and **Vuik, V.** (2014). Coastal state indicators to assess the morphological development of the Holland coast due to natural and anthropogenic pressure factors. *Ocean and Coastal Management*, **87**, 93–101.

Conference proceedings

1. **Vuik, V.**, and Jonkman, S. N. (2018). How vegetated foreshores affect probabilities and consequences of dike failure. In: *Coastal Engineering Proceedings*, Baltimore, US (Vol. 36).

2. **Vuik, V.**, Jonkman, S. N., and Van Vuren, S. (2016). Nature-based flood protection: using vegetated foreshores for reducing coastal risk. In: *Flood Risk Conference Proceedings*, Lyon, France (Vol. 7, p. 12008). EDP Sciences.
3. Penning, W. E., Steetzel, H. J., van Santen, R., De Lange, M., Ouwerkerk, S. J., **Vuik, V.**, and Van Thiel de Vries, J. S. M. (2016). Establishing vegetated foreshores to increase dike safety along lake shores. In: *Flood Risk Conference Proceedings*, Lyon, France (Vol. 7, p. 12008). EDP Sciences.
4. **Vuik, V.**, Jonkman, S. N., Borsje, B. W., Suzuki, T., Kratzer, I., and Bouma, T. J. (2014). Nature-based flood protection: the efficiency of vegetated foreshores in reducing wave run-up. In: *IAHR World Congress*, 28 June - 3 July 2014. Den Haag, The Netherlands.
5. Penning, W. E., Steetzel, H. J., Van Santen, R., Fiselier, J., De Lange, H. J., **Vuik, V.**, Ouwerkerk, S. J., and Van Thiel de Vries, J. S. M. (2014). Natural foreshores as an alternative to traditional dike re-enforecements: a field pilot in the large shallow lake Markermeer, the Netherlands. In: *IAHR World Congress*, 28 June - 3 July 2014. Den Haag, The Netherlands.
6. Van Balen, W., **Vuik, V.**, and Van Vuren, S. (2012). Probabilistic assessment of safety against dune retreat along the Northern-Holland coast. In: *Conference Proceedings NCK-days 2012*, Enschede, The Netherlands, ISBN: 978-90-365-3342-3.

PROFESSIONAL JOURNALS

1. **Vuik, V.** (2019). Toekomstbestendig met kwelders en andere brede waterkerende zones. *DeltaLinks*, Februari 2019.
2. De Vries, M. B., **Vuik, V.**, Olieman, M. A., and Jonkman, S. N. (2013). Voorlanden voor vergroten van waterveiligheid. *Land+Water*, Nr. 7/8, Juli 2013, 28-30.

BOOK CHAPTERS

1. Borsje, B. W., de Vries, S., Janssen, S. K., Luijendijk, A. P., and **Vuik, V.** (2017). Building with Nature as Coastal Protection Strategy in the Netherlands. In: Living Shorelines: The Science and Management of Nature-Based Coastal Protection, Bilkovic, D. M., La Peyre, M. K., Toft, J. D., & Mitchell, M. M. (Eds.), CRC Press. ISBN 9781498740029.